THE EFFECTIVENESS OF FILM COOLING

by

Bhaskar Ramchandra Pai

B.Tech., M.Sc.(Eng.), D.I.C.

Thesis submitted for the degree of
Doctor of Philosophy
in the Faculty of Engineering,
University of London.

October 1969

ABSTRACT

The present investigation is part of a research programme, committed to the development of a procedure for predicting the effectiveness of film cooling devices. The first step towards this objective is an understanding of the hydrodynamics and thermal performance of two-dimensional film cooling slots with tangential injection, by recourse to experimental and analytical techniques.

The present experimental programme investigated the influence of slot to mainstream velocity and density ratio and longitudinal pressure gradient on the impervious -wall effectiveness and flow-development downstream of a plane, two-dimensional slot with tangential injection, and the influence of velocity ratio and slot-lip thickness on the adiabatic-wall effectiveness and the heat transfer coefficient downstream of an axisymmetric slot.

A modified form of the Prandtl mixing-length hypothesis was used within the framework of the solution procedure of reference (49) to predict the flow downstream of two-dimensional slots. The appropriate physical inputs were obtained by examining experimental data and also by comparison of predicted and measured velocity and conserved-property profiles and wall properties over a practically useful range of velocity and density ratios and pressure gradients.

The predicted influence of velocity and density ratio, adverse and mild favourable pressure gradients and lip-thickness ratio on the impervious- or adiabatic-wall effectiveness showed, on the whole, a good correspondence with a wide range of experimental data, including those from the present investigation. Predictions of heat transfer coefficient in the presence of film cooling were also satisfactory.

The relevance of the present prediction procedure to a practical film-cooled combustion chamber was briefly examined. It was concluded that an accurate prediction of the flame-tube temperature required a precise knowledge of the conditions within the chamber and a prediction procedure for practical slot geometries. The author's suggestions in this connection are presented.

ACKNOWLEDGEMENT

I wish to express my gratitude to various persons whose guidance, help and encouragement were invaluable in the accomplishment of the present work. First, I am indebted to Dr. J.H. Whitelaw for his excellent supervision and deep personal interest in the project, which made my work challenging and interesting.

I wish to thank Professor D.B.Spalding for his help in the development of the prediction procedure and for his guidance of the project. My thanks are also due to Dr. S.V. Patankar for his invaluable help in the early stages of the project; to Dr. T. Mukerjee for the loan of his instrumented test section; to my colleague Mr. S.C. Kacker for helpful discussions and cooperation and to my family for their understanding and encouragement.

Finally, I wish to acknowledge the Council of Scientific and Industrial Research, India, for the award of the Burmah-Shell scholarship which was responsible for my presence at the Imperial College and to the Ministry of Technology Grant AT/2037/027/XR which enabled me to undertake the present research project.

CONTENTS

CHAPTER 1

1. Introduction.

1.1 Applications of film cooling.

Film cooling is a process for protecting a surface exposed to a high temperature gas stream by the injection of a cool fluid along the surface, to form a cooling film between the surface and the hot gas stream. The coolant is generally injected through slots, holes or porous sections in the surface to be cooled. In most of the applications the coolant is also gaseous and mixes with the hot gas downstream of the injection region. Film cooling is widely used in gas turbine combustion chambers, reheat nozzles of aircraft engines, turbine blades of gas turbines and in ram-jet and rocket nozzles. In all these applications the gas temperatures are very high (of the order of 2000^{o}C) and film cooling is essential to keep the temperature of the surfaces within metallurgical limits.

The cooling effect of a film is closely dependent on the mixing process between the coolant and the hot main stream: the greater the mixing, the shorter the distance downstream of the injection region which can be effectively film cooled. In the applications mentioned above, film cooling is supplementary to the more conven -tional convection cooling. For example, in the combustion chamber of a gas turbine, the flame tube is cooled on its outer surface by convection to the secondary air, part of which is bled into the chamber through slots for film cooling the inner surface of the flame tube,ie. the surface exposed to the flame.

Film cooling has been employed since the early days of the gas turbine. For example, the combustion chamber of the Whittle engine, which was of the counter flow type, had slots injecting tangentially in the circumferential direction (as opposed to axial). However the designs of film cooling slots in gas turbine combustion slots have since undergone considerable change and refinement. As the thermal loading of the combustion chambers has increased (ie., an increase in temperature, mass flow and pressure, and a decrease in the volume of the combustion chamber), the demands on the cooling system have also continually increased. These have been met with improved injection slot design and an increase in the number of film cooling strips. For example, in the early turbo-prop engines, film cooling was obtained by means of a few large holes at two regions of locally high flare in the flame tube, whereas a modern combustion chamber may have about thirteen ~~eight~~ film cooling strips, each comprising a machined ring designed to obtain a specific pressure drop and slot-to-mainstream velocity ratio at the slot exit. The design of film cooling slots is to date, an art rather than science.

When injected through slots, the coolant generally enters parallel to the surface, and the film can be considered as a 'wall-jet' in a moving stream. There are some applications closely related to film cooling by virtue of their wall-jet nature. These include the process of film heating for de-icing of aircraft wings or de-misting of windscreens by injection of warm air through slots or holes. Another related field is the application of wall jets to boundary layer control for example on helicopter rotors for increasing lift, or in diffusors to prevent separation at the walls.

The examples mentioned above have two common features: first, there is a surface and second, there is a gas stream with a principal direction of flow, such that the gradients of velocity and temperature normal to the surface are much greater than those along it and are confined to a narrow region adjacent the surface. These features are characteristic of boundary layers near walls and so flows downstream of a film cooling slot may be considered to be of the boundary-layer type, at least in the region far downstream of the injection region.

Though some aspects are particular to each of the above applications, a study of almost any of them would serve to high-light the main features of film cooling or the associated applications. Thus film cooling as applied to gas turbine combustion chambers serves as a useful case study for film cooling in general and much of the present treatment is biased in this direction.

1.2 Basic factors influencing film cooling.

This section is devoted to a qualitative description of the factors influencing film cooling in a gas turbine combustion chamber. The main object in cooling the flame tube is to maintain its temperature below the maximum acceptable metallurgical limit. To this end, the flame tube is cooled by means of the secondary air, which is approximately at the compressor delivery temperature. The temperature assumed by the flame tube is such that the net heat received by it through radiation and convection from the flame and heat lost through its outer surface by convection and radiation, are equal. Film cooling essentially influences the convective mode of heat transfer within the flame tube.

It is convenient to represent the convective heat transfer in the presence of film cooling through two quantities. The first is a quantity which depends on the mixing characteristics of the injected coolant and the main stream and is denoted as the adiabatic-wall effective -ness. This is defined as the ratio of the hot gas-to wall enthalpy difference at a location downstream of the slot, to the hot gas-to coolant enthalpy defference for an adiabatic wall. If the specific heat at constant pressure is assumed to be uniform within the flow, the enthalpies in the last sentence may be replaced by temperatures. Thus the adiabatic-wall effectiveness is given by the following expression:

$$\eta = \frac{h_G - h_{a,W}}{h_G - h_C} = \left[\frac{T_G - T_{a,W}}{T_G - T_C}\right]_{C_p = \text{const.}} \qquad 1.2.1$$

The adiabatic-wall effectiveness can be considered as a measure of the preservation of the identity of the cooling film: a value equal to unity signifies that the adiabatic-wall temperature is equal to the coolant temperature while a zero- value indicates an adiabatic-wall temperature equal to the hot gas temperature.

The adiabatic-wall effectiveness does not however provide any clue to the resistance of the film to heat transfer through it: for this a heat transfer coefficient based ~~of~~ on the adiabatic-wall temperature is useful:

$$h_f = \frac{\dot{q}''_W}{T_W - T_{a,W}} \qquad , \qquad 1.2.2.$$

where T_W is the temperature of the surface in the presence of the heat flux $\dot{q}''_W$ and $T_{a,W}$ is the wall temperature which would exist for the same initial conditions, and an adiabatic wall from the slot exit. Thus the adiabatic -wall effectiveness and the heat transfer coefficient h_f, defined in the above manner, serve to characterise the convective heat transfer in the presence of film cooling. Further, the distribution of these two quantities in the downstream direction gives a measure of the performance of the cooling slot and also provide part of the informa -tion from which the wall temperature can be computed.

It is to be expected that the effectiveness and the heat transfer coefficient will depend on several factors including the following:

geometry of the injection region;
distance from the slot exit;
gas velocities through the slot and mainstream ;
pressure gradients in the streamwise and cross-stream direction;
fluid properties (viz., molecular viscosity, conductivity and the Prandtl/Schmidt number);
turbulence intensities in the flow field.

This list of variables suggests that the flow downstream of a practical film cooling slot is very complex, since a large number of permutations and combinations of the above variables is possible and do exist in practice. It is useful therefore to indicate the ranges of the above variables which are likely to be encountered in gas turbine practice.

An impression of the wide range of injection geometries which are used in gas turbine applications can be found in reference (77). An ideal slot from the view of good performance is an unobstructed, two-dimensional slot which injects the fluid along the surface to be cooled. However such a design is not feasible in practice, as the components forming the slot have to be supported. The most commonly used designs are the 'wiggle strip' and the 'machined ring'. The former comprises a corrugated spacer mounted in an annular gap between two concentric overlapping sections of the flame tube, and the latter is a ring with discrete holes. Numerous variations on the design of practical devices is possible, but they have all one feature in common: the flow through them is invariably three dimensional, ie., apart from varying in directions normal to the wall and in the downstream direction, there is a variation in the spanwise direction also, at least in the region close to the slot. The width of the gap for practical slots (ie. the slot height) in modern gas turbine combustion chambers ranges from about 1.25 mm to 6 mm. The distance to be (or which can be sufficiently) cooled is of the order of 50 mm, which for the above range of slot heights corresponds from 8 to 40 slot heights.

The velocity ratios (ie., the mean velocity at slot exit to the main stream value) in practical devices range from about 0.5 to about 2.0. There is some incentive to set this value in the vicinity of unity and values slightly below this are often selected to optimise the coolant flow rate and effectiveness. The Mach numbers are generally low in combustion chambers (less than 0.3) and so compressibility is not generally of major importance. Density gradients due to temperature differences are however significant; slot to mainstream density ratios are greater than unity and values around three are common. Pressure gradients occur due to flare as well as to combustion and flow losses. Thus in the flared region near the primary zone an adverse presseure gradient is to be expected, whereas downstream a favourable pressure gradient due to combustion and geometry can be expected.

Fluid properties such as viscosity and conductivity can be expected to vary steeply in the regions of large temperature gradients. These gradients occur in the core of the flame tube due to combustion, and near the wall due to the cooling film and heat transfer.

The last item mentioned in the list of variables is the turbulence intensity. This can be expected to be high in the regions behind the fuel burner and colander and also where dilution streams mix with the primary stream. No measured values for this quantity are available for the case of a gas turbine combustion chamber.

Thus a considerable simplification of the flow downstream of a practical film cooling device is necessary to render it amenable to a systematic study.

1.3 Prediction of film cooling performance.

Procedures for the prediction of the adiabatic-wall effectiveness downstream of a film cooling slot have developed along two different lines. The first is the correlation of experimental data on the basis of dimensional analysis and guessed functional relationships between the relevant non-dimensional groups. The other is based on the analysis of the hydrodynamic and thermal flow field downstream of a film cooling slot, and may be considered a more fundamental approach than the first. The method of empirical correlations has the advantage of being simple in use but is severely limited by the data on which the correlations are based: their extension to include the effects of additional variables is tedious and needs a large amount of experimental data. Though empirical correlations may give satisfactory predictions over the range of experimental data on which they are based, the predictions are likely to be in error outside the range. The analytical approach, of which there are many variations, are invariably based on the equations of motion either in the differential or integrated form. It is wrong to suppose that analytical methods are superior to correlations because they do not need any empirical information. Analytical methods do need empirical information but at least some of it is of a general nature, and may be valid for a variety of flows. The amount of empirical information varies considerably with the method and the complexity of the model on which they are based. In general, the methods using the integrated equations of motion need more empirical information than those based on the differential equations: this matter will be discussed further in chapter 2. It should be mentioned that at present, analytical techniques are capable of handling only two- dimensional flows.

Most of the analytical methods currently available are valid only far downstream of the slot (say $x/y_C \geqslant 30$) and for a restricted range of velocity ratios (either much less or much greater than unity). Thus to date, analytical methods have not found much favour mainly because their validity is restricted to distances and velocity ratios which are not usually of interest to practical film cooling applications.

As regards the prediction of the heat transfer coefficient in the presence of film cooling, the present state of art is even more inadequate. In general, formulae valid for flat plates in zero-pressure gradient or fully developed pipe flow are used though, of course, neither is likely to be valid in the presence or film cooling.

1.4 Scope of the present investigation.

The present study is almost wholly concerned with two-dimensional slots. A study of two-dimensional slots is a useful step in the understanding of film cooling since they are, in principle, amenable to analysis. The use of a simple injection geometry also means that the task of controlled and independent variation of the individual factors is much easier.

On the experimental side the present investigation explores two-dimensional slots with tangential injection with particular reference to the adiabatic- or impervious-wall effectiveness and heat transfer coefficient, as they are influenced by the following parameters:

slot to mainstream velocity ratio;
slot to mainstream density ratio;
longitudinal pressure gradients;
slot lip thickness.

The data are obtained in suffient detail to test a prediction procedure for two-dimensional flows: this entails measurement of velocity and temperature (or mass fraction of slot fluid) profiles and the wall-shear stress, besides the impervious- or adiabatic-wall effectiveness and heat transfer coefficient.

Another objective of the present investigation is to apply a recent general prediction procedure due to

Patankar and Spalding (49) to the flow downstream of a two-dimensional slot with a view of predicting the influence of the factors mentioned above. As mentioned above, no fully satisfactory procedure exists, even for two-dimensional slots with tangential injection. The prediction procedure of reference (49) provides for the first time, a method for the solution of parabolic equations for boundary layer flows, which is sufficiently flexible, economical and general to be used in film cooling situations. This procedure requires the specification of the laws of turbulent exchange of momentum and mass before any predictions can be made, and the correctness of the predictions essentially rests on the validity of the exchange hypothesis chosen. The implications of the mixing length hypothesis of Prandtl (1925) for flows downstream of a film cooling slot are examined.

A final objective of the present study is to examine the relevance of prediction procedures, such as the one mentioned above, to practical applications of film cooling. An empirical procedure to extend the procedure to predict the performance of practical slots is suggested.

1.5 Outline of thesis content.

In order to place the present investigation in perspective, it is useful to survey the previous and concurrent investigations in film cooling. The next chapter (chapter 2) outlines and summarises the principal investigations in film cooling with tangential injection through two-dimensional slots, as well as available prediction procedures for effectiveness and heat transfer.

The steps leading to the development of a prediction procedure for the adiabatic-wall effectiveness and heat transfer coefficient may be enumerated as follows:

1. Selection of the type of prediction procedure
2. Procurement of experimental data against which to test the prediction procedure.
3. Specification of the physical inputs required for the prediction procedure.
4. Prediction of the effectiveness and heat transfer coefficient and comparison with the corresponding experimental data.

Chapters 3 to 6 deal with ~~these~~ problem in the above sequence. The salient features of the treatment in each of these chapters will now be briefly mentioned.

The first of the above steps implies the formulation of the mathematical and physical aspects of the problem, as well as a discussion on the relative merits of the various types of prediction procedures. This task is carried out in chapter 3.

Steps 2 and 3 in the above list need to be accomplished before the performance of the prediction procedure can be assesed. Accordingly, chapter 4 describes the experimental investigation which provides the requisite data as outlined in the previous section and, in chapter 5, the task of obtaining the appropriate physical inputs is undertaken. The latter exercise proceeds in two directions. The first is the direct examination of the physical inputs with reference to experimental data. The second (indirect) approach involves the comparison of predictions based on tentative assumptions about the physical inputs, with experimental hydrodynamic and conserved property data. For the latter exercise, the calculations are commenced from measured profiles, downstream of the slot (say $x/y_C \approx 20$) and consequently the predictions are of little direct utility.

Predictions of effectiveness and heat transfer coefficient, commencing from the slot exit and based on the physical inputs selected in chapter 5 are made in chapter 6 and compared with a wide range of experimental data. The influence of the variables listed in the previous section are examined.

Chapter 6 also examines the conditions within a practical gas turbine combustion chamber and the relative importance of the factors influencing the flame tube temperatures are discussed. The relevance of prediction procedures such as the present one are discussed and the chapter concludes with the author's suggestions for future research in film cooling.

CHAPTER 2

2. Brief review of previous and current investigations.

The object of the present section is to outline the major investigations in film cooling with two-dimensional slots with tangential injection. The various experimental investigations in this field are first briefly described, and their main findings are summarised. This is followed by a discussion of the various currently available prediction procedures. The limitations of these prediction procedures, as well as aspects needing further experimental investigation are pointed out.

Reviews of some of the investigations up to 1965 are to be found in references (76) and (77), while a summary of prediction procedures published before 1964 is to be found in reference (71).

2.1 Experimental studies of film cooling.

The systematic study of film cooling can be traced to the pioneering work of Wieghardt (75) at Göttingen in 1943. Wieghardt's interest was mainly in de-icing applications for aircraft wings by blowing through near-tangential slots. Brief particulars of Wieghardt's investigation as well as other subsequent comprehensive investigations of film cooling with two-dimensional tangential slots are shown in Table 2.1.1. There appears to be a gap of some thirteen years between the work of Wieghardt and the next publication on film cooling, after which there has been a sustained interest in the process. The general features of film cooling were revealed in Wieghardt's investigation and so it is appropriate to discuss these at the outset, so that the contributions of later workers can be viewed against this background.

The slot used by Wieghardt was designed to be flush with the surface (please see Table 2.1.1, col. 10): this caused the flow from the slot to emerge at a small angle to the surface, but the flow aligned itself to the plate within a short distance. As can be seen from the fourth column of the table, Wieghardt obtained data for a wide range of velocity ratios, but only for a very limited range of density (col. 5) and pressure (col.6) gradients.

TABLE 2.1.1. SUMMARY OF INVESTIGATIONS OF FILM COOLING WITH TANGENTIAL INJECTION THROUGH TWO DIMENSIONAL SLOTS

* VP - VELOCITY, TP - TEMPERATURE, CP - CONCENTRATION

1 AUTHOR	2 YEAR	3 x/y_C	4 i. $\bar{u}_C/u_G$ ii. $u_G(\frac{m}{s})$	5 DENSITY RATIO, ρ_C/ρ_G	6 PRESSURE GRADIENT	7 SLOT HEIGHT (mm) & INITIAL CONDITIONS.	8 PROFILES	9 OTHER VARIABLES INVESTIGATED	10 INJECTION GEOMETRY	11 PREDICTIONS
WIEGHARDT (75)	1944	to 800	i. 0.22-∞ ii. 16 - 32	0.80 - 0.91	ZERO; MILD FAVREL.; MILD ADVERSE.	y_C= 10; 5 $y_{G,C}$= 15; 17.	*VP: m= 0.22, 0.74, 1.01, 1.45 *TP: m= 0.74	i. Normal injection through slots. ii. Flow directions near slot exit.	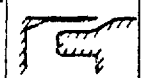	i. Empirical relation: $\eta = 21.8\cdot(x/my_C)^{-0.8}$; for $x/y_C > 100$ & m<1.
SEBAN, CHAN and SCESA (59)	1957	to 125	i. 0.08-0.92 ii. 13 - 38.	0.88 - 0.95	ZERO.	y_C= 3.2	VP, Outer surface of lip.	i. Normal injection through single slot. ii. Heat transfer coefficient; q_w constant.	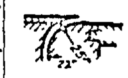	i. $\eta = 0.16\, R_C^{.33}(x/my_C)^{-b}$ b = 0.25 (x/my_C) < 40; = 0.70 > 40.
SEBAN (60) SEBAN & BACK (61), (62)	1960 1962	to 290	i. 0.20-23.7 ii. 1.5 - 37.0	0.88 - 0.95	ZERO (60), (61) FAVREL. (62) (2 values)	y_C= 1.6; 3.2; 6.3. $y_{G,C}$= 9.1; 31.6.	(61) VP, TP: m= .36 5 stations.	i. Heat transfer coefficient, q_w'' = constant		i. $\eta = 25\, m^{1.2}(x/my_C)^{-.8}$; m<1 = 1.09 $C^{-0.5}$; 1.00<m<2.5 $C = (\rho_C/\rho_G)^{-.5}(\frac{u_C - u_G}{u_C})^{2.3} R_{C}^{-0.3}(x/y_C)$
CHIN, SKIRVIN and HAYES (8)	1958	to 233	i. 0.26-2.85 ii. 19-54	0.83 - 1.17 (≠ 1.0)	ZERO	y_C= 2.7 $y_{G,C}$=20; 50.	VP, Outer surface of lip.	i. Influence of $y_{G;C}$.		i. $\eta = a\, A^{-b}$; see text for a,b; $A = (\frac{\rho_C}{\rho_G})^{-1.5}(\frac{u_G}{u_C}) R_C^{-0.3} R_{eff}^{0.14}(\frac{x}{y_C})$
HARTNETT, BIRKEBACK and ECKERT (22), (23)	1961 1962	to 138	i. 0.28 (22) 0.28 -1.1 (23) ii. 50	0.875	ZERO (22), (23) FAVREL., ADVERSE (23)	y_C= 3.1	VP, 5 stns. TP, 4 stns.	i. $(T_C - T_G)$ varied from 6 to 80°C. ii. Heat Transfer coefficient; q_w'' = constant	similar to WIEGHARDT (75)	i. $\eta = 16.9\,(x/my_C)^{-0.8}$
SAMUEL and JOUBERT (56)	1965	to 406	i. 0.23 2.90	1.1 - 1.25	ZERO	y_C= 3.2; 6.3; 9.4	VP: TP: } m=0.88, 10 stns	none.	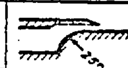	i. Similar to CHIN et.al. (8); separate expression for each y_C
GOLDSTEIN and HAJI-SHEIKH (20)	1966	to 160	m= 0-.41 (Air). m=.01;.02 (Helium) ii. Ma= 3	not specified	ZERO	y_C= 1.6; 3.1; 4.6 (Air) = 1.58 (Helium)	None.	i. Mach No. of free stream = 3. ii. Schlieren studies.		i. $\eta = a\cdot m^b\cdot(x/y_C)^c$ see text for a,b and c.
CARLSON and TALMOR (7)	1968	to 72	i. 0.19 0.90 ii. 64 - 132 (at x=0)	∼ 2.76	MODERATE FAVREL.	y_C= 1.58	None.	i. Free stream turbulence. = 12, 12, 22% ii. Heat Transfer Coefficient: without film cooling.	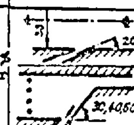	i. $\frac{1-\eta}{\eta} = 0.329\, a\, X_1$ where $X_1 = X f(\frac{\rho_G}{\rho_C}, Max)$; $X = R_{C}^{-0.3}\cdot Fe/R_C\cdot \xi(x)$; and a = $f((\bar{u'^2}/u_G), dp/dx)$.
WHITELAW (78), (79) WHITELAW & NICOLL (41) KACKER and WHITELAW (28), (30), (31)	1966 1969	to 288	i. 0.29 2.66 ii. 21	1.0	ZERO	y_C=1.88 to 12.7 (79) =0.243 (30) $\frac{t}{y_C}$ =0.128 to 1.90 (6 values) (30)	VP: $\frac{\bar{u}_C}{u_G}$ = 0.74; 1.33 (6 stns) (28) $\bar{u}_C/u_G$ = 0.75; 2.3, 3 stns (31), x/y_C (30).	i. c_f (28), (31) ii. x, $\overline{u'v'}$ profiles (28), (31) iii u' spectra (31).		i. Equations for R_2, R_3, R_ϕ are solved with auxilliary relations based on experiments. (41).
BURNS and STOLLERY (5), (6)	1968 1969	to 512	i. 0.58-4.0 (5) 0.30-1.42 (6) ii. 6.1; 17.3.	0.14; 4.17 (5), (6) 0.3; 0.6; 1.9; 1.38; 2.5. (5)	ZERO	y_C= 1.58 $\frac{t}{y_C}$ =(0), 1, 1.64, 2.7 (6). = (0), 2 (5). $y_{G,C}$=1.4; 4.	VP, *CP: $\bar{u}_C/u_G$ = 1.0; ρ_C/ρ_G = 0.14; 1.38; 4.17.	i. $y_{G,C}/y_C$= 0.89, 2.54 (5). ii. Colour Schlieren, ρ_C/ρ_G 0.14 (6)		i. Correlation of Ref (72).

One of the important conclusions from his study was that the adiabatic-wall effectiveness at a given station increased with the velocity ratio for mass velocity ratios less than approximately unity, but decreased with a further increase in the velocity ratio. Wieghardt also made detailed measurements of the velocity and temperature fields and came to the conclusion that the temperature profiles were relaitvely insensitive to the velocity ratio and were similar far downstream of the slot. The velocity field on the other hand was complex and allowed no simple analytical description. Far downstream of the slot, the velocity profiles approached a fully turbulent boundary layer shaper (ie., a 'power-law' profile). For velocity ratios greater than unity, the velocity profiles exhibited a maximum, which decayed in the downstream direction. Further, Wieghardt found that the effectiveness for any given non-dimensional distance x/y_C and velocity ratio, was practically the same for the two slot heights which he set up (see col. 7 of Table 2.1.1). He also found that the effect of a mild adverse or favourable pressure gradient, commencing fifty slot-heights downstream of the slot, was small.

One can now proceed to examine the other investigations on a comparative basis. First, some remarks about the slot geometries employed (see col. 10 of Table 2.1.1). The slots used by Hartnett et.al. (22), (23) and by Eckert and Birkeback (13) at the university of Minnesota were similar to the one used by Wieghardt. The slots used by all the other investigators shown in the table were of a backward facing step type and in principle, injected the fluid tangential to the surface. However, there are differences in the details of the various slots shown. The significant ones relate to the design of the slot lip; for example, its taper, thickness and overhang on the surface. The other design feature is the contraction leading to the slot exit. For example, in the slot used by Seban et.al. (59), and Chin et. al. (8), the contraction from the plenum chamber occurs far upstream of the slot exit and the lead-in to the slot is a curved constant-area duct. In the other examples shown, the contraction occurs close to the slot exit. In all the cases, the flow suffers a bend before emerging from the slot, which may introduce secondary vortices in the slot flow, particularly in the slot geometries of references (59) and (8). Inthe case of references (56), (20), (78), (30) and (5), the over-hang of the slot-lip tends to reduce any residual effects of this secondary flow. The slot heights used by the various investigators are shown in column 7 of Table 2.1.1.

With the exception of references (20), (57) and (7), all the investigations were carried out in low speed, turbulent flow (mainstream velocities of the order of 30 m/s), and consequently the slot to main stream density ratio were in the vicinity of unity, except where foreign gas was injected through the slot (20), (5), (6). Gases such as helium (20), (5), (6) or Arcton-12 (5), (6) were injected through the slot, to obtain large density ratios on either side of unity, without incurring the experimental problems associated with large temperatures. In the majority of the investigations with air injection (ie. references where the density ratios is slightly below unity), the secondary air was heated by some 30 to 40 deg C, whereas the mainstream was nominally at room temperature. This was mainly a matter of convenience, as the quantity of air to be heated was less if the secondary flow was heated. Reference (22) demonstrated that for a given mass flow through the slot, the same effectiveness was obtained with slot to mainstream temperature differences from 6 to 80 deg C.

The use of a mass transfer analogy to film cooling experiments was introduced by Whitelaw (78); a small quantity of helium was mixed in the secondary stream. The mass fraction of helium within the flow is analogous to the temperature (or enthalpy) field, provided the eddy-diffusivities for enthalpy and species transport are same (ie. if the turbulent Lewis number is equal to unity). The use of such a technique implies that mass concentration of the injected tracer are measured rather than temperatures. In particular, measurement of the mass concentration at the wall permits the evaluation of the impervious-wall effectiveness, analogous to the adiabatic-wall effectiveness. The advantage of the mass transfer analogue is that an impervious-wall condition can be realised more closely than an adiabatic-wall. Such a technique also permits the study of equal slot to free stream density.

The influence of longitudinal pressure gradients have been investigated in references (75), (62), (23), and (7). All, except reference (7), have noticed a small decrease in the effectiveness when the main stream is accelerated or decelerated. Reference (7) indicates a large influence due to favourable pressure gradient but, in this case, pressure gradients normal to the flow direction were also present (as can be expected from the slot geometry shown in Table 2.1.1). Also, the width of the test section of reference (7) was only 13 mm, which probably resulted in three-dimensional flow, especially in the vicinity of the injection region. In general, the range of pressure gradients investigated is small and the influence of pressure gradients in the presence of significant density gradients has not been investigated.

Information concerning the development of velocity and temperature (or mass fraction) profiles is useful, both for a qualitative understanding of the flow field and also for devising or asessing prediction procedures. When the two-dimensionality of the flow is good, the velocity and temperature profiles also permit the evaluation of wall-shear stress and eddy viscosity or diffusivity across the layer. Profiles of mean velocity and temperature (or mass fraction) have been provided by several authors shown in column 8 of Table 2.1.1.

Some of the other quantities investigated experimentally will now be briefly discussed. Heat transfer in the presence of film cooling has been investigated by Seban et. al. (59),(60),(61),(62) and by Hartnett et. al. (22),(23). Seban and Hartnett employed electrically heated walls, which resulted in nominally constant heat flux boundary conditions. The major conclusions reached by these authors was that for velocity ratios less than unity and for large distances fromthe slot ($x/y_C \geqslant 30$), the heat transfer coefficients (defined by eq. 1.2) approach values corresponding to a flat plate. The nature of the heat transfer coefficient near the slot was more complex and was a function of the velocity ratio.

The influence of the thickness of the boundary layer on the outer surface of the slot lip has been investigated by Chin et.al. (8), Seban and Back (61) and by Kacker and Whitelaw (27). The thickening of this boundary layer appears to result in a lowering of the effectiveness, but the effect is not very large, provided the lip-thickness ratio (t/y_C) is above about 0.4. For example, the data of reference (27) show a maximum decrease of about 4 percent (of unity) in the effectiveness for an increase of the boundary layer thickness from 2.4 to 10 slot-heights.

The influence of the slot-lip thickness on effectiveness has been investigated by Whitelaw et.al. (79), (64), (30), for uniform density flows and by Burns and Stollery (6) for non-uniform density cases. In reference (79), it was suggested that the influencing parameter for uniform density flows, is the ratio of the slot-lip thickness to the slot height (t/y_C) and this was confirmed by the work of references (64) and (30). Reference (79) describes measurements where the slot height was varied for a constant lip thickness, whereas references (64), (30), and (6) describe measurements for which the lip thickness was varied for a constant slot height. These investigations demonstrate that an increase in the lip thickness to slot height ratio (t/y_C) has a strong adverse influence of the effectiveness of film cooling. For example, the data of reference (30) show that for a velocity ratio of 0.86 and x/y_C of 28, the impervious-wall effectiveness decreases from 0.85 to 0.45 as the lip thickness ratio is increased from 0.128 to 1.14. For large downstream distances, the impervious-wall effectiveness with a thick lip tends towards the thin lip value. These statements are valid for the case of uniform density cases. For the case of Arcton-12 injection ($\rho_C/\rho_G = 4.17$) however, the influence of the lip thickness diminishes with increasing velocity ratio (6). Another interesting finding of reference (79) and (30) is that for values of t/y_C greater than about 0.4, the maxima in effectiveness for velocity ratios in the vicinity of unity, disappears: the value of effectiveness for a given downstream distance remains practically constant for velocity ratios greater than approximately unity.

Further variables investigated by Kacker and Whitelaw (28), (31) are mainly concerned with the hydrodynamics of the flow downstream of film cooling slot, in uniform density and pressure flows. These include the measurement of turbulence intensities, kinetic energy of turbulent motion, u'-spectra , wall-shear stress and the distribution of the turbulent shear stress across the layer. The data provide a basis for assesing a hypothesis of turbulent momentum transport in the elliptic and parabolic flow regimes.

An examination of the hydrodynamics of a wall-jet in stagnant surroundings has been made by Tailland and Mathieu (73) and by Gartshore (17), and for wall-jets in a moving stream by Bradshaw and Gee (4). Wall-jets in adverse pressure gradients have been investigated by Eskinazi and Kruka (26), Patel and Newman(50). Heat transfer to a wall-jet in stagnant surroundings has been studied by Myers et.al. (40). These studies are relevant to film cooling in so far as the velocity profiles have a velocity maximum such as thatoccurringin a film cooling situation for velocity ratios in excess of unity.

Though there have been numerous experimental investigations in film cooling, all the influencing factors have not been systematically investigated. For example, there is a need for experiments in which the injection geometry (ie. the slot height) and initial conditions at the slot exit are kept unaltered while the variables such as velocity ratio, density ratio and pressure gradients are varied independently as well as simultaneously and sufficient measurements concerning wall properties and profiles are obtained to asses prediction procedures. A certain amount of overlap with previous investigations is desirable in order to asses the consensus or otherwise between the various sets of data.

2.2 Brief review of previous prediction procedures.

Every experimenter at the conclusion of his investigation, wishes to see some order or regularity in his data, such that a simple analytical expression or law can be found to charaterise his findings. On the other hand, a designer wishes to predict the performance of a film cooling device for a projected application. Thus there is a need to predict, amongst other things, the film cooling effectiveness and heat transfer coefficient downstream of a two-dimensional slot. As mentioned in the introduction, the distance generally of interest in propulsion applications, is of the order of 40 slot-heights downstream of the slot.

Prediction procedures may be classified under the following categories:

1. Correlations;
2. Integral methods;
3. Differential methods.

The following three sub-sections briefly outline the various proposals in the above categories and a discussion on them is included in section 2.2.4.

<u>2.2.1 Correlations.</u> In correlating experimental data, use is made of dimensional analysis and some observed regularity when the data are plotted in these dimensionless groups. They are not generally based on any physical or transport hypothesis. There are numerous examples under this category. Wieghardt (75) in his pioneering paper on film cooling found that all his effectiveness data for $m < 1$, tended to fall on a single straight line when plotted on log-log paper against the parameter (x/my_C). Consequently he found that the equation shown in column 11 of Table 2.1.1 correlated his data for large distances from the slot $(x/y_C > 100)$ and $m < 1$. Seban et.al. (60) found a correlation for the 'potential core' region (ie., the distance from the slot for which the effectiveness is unity) and used this relation, in conjunction with a power-law relationship, to correlate their data for mass velocity ratios less than unity. They found that their data displayed a power-law decay with x/y_C at large distances from the slot: the power being 0.8 for m less than unity and 0.5 for m greater than unity. Chin et.al. provided another correlation, which included a correction for the hydrodynamic starting length $(R_{x,C})$. Three different power law regimes were discerned and the coefficients of the equation shown in Table.2.1.1 are as follows:

$$\begin{array}{lll} a = 1, & b = 0 & A < 15 \\ a = 1.5, & b = 0.15 & 15 < A < 72 \\ a = 12.7, & b = 0.65 & 72 < A \qquad u_C/u_G < 1 \end{array}$$

where the correlating parameter A is as defined in the table. A similar correlation was provided for velocity ratios between 1 and 2. Samuel and Joubert (56) correlated their data in a similar way, but they found that a separate correlation was needed for each of the slot heights.

A correlation developed by the Lucas Research Laboratories, Burnley (34), employed an exponential function. The advantage of the exponential function chosen was that it indicated a smooth decrease in the effectiveness from a value of unity near the slot. The recommended equation in this reference is:

$$\eta = 1 - \exp\left[\frac{-\ 44.1}{m^{-0.8}(T_G/T_C)^{0.6}(x^{0.8}/y_C).X}\right] \quad ,$$

$$\text{where} \quad X = 1 \qquad \frac{\bar{u}_C}{u_G} \leqslant 1.25 \quad ,$$

$$X = \left[\frac{u_G}{u_C} + 0.2\right]^{-1.2} \qquad \frac{u_C}{u_G} > 1.25 \quad . \qquad 2.2.1$$

(note that x and y_C are to be measured in inches).

Another simple correlation, provided by Spalding, Jain and Nicoll (65), which is valid for velocity ratios on either side of unity is as follows:

$$\eta = 1 \qquad X < 7 \quad ;$$

$$\eta = 7/X \qquad X \geqslant 7 \quad ,$$

$$\text{where} \quad X = 0.91\left[\frac{u_G\ x}{u_C\ y_C}\right]^{0.8} R_C^{\ -0.2} + 1.41\left\{\left|1 - \frac{u_G}{u_C}\ \frac{x}{y_C}\right|\right\}^{0.5}$$

2.2.2

This expression is based on the notion that near the slot, the flow is jet-like and reverts to a boundary layer far downstream of the slot.

<u>2.2.2 Integral methods.</u> Under this category are implied methods which solve the integrated forms of the conservation equations applicable to boundary layers. Numerous varieties and hybrids of the integral methods exist (see for example the introduction in reference (49)). For film cooling applications, most of them solve the integral thermal energy (or species) conservation equation, after solving (or assuming) a solution of the integral hydrodynamic properties of the flow. The solution of the integral equations require auxiliary relations between the various dependent variables and other quantities appearing in the equations. These may either be explicit functions derived from experimental data (in which case the method is called an 'explicit integral method', for example reference (41)) or they may be derived from a general hypothesis for eddy transport. The latter

variety may be called the 'implicit' type (see for example (48)). Integral methods employ assumptions regarding the shape of the velocity and temperature profiles, which thereby permit some of the relations between the integral properties to be worked out. For example, several of the methods (Wieghardt (75), Stollery and El-Ehwany (71)), assume that the velocity profiles are similar and can be described by a power-law relation of the type $u/u_G = (y/y_G)^n$, where n is approximately equal to 1/7. Similar assumptions are made concerning the temperature or species profiles.

Again, it is fair to cite Wieghardt's case as a typical integral method of the 'explicit' type, and then to point out the differences of later proposals. Wieghardt solved the energy equation assuming similarity in the velocity and temperature profiles - a power law for the former and an exponential for the latter. He obtained the result that for a power-law exponenent of 1/7, the effectiveness far downstream of a film cooling slot is given by the equation

$$\eta = 2.01 \; m \, (y_C/y_G) \, . \qquad 2.2.3$$

The x-wise distribution of effectiveness can be obtained from this equation if a relation betweent the boundary layer thickness y_G and the distance x is assumed. Thus, if y_G is taken from the relation

$$\frac{y_G}{x} = 0.37 \, R_x^{-0.2} \; , \qquad 2.2.4$$

which is known to be valid for flat-plate boundary layers in zero pressure gradient (58), one obtains

$$\eta = 5.44 \, (x/my_C)^{-0.8} R_C^{\;0.2} \, . \qquad 2.2.5$$

It should be pointed out that the exponential form for the temperature profiles was obtained by Wieghardt by integrating the energy equation along with the continuity equation and assuming that the eddy viscosity at any station was constant across the layer.

The expressions obtained by Hartnett et.al. (22), Klein and Tribus (32), Stollery and El-Ehwany (71) are similar to the above expression and differ essentially in the value of the constant in the equation. The procedures of these authors differ mainly with regard to the assumption of the shape of the temperature profile.

One integral method which differs markedly from the above methods is that of reference (41). In this procedure, three integral equations are solved. These are the integral momentum-deficit, integral kinetic-energy-deficit and the energy (or species) equations. Empirical relations, based on experimental data between the dependent variables R_2 and R_3 and the other quantities such as H, H_{32}, $c_f/2$ and $\bar{s}$ are employed, which then permit the solution of the three ordinary differential equations, for example by forward integration procedures. Further empirical relations between conditions at the slot exit and the values at a downstream station are provided, which permit the prediction of effectiveness, commencing from the slot exit.

2.2.3 Differential methods. Under this category are implied methods which solve the parabolic, partial differential equations valid for boundary layers. Methods for solving these equations are of the numerical, finite-difference type, which may either be of the

marching integration or
cross-stream integration

type. Finite difference methods for turbulent boundary layers have only recently found general application (49). Procedures available prior to that of reference (49) were expensive in computer time and had inherent problems such as instabilities due to step size. Previous application of numerical methods to film cooling problems are not known to the author. Brief particulars of the two types of finite difference procedures mentioned above are given in the next chapter (3.3).

It is relevant to mention that methods of the 'parametric integral' type also solve the parabolic equations, after reducing them to a set of first order ordinary differential equations (for example Patankar and Spalding (48)); however, the solutions of the integral equations tend to that of the parabolic equations only when the number of parameters becomes very large.

2.2.4 Discussion of previous prediction procedures.

In the above three sub-sections, the various methods for the prediction of film cooling effectiveness have been presented without comment. In the present section, the advantages, limitations and successes of the various procedures are briefly discussed.

The correlations of references (75), (59), (22), and (72) which are based on assumptions valid for flat-plate boundary layers, are valid in the presence of film cooling, only at large distances from the slot and for mass velocity ratios less than unity. For example, Wieghardt found his correlation was valid for x/y_C greater than about 100. The use of such correlations for values of (x/my_C) less than about 50 appears to be unreliable. Even for large values of this parameter, the scatter of data from different sources around any of the above correlations is of the order of $\pm$ 40 percent of the local values of effectiveness (22),(72). This clearly indicates the limited use of such correlations from a practical view-point, since the distance of practical importance in gas turbine applications is seldom more than 40 slot-heights and mass velocity ratios greater or equal to unity are common. Further such methods are not capable of including the effects of factors in the near-slot region. These limitations are essentially due to the over simplifying assumptions concerning the velocity profiles: velocity profiles in the vicinity of a film cooling slot exhibit a maximum and a minimum, whereas the profiles assumed in the analysis are monotonic. The correlation of reference (36) and (65) do not suffer from these two limitations.

The explicit integral method of reference(41) is based on more intricate equations and a considerable amount of experimental data is needed to devise the auxiliary relations used in the method. For example, for the simplest case of uniform density and pressure flows, the total number of constants to be obtained by reference to experiment is 24. Extension to include the influence of further variables (such as density and pressure gradients) would increase this number even further and the amount of experimental data required to base the auxiliary equations would be formidable. Even so, the method fails to provide realistic predictions of effectiveness for velocity ratios in the vicinity of unity, and in the near-slot region.

The main conclusion that can be drawn from the above discussion is that, at present, there is no single procedure which can satisfactorily predict the effectiveness of a two-dimensional film cooling slot for a practically useful range of distance from the slot exit, velocity ratio, density ratio and pressure gradients and which takes some cognizance of the conditions at the slot exit. It is likely that further progress in this direction would be made by prediction procedures having as their basis, the partial differential equations which describe the flow downstream of a film cooling slot.

CHAPTER 3

3. The flow downstream of a two-dimensionsl, film cooling slot.

The purpose of this chapter is threefold: first, to provide a qualitative description of the flow downstream of a two-dimensional slot and to identify the different flow regimes. Second to introduce the equations governing such flows and thirdly, to outline the solution procedure which is considered most suitable. The third objective implies a brief discussion of the various calculation procedures avilable, to enable a selection to be made.

3.1 Qualitative description of the flow field.

The flow development downstream of a film cooling slot is sketched in Fig.3.1.1. The figure indicates the shapes of the velocity and enthalpy profiles and effectiveness for a velocity ratio close to unity, as well as the relevant notation.

The velocity profiles in this figure have been normalised with the freestream value. At the slot exit, three boundary layers can be discerned: two within the slot and one on the outer surface of the slot lip. In the example shown, the two boundary layers within the slot exit are separated by a region of uniform velocity. Immediately behind the slot lip, there is a region of separated and recirculating flow. The two boundary layers on either side of the slot lip converge downstream of the this separated flow region and develop as a 'mixing layer', up to the point where it joins the boundary layer growing on the wall. Thereafter the layer develops a wall boundary layer. The shape of the velocity profiles near the slot depends mainly on the velocity ratio at the slot exit. The example shown in Fig.3.1.1 corresponds to a slot to mainstream velocity ratio of approximately unity. For velocity ratios less than this value, the velocity profiles would have a larger defect near the wall, whereas for velocity ratios greater than unity, the velocity profiles resemble that of a wall-jet, with a velocity maximum greater than the free stream value. Both the peak and trough in the velocity profiles decay in the downstream direction as a result of momentum exchange, till far downstream, the velocity profiles are monotonic and similar to those existing on a flat plate in a uniforn velocity stream.

The enthalpy profiles shown in Fig.3.1.1.have been normalised with the free-stream and wall values in the following manner:

$$h' = \frac{h - h_G}{h_W - h_G} .$$

The wall value of enthalpy appears in the adiabatic-wall effectiveness, as defined in equation 1.2.1. The temperature (or enthalpy) profile at slot exit is of a 'top hat' shape: there is a steep gradient at the lip from the value in the slot to the free stream value. As the mixing between the coolant and the mainstream progresses, the step in the temperature profile is smoothed out and the profiles become S- shaped far downstream. The gradient of the temperature profile is of course zero at the wall, for the case of an adiabatic wall. The profiles of mass fraction of the coolant are similar to the enthalpy profiles and are exactly analogous if the turbulent Lewis number is unity. This is tacitly assumed to be true in this thesis and so enthalpy and mass fraction of coolant are sometines used interchangeably in particular, the adiabatic-wall and impervious-wall effectiveness are assumed to be equal, and merely referred to as effectiveness. The effectiveness as indicated in Fig.3.1.1. is equal to unity near the slot but decreases downstream as the coolant mixes with the free stream. In the immediate vicinity of the slot, the flow can be expected to be significantly influenced by the slot geometry and initial conditions such as the thickness of the boundary layer on the outer surface of the slot-lip ($y_{G,C}$) or the shape of the velocity profile within the slot. In particular, due to the finite thickness of the slot lip and the separated flow region behind it, the streamlines close to the slot lip would show significant curvature and there would be pressure gradients normal to the predominant flow direction. Thus in this region the flow is not of the boundary layer type, and departures from it are likely to increase with an increase in the lip thickness or as the velocity ratio approaches zero. The extent of the 'initial region' near the slot is hard to define precisely, and several definitions are in vogue. Some authors define it as the 'potential core' length, the distance from the slot at which the effectiveness begins to depart from unity, while others define is as the point of intersection between the mixing layer originating from the slot lip and the wall boundary layer. The concept of an initial region is no longer of particular significance and in the present work it will be taken to mean the region close to the slot where the geometry of the injection region can be expected to have a significant influence (about 10 to 30 slot-heights, depending on the lip-thickness ratio).

3.2 Equations governing the flow.

For the present purpose the flow downstream of a film cooling slot will be assumed to be that of a perfect gas; steady, incompressible, fully turbulent, with negligible body forces and two-dimensional (ie. there are property variations normal to the wall and in the downstream direction only). The equations which govern fluid flow of this type are the following:

the Navier-Stokes equations in two-dimensions;
the equation of continuity;
the first law of thermodynamics;
the perfect gas relationships between pressure, density and temperature.

The Navier-Stokes equations for turbulent flow have to be considered on a time averaged basis to render them amenable to present day solution procedures. With these restrictions, the relevant set of equations in Cartesian coordinates are:

$$u\,\frac{\partial u}{\partial x} + v\,\frac{\partial u}{\partial y} = -\frac{1}{\rho}\frac{\partial p}{\partial x} + \nu\left\{\left(\frac{\partial^2 u}{\partial x^2}\right) + \left(\frac{\partial^2 u}{\partial y^2}\right)\right\} - \frac{1}{\rho}\left(\frac{\partial\,\overline{\rho u'^2}}{\partial x} + \frac{\partial\,\overline{\rho u'v'}}{\partial y}\right) \qquad 3.2.1$$

$$u\,\frac{\partial v}{\partial x} + v\,\frac{\partial v}{\partial y} = -\frac{1}{\rho}\,\frac{\partial p}{\partial y} + \nu\left\{\left(\frac{\partial^2 v}{\partial x^2}\right) + \left(\frac{\partial^2 v}{\partial^2 y^2}\right)\right\} - \frac{1}{\rho}\left(\frac{\partial\overline{u'v'}}{\partial x} + \frac{\partial\,\overline{\rho v'^2}}{\partial y}\right) \qquad 3.2.2$$

$$\frac{\partial\,(\rho u)}{\partial x} = -\,\frac{\partial\,(\rho v)}{\partial y} \qquad 3.2.3$$

$$u \frac{\partial h}{\partial x} + v \frac{\partial h}{\partial y} = \frac{\kappa}{\rho} \left\{ \left(\frac{\partial^2 h}{\partial x^2} \right) + \left(\frac{\partial^2 h}{\partial y^2} \right) \right\} - \left(\frac{\partial \overline{u'h'}}{\partial x} + \frac{\partial \overline{v'h'}}{\partial y} \right)$$

$$+ \nu \Phi \qquad 3.2.4$$

$$1/\rho = \bar{R}\, T/p \qquad 3.2.5$$

Thus there are five equations and five unknowns viz. u, v, h, p and ρ, and so in principle form a soluble set, provided the turbulent stresses in eq. 3.2.1 and 3.2.2 and the turbulent enthalpy fluxes in eq. 3.2.4 can be expressed as functions of the other dependent variables. The last proviso, which is an important one, will be discussed later in this chapter.

The Navier-Stokes equations shown above are elliptic in nature and are capable of describing flows with or without recirculation and pressure gradients in both directions. Consequently the above equations are valid in the immediate vicinity of the slot as well as further downstream. Numerical methods for the solution of the equations of the above type have recently been devised and are under development (19). However, they are quite expensive in computer time and need considerable experimenting before satisfactory solutions can be obtained.

For slots with fairly thin lips (say $t/y_C \leqslant 0.5$), the factors which cause a violation of the boundary layer assumptions due to Prandtl (58), namely recirculation and pressure gradients normal to the flow direction, can be expected to vanish fairly close to the slot (28). Thus for practical purposes the flow downstream of a film cooling slot can be considered to be of the boundary layer type, except in the immediate vicinity of the slot lip. This implies that the elliptic equations (3.2.1) and (3.2.2) may be reduced to parabolic ones using the well known boundary layer assumptions. These imply that the thickness of the boundary layer is small in comparison with a characteristic dimension of the flow and that there is no region of recirculation. An order of magnitude analysis of the various terms in equations 3.2.1 and 3.2.2, permits them to be reduced to the following:

$$u \frac{\partial u}{\partial x} + v \frac{\partial u}{\partial y} = - \frac{1}{\rho} \frac{dp}{dx} + \nu \frac{\partial^2 u}{\partial y^2} - \frac{1}{\rho} \frac{\partial \overline{\rho u'v'}}{\partial y} \quad , \quad 3.2.6$$

and
$$\frac{dp}{dy} \approx 0 \quad . \quad 3.2.7$$

Essentially, the second derivatives of velocity in the x-direction have been neglected in comparison with the corresponding term in the y- dirextion, since the latter is of an order $(1/y_G)^2$ greater than the former. Eq. 3.2.2 is truncated to the above form (eq.3.2.7) due to the fact that all the terms in it are of the order (y_G) which is small in comparison with the terms of eq.3.2.6, which are of order unity. Further, the contributions of the normal turbulent stresses have been neglected in comparison with the turbulent shear stresses. The main implications of the parabolic equations 3.2.6 are as follows. First, the pressure distribution is no longer an unknown: the x-direction pressure gradient is taken to be the same as that existing at the outer edge of the layer (which is generally known, or calculable from the data of the problem) and the y-direction pressure gradient is assumed to be zero (eq. 3.2.7). Second, it is necessary to specify the boundary and initial conditions on only three sides of the flow domain: the wall, the free stream and along a normal to the wall at the initial value of x, whereas the elliptic equations 3.2.1 and 3.2.2 need boundary and initial conditions within an enclosed domain. The implication of this statement is that for the parabolic equations, there is no downstream influence and they can be solved by a method of marching integration, which is a relatively cheap (in computer time) process.

The energy equation, 3.2.4 is also further simplified as a result of the boundary layer assumptions. In particular, the second derivative of h in the x-direction and the term containing $\overline{u'h'}$ are neglected. Further, the dissipation term $\nu\Phi$ is neglected for low-speed flow and for fluids of low viscosity.

However, equations 3.2.6 and the reduced form of equation 3.2.4 are still non-linear, partial differential equations for which general analytical solutions are not available. Possible methods of solution are outlined in the next section.

In connection with the elliptic equations 3.2.1 and 3.2.2 it was stated that they form a soluble set, along with eqns. 3.2.3 to 3.2.5, provided the turbulent stresses and diffusional fluxes can be related to the other variables. This proviso still holds for the parabolic form of the equations, and in fact constitutes the central problem of the physical aspects of turbulent flow.

By far the most common practice is to relate the turbulent stresses and heat fluxes to the gradients of mean velocity and enthalpy (or the respective scalar conserved property), in the manner analogous to laminar flow:.

ie., $$\tau_{eff} = \mu_{eff} \frac{du}{dy} \quad , \quad 3.2.8$$

and $$J_h = -\frac{\mu_{eff}}{\sigma_{eff}} \frac{dh}{dy} \quad . \quad 3.2.9$$

Here τ_{eff} and J_h represent the total (ie., the sum of laminar and turbulent components) shear stress and diffusive enthalpy flux, while μ_{eff} represents the effective viscosity and σ_{eff}, the ratio of the effective viscosity to diffussivity. Unlike laminar flow, μ_{eff} and σ_{eff} are not unique thermodynamic properties of the fluid, but are function of the flow field as well. Before proceeding to the various proposals for the effective transport coefficients, it should be mentioned that the concept of an eddy (or effective) exchange coefficient is not the only possible way of accounting for the turbulent quantities. For example, it is possible to obtain from the Navier-Stokes equations, a differential equation for the turbulent shear stress which in principle, can be solved along with the other equations (55). This possibility has not been explored to any depth at present.

Several hypotheses have been proposed in the past for eddy viscosity and a fairly comprehensive list of these can be found in (68). All of them are empirical, but some are based on a heuristic model for the motion of eddies while others are based purely on dimensional analysis. In spite of the large number of proposals for eddy viscosity relationships, it is fair to say that no single entirely satisfactory and general hypothesis is yet available: each proposal has its advantages and limitations. It is not the intention here to discuss the merits and demerits of all available hypotheses: instead three hypotheses which have been widely used and one which is currently being investigated will be mentioned. These are the hypotheses due to Prandtl (1925), Clauser (1954) and Kolmogorov - Prandtl (1942-45). The first two of these have been adequately described in reference (58), whereas the third and fourth have been described in chapter 2 of reference (68). These four hypotheses are relevant to the present problem, but a selection from these is deferred to chapter 5.

3.3 Choice of solution procedure.

The mathematical problem is thus the solution of a set of four equations, 3.2.6, 3.2.3, 3.2.4 and 3.4.5, three of which are partial differential equations, in conjunction with some specific relations for the eddy viscosity and diffusivity, and appropriate boundary and initial conditions.

As mentioned earlier there are no general analytic solutions for the set of equations mentioned above. There are two possible lines of attack: the first is to reduce the partial differential equations to ordinary differential equations, which are soluble by standard techniques and the second is the finite-difference type numerical methods.

There are a number of methods under the first category. The first is to multiply the partial differential equations with weighting functions (which may equal unity or be functions of velocity etc.) and integrate across the layer. The result is a set of ordinary differential equations, with the integral properties (such as the momentum thickness, shape factor etc.) as the dependent variables and the stream-wise distances as the independent variable. These can be solved, for example by forward integration, in conjunction with certain auxiliary relations. These relations can be in the form of explicit functional relations between the dependent variables and other variables occuring in the equations (this includes a drag law) or they can be related to the shape of the velocity and temperature profiles. The latter possibility is the basis of the 'parametric integral' technique, for example ref (48). As pointed out by the authors of this reference, this method is not an approximate one and its accuracy can be increased with the number of free parameters (and consequently the number of integral equations).

The partial differential equation reduce to ordinary ones for a certain class of flows which are called equilibrium flows. In such flows the velocity profiles become 'similar' to one another, when non-dimensionalised with a suitable para-meter, for example the boundary-layer thickness. Flows of the equilibrium type require certain non-dimensional groups, representing longitudinal gradients of free stream velocity, stream function and mass transfer through the wall, to be constant. The derivation of the relevant equations may be found in section IV, p. 18 of reference (67). When the above conditions are satisfied, the partial differential equations reduce to ordinary ones, which can be solved numerically by forward integration.

Under the second category, there are two main varieties: one is denoted the 'cross-stream integration' and the other is the 'marching integration' procedure. The cross stream integration procedure involves the reduction of the partial differential equations to ordinary differential equations, valid for successive sections across the layer. This set of ordinary differential equations may then be solved numerically, for example by forward integration. Iteration is however necessary, since boundary conditions on either edge of the domain have to be satisfied. This latter condition implies a considerable increase of computing time and storage over methods which do not need iteration.

The marching integration procedure on the other hand, posses the desirable characteristic that no iteration is necessary. In this procedure, the calculation proceeds downstream by means of a forward step: commencing with the appropriate boundary conditions, the unknowns at a short distance downstream are calculated. The computed values at the downstream station then become the 'upstream' conditions for the next step and thus the calculation progressively solves the flow field. The partial differential equations are reduced to a set of linear algebraic equations which can be solved by matrix inversion or, the cheaper, recurrence formulae. Thus the marching integration procedure appears attractive since iteration can be avoided and only linear, algebraic equations have to be solved. The elements of this method have been known for a long time, but it is only recently that a form particularly suited for boundary layer-type flows (both laminar and turbulent) has been devised (Patankar ans Spalding (49)). This general solution procedure provides the framework for the solution of the parabolic equations valid for boundary layers for a wide range of boundary conditions such as heat or mass transfer through the wall, or stream-wise pressure gradients. It is equally applicable to both free flows and flows in the vicinity of walls. It is of the implicit, marching integration type and consequently is stable for all step lengths. It is economical in computer time and is flexible enough to accomodate almost any hypothesis for turbulent exchange.

The choice of the solution procedure to be used for the present problem can now be made on the basis of the brief outline of the various methods given above. The methods under the first category, which reduce the parabolic equations to ordinary ones may be discarded for the following reasons. The integral techniques using explicit auxiliary relations have the disadvantage of requiring a vast amount of experimental data: as mentioned in chapter 2.2.2. The parameteric integral method has two major drawbacks : its complexity increases with the number of free parameters used, and secondly, as reported by the authors of reference (48), matrix singularity, encountered ocassionally during the solution procedure, can be troublesome. The procedure valid for equilibrium flows may be ruled out, since in general, the flow near a film cooling slot is not of this type.

The choice is then between the two finite difference schemes: the cross-stream integration and the forward integration procedures. As mentioned earlier, the former needs a trial and error forward integration procedure and considerable computer storage in comparison with the marching integration procedure. Thus the logical choice is a marching integration technique, preferably of the 'implicit' type, since this is relatively free from restrictions on the step length. The procedure of reference (49) provides just such a solution procedure, and will be used as the basis for the present work. A brief outline of this method is given in the next section.

3.4 Brief description of the marching integration procedure of Patankar and Spalding (49).

The conservation equations (3.2.3, 3.2.4 and 3.2.6) are cast into the von Mises form by the introduction of the stream function. These read, in axisymmetric coordinates as:

$$\left.\frac{\partial u}{\partial x}\right|_{\psi} = \left.\frac{\partial(\tau r)}{\partial \psi}\right|_{x} - \frac{1}{\rho u}\frac{dp}{dx} \qquad 3.4.1$$

$$\left.\frac{\partial \varphi}{\partial x}\right|_{\psi} = \left.\frac{\partial(J_j r)}{\partial \psi}\right|_{x} + \frac{R_j}{\rho u} \qquad 3.4.2$$

$$d\psi = \rho u r \; dy \qquad 3.4.3$$

where φ is some scalar conserved property (such as mass fraction of the coolant or the total enthalpy). Equation 3.4.1 signifies the conservation of the x-direction momentum, and equation 3.4.2, the conservation of φ.

The independent variable ψ is transformed to a non-domensional stream function ω defined as

$$\omega = \frac{\psi - \psi_I}{\psi_E - \psi_I} \qquad 3.4.4$$

where I and E refer to the internal and external edges of the boundary layer. Thus the value of ω is 0 at the inner edge and 1 at the outer edge of the layer, a fact which ensures that computation is always limited to the boundary layer region. Thus equations 3.4.1, 3.4.3 and 3.4.4 yield,

$$\left.\frac{\partial \varphi}{\partial x}\right|_{\omega} + (a + b\omega)\left.\frac{\partial \varphi}{\partial \omega}\right|_{x} = \left.\frac{\partial}{\partial \omega}\left(\frac{c\,\partial\varphi}{\partial \omega}\right)\right|_{x} + d \qquad 3.4.5$$

where
$$a = r_I \dot{m}_I'' \; / \; (\psi_E - \psi_I)$$
$$b = (r_E \dot{m}_E'' - r_I \dot{m}_I'') \; / \; (\psi_E - \psi_I)$$
$$c = r^2 \rho u \mu_{eff} \; / \; \{(\psi_E - \psi_I)^2 \cdot \sigma_{eff}\}$$

The next step is to obtain a finite difference form of the above equations. The calculations are based on an orthogonal x- ω grid as indicated in Fig. 3.4.1.

The values of the dependent variables are known at discrete points (eg. at U, U^+, U^-) at the upstream station, while those at the downstream station are unknown. The finite difference equations are obtained by using an integ. -rated average over a control colume around a grid line, indicated by the shaded area in Fig.3.4.1, of the various terms in the partial differential equations 3.4.5. The details of this averaging procedure are as follows. The finite difference expressions for the convection terms (ie. the left hand side of equation 3.4.5) are obtained by integrating the terms in the ω- and x- directions over the control volume, in conjunction with an assumed (linear) profile of the dependent variable between the grid lines in the ω-direction. This process is indicated by the following equations:

$$\frac{\partial \varphi}{\partial x} \approx \left\{\int_{x_U}^{x_D}\int_{\omega_{DD-}}^{\omega_{DD+}} \frac{\partial \varphi}{\partial x}\, d\omega . dx\right\} / \left\{(x_D - x_U)(\omega_{DD+} - \omega_{DD-})\right\} \qquad 3.4.6$$

$$(a + b\omega)\left(\frac{\partial \varphi}{\partial \omega}\right) = \left\{\int_{\omega_{DD-}}^{\omega_{DD+}} (a+b\omega) \left.\frac{\partial \varphi}{\partial x}\right|_{x=x_D} d\omega\right\} / (\omega_{DD+} - \omega_{DD-}) \qquad 3.4.7$$

$$\frac{\partial \varphi}{\partial x} + (a + b\omega) \frac{\partial \varphi}{\partial \omega} \approx g_1 \, {}_{D+} + g_2 \, {}_{D} + g_3 \, {}_{D} \pm g_4 \qquad 3.4.8$$

where the g's are functions of ω, x, a and b, which are known quantities. Further, only the downstream values of φ appear in the equations, which makes the equations of the implicit type.

The flux terms are similarly treated, noting that a step -variation of φ in the downstream direction is assumed: φ is assumed to have a uniform value, equal to φ_D, except at x= x_U, where φ has the upstream value. One obtains for the flux terms:

$$\frac{\partial}{\partial \omega}\left(c \frac{\partial \varphi}{\partial \omega}\right) \approx \frac{2}{\omega_{D+} - \omega_{D-}} \left\{ c_{UU+}\left(\frac{\varphi_{D+} - \varphi_{D-}}{\omega_{D+} - \omega_{D-}}\right) - c_{UU-} \frac{(\varphi_D - \varphi_{D-})}{(\omega_D - \omega_{D-})} \right\} \qquad 3.4.9$$

$$\approx g_5(\varphi_{D+}-\varphi_D) - g_6(\varphi_D - \varphi_{D-}) \qquad , \qquad 3.4.9$$

where the g's are functions of ω and the upstream values of c, which contains the all-important eddy exchange coefficients.

Finally the finite difference version of the source term d, is obtained by a linearising procedure:

$$d_D \approx d_U + \left.\frac{\partial d}{\partial \varphi}\right|_U (\varphi_D - \varphi_U) \qquad . \qquad 3.4.10$$

For the velocity equation, for which $d = -(1/\rho u)dp/dx$, a linear variation of d with ω is assumed and one obtains:

$$d \approx \int_{\omega_{DD-}}^{\omega_{DD+}} (d)_{x=x_D} \, d\omega \; / \; (\omega_{DD+} - \omega_{DD-}) \qquad ,$$

or

$$d_{x=x_D} \approx s_1 u_{D+} + s_2 u_D + s_3 u_{D-} + s_4 \qquad . \qquad 3.4.11$$

where the s's are known functions of the pressure gradient and other variables at the upstream station.

The final difference equation is of the form

$$\varphi_D = A\,\varphi_{D+} + B\,\varphi_{D-} + C \qquad , \qquad 3.4.12$$

where

$$A = \frac{g_5 - g_1}{g_2 + g_5 + g_6 - (\partial d/\partial \varphi)_U} \qquad ,$$

$$B = \frac{g_6 - g_3}{g_2 + g_5 + g_6 - (\partial d/\partial \varphi)_U} \qquad ,$$

$$C = \frac{d_U - (\partial d/\partial \varphi)_U \; {}_U - g_4}{g_2 + g_5 + g_6 - (\partial d/\partial \varphi)_U} \qquad .$$

The coefficients A, B and C are all calculable from known quantities at the upstream station.

The main advantage of the above micro-integral formulation is that the conservation across the whole boundary layer is automatically satisfied. An equation of the form of eq. 3.4.12 is obtained for each of the grid lines and the result is a set of linear, algebraic equations which are soluble with standard techniques such as matrix inversion. However, since the matrix turns out to be one with three non-vanishing diagonals, a simple recurrence formula of the successive-substitution type is used. For this procedure, the computing effort is proportional to the number of equations (or grid intervals), whereas for matrix inversion techniques, it is proportional to the square or cube of the number of equations to be solved.

Special procedures are adopted near the wall to obviate the need of having a large number of grid lines to cover the region of steep gradients of velocity and temperature. The flow is assumed to be one-dimensional in the vicinity of the wall, since the x-convection is locally negligible in this region, since the velocities are low. Couette flow solutions using the van Driest's hypothesis (74) for the mixing length distribution are obtained and expressed as explicit algebraic functions. Thus the non-dimensional wall shear stress and heat flux are expressed as functions of the local Reynolds number R ($\equiv uy/\nu$), a mass transfer and a pressure gradient parameter. The Couette flow solution near the wall is matched with the adjacent grid value such that the slope and value of φ at the matching point are the same for the Couette flow and the adjacent control volume. Two types of boundary conditions are permitted at the wall. The first is the case where the value of the variable along the wall is specified (eg. u= 0, or T_W = constant), and the second is when the total flux through the wall is specified (eg. $\mathring{q}''_W$= constant). The case of an adiabatic wall is a boundary condition of the second type when the heat flux through the wall is zero.

One novel feature of the procedure of reference (49) is that the width of the computational grid grows or diminishes in correspondence with the boundary-layer thickness. This is accomplished by incorporating an entrainment law which is based on the equations of motion and the viscosity hypothesis. This ensures that the ω= 1 or ω = 0 line (depending on which is adjacent to a free stream) is located along the edge of the boundary layer. For a fluid assumed to obey the mixing length hypothesis, the outer edge is defined as the point where the eddy viscosity goes to zero. For such flows flows it can be shown that the entrainment is proportional to the second derivative of the velocity at the outer edge (which is generally non-zero). The assumption of a parabolic velocity profile permits the evaluation of this derivative.

It should be pointed out that any entrainment formula would serve, so long as it ensured that sufficient number of grid lines were present within the region of significant velocity and temperature gradients.

CHAPTER 4

4. The experimental investigation.

The purpose of the present experimental program was to investigate the influence of the velocity ratio ($\bar{u}_C / u_G$), distance from the slot exit (x/y_C), density ratio (ρ_C / ρ_G), and the longitudinal pressure gradient(dp/dx) on the effectiveness, heat transfer, velocity and mass fraction profiles and wall-shear stress downstream of two-dimensional slots with tangential injection.

The measurements were carried out in two low-speed wind tunnels; the test section of one was rectangular in cross section (apparatus A) and that of the other was circular (apparatus B). Apparatus A had a plane, two-dimensional slot and an impervious wall, with the provision or the injection of air or foreign gases through the slot, in order to attain significant density gradients, and an adjustable false roof to apply longitudinal pressure gradients. Apparatus B had an axisymmetric slot with a heated wall, to permit the study of heat transfer.

The next two section (4.1 and 4.2) describe the investigation with apparatus A, and the subsequent two (4.3 and 4.4) describe the investigation with apparatus B. The description of apparatus, method of operation, presentation and discussion of results are dealt with in turn for each apparatus. For apparatus A, the experiments with nominally zero pressure gradient are discussed first, followed by those in non-zero pressure gradients.

4.1.1 Description of apparatus A.

The low speed, once through wind tunnel with provision for tangential injection through a plane, two-dimensional slot is shown schematically in Fig.4.1.1. The wind tunnel comprised a primary and secondary circuit: the primary circuit included an entry section, the test section, the plenum chamber, the centrifugal fan and an exit diffusor; the secondary circuit included a source of injected fluid an orifice plate for metering the flow, a plenum chamber and a slot, venting into the test section. These items, together with the auxiliary equipment used for the experiments, are described below.

The wind tunnel designed by Nicoll (42) was intended for use in the present investigation. Several modifications to the tunnel were found necessary and it turned out that only the test section, the injection slot and the secondary blower from the original tunnel were retained for the present investigation.

The main difficulty encountered with the tunnel of ref. (42) was the presence of large, low frequency fluctuations in the total and static pressures (around 20 percent of the local dynamic head) The cause of the unsteadiness was traced to the entrance section which in the original tunnel comprised a bell-mouth with a radius of approximately 40 mm. An improved entry section (fig,4.1.2 (a)) described below was installed and removed the unsteadiness in the flow, almost entirely. Other alterations to the tunnel included a new secondary circuit with an orifice meter and arrangement for the injection of Arcton-12 and hydrogen through the slot.

The primary circuit.

The entry section. (Fig. 4.1.2 (a)) The entry section was formed by a plenum chamber leading to a contraction section with an area ratio of 19.2. The plenum chamber was fitted with a row of 13 mm x 13 mm x 51 mm honeycomb flow straightener, followed by two 28 x 20 s.w.g. mesh, wire screens, 355 mm apart. The exit of the contraction section was lined with a 25 mm- wide strip of coarse emery cloth to act as a boundary-layer trip.

The test section. (Fig. 4.1.2 (b)) The test section was rectangular in cross-section (152 mm x 127 mm) and 1.8 m long, with a 6.3 mm- thick Dural base plate, and perspex windows in the side walls. 0.51 mm-diameter static pressure holes were located on the centre line of the base plate as well as on one of the side walls. The top of the test section had a slot for the insertion of probes mounted on a traversing gear.

Provision was made for mounting of a 152 mm-wide Dural plate inside the test section to form a false roof, which permitted favourable or adverse pressure gradients to be applied. Five holes were located along the centre line of this plate for the insertion of probes for measurement of velocity and concentration profiles. Fairing between the edges of the plate and the tunnel roof was provided by flexible sheet-metal sections.

The plenum chamber and fan. The plenum chmaber downstream of the test section was 620 mm x 620 mm and contained two wire screens 355 mm apart and a honeycomb section flush with the inlet flange of the fan. The function of the plenum chamber was to remove any upstream influence of the fan.

A radial flow fan, throttled on its pressure side and driven by a 6 kW, 3 phase induction motor provided the primary stream, continuously variable from 0 to 45 m/s. The free-stream turbulence intensity was approximately 0.35 percent at 20 m/s tunnel velccity.

The secondary circuit.

Injected gases. Air, hydrogen, argon and Arcton-12 (di-chloro-di-fluoro methane) were injectdd in turn through the slot, resulting in a slot to mainstream density ratio of 1.0, 0.069, 1.38 and 4.17 respectively. The secondary air stream was provided by a small radial blower, fitted with a sliding throttle on its suction flange. Hydrogen and argon were available in high pressure (14×10^6 N/m²) bottles, while Arcton-12 was available in bottles at relatively low pressures (0.49×10^{-6}N/m² approx). Consequently, regulating valves were used with the first two, while care was taken to minimise the pressure losses in the secondary line for Arcton-12 injection, inorder to achieve sufficiently high velocity at the slot exit. Three or four bottles were used in parallel, each being connected to a manifold upstream of a pressure regulating valve.

Metering section. The manifold (or the exit flange of the blower, in case of air injection) was connected to a length of 76 mm inside diameter pipe, fitted with a "D and D/2" orifice meter designed in accordance with B.S. 1042 (1966). This pipe was coupled to a plenum chamber, 71 mm x 150 mm x 730 mm, leading to the slot assembly.

The slot. Details of the slot assembly are shown in Fig. 4.1.3. It comprised a contraction section with an area ratio of 35, from the plenum chamber to the slot exit. The lip of the slot was tapered, with a trailing edge thickness of approximately 0.25 mm. The slot height was set to 2.5 mm with a spanwise variation of $\pm$ 50 μ. This setting of the slot height was used for all the experiments.

4.1.2 Auxiliary apparatus.

Gas sampling devices. Gas samples were drawn through static-pressure holes in the base plate of the tunnel by means of a vacuum pump and stored in sample bottles shown in Fig.4.1.4. Each sample bottle had a gas-tight cock at inlet and exit, and a serum cap for the extraction of samples with a hypodermic syringe.

Gas samples from locations within the flow field were sucked through a hand-pump arrangement and collected over mercury in a bank of cylindrical sample bottles, shown in Fig. A.1.1. A detailed description of the sampling system is given in appendix A.1.1.

Gas-chromatographic equipment.

A Shandon KG-2 gas chromatograph with a 2 m- long molecular sieve column and a 'GOWMAC' double filament thermal conductivity cell was used for the analysis of the gas samples. The thermal conductivity cell and the column were mounted within a temperature controlled oven and nitrogen was used as the carrier gas. The gas samples were injected into the chromatograph by means of a 1 ml Hamilton gas syringe and the output of the thermal conductivity cell was recorded on a Honeywell chart recorder, with a 1 mv full scale deflection. The peak-heights recorded on the chart recorder were used as a measure of the concentration of the respective constituent; the chromatograph was periodically calibrated against samples of known concentration of the relevant gas mixtures. Fig.4.1.5 shows typical calibrations of the chromatograph for hydrogen-air, helium-air, argon-air and Arcton-12- air mixtures; Fig.4.1.6 shows typical chromatograms corresponding to these mixtures. Helium-air mixtures for the calibration were prepared in a gas jar of approximately 1000 ml, whereas the other mixtures were prepared in the botlles shown in Fig.A.1-1.

Pressure measuring devices.

A Hilger-Watt electonic micro-manometer with a variable-capacitance pressure transducer (range 0 to $\pm$ 50mm of water), connected to a Honeywell chart recorder was used to record total pressure from an impact tube. A bank of inclined-tube manometers containing paraffin (specific gravity 0.787) was used to measure the streamwise static pressure distribution and a Betz manometer was used for the measurement of the pressure difference across the orifice meter in the secondary circuit. Differential pressures between a number of pairs of static pressure holes were measured by successively coupling them to a micro-manometer. This operation was facilitated by a pressure switch, designed by the author which employed a mercury seal. Details of this pressure switch are given in appendix A.1.2.

Traverse gear and impact probe.

The traverse gear for impact probes etc. is shown in Fig. 4.1.7. It comprised a micrometer mounted on a block which could be locked at any position along two vertical parallel rods. The micrometer which was graduated in 0.001 inch divisions, propelled a sliding member which carried the impact probe at the end of a 6.35 mm-diameter tube.

The impact tubes were constructed from flattened stainless steel hypodermic tubing, 2 mm outside diameter. The finished dimensions were approximately 0.35 mm x 1.5 mm on the outside and 0.1 mm x 1.0 mm inside. The impact probes were also used for the extraction of gas samples from within the flow field. In some experiments a rake of twelve impact probes was used, but its use for sequential measurement of total pressure and gas sampling was found to be cumbersome, and the use of a single probe was preferred.

4.1.3 Operation of apparatus A.

Apparatus A was used for the measurement of impervious-wall effectiveness, velocity and mass-fraction profiles and wall-shear stress. The procedure for performing these measurements will now be briefly described.

The tunnel was set to operate at the desired velocity ratio by operating the throttles in the primary and secondary circuits: the free-stream velocity was inferred from the static and total free-stream pressures in the plane of the slot exit, while the slot velocity was obtained from the orifice-meter in the secondary line. For the case of air injection, a small amount of helium (of the order of 1 percent by volume) was introduced into the secondary stream through a rake just downstream of the secondary blower, to function as a tracer during effectiveness and concentration profile measurements. Gas samples were sucked through the static-pressure holes in the tunnel floor and plenum chamber upstream of the slot, and stored in the bank of sample bottles, Fig.4.1.4. The sampling rate was kept sufficiently low to ensure that the measured concentration was not influenced by the sampling rate. The gas samples were later analysed in the gas chromatograph described in section 4.1.2 above.

Velocity and mass fraction profiles were obtained by traversing an impact probe across the boundary layer: , total pressures were recorded through a pressure transducer or liquid-manometer, while gas samples were drawn through impact probes and collected in the sample bottles described in appendix A.1.1 and later analysed with the gas chromatograph. The static pressure at the measuring stations was obtained from the longitudinal pressure distribution existing in the test section in the absence of the traversing gear. Velocity profiles were computed from a knowledge of the total and static pressure and the local density.

Values of wall-shear stress were inferred from two independent procedures: first from the 'Clauser plot' and second from the razor-blade technique: wall shear stress measurements were carried out only for the case of air injection. The Clauser plot method is well known and will not be described here: this method implies a logarithmic velocity distribution in the wall layer, characterised by two 'universal' constants K and E.

The use of razor-blades for the measurement of the wall-shear stress has been described in reference (46). It was demonstrated that a razor-blade segment, fixed over a static-pressure hole with adhesive tape or cement, was a viable instrument for the measurement of wall-shear stress. Razor-blade segments located in this manner were calibrated in a fully-developed channel flow, set up for the purpose, and then relocated over static pressure holes in the tunnel floor, downstream of the injection slot. The reproducibility of the shear stress measurements was $\pm$ 4 percent in case of the 229 μ- thich blade segments secured with adhesive tape. The reproducibility of the 102 μ- thick blade segments secured with cement was subequently found to be worse than that claimed in reference (46) and an 'in situ' calibration in a fully developed channel flow was preferred. The use of the razor-blade technique is preferred in wall-jet and wall-wake flows, since they are generally submerged in the sub-layer and are relatively uninfluenced by the outer region of the flow, or by pressure gradients.

4.2 Presentation and discussion of experimental results- apparatus A.

The measurements of impervious-wall effectiveness, hydrodynamic and species properties made with apparatus A are described in this section. Experiments in nominally zero pressure gradient are presented first, followed by those in significant longitudinal pressure gradients. Some of the present data for the nominally zero pressure gradient have previously been reported in references (44), (46) and (29), while some of the data for non-zero pressure gradients have been reported in reference (47). The present data are given in tabular form in appendix 3.

4.2.1 Experiments in nominally zero pressure gradient.

The test section, in the absence of the false roof, was of uniform cross section and provided a small favourable pressure gradient in the flow direction (0.5 mm of water in a distance of 300 mm at a free-stream velocity of 20 m/s). This pressure gradient is negligibly small for present purposes.

Impervious-wall effectiveness.

Measurements of the impervious-wall effectiveness are given in tabular form in appendix A.3.1. Fig. 6.1.2 (a)* to (h) show some of the measured values of impervious-wall effectiveness for air injection plotted against the non-dimensional distance from the slot, x/y_c for eight velocity ratios. The data are represented by the points while the lines are predictions which will be discussed in chapter 6: this convention is adopted throughout this study, wherever experiment and predictions are shown in the same figure. Fig. 6.1.3 (a) to (h) show similar plots

---

* Footnote: This reference to a figure in chapter 6 is due to the intention to present predictions of available data in a sequence in that chapter. This remark also applies to references to figures in chapter 5, later in this chapter.

for the case of argon and Arcton-12 injection through the slot; these resulted in slot to mainstream density ratios of 1.38 and 4.17 respectively. Fig. 6.1.4 (a) to (d) show similar data for hydrogen injection, ie. a density ratio of 0.069.

The influence of velocity ratio on the effectiveness is clearly indicated in Fig. 4.2.1 (a) to (d). In each of these figures, the effectiveness is plotted against the velocity ratio for four values of x/y_C and for a constant density ratio. The points represent experimental data and the lines are smooth curves through them. It can be seen that for all the cases, the effectiveness increases with the velocity ratio up to approximately unity. For the case of air injection, a small decrease in effectiveness for velocity ratios greater than unity is noticeable whereas for argon injection effectiveness is practically constant in this range. For hydrogen and Arcton-12 injection, the effectiveness increases for velocity ratios above unity, though for the latter case the increase is quite small. The figure implies that for density ratios less than unity it is highly advantageous to employ a velocity ratio greater than unity; for density ratios around unity it can be disadvantageous; and for large density ratios it is not significantly advantageous.

Fig. 4.2.2 clearly shows the influence of density ratio on effectiveness: in this figure, effectiveness is plotted against the density ratio for constant values of x/y_C and $\bar{u}_C/u_G$. As expected, for a particular velocity ratio and distance from the slot, the effectiveness increases with the density of the injected gas.

It is interesting to compare the present measurements with those obtained by other investigators. Exact agreement is hardly to be expected since, apart from experimental uncertainties, differences in geometry and initial conditions at the slot exit may cause differences in the measured values of the impervious-wall effectiveness. Fig. 4.2.3 (a) compares the present measurements for air injection with those of reference (30) for a lip-thickness ratio (t/y_C) of 0.126. The present slot configuration had a tapered lip, whose effective lip thickness was unknown. The good agreement between the two sets of data (maximum discrepancy around

7 percent of effectiveness at a distance of 52 slot-heights) suggests that the present tapered lip effectively functioned as a thin lip. However, the presence of other differences between the two apparatus, such as the thickness of the boundary layer on the outer surface of the lip; the shape of the velocity profile within the slot, render a further resolution of the differences between the two sets of data, impractical. Fig. 4.2.3 (b) shows a similar comparison with the data of reference (5) for the injection of Arcton-12 ($\rho_C/\rho_G = 4.17$). The agreement is again good (maximum differences are around 6 percent of effectiveness at 112 slot-heights). The geometry of reference (5) was similar to the present one and so good agreement between the two sets of data was not unexpected.

Hydrodynamic and species properties.

Profiles of mean velocity and concentration were measured at several downstream locations for representative values of density and velocity ratios. These are tabulated in appendices A.3.2 and A.3.3 respectively. Values of the skin friction coefficient obtained from the razor-blade technique are also tabulated (A.3.4).

Profiles of a representative selection of velocity ratios are plotted in Figs. 5.2.3 (a) to (d), (j) and (k). The velocity ratios selected for constant-density flows, include two values less than, one slightly above and one significantly above unity. The experimental data are shown as points and the lines are predictions, and will be discussed later (chapter 5). In these figures, the velocities have been normalised with the free-stream values and the concentration values with the corresponding value at the wall.

Velocity profiles corresponding to velocity ratios less than unity exhibit a wake-like profile at x/y_C of 20 (Fig.5.2.3 (b)): the velocity defect is larger than for a conventional flat-plate boundary layer and the wake due to the lip- boundary layers is noticeable. Further downstream ($x/y_C \geqslant 50$), the profiles closely resemble conventional flat-plate boundary layers in zero-pressure gradient. The integral property R_2 and the shape factor H, corresponding to a velocity ratio of 0.55, are shown in Fig. 5.2.5 (d).

As expected, R_2 increases in the downstream direction and the shape factor H tends towards the value for a flat-plate boundary layer in zero pressure gradient (ie. approximately equal to 1.28). This figure also shows the skin friction coefficient, which is approximately constant for x/y_c greater than 50.

Velocity profiles corresponding to velocity ratios greater than unity (Fig.5.2.3 (c) and (d)) exhibit a velocity maximum akin to a wall-jet. The wake due to the slot-lip is noticeable at x/y_C of approximately 20. For the velocity ratio of 1.85 (Fig.5.2.3 (d)), the velocity maximum is noticeable at x/y_C of 100, but for the velocity ratio of 1.23 (Fig.5.2.3 (c)), the maximum has almost vanished at x/y_C of 75. The decay of the velocity maximum, as well as the growth rate of the layer, as characterised by the increase in y_{HALF} for the former case is shown in Fig.5.2.5 (a). This figure also indicates the downstream distribution of the skin friction coefficient: as expected, it decreases with x and the values are much greater than those for velocity ratios less than unity.

4.2.2 Experiments in presence of significant pressure gradients.

The influence of favourable and adverse pressure gradients on the flow development and the impervious-wall effectiveness was investigated for three cases of favourable and one adverse pressure gradient. The pressure gradient was applied by means of the straight adjustable roof, resulting in a wedge-shaped flow passage. It is easy to show that for such a flow passage, the parameter $K_p\left(\equiv \frac{\nu}{u_G^2}\frac{du_G}{dx}\right)$ is constant for a particular wedge angle and velocity at the entry to the wedge, provided the boundary layers are thin (or similar in shape). The nominal values of K_p for the four non-zero pressure gradients, and the corresponding inclinations of the false roof are indicated an Fig.4.2.4.

Pressure gradient designated PG1 may be regarded as a mild acceleration, PG2 a moderate and PG3, a strong favourable pressure gradient, since it is known that for values of K_p greater than approximately 2×10^{-6}, a conventional turbulent boundary layer gradually reverts to a laminar state (33), (1).

The values of the free stream velocities at slot exit were different for the favourable and adverse pressure gradient situations: they were 10 m/s and 21 m/s respectively. This change in the initial velocity was necessary to permit large values of K_p to be attained for the favourable pressure gradients and to prevent side-wall separation for the adverse pressure gradient. However, the different initial free-stream velocities resulted in different values of the slot Reynolds number R_C, for the same velocity ratio. Consequently, zero-pressure gradient data needed for comparison was obtained for each of the values of the initial free stream velocity.

The longitudinal static pressure distributions for the various settings of the roof and for a velocity ratio less than unity is shown in Fig. 4.2.5. The pressure distributions did not vary appreciably with the velocity ratio, except in the immediate vicinity of the slot. Fig. 4.2.5 also shows the symbols used to represent the data for the various pressure gradients in subsequent figures.

Impervious-wall effectiveness.

The influence of pressure gradients on the impervious-wall effectiveness for constant density flows is described first, followed by the case of non-uniform density.

Fig. 4.2.6 shows the influence of the above - mentioned pressure gradients on the impervious-wall effectiveness; Fig.4.2.6 (a) refers to the favourable pressure gradients and Fig. 4.2.6 (b) to the adverse pressere gradient. It is evident that the influence of pressure gradients, both favourable and adverse is to reduce the effectiveness below the zero-pressure gradient values. Further, this influence decreases with increasing the velocity ratio. For the favourable pressure gradients, the influence of the pressure gradients increases with the severity of the pressure gradient. In general, the influence of both the favourable and adverse pressure gradient on effectiveness is small (less than 5 per cent of unity), except for the case of the strongest favourable pressure gradient, PG3, for which the maximum reduction in effectiveness was of the order of 20 percent of unity. Am examination of the hydrodynamics of the flow in the strongest favourable pressure gradient (presented later in this section), reveals that the flow was no longer fully turbulent in this case.

Fig. 4.2.7 shows the influence of the favourable pressure gradient PG2 and adverse pressure gradient PG4 on the impervious-wall effectiveness for the case of Arcton-12 and hydrogen injection. The influence of the favourable pressure gradient is similar to the uniform density case: a small reduction in effectiveness with the influence decreasing with increasing velocity ratio. The adverse pressure gradient appears to have no significant influence for the cases of Arcton-12 and hydrogen injection shown.

Influence of the slot Reynolds number, R_C.

As mentioned above, the use of two values of the initial free strean velocities resulted in a change of the slot Reynolds number, for a given velocity ratio. The observed influence of the slot Reynolds number for the case of uniform density and pressure flow is shown in Fig.4.2.8 for two velocity ratios. It is evident that for a prescribed velocity ratio, and distance from the slot, the effectiveness increases with an increase in R_C: far downstream the increase is approximately proportional to $R_C^{0.2}$. This is in accord with the boundary layer model of reference (72). At distances closer to the slot, the influence of R_C appears to be greater than that suggested by this relation. The reasons for this may be associated with changes in the initial conditions at slot exit, such as the boundary layer thickness, $y_{G,C}$ and the shape of the velocity profile in the slot exit, brought about by a change in the Reynolds number.
It should be noted that a change in R_C brought about by a change in $\bar{u}_C$ is not necessarily equivalent to that due to a change in y_C, ρ_C or μ_C.

Hydrodynamics and species properties.

Measurements of the mean velocity and concentration profiles and wall-shear stress were obtained for the case of uniform density injection only. These are tabulated in appendices A.3.2, A.3.3 and A.3.4 respectively. The velocity profiles corresponding to velocity ratio less than unity and for the favourable (PG2) and the adverse (PG4) pressure gradient are shown in Fig. 5.2.9 (a) and (b), while the corresponding profiles for a velocity ratio greater than unity are shown in Fig.5.2.9 (c) and (d).

The following observations are relevant in connection with these profiles. First for velocity ratios less than unity, the thickness of the velocity profiles decreases in the downstream direction in case of the favourable pressure gradient and increases for the adverse pressure gradient. Again, for these velocity ratios, the velocity defect is much smaller for the case of the favourable pressure gradient than for the adverse pressure gradient case. The velocity profiles corresponding to velocity ratios greater than unity are not qualitatively different from the corresponding zero pressure gradient profiles. The decay of the velocity maxima, growth of y_{HALF} and the wall-shear stress are indicated in Fig. 5.2.11.

The shape and thickness of the concentration profiles (Fig.5.2.9) on the other hand are relatively uninfluenced by the pressure gradients, for all velocity ratios. Further, the thickness of the concentrations profiles tends to be larger than that of the velocity profiles in the case of the favourable pressure gradients. This is to be expected, since the species conservation equation (eq. 3.4.2) does not contain a pressure gradient term.

It is of interest to note the influence of pressure gradients on the momentum- thickness Reynolds number R_2. These are plotted in Figs. 4.2.9 and 5.2.10. It can be seen (Fig.4.2.9) that for velocity ratios less than unity, the influence of the favourable pressure gradients is to decrease R_2 below the corresponding zero-pressure gradient value. It can be shown that for constant-K_p flows, there exists an equilibrium value of R_2 and shape factor H for each value of K_p (33). Figs. 11 and 12 of this reference permit the equilibrium values computed for laminar and turbulent flow (on the basis of a mixing length assumption) to be obtained. Though equilibrium conditions were not reached within the test section, the values of R_2 and H measured at the last measuring station for PG2 and PG3 corresponding to a velocity ratio of 0.54 are shown in Table 4.2.1 below, along with the equilibrium values obtained from (33).

Table. 4.2.1 Measured and equilibrium values of R_2 and H

Quantity.	$K_p\ 10^6$	Pressure Gradient	Equilibrium value lam.	Equilibrium value turb.	measured value at last stn.
R_2	1.82	PG2	270	760	500
	3.30	PG3	190	450	260
H	1.82	PG2	2.0	1.28	1.49
	3.30	PG3	2.0	1.30	2.50

From this table it is evident that for the case of pressure gradients PG2 and PG3 the flow is tending towards a laminar state (please see Fig.5.2.10). Though the criteria for reverse transition have not yet been fully established, (33), (51), (1), values of K_p corresponding to PG2 and PG3 appear to be large enough for the onset of reverse transition. The value of the measured shape factor for PG3 in the above table is seen to be higher than the laminar value of reference (33): in fact the value of H for a Blasius-type profile is 2.6 (58). Besides, the boundary layer thickness was small, causing some experimental uncertainty in the value of H. A criterion proposed by Patel (51) for the onset of reverse transition is that the value of $\Delta_p \equiv -K_p(c_f/2)^{-3/2}$ should exceed about-0.0245. For this value of Δ_p, departures from the logarithmic law of the wall occur and the velocity profiles indicate an "overshoot" above the log-law line.

The present velocity profiles in the vicinity of the slot ($x/y_c \lesssim 30$) indicated an overshoot above the log-law line for all the cases with the initial free stream velocity of 10 m/s. The reason for this is probably the low Reynolds number as well as the effects of the slot-geometry, resulting in a low wall-shear stress in the region. For the case of the strongest pressure gradient PG3 and for velocity ratios less than and greater than unity, the downstream profiles indicated a prominent overshoot above the log-law line, at locations where Δ_p exceeded -0.0245. Thus the present data for wall-jet and wall-wake flows are in accord with Patel's criterion for the onset of retransition.

4.2.3 Precision and accuracy of the experimental data.

The uncertainties in any experimental data in fluid flow are of two kinds: those due to departures of the flow from that which the experimenter believes it to be and those due to the imprecision and inaccuracy of the measuring techniques. In the present context, departure from two-dimen - sional turbulent flow is implied in the first category while errors in the measurement of pressure, concentration etc., are implied in the second. These will now be examined in turn.

Two dimensionality of the flow implies that there are no spanwise variations in the hydrodynamic or species quantities, such as mean velocity, shear-stress, intensity or scale of turbulence, or concentration. Clearly in a plane "two-dimensional" tunnel, this is possible only in the vicinity of the central span of the slot. Some of the obvious factors influencing the two-dimensionality of the flow include the spanwise uniformity of the slot-height, uniform tripping of the boundary layers on the slot lip and the squareness of the test section. In the present apparatus, the slot height was uniform to within 2 percent, the boundary layers were tripped at the entry to the test section and the squareness of the tunnel cross section was better than one percent.

Further, velocity profiles were measured at three spanwise locations, 10 slot- heights on either side of the centre line and on the centre line, for a velocity ratio equal to 1.85, and for four values of x/y_C (x/y_C= 0, 43, 93 and 200). The salient information from these tests was as as follows:

> The maximum spanwise variation in the value of the velocity maxima, wall-shear stress (as obtained from 'Clauser plot'), and momentum thickness Reynolds number R_2 were $\pm$ 1.5, $\pm$ 3.0 and $\pm$ 20 percent respectively.

The mean velocity profiles at a constant x/y_C exhibited good agreement in the log-law region: whence the good agreement in the wall-shear stress; but they showed a relatively large variation in the outer region of the layers. This is reflected in the large spanwise variation of the integral property, R_2. Agreement with the two-dimensional integral momentum equation was erratic: values of the wall-shear stress deduced from the momentum balance between adjacent profiles were in agreement with those deduced from 'Clauser plot' in some instances, but differed by as much as 100 percent for the case for velocity ratios less than unity and x/y_c less than about 50. The discrepancies were attributed to the non-two dimensionality of the flow, and the uncertainty in obtaining x-derivatives of the measured integral quantities, which change but slowly in the x-direction.

Measurementerrors in the experimental data relate to the primary and secondary mass flow rates, the impervious- wall effectiveness, velocity and concentration profiles. These will now be briefly discussed.

Errors in the flow measurement were estimated to be around 2 percent; the values of the mean slot velocity $\bar{u}_c$ obtained by the integration of the slot-velocity profile agreed with that obtained from the orifice meter within about 2 percent, for air injection.

Errors in the measurement of effectiveness arose from the sampling technique and chromatographic analysis. Tests at a number of sampling rates indicated that the measured values of the wall concentration were insensitive to the sampling rate. The precision of the values of the impervious-wall effectiveness was around 3 percent of unity for the case of air (plus helium tracer) injection. This is in agreement with the observation of Whitelaw(78). Marginally worse precision was obtained for the injection of Arcton-12, argon and hydrogen, since in these cases, there was no oxygen peak to provide an additional check on the quantity of sample injected each time.

Errors in the measurement of velocity profiles were due to errors in the probe location, pressure and density measurement and the interaction between the flow and the probe. The accuracy of the probe location was of the order of $\pm$ 25μ in the y- direction. Total pressures were measured with a pressure transducer whose linearity was found to be better than 2 percent; the transducer was periodically calibrated with a Betz manometer, graduated in 0.1 mm of water-column. In case of foreign gas injection, the errors in density measurement corresponded to the error in concentration measurement, discussed below. It is known impact tubes are influenced by the proximity to the wall, velocity gradients, turbulence intensity and the Reynolds number. The influence of the last three factors was expected to be negligibly small for the present experiments. The y-values of the probe were increased by 15 percent of the outside dimension of the impact probe, in order to allow for the influence of the first two of the above factors, as suggested by McMillan (37).

Errors in the measurement of the concentration profiles were due to errors in the probe location (as for the velocity profiles) and errors in the concentration measurement. The latter were similar in magnitude to the errors in the effectiveness measurements discussed above.

4.2.4 Summary of results with apparatus A.

To conclude the present section, the main results with apparatus A are enumerated below.

1. Measurements which demonstrate the influence of velocity ratio, distance from the slot exit, density ratio and pressure gradients on the impervious-wall effectiveness, velocity and concentration profiles and wall-shear stress are presented. (Tabulated in appendix A.3)

2. The qualitative influence of the velocity and density ratio on the impervious-wall effectiveness is as follows:

$\bar{u}_C/u_G$	ρ_C/ρ_G	Effectiveness at constant x/y_C
$\lesssim 1.0$	0.069 to 4.17	increases with u_C/u_G.
$\gtrsim 1.0$	≈ 1.0	decreases with increasing u_C/u_G.
	$<< 1.0$ $>> 1.0$	increases with u_C/u_G.

3. The present data of the impervious-wall effectiveness for air injection are in good agreement (within 7 percent of unity) with those of reference (30) for t/y_C of 0.126 and suggest that the present tapered lip functions as a thin lip. The present data for Arcton-12 injection ($\rho_C/\rho_G = 4.17$) are in good

agreement (within 6 percent of unity) with those of reference (5).

4. The influence of favourable and adverse longitudinal pressure gradients in the range $-1.0 < K_p \times 10^6 < 1.8$ for constant-density flows was to cause a small reduction in the impervious-wall effectiveness (less than 5 percent of unity). The influence of pressure gradient decreases with increasing velocity ratio.

5. The influence of a strong favourable pressure gradient ($K_p \times 10^6 \approx 3.8$) was to decrease the impervious-wall effectiveness by a maximum of about 20 percent of unity, for velocity ratios less than 1.2.

6. The influence of pressure gradients ($K_p \times 10^6 \approx -1.0$ and 1.8) on the impervious-wall effectiveness in the presence of density gradients (ρ_C/ρ_G = 0.069 and 4.17) was similar to that for the uniform-density case.

7. Velocity profiles, for which the pressure gradient parameter Δ_p was greater than -0.0245, showed an over-shoot above the log-law line, indicating the presence of re-laminarisation. This phenomenon was also indicated for the case of $u_C/u_G < 1.0$, by values of R_2 below and H above, the equilibrium values for turbulent flows with constant K_p.

8. The influence of an increase in R_C in constant density flows, due to a change in $\bar{u}_C$ only, was to increase the impervious-wall effectiveness. This increase was approximately proportional to $R_C^{0.2}$ far downstream, but was greater closer to the slot.

4.3.1 Description of apparatus B.

The once-through, low speed wind tunnel with an axi-symmetric slot configuration is shown schematically in Fig.4.3.1 and a photograph of the same appears in Fig. 4.3.2 (a) and (b). This apparatus was designed to obtain measurements of the adiabatic-wall effectiveness and the heat-transfer coefficient in the presence of tangential injection.

The wind tunnel comprised a drum assembly (see Fig.4.3.1) concentric with a test section of inside diameter approximately equal to 73 mm. The test section was coupled to a source of vacuum through a run of 51 mm 'Durapipe' with an orifice meter (designed in accordance with B.S. 1042, 1966) installed within it.

The plenum chamber was connected to a source of compressed air through a run of 38 mm-Durapipe and an electric air heater. An orifice meter was included in the Durapipe section to meter the secondary air.

The drum assembly, the test section and the auxiliary equipment will now be described in turn. A discussion on the design and development of the apparatus follows thereafter (section 4.3.2).

The drum assembly. (Fig.4.3.3 (a)) comprised a drum, 355 mm in diameter, one side of which carried a bell-mouth made from fibre-glass. The bell-mouth terminated in a cylindrical pyrex tube of 1.6 mm-wall-thickness and 63 mm-outside diameter, to form the 'slot lip'. A ring of 6 mm-thick plywood, was fixed in the plenum chamber to diffuse the air entering it. A wooden fairing ring provided a smooth contraction from the plenum chamber to the slot exit.

The test section, Fig. 4.3.3 (b) was formed from a 126μ-thick stainless steel sheet rolled into a cylinder, 73 mm in diameter and 510 mm long, with its longitud nal extremeties bent outwards. The s.s. sheet was bonded with Araldite to the inner surface of a split- 'Tufnol' pipe of 73 mm-inside diameter and 510 mm long. Two copper bars, 510 mm x 28 mm x 6.3 mm were clamped along the extremeties of the s.s. sheet and were separated from one another by a 1.6 mm-thick bakelite sheet. Thermocouples made from 35 s.w.g copper and 34 s.w.g. constantan enamelled wires were spot-welded on the outer surface of the sheet at locations indicated in Fig.4.3.3 (c). The thermocouple wires were laid on the sheet at right angles to the axis of the test section before bonding to the Tufnol halves. Three thermocouples were located at the slot exit, 120 degrees apart. The thermocouple wires led to a set of selector switches and a reference junction at room temperature.

Auxiliary equipment.

A highamperage (0 to 1000 amperes), variac was used to supply the current for heating the s.s. sheet in the test section. A calibrated, temperature compensated resistance (equal to 333 $\mu\Omega$) was connected in series with the s.s.heater; the voltage drop across it was a measure of the current through the heater. A "Solartron" precision a.c. valve mili-voltmeter was used for measuring a.c. potentials and a "Fenlow" digital voltmeter with a resolu -tion of 10 μv was used for recording the thermo-e.m.f.-s.

Manometers filled with water or mercury were used for the measurement of differential and absolute pressures at the two orifice meters.

4.3.2 Design and development of apparatus B.

The measurement of heat transfer coefficients in the presence of film cooling was not envisaged in the early stages of the present investigation. The realisation of the lack of sufficient experimental data of this important quantity coincided with the availability of a test section with a large number of heat-flux meters, previously used by Mukerjee (39) for the investigation of heat transfer in a supersonic-parallel diffuser. It was decided to design a suitable annular slot to match this test section, to study the adiabatic-wall effectiveness and heat transfer in the presence of film cooling, under subsonic conditions; the College supply of compressed air and vacuum provided a ready source for the two air streams.

With this intention the drum assembly and the rest of the apparatus described in the last section was constructed. Fibre-glass and pyrex were selected for the bell-mouth and slot-lip to reduce the heat transfer bewteen the mainstream and secondary stream , upstream of the slot. The thickness of the slot lip was dictated by the minimum wall-thickness of the pyrex tube which could be readily fabricated. The slot-height was chosen to obtain areasonable percentage uniformity ($\pm$ 5 percent) of the annular gap with the available test section.

Details of the test section used by Mukerjee (39) are shown in Fig. 4.3.4. It comprised a 73 mm-inside diameter Tufnol pipe, with 47 heat-flux meters located along a line parallel to its axis. Each of the heat flux meters comprised a 0.8 mm-thick polypropelene sheet, sand - wiched between the two copper studs, one of which was flush with the inner surface of the Tufnol pipe and the other immersed in a water-jacket. A copper-constantan thermocouple was located in each of the copper studs.

In principle, the steady state heat flux through the meters could be inferred from the temperature difference across the plastic material, its thermal conductivity and its thickness.

Experiments conducted with the above test section yielded values of the heat-transfer coefficient which were about seven times larger than that expected on the basis of previous experiments (62), (22). The reasons for this large discrepancy was attributed to the following:

i. Thermal starting length effect;

ii. Uneven contact between the plastic sheet and copper studs (ie. air gaps);

iii. Errors in temperature measurement.

The first of the above reasons appeared to be most important, since the leading edge of each of the copper studs presented a step in the wall heat flux; the Tufnol was a near-adiabatic surface, followed by a region of finite heat flux through the copper studs. Thus a new thermal boundary layer was initiated at the leading edge of each of the heat flux meters. It is well known that for such a boundary condition, the heat transfer coefficient is locally much higher than that for the case of a thermal layer starting coincidentally with the velocity- boundary layer (53), (12). It can be expected that the arrangement used would lead to high local heat fluxes, and consequently to a high heat transfer coefficient. It is not possible to allow for this effect on a theoretical basis, mainly because the thermal boundary layer was three-dimensional. Attempts were made to calibrate the heat flux meters 'in situ', by making the test section a part of a fully developed pipe flow. Details of the calibration procedure and the results obtained are given in appendix A.2.

The main conclusion from these tests was that an 'in situ' calibration of the heat flux meters is essential and that an adiabatic wall with intermittent heat sinks (or sources) was not a desirable boundary condition for the measurement of heat transfer coeffiencient. It is interesting to note that other investigators using similar heat-flux measuring devices have also reported inexplicably high values of the heat-transfer coefficient (2), (11). It seems probable that the discrepancies can be partly explained on the basis of a thermal starting length effect. Thus the test section described in the previous section, with an electrically heated wall was developed.

One important consideration in the design of an electrically heated test-section was the heat loss through the buss bars which renders the heat-flux into the flow in the vicinity of the buss-bars difficult to determine precisely (21). A design in which the buss-bars are attached at right angles to the ends of pipe section is more susceptible to this error than the design shown in Fig.4.3.3, in which the influence of the buss bars is limited to a narrow, circumferential region of the flow, not in the vicinity of the measuring thermocouples. The 50 mm- lead-in between the buss bars and the interior of the test section ensured that the electric field within the s.s.sheet was uniform. The thin s.s. sheet provided a sufficiently high elecrical resistance and minimised axial heat-conduction effects.

4.3.3 Operation of apparatus B.

The test section was subjected to a heat loss test to determine the heat transfer coefficient between the heated s.s. sheet and the surroundings. For this test, the ends of the test section were sealed with 12mm-thick ply-wood discs and a certain current passed through the s.s. sheet. Under steady state conditions, the electrical power input into the s.s. sheet was equal to the heat lost by it to the surroundings. Measurement of the temperature distribution on the sheet surface permitted the heat transfer coefficient between the s.s. sheet and the surroundings (h_2) to be determined. The s.s. sheet was heated by some 15 to 25 deg C above room temperature and the heat transfer coefficient h_2 was found to be practically independent of the temperature difference in this range.

The procedure for obtaining the adiabatic-wall effectivness and the heat-transfer coefficient was as follows. The desired velocity ratio (deduced from the readings of the two orifice meters) was set and the secondary air stream heated by some 22 deg C above room temperature. When conditions were steady (in about one and a half hours), the temperature distributions in the s.s. sheet and the slot were recorded by noting the thermo-e.m.f.-s developed by the thermocouples. Next, a current of approximately 250 A was passed through the sheet. The velocities and temperatures at the slot were maintained at their previous values. When conditions were steady, (in approximately one hour), the thermo-e.m.f.-s, the a.c. potential distribution in the s.s. sheet, as well as the voltage drop across the standard resistance in series with the s.s. sheet were recorded. The data reduction procedure was as follows. The rate of heat generation was calculated from the product of the current through the s.s. sheet and the local a.c. voltage gradient across the s.s. sheet. The latter was obtained by a least-squares fit between the a.c. potential distribution and the spanwise distance measured along the curved surface of the sheet. The potential distribution on the s.s.sheet was measured with an a.c. milivoltmeter, using the spot-welds of the thermocouples as the measuring nodes. The heat loss to the surroundings was computed foom the heat transfer coefficients on the outer surface of the s.s. sheet (h_2) and the local wall-to- room temperature difference. A heat balance for an element of the s.s. sheet leads to (neglecting axial heat conduction) the relation

$$\dot{q}''_{gen} = h_1 (T_W - T_{a,W}) + h_2 (T_W - T_G). \qquad 4.3.1$$

Since for each velocity ratio, the experiments were carried out for two values of $\dot{q}''_{gen}$ (equal to zero and one non-zero value), the two unknowns in the above equation, h_1 and $T_{a,W}$ (whence η) could be readily computed.

This assumed that the heat transfer coefficient h_1 was independent of $\dot{q}''_{gen}$: this was confirmed by obtaining h_1 for two different, non-zero values of $\dot{q}''_{gen}$.

4.4 Presentation and discussion of experimental results - apparatus B.

The following section describes the results obtained with apparatus B and corresponding to a lip thickness ratio t/y_C, of 0.35. Experiments conducted with a lip insert which resulted in a lip thickness ratio of unity are described in section 4.4.2, which is followed by a discussion of the experimental inaccuracies (section 4.4.3), and a summary of experimental results (section 4.4.4). The density ratio was approximatley 0.93 and the pressure gradient negligible, for all the runs.

4.4.1 Influence of the velocity ratio on the effectiveness and heat-transfer coefficient.

Effectiveness. The solid circles in Fig. 6.2.3 (a) to (g) represent the measured values of the adiabatic-wall effectiveness for seven velocity ratios in the range 0.389 to 3.55, and for a lip thickness ratio of 0.35. The data shown were obtained from the bottom row of thermocouples (Fig.4.2.2 (b)). The qualitative behaviour of the adiabatic-wall effectiveness is similar to the impervious-wall effectiveness measured with the plane slot, apparatus A. Fig.4.4.1 shows the adiabatic-wall effectiveness for three values of x/y_C plotted against the mass-velocity ratio. The points refer to measurements with apparatus B (interpolated for the values of x/y_C shown), and the broken lines represent faired curves through the corresponding measurements with apparatus A. Despite the numerous differences between the two apparatus, the agreement in the measured impervious / adiabatic- wall effectiveness is remarkable: the largest discrepancy is about 5 percent of unity at x/y_C of 32.5 and about 10 percent of unity at x/y_C of 52.2. This essentially indicates that the differences in the two apparatus had compensating influences on effectiveness. For example, the lip thickness ratio for apparatus B was 0.35, whereas the corresponding value for apparatus A (with a tapered lip) was probably lower. Thus in this respect, apparatus B would have a lower effectiveness than that of apparatus A. On the other hand, apparatus B was axisymmetric, with a radius ratio (inner radius of slot annulus to test section radius) equal to 0.825 as compared with the value of unity for the plane slot. This means that in the vicinity of the slot, the interface area between the mainstream and secondary stream was roughly 20 percent less in apparatus B than for apparatus A. Other factors remaining the same, this would lead to a lower degree of mixing between the two streams for apparatus B, and consequently higher effectiveness. Though the good agreement between the effectiveness measured with the two apparatus cannot be taken as conclusive evidence for the unity-value of the turbulent Lewis number, it does indicate the plausibility of this value.

Heat transfer coefficient. The solid circles in Fig.6.2.3 (h) to (n) represent the measured values of the heat transfer coefficient (expressed as a Nusselt number based on slot-height and conductivity at slot temperature) corresponding to the velocity ratios indicated in Fig. 6.2.3 (a) to (g). The heat transfer coefficient is based on the adiabatic-wall temperature defined in eq.1.2.1. The lines in Fig.6.2.3 (h) to (n) are predictions which will be discussed in chapter 6.

Some scatter is evident in the data, especially in the vicinity of the slot ($x/y_C < 5$), but the trends in the range $10 < x/y_C < 50$ are clearly indicated. For velocity ratios less than about 1.2, the Nusselt numbers tend to a value lower than the value corresponding to fully-developed pipe flow, for the same bulk-Reynolds number, based on the pipe diameter (obtained from the Colburn-analogy (26)) by some 15 percent. The latter are indicated by the short chain -dotted lines in the figures. For velocity ratios greater than 1.2, the Nusselt numbers are higher than the pipe flow values. The authors of references (23) and (60) have found that, for velocity ratios less than unity and x/y_C greater than about 30, the heat-transfer coefficients agree with flat -plate values within $\pm$ 10 percent. The present data do not support this conclusion; these are lower than the flat plate values (R_x based in the distance from the slot exit) by about 30 percent for velocity ratios less than unity and x/y_C greater than 30. The agreeement with flat plate values based on the distance from the 'effective origin' of the boundary layer rather than the slot exit, is likely to be better : this has not been examined partly because the prediction method described later (chapter 6) does not require this information and partly because the effective origin of the velocity boundary-layer was not known in the present instance.

The influence of the velocity ratio on the heat transfer coefficient is clearly demonstrated in Fig.4.4.2, in which the Nusselt number for three values of x/y_C is plotted against the mass-velocity ratio. The figure shows that, at a particular location, the heat-transfer coefficient increases with the velocity ratio - or, since the free-stream velocity was approximately the same for all the runs, with the slot Reynolds number. This increase is rapid for velocity ratios in excess of unity and is relatively small for velocity ratios less than unity. This implies that for velocity ratios greater than unity, the velocity of the secondary stream is the governing parameter for the heat-transfer coefficient while, for velocity ratios less than approximately unity, the free stream velocity is of primary importance.

4.4.2 Influence of slot-lip thickness.

The influence of the slot lip thickness on the impervious-wall effectiveness has been shown to be significant (79), (64), (30). The object of the present experiments was to examine the influence of this parameter on the heat-transfer coefficient and the adiabatic-wall effectiveness. The measurements of adiabatic-wall effectiveness and heat transfer coefficients in presence of a lip insert resulting in a lip thickness ratio of unity, are indicated by the open squares for two velocity ratios in Fig.6.2.3 (b), (f), (i) and (m). It is clear that the adiabatic-wall effectiveness is reduced by an increase in the lip thickness ratio, t/y_C. On the other hand, the influence on the heat-transfer coefficient in the range $10 < x/y_C < 50$ is practically negligible. In the immediate vicinity of the slot ($x/y_C<10$) the behaviour of the heat transfer coefficient is complex: for velocity ratio less than unity, there appears to be a small increase whereas for the velocity ratio greater than unity, there is a significant reduction over the thin lip case.

The above finding concerning the insensitivity of the heat transfer coefficient to the lip thickness is of considerable engineering utility. It is compatible with the observation of Kestin et. al. (24) that the free-stream turbulence intensity has little influence on the heat transfer coefficient in the fully turbulent regime of a flat-plate boundary layer in zero pressure gradient, since one of the effects of the increased lip thickness is an increase in the turbulence intensity (see for example reference (31)). It also indicates another advantage of basing the heat transfer coefficient on the adiabatic wall temperature (which is influenced by the lip thickness ratio).

It should be noted that though the heat transfer coefficient is not appreciably altered due to an increase in the lip thickness, the value of the heat transferred for a given boundary condition would alter, since the adiabatic-wall temperature (on which the heat-transfer coefficient is based) is altered. For example, in the case where the wall temperature is maintained at a certain value which is below tht adiabatic-wall temperature, an increase in the lip thickness would result in a reduction in the heat flux through the wall.

4.4.3 Experimental uncertainties.

The uncertainties in the experimental data for effectiveness and heat-transfer coefficient were mainly due to non-two dimensionality of the flow, errors in the measurement of temperature and heat-flux and effects of heat conduction within the s.s. sheet. The slot height was uniform to within 2 percent, as estimated by the insertion of a tapered plug. The spanwise variation in effectiveness, as measured by the thermocouples at three circumferential locations (Fig.4.2.2(b)) was of the order of 6 percent of unity.

The errors in the observed temperatures were mainly due to errors in the measurement of the thermo-e.m.f.-s. These were measured with a digital voltmeter with a resolution of 10 μV (equivalent to 0.27 deg C for the copper-constantan thermocouples used). This corresponds to about 1 percent of the temperature difference between the slot and the free stream. Variations up to 3 deg C occured in the ambient temperature during the day: the influence of this variation was minimised by keeping the reference junction at the temperature of the mainstream, ie., the room temperature. Conduction errors through the thermocouple leads was negligible since they were placed along isotherms for a length of at least 60 mm along the s.s. sheet.

Uncertainty in the value of the heat flux was mainly due to instrument errors in the a.c. valve voltmeter and errors in the determination of the voltage gradient across the s.s. sheet. The accuracy of the ACVM was estimated at around 2 percent at full scale deflection, the resulting error in the power input being 4 percent. The scatter of the voltage gradient across the sheet at four x- stations was around $\pm$ 2 percent about the mean value. The estimated error in the wall temperature due to axial conduction was less than one percent. Thus the cumulative error in the heat transfer coefficient was approximately $\pm$ 6 percent.

4.4.4 Summary of results with apparatus B.

The main results of the investigation with apparatus B are enumerated below.

1. Measurement of the adiabatic-wall effectiveness and the heat transfer coefficient downstream of an axisymmetric slot are presented. (Tabulated in appendix A.4)

2. Measurements of the adiabatic-wall effectiveness with apparatus B show good agreement (within 5 percent of unity) with the impervious-wall effectiveness measured with apparatus A. This suggests compensating differences between the two apparatus and the plausibility of a unity-value of the turbulent Lewis number.

3. The heat-transfer coefficient, in the presence of film cooling, is a function of the velocity

ratio and cannot be represented accurately either by the flat-plate or pipe-flow formulae.

4. An increase in the lip-thickness ratio from 0.35 to 1.0 leads to a significant decrease in the adiabatic-wall effectiveness (up to 20 percent of unity), but the heat-transfer coefficient (based on the adiabatic-wall effectiveness) in the range $10 < x/y_C < 50$ is negligibly influenced.

CHAPTER 5.

5. The physical inputs to the prediction procedure.

Introduction.

In chapter 3 the mathematical problem associated with the prediction of the flow downstream of a two-dimensional film cooling slot was identified and a solution procedure for the purpose was selected. It was pointed out that the relevant parabolic partial differential equations can be solved provided relations are available, linking the total (ie., sum of laminar and turbulent) shear stress, and the diffusive flux of conserved property such as enthalpy to some time averaged quantity. This implied the specification of an eddy transport hypothesis, The assumption of an eddy transport hypothesis (equations 3.2.8 and 3.2.9) tacitly implies that the shear stress and diffusive fluxes can be related to the gradients of mean velocity and conserved property respectively. The invalidity of this assumption is in some instances obvious. For example, it is known that in a wall-jet there is a finite shear stress at the location of zero mean-velocity gradient (73), (16). However, there are many cases of boundary layer and pipe flows where such a turbulent exchange postulate, in conjunction with a specific eddy transport hypothesis yields satisfactory solutions. The implications of any hypothesis have to be worked out by comparing calculations based upon it with the relevant experimental data. As mentioned in chapter 3, four eddy viscosity hypotheses which are likey to be of relevance to the present problem are those of Prandtl (1925 and 1942), Clauser (1954) and Kolmogorov-Prandtl (1942-45). These hypotheses are represented by the following equations:

$$\mu_{eff} = \mu + \rho \ell^2 \left|\frac{du}{dy}\right| \qquad \text{Prandtl (1925)} \qquad 5.0.1$$

$$\mu_{eff} = \mu + \text{const.}\ \ell \rho \left|(u_{max} - u_{min})\right| \qquad \text{Prandtl (1942)} \qquad 5.0.2$$

$$\mu_{eff} = \mu + 0.018\ \rho u_G \delta_1 \qquad \text{Clauser (1954)} \qquad 5.0.3$$

$$\mu_{eff} = \mu + k^{\frac{1}{2}} \ell\ f(\rho k^{\frac{1}{2}} \ell / \mu) \qquad \text{Kolmogorov (1942) Prandtl (1945)} \qquad 5.0.4$$

The ℓ-s in the above equations denote length scales which have to be specified empirically. The second term on the right hand side in the above equations represents the turbulent component which far out-weighs the laminar viscosity except very close to the wall.

Equation 5.0.1 above has been used with some success for turbulent flow in pipes and boundary layers on flat plates (58), (35), It is applicable to flows with or without velocity maxima, except for the deficiency that it indicates a zero-value for the turbulent viscosity at a location of zero velocity gradient.

Equation 5.0.2 was formulated by Prandtl for free flows such as jets and wakes. It may thus be of relevance in a film cooling situation for the wake region behind the slot-lip.

Equation 5.0.3 was devised by Clauser (9) for boundary layers in adverse pressure gradients, for which the displacement thickness δ_1 is positive. In a film cooling situation, this is the case only for velcoity ratios less than unity. Since velocity ratios on either side of unity are of practical importance, it would be unwise to select this hypothesis for the present problem.

The potential of the last of the hypotheses mentioned above (eq. 5.0.4) has only recently been investigated to any extent (70). Its aesthetic superiority over equation 5.0.1 lies in the fact that it predicts a finite eddy viscosity at the point of zero mean velocity gradient, and that it is also capable of taking into account, the influence of free-stream turbulence. However, it requires the solution of an additional partial differential equation for the conservation of k, the kinetic energy of turblulent motion. The empirical information needed is in no way less than that for the simple mixing length theory, eq.5.0.1, since the length scale of turbulence has still to be specified. In fact, the empirical information needed is greater since the constants expressing the transport of the kinetic energy of turbulence have to be specified. Further it provides no explanation for the existence of a finite shear-stress at a zero-velocity gradient location mentioned earlier in the chapter. Thus it would appear that the use of eqution 5.0.4 in a film cooling situation would be justified only if the performance of the simple mixing length theory, eq. 5.0.1 is found to be seriously inadequate.

The previous sentence implies that the objectives of any prediction procedure need to be clearly stated. The quantities which are of direct interest in the present study of film cooling (in order of practical importance) are the following:

properties at the wall (ie., adiabatic- or impervious-wall effectiveness, heat transfer coefficient and skin friction);

profiles of time-mean quantities (such as velocity, mass-fraction or enthalpy);

and integral properties (such as momentum thickness, shape-factor, energy thickness).

The above discusiion suggests that the Prandtl mixing-length hypothesis (eq. 5.0.1) with some modification may suffice to permit the prediction of the above quantities. The implications of any eddy transport hypothesis should be regarded in the manner in which they influence the above variables. For example, the implication of a vanishing eddy diffusivity at a zero velocity gradient prevents the diffusion of the conserved property (enthalpy or mass-fraction) across the velocity maximum or minimum, resulting in kinks in the conserved property profiles.

Another implication of the Prandtl mixing-length hypothesis is that it tacitly assumes local equilibrium between the production and dissipation of the kinetic energy of turbulence. This is approximately true in the fully turbulent region of flows near walls in mild pressure gradients, but not for example, in flows with strong favourable pressure gradients or in which abrupt streamwise changes in the wall boundary conditions occur. In such cases, the predictions of all the quantities mentioned above are likely to de deficient.

Finally, distributions of the mixing length and effective Prandtl or Schmidt number have to be specified before calculations can be performed. This is essentially an empirical process since the mixing length and the effective Prandtl or Schmidt number are not fundamental physical properties. There are two ways by which suitable mixing length and effective Prandtl/Schmidt number distributions can be obtained. The first is to deduce the distributions of these quantities by reference to experimental data. This may be referred to as the direct approach.

The indirect approach is to perform calculations on the basis of a certain tentative distribution of the mixing length and the effective Prandtl/Schmidt number and to compare the resulting profiles of mean velocity, conserved property and the wall properties with the experimental data. The assumed distributions may be considered satisfactory if the comparison with the experimental data is satifactory. Both these avenues are explored in the present chapter.

5.1 Determination of the mixing coefficients from experimental data.

Introduction. Inorder to deduce mixing lengths and the effective Prandtl/Schmidt numbers from equations 3.2.8, 3.2.9 and 5.0.1, profiles of mean velocity, conserved property, shear stress and diffusive flux across the boundary layer are required. In the absence of direct measurements of the last two quantities, it is possible, in principle, to obtain them by applying the conservation equations for mass, momentum and energy (or species).

Such an exercise for the determination of mixing length distributions in boundary layers and wall-jets has been previously carried our by Escudier (14). The tentative conclusion reached by him was that the mixing length distributions in a number of boundary layers and a limited number of wall-jets examined by him could be approximately represented by a ramp function of the form

$$\ell = K\,y \quad , \qquad 0 < y \leq y_G\lambda/K$$
$$\ell = \lambda \quad , \qquad \frac{\lambda y_G}{K} < y \leq y_G \quad . \qquad 5.1.1$$

The mixing length distributions presented in this reference show considerable scatter and values of K from 0.28 to 0.6 and λ from 0.05 to 0.11 are prevalent. These numbers refer to experiments in which the shear stress was measured with hot-wire equipment; the scatter was even greater for experiments in which the shear stress was obtained by momentum balanace. The representative values suggested by Escudier were K = 0.41 to 0.45 and λ = 0.075.

Though the ramp-distribution (eq.5.1.1) is by no means conclusive, it does provide a simple and reasonable approximation to available data in boundary layers and wall-jets. However, its validity to flows downstream of a film cooling slot remains to be demonstrated.

Evaluation of the effective Prandtl or Schmidt number for flows downstream of a film cooling slot have not previously been reported except in reference (29), whose findings are presented later in this chapter. The status of the experimental information on the turbulent Prandtl number in boundary layers and pipe flows has been reviewed in references (25) and (3). Despite several experimental investigations, two basic questions, namely, the influence of the molecular Prandtl or Schmidt number on the turbulent counterparts (if any), and the distribution of the turbulent Prandtl or Schmidt number across the boundary layer, remain to be conclusively answered. For example, reference (3) indicates values of the turbulent Prandtl number for gases (of molecular Prandtl number in the vicinity of unity) ranging from 0.15 to 1.5, with the majority of the data points between 0.7 and 1.0, while referencee(25) indicated values of the turbulent Prandtl number from 1.1 to 2.0 for mercury (molecular Prandtl number of 0.025). Results from recent experiments have been equally conflicting. The data of reference (63), for air flow over porous flat-plates with air injection and suction, indicate that the turbulent Prandtl number lies between 0.8 and 1.0 for a substantial part of the boundary layer ($0.1 \leqslant y/y_G \leqslant 0.8$). On the other hand, data of reference (18) for the turbulent diffusion of foreign gases into air indicate variations of the turbulent Schmidt number ranging from 1.0 to 3.0 for helium, 0.6 to 1.4 for carbon dioxide and 0.17 to 1.0 for n- octane.

5.1.1 Measurements with apparatus A.

The data for two velocity ratios, equal to 0.55 and 1.85 (Runs 9 and 10) for air injection with nominally zero pressure gradient were examined with the view to obtaining mixing length and effective Schmidt number distributions. Since there were no measurements of the shear stress or diffusional flux of species across the layer, these quantities had to be obtained by the use of the two-dimensional conservation equations. It was found that good integral momentum balance was not obtained at all locations. Fig.5.1.1 (a) and (b) shows the values of wall-shear stress obtained by four methods, viz. : Clauser plot, calibrated razor-blades, momentum balance between adjacent profiles and momentum balance using a least-squared cubic fit through measured values of R_2, H and u_G in the streamwise direction. It may be seen that while there is reasonable agreement between the values of skin friction obtained by Clauser plot and razor-blade methods, there is considerable scatter in those obtained through momentum balance. This is a combined effect of non-two dimensionality in the flow, errors in the measurement and the procedure for obtaining x- wise derivatives of quantities that change slowly in the x- direction.

Fig. 5.1.2 (a) and (b) show a selection of the mixing length distributions deduced from the data of runs 9 and 10 respectively. The mixing lengths and the y-values have been non-dimensionalised with the boundary layer thickness y_G (defined as the distance from the wall where the velocity is 0.99 times the free-stream value). In general the ramp mixing length distribution, eq. 5.1.1 (indicated by the broken lines in Fig.5.1.2) is not a bad representation of the majority of the data points shown, except in the vicinity of the velocity maxima (run 10) and the outer edges of the boundary layer. Near the velocity maximum the mixing length tends to infinity since the shear stress is finite at this point. A short distance from the velocity maxima towards the wall, the mixing length goes towards zero, at the location of zero- shear stress. Towards the outer edge of the layer, the mixing length tends to large values: significance can hardly be attached to this in view of the experimental uncertainties in this region.

In obtaining the mixing lengths, the shear stress distribution was obtained by momentum balance between adjacent profiles; the velocity gradient (du/dy) was taken as the mean between the adjacent profiles (for a constant y) and was obtained by fitting a parabola through three adjacent points in each profile.

Fig.5.1.1 (c) and (d) shows the integral mass balance at different x-locations at which concentration profiles were measered. A unity- value of the ordinate $(R_{\varphi} \cdot \eta / R_C)$, indicates an exact balance. The majority of the points are within $\pm$10 percent of this value and the worst deviation is about 20 percent.

Effective Schmidt numbers were obtained by evaluating the diffusive flux at each y-location through species balance between adjacent profiles and the y-direction gradient of the concentration profiles smoothed 'by eye'. Some of the deduced Schmidt numbers, between locations where reasonable over-all species and momentum conservation were obtained, are shown in Fig. 5.1.3 (a) and (b). There is considerable scatter and the results allow only the limited conclusion that the majority of the points are in the range 1.0 $\pm$ 0.3.

5.1.2 Results with the data of reference (29).

Mass fraction profiles measured by the author in the wind tunnel of reference (30) indicated a good integral species balance (within 2 percent). Consequently, mixing lengths and the effective Schmidt number were deduced in the manner described and presented in reference (29). In this case the shear stress distribution across the layer was obtained with an inclined, constant temperature hot-wire and the diffusive flux by a species balance between adjacent profiles. Typical mixing lengths obtained in this investigation are shown in Fig. 1 of reference (29). Though there is considerable scatter, the data suggest that, except in the vicinity of the velocity maxima, a ramp mixing-length distribution is a fair representation of the data. There seems to be a tendency for the value of λ to increase downstream. Fig. 3 of this reference shows the typical effective Schmidt numbers deduced from the data. Again, the scatter is large and the allows the limited conclusion that an effective Schmidt number of 0.5 $\pm$ 0.3 is representative of most of the data points.

5.1.3 Discussion of procedure and results.

The above results emphasise the difficulties in deducing the mixing lengths and turbulent Schmidt numbers from profile data in non-equilibrium flows. The problem may be expected to be somewhat simpler in equilibrium flows, such as fully developed flow in pipes and channels, where the x-derivatives are zero and the shear-stress distribution across the layer is precisely known.

The reasons for the large scatter in the mixing length distributions presented above and elsewhere (14),(29), may be attributed to the following:

1. that similarity in the mixing length, normalised with the thickness of the boundary layer, does not exist;

2. sensitivity of the deduced mixing lengths to data-reduction procedures and experimental inaccuracies of the dependent variables, namely

i. Determination of y_G from experimental data;
ii. differentiation of experimental velocity profiles to obtain the velocity gradients, (du/dy);
iii. Errors in the shear-stress distribution deduced from the integral momentum equation, due to the non-twodimensionality of the flow and differentiation of the experimental integral quantities in the x-direction.

Although reason 1 above is likely to be true, the uncertainties under 2 make it difficult to asses the lack of similarity. The assumption of similarity in mixing length distribution is a very useful simplification in the development of prediction procedures.

There is no conclusive evidence on the value of the turbulent Prandtl or Schmidt number. While it is likeky that a unique value for the turbulent Prandtl or Schmidt number does not exist, difficulties in the experiments prevent this to be proved one way or other. However, there seems to be considerable experimental and theoretical reason to suggest that for the turbulent flow of air over solid surfaces, the turbulent Prandtl or Schmidt number is in the vicinity of unity.

The use of the two dimensional conservation equations to obtain the shear stress and the diffusional fluxes appears to be unreliable, unless the two-dimensionality of the flow is exceptionally good. The use of an inclined hot-wire to measure shear stress distribution can be expected to be more reliable. The use of hot wires to measure the turbulent heat and species fluxes may eventually yield more reliable information about the distribution of these quantities.

The relative importance of the quantities appearing in equations 3.2.8, 3.2.9, and 5.0.1 are indicated in the following equations, obtained by differentialing the above equations:

$$\frac{d\ell}{\ell} = \frac{1}{2}\frac{d\tau}{\tau} - \frac{d\,(u')}{u'} \quad , \qquad 5.1.2$$

$$\frac{d\sigma_{eff}}{\sigma_{eff}} = -\frac{d(u')}{u'} + \frac{d\,c'}{c'} + \frac{d\tau}{\tau} - \frac{dJ}{J} ; \qquad 5.1.3$$

In these equations the primes denote differentiation with respect to y. From equation 5.1.2 it is evident that the percentage error in the mixing length is the sum of half the percentage error in the shear stress and the error in the velocity gradient. For the effective Schmidt number, the influence of an error in the shear stress is twice as significant, and two additional sources of error are present. The percentage error in the velocity gradient is likely to be large near the velocity maximum and near the wall, while the error in shear stress is likely to be large near a velocity maximum. The error in the diffusive flux J is likely to be large near the wall (for an impervious wall), while errors in the concentration gradients are likely to be important in the outer part of the layer. Thus meaningful results may be expected in a limited region between the velocity maximum and the outer edge of the layer.

Finally it is appropriate to enumerate the main findings of the present section.

1. The mixing length distribution presented in the two preceding sub-sections provide additional plausibility to the ramp-mixing length distribtuion for flows downstream of a film cooling slot, except in the vicinity of velocity maxima. Though the uncertainties in the data preclude the positive confirmation of the constants in the ramp-function, the values K = 0.41 and λ = 0.09 appear to be a reasonable

first approximation to the data.

2. The present experimental data do not reveal a universal value of the turbulent Schmidt number. The data from apparatus A suggests a value of 1.0 ± 0.3 in the outer region of the boundary layer, while that of reference (29) suggests a value of 0.5 ± 0.3. However the uncertainties in the data and data reduction procedures preclude a resolution of this difference.

5.2 Predictions based on the mixing length and effective Prandtl/Schmidt number hypothesis.

Some guidance about the mixing length distributions and the effective Prandtl/Schmidt number was obtained in the previous section: this was by no means conclusive or universal. However, it remains to ascertain whether it is possible to obtain acceptable predictions using the mixinglength and the effective Prandtl/Schmidt number hypothesis, within the framework of the calculation procedure of reference (49), described briefly in chapter 3.4. This possibility is examined in the present section by comparing predictions based on tentative distributions of the mixing length and effective Prandtl/Schmidt number, with available experimental data.

5.2.1 Procedure.

A finite difference grid was located on measured profiles of velocity and concentration (or enthalpy) downstream of an injection slot, in a region where the effects due to slot-geometry could be expected to be small (about 20 slot-heights downstream). The appropriate boundary conditions along the wall and the free stream were specified. Integration of the momentum and species (or enthalpy) equations was commenced using the procedure of reference (49), which yielded downstream profiles of velocity and species, along with the quantities such as the impervious-wall effectiveness, wall-shear stress, momentum thickness etc. The object of the exercise was to perform these calculations for a specific distribution of the mixing-length and effective Prandtl/Schmidt number and to alter the chosen distribution, if necessary, to obtain the best over-all agreement with selected experimental data.

At this stage it is desirable to quantify the criterion for satisfactory prediction of the impervious-adiabatic-wall effectiveness, because of its importance to film cooling. Two quantities are sufficient to characterise the the quality of prediction: (a) the maximum deviation (D_{max}) between the prediction and the experimental data over a specified distance from the slot and (b) the quantity defined by

$$\Lambda^2 = \frac{1}{L}\int_0^L (\eta_{PRD} - \eta_{EXPT})^2 \, dx \quad , \qquad 5.2.1$$

where $\eta_{EXPT}(x)$ represents a smooth curve through the data-ponts and η_{PRD} the predicted distribution of effectiveness. Thus Λ can be considered as the root-mean square deviation between the predicted and experimental effectiveness, with the streamwise distance as the weighting function (see Fig. 5.2.1). A mean value of Λ for a number of sets of data (say NSETS) can be evaluated through the expression:

$$\bar{\Lambda}^2 \equiv \sum_{i=1}^{NSETS} \Lambda_i^2 L_i \Big/ \sum_{i=1}^{NSETS} L_i \quad . \qquad 5.2.2$$

<u>5.2.2 Data for comparison.</u>

For the present exercise only those measurements which include downstream profiles of velocity and concentration (or enthalpy) are of interest. This considerably limits the number of experimental data available. The data of references (5), (56), (61), (23) and (29) are relevant and along with the present measurements, are used for comparison with predictions. The above data cover a useful and wide range of conditions:

$$0.36 < u_C/u_G < 1.85 \quad ;$$

$$0.88 < \rho_C/\rho_G < 4.17 \quad ;$$

$$1970 < R_C < 17400 \quad ;$$

$$-1.0 < K_p 10^6 < 3.8 \quad .$$

Besides the above data, references (28), (73), (16), (4) and (17) present hydrodynamic quantities such as profiles of mean velocity and wall-shear stress. The case of the pure wall-jet ($u_G \rightarrow \infty$) isincluded (73) and (17). The prediction of these data is also examined, to extend the range of variables covered.

A check on the internal consistency of the data is provided by evaluating the integral of the species or enthalpy flux, $\int_0^{y_G} \rho u \varphi \, dy$ for each set of velocity and concentration profiles, which should equal the enthalpy or mass flux through the slot. Such a check was carried out and the results showed discrepancies in the integral species (or enthalpy) conservation of upto 30 percent, and the majority of the points were within 10 percent. This may be considered satisfactory in view of the compounding of the errors which occur in the evaluation of the integral and inaccuracies in the measurement of concentration /enthalpy profiles in the outer region of the flow.

5.2.3. The choice of the mixing length and effective Prandtl/ Schmidt number distribution.

The ramp mixing-length distribution discussed in chapter 5.1.1 was tentatively adopted for the present calculations. The value of K and λ are taken as 0.419 and 0.09 respectively. The former is a fairly well accepted value for turbulent boundary layers (51), (14) and shown to be valid for wall-jets (45). The latter is a value representative of the experimental data examined in references (14) and (29) and the data presented in the previous section.

In view of its importance to film cooling, it is preferable to optimise the predictions for the impervious-adiabatic- wall effectiveness, by examining the predictions corresponding to a number of plausible distributions of the effective Prandtl or Schmidt number. Various values of the effective Prandtl /Schmidt number were tried, including σ_{eff} of 0.5 and 1.0, as suggested by the experiments in the previous section.

The mixing-lengththeory yields zero eddy viscosity and diffusivity at the point of zero-velocity-gradient.

As this is unrealistic, the simple expedient of bridging the region of zero eddy diffusivity with a straight line between the points of highest eddy diffusivity was employed (please see Fig. 5.2.2)

The distributions of mixing length and the procedure near zero velocity gradient outlined above appear crude over simplifications of the processes taking place within the flow and indeed this is so. It is the object of the present exercise to examine the predictions that result with this crude hypothesis and to outline areas where a more sophisticated hypothesis is necessary. It is in the nature of turbulent flow that its gross properties are not always sensitive to assumptions about its complex internal structure.

5.2.4 Comparison of predictions with experimental data: flows in uniform pressure.

The results of computations using the above mixing length and effective Prandtl/Schmidt number are presented in this section. Fig.5.2.3 (a) to (m) shows predicted profiles of mean velocity and concentration (or enthalpy) for thirteen sets of data from the references mentioned in section 5.2.2 above, along with the measured profiles. The corresponding predictions of effectiveness are shown in Fig. 5.2.4 (a) to (m). The predictions are shown as full lines and the data as points. The constants used for these computations, K, λ, and σ_{eff} are 0.419, 0.09 and 1.0 respectively. Table 5.2.1 presents a summary of the data along with the quantitative measure of agreement between predicted and measured values of effectivenees mentioned previously, viz. Λ and D_{max}.

It can be seen from Fig.5.2.3 that the predictions of velocity profiles is on the whole satisfactory for all the cases, including a wall-jet, a wall-wake and a weak wall-jet which decays to a normal turbulent boundary layer, far downstream. There are small discrepancies between the predictions and measurements but these do not appear to be systematic. The largest discrepancy (around 8 percent of velocity) in Fig. 5.2.3 (h) occurs for the lowest velocity ratio considered ($\bar{u}_C/u_G = 0.36$).

Before proceeding to examine the predictions of effectiveness and concentration profiles, the predictions

TABLE 5.2.1 Summary of comparison of predicted and measured effeciiveness.

No.	DATA	$\bar{u}_C/u_G$	R_C	ρ_C/ρ_G	$\sigma_t = 1.0$ $\Lambda\vert_{x/y_c=100}$	D_{max}		$\sigma_t = 0.5$ $\Lambda\vert_{x/y_c=100}$	D_{max}		$\sigma_t =$ 0.5 / 1.75 $\Lambda\vert_{x/y_c=100}$	D_{max}	
a	Run 9	0.55	1970	1.0	0.030	+0.03	GOOD	0.090	−0.07	FAIR	0.103	+0.12	FAIR
b	Run 4	0.76	2620	1.0	0.034	±0.03	GOOD	0.143	−0.15	POOR	0.037	+0.04	GOOD
c	Run 1	1.23	4170	1.0	0.024	+0.02	GOOD	0.090	−0.10	FAIR	0.075	+0.10	FAIR
d	Run 10	1.85	6330	1.0	0.063	+0.07	FAIR	0.055	−0.05	FAIR	0.122	+0.08	POOR
e	Ref(29)	0.76	5570	1.0	0.099	+0.11	FAIR	0.048	−0.03	GOOD	0.174	+0.22	POOR
f	Ref(29)	2.30	17400	1.0	0.107	+0.14	FAIR	0.024	±0.02	GOOD	0.176	+0.24	POOR
g	Ref(23)	0.67	5670	≈1.0	0.038	−0.06	GOOD	0.153	−0.17	POOR	0.043	+0.07	GOOD
h	Ref(61)	0.36	4300	≈1.0	0.091	+0.10	FAIR	0.025	±0.03	GOOD	0.148	+0.17	POOR
i	Ref(56)	0.88	4580	≈1.0	0.021	±0.03	GOOD	0.102	−0.12	FAIR	0.080	+0.08	FAIR
j	Run 2	0.58	5150	4.17	0.012	±0.02	GOOD	0.112	−0.15	POOR	0.012	+0.05	GOOD
k	Run 6	1.65	14250	4.17	0.018	−0.07	GOOD	0.093	−0.15	FAIR	0.048	±0.02	GOOD
l	Ref(5)	1.01	9800	4.17	0.013	−0.05	GOOD	0.085	−0.13	FAIR	0.027	+0.03	GOOD
m	Ref(5)	1.01	1990	1.38	0.028	±0.03	GOOD	0.080	−0.15	FAIR	0.087	+0.08	FAIR
				$\bar{\Lambda}$	0.054			0.112			0.101		

RATINGS

	$\Lambda < 0.05$	GOOD
$0.05 <$	$\Lambda < 0.11$	FAIR
$0.11 <$	Λ	POOR

of some additional hydrodynamic quantities will now be discussed. Fig. 5.2.5 (a) and (b) show predicted and measured growth rate, decay of velocity maxima and wall-shear stress for two velocity ratios greater than unity. The data shown in (a) are present measurements and those in (b) are from reference (28). The predictions are satisfactory. Fig. 5.2.5 (c) shows the prediction of integral properties and wall-shear stress for the case of a weak wall-jet where the velocity maxima disappears downstream and R_2 passes from negative to positive values. There is also a discontinuity in the shape factor H. Fig. 5.2.5 (d) and (e) show similar predictions for two velocity ratios less than unity. Again one set of data is from reference (28), and the other is present measurement . The agreement between the predictions and experiment is satisfactory.

The largest velocity ratio examined so far is 2.74 and the predictions found to be satisfactory. It is of interest to see whether this is valid for the case of the wall-jet in still surroundings ($u_C/u_G \rightarrow \infty$) Fig. 5.2.6 shows predictions of the growth rate of y_{HALF} and decay of u_{MAX} for the data of Gartshore (17) and Tailland and Mathieu (73): wall-shear stres data is also shown for the data of reference (73). The corresponding velocity profiles are shown in Fig.5.2.7. It may be seen from the full lines in Fig.5.2.6 that the use of the constants K= 0.419 and λ=0.09, lead to satisfactory predictions of y_{HALF} and u_{MAX} and the wall-shear stress. The predicted velocity profile is defective, as shown in Fig.5.2.7, in that the velocity maximum occurs too close to the wall and exhibits a peaky shape. The velocity profile can be corrected by reducing λ to give K/λ of 7, but this leads to excessively low rates of spread and velocity maximum decay. This is shown by the broken lines in Fig.5.2.6 and 5.2.7. It may be concluded that for the case of the pure wall-jet, no one set of values of K and λ will result in satisfactory predictions of more than two of

the shape of the mean velocity profile,

y_{HALF} and u_{MAX}

and $c_f/2$.

Since the shape of the mean velocity profile is the least important of these, the value of 0.419 and 0.09 for K and λ are considered most satifactory. The data of Bradshaw and Gee (7) and Eskinazi and Kruka (16) for a velocity ratio of 10 were also examined and similar conclusions were found to be appropriate.

Thus it may be concluded that the simple ramp- mixing length distribution gives fairly satisfactory predictions of the hydrodynamic quantities over a wide range of velocity and density ratios. For high velocity ratios the mean velocity profile is incorrectly predicted but this is not considered a serious draw back.

Returning to the problem of predicting concentration profiles and effectiveness, it is evident from Figs. 5.2.3 and 5.2.4 that both these quantities are well predicted with an effective Prandtl/Schmidt number of 1.0. The shape of the concentration profile (normalised with the value at the wall) is in good qualitative agreement with the experimental profiles. The discrepanciss are mainly in the outer regions of low concentrations where the accuracy of the measurements is low.

The predictions of effectiveness carried out with three different specifications of the turbulent Prandtl/ Schmidt number, viz. σ_t of 1.0 (full lines), 0.5 (broken lines) and a linear distribution across the layer from 1.75 at the wall to 0.5 in the free stream (chain dotted lines) are shown in Fig.5.2.4. It can be seen that the best over-all agreement is obtained with $\sigma_t = 1.0$. This may be substantiated by comparing the values of Λ (as explained in section 5.2.1) . Table 5.2.1 (p. 85) indicates the value of Λ evaluated at a distance of 100 slot-heights along with the maximum deviation between the predicted and measured effectiveness, for each of the above specifica -tions for σ_t. It can be seen that there is a certain amount of compensation amongst the predictions for the different sets of data, ie., no one specification of σ_t predicts all the data equally well. However, the predictions obtained with σ_t of 1.0 gives the lowest value for the $\bar{\Lambda}$, equal to 0.054 percent of effectiveness as compared to $\bar{\Lambda}$ of 0.112 and 0.101 for σ_t of 0.5 and the linear distribution of σ_t respectively.

The present conclusion regarding the best value for σ_t is at variance with the suggestion of reference (29), of the linear distribution across the layer. There are two reasons for this reconsideration. First, that certain data (shown in Fig, 5.2.4 (e), (f), and (i)), examined since the writing of the report, were poorly predicied with the linear distribution of σ_t. The second reason stems from the use of the Couette-flow assumption in the procedure of reference (49). The consequences of this assumption were (a) that the conservation of species across the flow was not precisely observed and (b) it caused the non-dimensional concentration profile to bulge outwards due to the incorrect slope at the first grid interval near the wall. Subsequently, the formulation near the wall was revised (69) to allow for the convection in the half-interval near the wall. An example of the velocity and concentration profile obtained with the original and modified procedures, for a constant σ_t of 1.0 is shown in Fig. 5.2.8. The new formulation results in a higher value of the effectiveness and a 'flatter' non-dimensional concentration profile. A similar effect was previously obtained by the use of a linear distribution of σ_t.

5.2.5 Flows in the presence of streamwise pressure gradients.

In chapter 4.2.2 data pertaining to the flow downstream of a two-dimensional film cooling slot in the presence of pressure gradients were presented. It is of interest to examine the prediction of these data with the simple mixing-length hypothesis, in conjunction with the mixing length and effective Prandtl or Schmidt number adopted in the previous section.

The procedure for the calculations was basically similar to the one for the zero-pressure gradient flows discussed in the last section. The appropriate boundary conditions along the free stream implied that the free-stream velocity was varied in the streamwise direction to correspond with the experimental data. The value of the free stream velocity at a downstream station during the marching integration procedure was obtained from polynomials fitted to the experimental values of K_p.

Before proceeding to examine the results of these computations, two factors pertinent to flows with pressure gradients should be mentioned. First, that the wall functions incorporated in the calculation procedure of reference (49) were based on the van Driest's hypothesis (74), extended to include the influence of pressure gradients and mass transfer, on the drag and heat transfer in turbulent flow. The validity of these functions for heat transfer in adverse pressure gradients has been examined by the present author (43) and by the authors of ref.(49) for several boundary layers with favourable and adverse pressure gradients. They have been found to be satisfactory for all the cases except those in presence of strong favourable pressure gradients.

The second remark is to note that predictions obtained with the mixing-length distribution used in the previous section are not valid as such, to flows in strong favourable pressure gradients, such as PG2 and PG3 (described in chapter 4), in which re-transition to laminar flow is imminent. In such cases, the deviation between the predictions and experiments is an indication of re-transition.

It is also pertinent to note that in majority of the applications of film cooling, the favourable pressure gradients are unlikely to be strong enough to induce re-transition.

The calculations and comparison with the experimental data will now be presented. Fig. 5.2.9 (a) and (c) show predicted and measured profiles of mean velocity and concentration(of helium tracer) corresponding to the favourable pressure gradient PG2 (K_p(nominal) = 1.8×10^{-6}), for two velocity ratios. Fig. 5.2.9 (b) and (d) present similar information for the case of the adverse pressure gradient PG4 (K_p (nominal) = -1.0×10^{-6}). The velocity profiles have been normalised with the local free stream velocity.

It is evident from Fig. 5.2.9 (a) that significant discrepancies exist between the prediction based on the assumption of fully turbulent flow and the experimental velocity profiles for the case of the favourable pressure gradient, PG2. In particular, the predicitions underestimate the thickness of the viscous sub-layer and indicate a greater velocity defect than that shown by the experimental data. However, for the velocity ratio greater than unity, and for the same nominal value of K_p,(Fig.5.2.9 (c)) the velocity profiles appear to be well predicted. It should be noted that the value of the pressure gradient parameter Δ_p for this velocity ratio is lower than that for the lower velocity ratio (Fig.5.2.9 (a)); consequently, PG2 constitutes a milder pressure gradient for this case.

The above observations are also reflected in the predictions of integral quantities and skin-friction coefficient. Fig.5.2.10 (a) shows measured and predicted values of R_2, H and $c_f/2$ for the run shown in Fig.5.2.9 (a) (ie. PG2, $\overline{u}_C/u_G = 0.58$). The predicted value of R_2 tends towards the equilibrium value for turbulent flow, corresponding to the prevailing value of K_p, as obtained from Fig. 11 of reference (33), while the experimental data tend towards the corresponding asymptote for laminar flow. The predicted and measured values of the shape factor H, do not show much change except far downstream, where the experimental values begin to rise towards a laminar asymptote and the predictions towards a turbulent asymptote. The measured skin friction coefficients are everywhere below the predictions based on the assumption of turbulent flow. The trends shown in Fig.5.2.10 (a) are more clearly illustrated in Fig.5.2.10 (b) for the stronger favourable pressure gradient PG3, and for the same velocity ratio. In this figure, the experimental values of R_2 and H are close to the equilibrium laminar values while the corresponding predictions tend towards the turbulent asymptotes. The predicted skin-friction coefficients increase with the downstream direction, while the measured values indicate a sharp decrease at about 100 slot-heights.

The predicted and measured growth of y_{HALF}, decay in the velocity maximum and the skin-friction coefficient for the favourable pressure gradient PG2 and a velocity ratio greater than unity, are shown in Fig.5.2.11 (a). The agreement between the predictions and experiment are excellent. This is not surprising since, as as suggested above, the pressure gradient PG2 constitutes a mild pressure gradient for this velocity ratio. The predictions and measurement indicate a decrease in the velocity maximum upto a distance of about 70 slot-heights, followed by an increase further downstream. This suggests that in the initial region the loss of momentum due to viscous forces is dominant, but far downstream, its increase due to the acceleration is greater. The predictions also indicate a decrease in the thickness of the layer from x/y_C of approxi -mately 130. The good agreement between the predicted and measured skin friction coefficients suggests that the flow is still turbulent in the wall region.

The above comparison of predictions based on the assumption of turbulent flow and the experiments in flows with imminent re-transition does not provide any positive criterion for the onset of reverse transition. The reason for this is partly because reverse transition is a gradual process and there can be a lag in space and time between its manifestations in the various mean properties. For example, a decrease in the skin-friction coefficient does not always coincide with the minimum in the shape factor (see for example, Figs. 5 and 9 of reference (1)), which has been cited as an approximate criterion for the onset of reverse transition (52). However, in the present problem of wall-jet and wall-wake flows, numerical values of quantities such as R_2 and H do not always connote the same meaning as corresponding values for conventional boundary layers and thus the criteria for reverse transition based on these quantities has limited relevance. For present purposes, significant departures from predictions based on turbulent-flow assumption is a fair indication that reverse transition is taking place.

Predictions of the hydrodynamic quantities in the adverse pressure gradient PG4 will now be examined. As mentioned earlier, Fig.5.2.9 (b) and (d) show measured and predicted profiles for two velocity ratios on either side of unity. In general, the mean velocity profiles are well predicted, except for some discrepancy far downstream, in the outer regions of the layer and for the case of velocity ratio less than unity. Part of this discrepancy may be attributed to the non-two dimensionality of the flow in this region. The rapid increase in the layer thickness is well demonstrated by the predictions and experimental data. Fig.5.2.10 (c) shows the predicted and measured values of integral properties R_2 and H and the skin-friction coefficient. The prediction for R_2 and H are satisfactory, while the skin friction is well predicted far downstream. Closer to the slot, the experimental data for skin friction are lower than the predicted values. Fig.5.2.11 (b) shows predicted and measured growth of y_{HALF}, decay of velocity maximum and the skin-friction coefficient corresponding to a velocity ratio greater than unity, and for the adverse pressure gradient PG4. Again the agreement between the predictions and experiments is very satisfactory.

Finally, Fig.5.2.12 (a) to (d) show the predicted and measured values of the impervious-wall effectiveness in the presence of pressure gradients. Fig.5.2.12 (a) and (b) correspond to the favourable pressure gradient PG2 while (c) and (d) correspond to the adverse pressure gradient PG4. Predictions for the case of the strong favourable pressure gradient over-estimate the effectiveness far downstream. This demonstrates the unsatisfactoriness of the mixing length and effective Schmidt- number concept in flows in which reverse transition is either taking place or is imminent. It is plausible that for such flows, the laminar Schmidt number ($\sigma = 0.22$ for the diffusion of helium into air) will influence the effective Schmidt number over a considerable part of the flow.

The prediction of the impervious-wall effectiveness and concentration profiles for the case of the adverse pressure gradient PG4, shown in Figs. 5.2.12 (c), (d) and 5.2.9 (b) and (d), are very satisfactory.

5.2.6 Conclusions and summary.

The main object of this section was to asses the validity of the simple mixing-length theory to predict the time-mean properties of turbulent flow downstream of a film cooling slot. Available experimental data, corresponding to a wide range of velocity ratios, density and pressure gradients, have been compared with the predictions of mean velocity and concentration (or enthalpy) profiles, the impervious- or adiabatic- wall effectiveness, wall-shear stress and integral properties.

The principal conclusion that can be drawn is that the ramp-distribution of the mixing-length (eq.5.1.1) and a unity value of the effective Prandtl or Schmidt number can provide acceptable predictions of the above quantities for all the cases examined, except those in favourable pressure gradients, strong enough to re-laminarise the boundary layers.

CHAPTER 6

6. The prediction of effectiveness and heat transfer downstream of a film cooling slot.

Introduction.

In the previous chapter, the validity of the mixing length hypothesis was examined in the region sufficiently downstream of the slot, where the effects of the slot geometry were likely to be of less importance. For this exercise, integration was commenced from measured profiles of velocity and conserved property downstream of the slot. However in most practical situations profiles at a downstream station are not available and only the conditions at the slot exit are known. For example, the velocity and temperature prevailing in the slot and main -stream may be known or deducible and it is desired to predict the adiabatic-wall effectiveness and heat-transfer coefficient downstream of the slot exit. In some applications, neither the wall temperature nor the heat flux are known a priori; these can be determined from the predicted adiabatic-wall temperature and a heat-transfer coefficient based on this temperature.

In this chapter the possibility of obtaining predictions of film cooling effectiveness and the heat-transfer coefficient from the slot exit, using the prediction procedure discussed in the previous chapter is examined. It must be pointed out that close to the slot exit, the assumptions leading to the parabolic, boundary-layer equations, are not strictly valid, due to the presence of cross-stream pressure gradients and recirculation behind the slot lip. This region is more accurately represented by the Navier Stokes equations in their entirety: these equations are partial, elliptic differential equations and their solution involves greater computer time and complexity.[1] It is therefore interesting to examine the performance of the marching integration procedure for parabolic equations, commencing from the slot exit. However, in view of the inconsistency of using parabolic equations in the

---

1. This approach has been concurrently examined at Imperial College. See for example, Kacker, S.C., Ph.D. thesis (1969)

vicinity of the slot, discrepancies between the predictions and experiment are to be expected; it is to be hoped however, that these will affect the details of the flow pattern rather than the wall properties, such as the effectiveness of film cooling and the heat-transfer coefficient.

As suggested by the experimental data presented in chapter 4 and the literature survey of chapter 2, the effectiveness of a film cooling slot is influenced by several variables. The important ones were shown to be the slot to mainstream velocity and density ratio, the geometry of the injection region and to a lesser extent, the longitudinal pressure gradient and the initial conditions at the slot exit, such as the thickness of the boundary layer on the outer surface of the slot lip. Further, in most applications of film cooling, heat transfer through the film cooled wall is present and it is to be expected that this quantity will also be influenced by the variables mentioned above. Out of these variables, the geometry of the injection region is probably the most complex, since the number of geometriaal parameters is large; only a few of them have been systematically investigated (79), (30), (64). Most geometries used in practical applications render the flow three dimensional and thus go beyond present analytical capability. One variable which has been experimentally investigated for two dimensional flows and shown to have a practically important influence, is the slot-lip thickness to height ratio, t/y_C (79), (30).

In the present chapter, the predicted trends with respect to the above-mentioned variables and their agreement with available experimental data for two-dimensional flow are examined. Where a serious shortcoming of the turbulence model used is encountered, attempt has been made to overcome it by empirical means. This artifice was found to be necessary, for example in the prediction of the influence of the lip thickness on effectiveness.

A further exercise which has been attempted in this chapter relates to the prediction of wall temperatures in a gas turbine combustion chamber. The motivation for this exercise is two fold: first to demonstrate the relative importance of the variables which influence the temperature of a film cooled surface, and second, to outline the role of prediction procedures such as the present one, in the prediction of wall-temperatures in practical devices.

The chapter commences with the case of tangential injection through a plane two-dimensional slot with a nominally thin slot lip, and in flows with uniform density and pressure, bounded by an adiabatic or impervious wall. The effects of density ratio and slot lip thickness are examined next. Film cooling in the presence of heat transfer at the wall is then considered, followed by the effects of longitudinal pressure gradients on the effectiveness of film cooling. This is followed by a brief discussion on film cooling in gas turbines. Comparison with available data is made for each of the factors mentioned above. The chapter concludes with the author's suggestion for future research in film cooling. A listing of the computer programme for the prediction of the flow development, effectiveness and heat transfer coefficient is given in appendix A.5, together with explanatory notes.

6.1 Prediction of adiabatic- or impervious- wall effectiveness: case of uniform pressure and thin slot lip.

The flow downstream of a film cooling slot has been qualitatively described in chapter 3 (see Fig. 3.1.1). Three boundary layers growing in the vicinity of the slot may be distinguished: one on either side of the slot lip and one on the surface to be cooled. The ones growing on the slot lip merge just downstream of the slot exit, and develop as a mixing layer. This mixing layer merges with the wall boundary layer further downstream. There is also a region of separated flow immediately behind the slot lip.

In order to apply the prediction procedure in this region, one has to decide on two matters: first the location of the grid, and second, the choice of characteristic lengths in the various regions of the flow. These will be discussed in turn.

The grid location.

The simplest possibility is to locate the finite difference grid from the wall to the outer edge of the boundary layer on the outer surface of the lip. This is procedure adopted here and a typical grid is shown in

Fig.6.1.1. The grid lines are not uniformly spaced: a larger number is provided in regions of large velocity gradients. In the region directly behind the lip, a small forward velocity (say 10 percent of the free stream value) is assumed. This is incorrect, but preserves compatibility with the parabolic nature of the solution procedure. With this set-up, it is necessary to specify the profiles of velocity and conserved property (enthalpy or mass fraction) across the slot. This can be obtained from measured profiles or guessed from a knowledge of the mass flow rates through the slot and free stream and assumed profile shapes. For instance, in the example shown in Fig.6.1.1, the velocity profile at the slot exit is composed of three power-law profiles, representing the three boundary layers mentioned above. The two boundary layers within the slot are separated by a region of uniform velocity. The advantage of the present practice of grid location is that the presence of the boundary layer within the slot and on the outer surface of the lip is taken into consideration. A different approach was used by the authors of reference (10): the development of a mixing layer originating from a point near the tip of the slot lip was calculated, up to the station where this layer impinged on the wall. Thereafter the calculation proceeded as for a wall boundary layer. The initial conditions assumed in this method were unrealistic as they do not include the effects of the boundary layers at the slot exit. Consequently, the predictions from this procedure are poor in the initial region, particularly for velocity ratios close to unity.

Characteristic lengths.

The mixing lengths are generally specified in relation to a characteristic width of the layer being calculated. For example, in the previous chapter, the characteristic length was taken as the distance from the wall to the point where the velocity differed from the free stream value by one percent. The question arises, whether this practice should be retained in the region near the slot, where two layers can be identified, ie., the mixing layer and the wall boundary layer. It might be more appropriate, for example, to use two characteristic lengths, one for each of the two regions. Further downstream where the velocity defect due to the lip has vanished, only one characteristic length would suffice. This possibility has been investigated by the present author in reference (45). Fairly satisfactory predictions of the impervious-wall effectiveness were obtained for velocity ratios outside the range 0.9 to 1.5 and for a desity ratio of unity. Within this range of velocity ratio, the effectiveness was over estimated. It is also worth while to explore the possibility of using the width of the whole layer, ie. from the wall to the outermost point where the velocity differs from the free stream value by say one percent , as the characteristic length. This practice, apart from being simpler, has the advantage that there is no abrupt change in the characteristic length: the two-layer model suffered from this at the station where the velocity defect behind the lip disappeared. Resluts of calculations performed with with the width of the whole layer as the characteristic length are discussed below.

Details of the calculation procedure.

The prediction of impervious-wall effectiveness and heat transfer coefficient were made with the following values of the numerical and physical parameters:

number of grid lines	35
K	0.419
λ	0.09
σ_t	1.0
Step length	Such that mass flow entrained in each forward step is 2.5 percent of the mass flow in the layer, provided the step legth does not exceed the following: $dx < .05\ y_G;\ 0<x/y_C<10$; $< .15\ y_G;\ 10<x/y_C<20$; $< .30\ y_G;\ 20<x/y_C$.

The characteristic length was taken as the distance from the wall to the point where the velocity differed from the free stream value by one percent. Further, the eddy diffusivity profile was bridged across the peaks as explained in chapter 5.

Comparison of predicted and measured impervious-wall effectiveness.

Fig. 6.1.2 (a) to (h) show predicted and measured values of the impervious-wall effectiveness for eight values of the velocity ratio, ranging from 0.37 to 3.12 and for a density ratio of unity. The experimental data, shown by the solid circles are present measurements for air injection through a 2.54 mm-plane slot (apparatus A, chapter 4). This slot had a tapered lip and for present purposes can be considered as a lip of vanishing effective thickness. The diagrams are plotted on a semi-logarithmic axes and unlike Fig.5.2.4, the predictions extend from the slot exit. It can be seen that the agreement between the predictions and experiment is, on the whole, good. This is true even for the case of velocity ratio in the vicinity of unity((d) and (e)). For the lowest velocity ratio ($\bar{u}_C/u_G = 0.37$), the predictions are pessimistic in the initial region but agree with the experimental data further downstream. For the two highest velocity ratios, the predictions overestimate the effectiveness far down -stream. In fact the predicted effectiveness for a constant downstream distance is practically the same for velocity ratios greater than about 1.2, whereas the experimental values decrease slightly with increasing velocity ratio. It may be noted that this decrease has been observed only for unobstructed slots with thin lips ($t/y_C \leqslant 0.4$) (30), (79). In spite of this deficiency, the predictions are acceptable. It may be noted that the two-layer model (45) did indicate a decrease of effectiveness with an increase of velocity ratio in excess of unity. However, the predictions shown in Fig.6.1.2 are to be preferred, in view of their better agreement with experiment especially for velocity ratios in the vicinity of unity.

Fig.6.1.3 shows similar computations for cases of density ratios greater than unity. Fig.6.1.3 (a) to (d) show predicted and measured impervious-wall effectiveness for the injection of argon through the slot; this corresponds to a density ratio of 1.38. Figure 6.1.3 (e) to (h) relate to a density ratio of 4.17, obtained by the injection of Arcton-12. Again the agreement between the predictions and experiment is satisfactory: the predictions differ from experiment by less than ten percent of unity. In most cases there is a tendency for the predictions to slightly underestimate the effectiveness far downstream.

Predictions for the case of density ratios much less than unity (for example hydrogen injection, which resulted in a density ratio 0.069) present a special difficulty, since the flow is likely to be not fully turbulent in the initial region, due to the low Reynolds numbers. Predictions obtained by assuming fully turbulent flow, with the eddy viscosity and diffusivity augmented with the laminar values are shown for four velocity ratios in Fig.6.1.4. It can be seen that the predictions are of the right order, but tend to over estimate the effectiveness in the downstream region. It is possible that for low Reynolds numbers, the turbulent Schmid number may be appreciably influenced by the laminar value (0.22 for hydrogen diffusing into air). The mixing length distribution is also likely to be significantly different from the one assumed here. For such a possibility to be examined, detailed information of the velocity and concentration profiles as well as the wall-shear stress are needed. Such information is not available at present. Light-gas injection has no immediate film cooling application and so the prediction of hydrogen-injection-data will not be pursued further in this study.

Before proceeding to examine the influence of other variables, it is instructive to examine briefly the predictions for the above data for density ratios greater and equal to unity, obtained from some of the empirical correlations mentioned in the literature survey of chapter 2. Three of these are of particular interest: that of Spalding et. al. (65), Stollery and El-Ehwany (71) and that developed by the Lucas Gas-turbine Equipment Ltd. (36). The expression of reference (65) is chosen in view of its validity for velocity ratios greater and less than unity, and that of reference (71) for its theoretical foundation. The Lucas correlation has been included in view of its wide use in industry.

Predictions of the impervious-wall effectiveness obtained from the above correlations for the initial conditions appropriate to the present data are shown in Fig.6.1.5 (a) to (p). It should be mentioned that the expression of reference (65) has been generalised to non-uniform density cases by replacing the velocity ratio $\bar{u}_C/u_G$, by the mass-velocity ratio, m. The following conclusions can be drawn concerning the agreement of these predictions with the present measurements. For the uniform density case, the Lucas correlation seems to give the best agreement with the data, except for the lowest velocity ratio, where it tends to over estimate the effectiveness. For the lowest velocity ratio, the boundary layer model of Stollery and El-Ehwany gives good agreement, but the predictions from this model deteriorate rapidly with increasing velocity and density ratio. The correlation of Spalding et. al. appears to give good predictions for the uniform density case, for velocity ratios not close to unity. For the higher velocity ratios, the correlation of Spalding et. al. tends to overestimate the so called 'poten -tial core' region by a significant amount. The predictions for the cases with density ratios greater than unity show greater discrepancies and all except the data for the lowest velocity ratio for argon are poorly predicted with the correlations of references (65) and (71). Also the Lucas correlation greatly under estimates the effectiveness for velocity ratios greater than about 0.5. Thus the general conclusion that can be drawn regarding these three correlations is that they provide acceptable predictions in certain limited ranges of velocity and density ratios, but that outside these ranges, the predictions are poor. In particular the Lucas correlation can under estimate effectiveness by about 25 percent of unity for density ratios greater than unity and x/y_C of approximately 30.

6.2 Influence of the slot lip thickness on effectiveness.

In specifying the velocity profile at the slot exit, the region hehind the slot lip was represented by a region of low forward velocity of corresponding width. Computations of adiabatic-wall effectiveness for a constant velocity ratio and varying lip thickness indicated very little influence of this parameter. This is contrary to the experimental findings of references (30) and (63), which report a significant decrease in effectiveness with increase of the slot lip thickness-to-height ratio. The discrepancy between predicted and experimental trends can be attributed partly to the turbulent exchange hypothesis and partly to the use of the boundary layer equations in the vicinity of the slot. The former reason seems to be more important: an increase in the lip thickness leads to higher turbulent kinetic energy in the mixing layer behind the lip (as substantiated by the measurements of reference (31)). One would expect on the basis of the hypothesis of Prandtl and Kolmogorov (eq.5.0.4) that the eddy diffusivity (and hence the mixing) would consequently increase and result in a lowering of the effectiveness. The mixing length theory does not indicate a marked increase in the diffusivity, since the velocity gradients are not very different for the thick and thin lips. Thus logically one must abandon the simple mixing-length theory and adopt a more general theory of turbulence, which would, amongst other things, predict quantitatively, the observed decrease of effectiveness with an increase in the slot lip thickness. Unfortunately such a model of turbulence is not yet forthcoming: the higher order models of turbulence invariably need a greater number of empirical constants whose specification and generality is, to date, in a nebulous state. Thus one is tempted to retain the mixing length concept, particularly in view of satisfactory predictions for the thin- lip configuration. It is however necessary to introduce further empiricism with respect to the eddy diffusivity, such that the predictions of effectiveness accord with experiment. One such attempt will be described presently. It is based in the notion that there is a relationship between tha eddy diffusivity downstream of the lip and the lip-thickness to slot-height ratio. The other tacit requirement is that the effect due to the lip diminishes in the streamwise direction. Thus one could, as a first approximation, merely add to the eddy diffusivity specification used in the last section, a term which is related to the lip thickness and which diminshes in the downstream direction.

The present procedure for enhancing the diffusivity in the wake region in indicated in Fig.6.2.1. Γ_o represents the effective viscosity or diffusivity profile resulting from the Prandtl mixing-length hypothesis, as modified by the bridging procedure described in chapter 5.2.3. In the region between the two outer peaks of the eddy diffusivity profiles, an additive diffusivity Γ_{add} is imposed to represent the effect of the lip thickness. Γ_{add} is computed from a form of the eddy viscosity hypothesis suggested by Prandtl (58) for free flows:

$$\Gamma_{add} = \frac{\xi}{\sigma_t} \rho \, \ell_w u_w \qquad , \qquad 6.2.1$$

where ξ represents a function to be specified empirically, ℓ_w is a characteristic width and u_w is a characteristic velocity of the wake. In the region between the two inner peaks of the diffusivity profile, the diffusivity is assumed to vary linearly from the value at the innermost peak to the augmented value at the adjacent peak. Thus the resulting eddy diffusivity profile is continuous across the layer and exhibits an increased value on the wake region behind the lip. The additive term Γ_{add} decreases to zero as the wake disappears.

The next problen is the specification of the quantities in equation 6.2.1. ρ is taken as the local density, which therby permits the application of the above expression to cases of non-uniform density; ℓ_w is taken as the distance between two points near the edges of the wake region where the velocity differs from the free stream and velocity maxima by one percent, and u_w is taken as the velocity difference between the minimum velocity in the wake and the mean of the free stream and velocity maxima (see Fig.6.2.1). As mentioned above ξ is a quantity to be specified empirically. It would be convenient for example, to obtain a relation between ξ and the lip thickness to slot height ratio, which would result in satisfactory predictions of the adiabatic-wall effectiveness over a useful range of velocity ratios. An attempt has been made to obtain this function by trial and error, so as to obtain agreement with the measured values of effectiveness for the data of Kacker and Whitelaw (30) for the following range of variables:

$$0.13 < t/y_C < 1.1 \quad ,$$
$$1.0 < x/y_C < 100 \quad ,$$
$$0.75 < \bar{u}_C/u_G < 2.3 \quad ,$$

and $$\rho_C/\rho_G = 1.0 \quad .$$

This may be considered a useful practical range of variables for film cooling application, except that the density ratio is frequently greater than unity. The following power-law relationship between ξ and t/y_C has been found to yield reasonable predictions of the impervious-wall effectiveness:

$$\xi = 0.28\,(t/y_C)^2 \qquad . \qquad 6.2.2$$

According to this expression ξ varies from 0.0047 to 0.34 for the range of t/y_C indicated above.

Predictions of the impervious-wall effectiveness obtained with the above expression for ξ in conjunction with the eddy diffusivity distribution described in Fig.6.2.1 are shown in Fig.6.2.2, along with the experimental data from reference (30). Predictions and measured values of effectiveness for five values of lip thickness ratio and five values of the velocity ratio are shown in this figure. The predictions for the velocity ratio up to 1.27 and t/y_C of 0.63 are highly satisfactory. For the highest velocity ratio, the predictions overestimate the effectiveness in the far downstream region ($x/y_C > 70$). The predictions for the largest value of t/y_C (of 1.14) can be considered satisfactory for all the velocity ratios, but the predictions for t/y_C equal to 0.89 are conservative for velocity ratios greater than unity. The experimental data for this lip thickness (0.89) and the largest velocity ratio shows a rather unexpected (high) value of effectiveness around 30 slot-heights downstream.

In general, the ability of the above simple expression for ξ to provide acceptable predictions over such a range of velocity and lip thickness is encouraging. However, its ultimate utility depends on its ability to predict data from other sources, with or without density gradients. It may be noted that the present data discussed in the previous section, were obtained in a plane two-dimensional slot with tapered lip, whose effective thickness is not known. In light of the present predictions indicating the effect of lip thickness, such a tapered lip is suggestive of a vanishing effective lip thickness. Further available data will now be examined.

Fig. 6.2.3 (a) to (g) shows measured and predicted values of the adiabatic-wall effectiveness for a density ratio of 0.93. The data points are present measurements made in an axisymmetric flow configuration presented in chapter 4.4 (apparatus B). The slot-lip thickness to height ratio was 0.35 for all the runs except the data indicated by the square symbols in (b) and (f). These correspond to tests conducted with a lip insert which resulted in a lip-thickness ratio of unity. Predictions corresponding to a value of t/y_C of 0.35 and a value of ξ obtained from equation 6.2.2 are shown as full lines. These predictions agree very satisfactorily with the experimental values, except for the lowest and highest velocity ratios, where the predictions tend to overestimate the effectiveness by about 10 percent of unity. The discrepancy for the largest velocity ratio ($\overline{u}_C/u_G$ = 3.54) is not surprising as the present procedure does not predict a significant lowering of effectiveness for velocity ratios in excess of unity. The discrepancy for the lowest velocity ratio is rather unexpected as this suggests an effect of the circumferential radius of curvature for low velocity ratios which is contrary to the predicted trend: the broken line in Fig.6.2.3 (a) represents a prediction for a plane slot with identical initial conditions. The measurements are not sufficiently detailed to explain this discrepancy. The chain - dotted lines in (b) and (f) represent predictions corresponding to a slot lip thickness to height ratio of unity. Agreement with the measurements, represented by the square symbols, is satisfactory for distances greater than 20 slot-heights. Thus the predictions shown in Fig.6.2.3 (a) to (g) lend further support to the prediction procedure described in this chapter.

Finally, Fig.6.2.4 (a) to (i) show predicted and measured effectiveness for the data of Seban (60), Samuel and Joubert (56), Burns and Stollery (5),(6). For the tapered lip of references (56), (5) and (6), the value of ξ has been calculated from equation 6.2.2 corresponding to a small lip thickness (t/y_C of 0.1). The predictions for the thin lip cases and all the density ratios are satisfactory. The preditions for the data of Burns and Stollery (6) for a value of t/y_C of unity (see Fig 6.2.4 (f),(g) and (i)) are fair only for velocity ratios less than 0.5. For the two higher velocity ratios, the predictions over-estimate the detrimental influence of the lip thickness. This would suggest that for large density and velocity ratios the simple formula given by equation 6.2.2. fails to give acceptable predictions. However, the density ratio for Arcton 12 is 4.17, which is greater than that likely to be found in gas turbine practice. It would therefore be interesting to examine the largest value of density and velocity ratio for which the present procedure will provide acceptable predictions. Beyond these limiting values the empirical expression, eq. 6.2.2, will have to be modified and further free parameters introduced. This has not been attempted at present.

It is, however, interesting to note the predicted influence of the density ratio on effectiveness for various lip thickness ratios, on the basis of equation 6.2.2. Fig. 6.2.5(a) shows the predicted values of effectiveness at a distance of 32.5 slot-heights corresponding to a velocity ratio of 0.8 and for three values of the lip thickness ratio (t/y_C = 0.2, 0.5 and 1.0), plotted against the density ratio. Fig. 6.2.5(b) shows similar predictions for a velocity ratio equal to 1.5 and a slot Reynolds number of 5000. The predictions indicate, as one would expect, that the influence of the lip thickness ratio decreases with increasing density ratio. This trend is more pronounced at the larger velocity ratio. Further judgement on the validity of equation 6.2.2 should await additional experimental data for a range of density ratios between 1 and 4, in order to confirm or negate the accuracy of the trends predicted in this figure.

In making the above predictions, the thickness of the boundary layer on the outer surface of the lip ($y_{G,C}$) was chosen to correspond with the experimental value, where available. The present procedure indicates a lowering of effectiveness with increasing thickness of the boundary layer. This trend is in accord with the measurements of Kacker and Whitelaw (27). The predictions indicate that the effect of the boundary layer thickness is significant for $y_{G,C}/y_C$ less than about 2.5. For the value of this ratio greater than about 3, the predicted effectiveness appears to be only weakly dependent on this quantity. The predicted influence of $y_{G,C}$ is greater than that indicated by the measurements of ref. (27). However, these predictions refer to a thin lip configuration, whereas the measurements of reference (27) correspond to a lip-thickness to slot-height of 0.42. It is possible that for values of this parameter above a certain value, the influence of the lip boundary layer diminishes and the influence of the lip thickness itself becomes the controlling factor.

6.3 Prediction of heat transfer in presence of film cooling:

So far the predictions have been made for an adiabatic- or impervious-wall boundary condition, but frequently film cooling is accompanied by heat transfer at the wall. If the thermal boundary condition at the wall is known a priori, a prediction of the unknown quantity can be readily made using the prediction procedure of reference (49). For example, if the heat flux at the wall is prescribed, the wall temperature can be predicted using the prediction procedure, or vice-versa. Thus, the conventional concept of a heat-transfer coefficient becomes unnecessary. However, in some situations, neither the heat flux at the wall nor the wall temperature is known in advance, and in such situations, it is convenient to define and compute a heat transfer coefficient based on the adiabatic-wall temperature. The adiabatic-wall temperature has thus to be initially computed: this follows readily from a prediction of the adiabatic-wall effectiveness on the lines outlined in the previous section. For fluids with Prandtl number close to unity and for small values of the heat flux at the wall, the heat transfer coefficient defined in the above manner is likely to be independent of the wall temperature or heat flux distribution. Thus, a possible sequence for the computation of the heat transfer coefficient corresponding to a set of initial conditions at the slot exit is as follows: first, a prediction of the adiabatic-wall temperature is made on the lines outlined in the previous two sections, and the values stored as a function of the distance from the slot. Next, a calculation of the wall temperature is made, commencing from the slot exit and corresponding to a (arbitrary) constant heat flux at the wall. The heat-transfer coefficient can then be readily calculated.

Calculations in this sequence were carried out corresponding to the initial conditions of runs 1 to 7 with the axisymmetric test-section (Apparatus B, chapter 4) and a realistic boundary condition. A constant heat flux equal to 630 W/m^2 extending from the slot exit was used for the computations. A check calculation with a heat flux equal to 950 W/m^2 yielded practically the same values of the heat transfer coefficient, thus confirming the insensitivity of this quantity to the magnitude of the heat flux for the range of the experiments. The mixing length constants were the same as used previously.

The results of these calculations are shown in Fig. 6.2.3. along with the experimental data which are shown as points: (a) to (g) display the predicted and measured adiabatic-wall effectiveness which have been discussed in the previous section. (h) to (i) show the streamwise distribution of the heat-transfer coefficient (expressed as a Nusselt number based on the slot height and conductivity at slot temperature) for the initial conditions indicated in (a) to (g). For distances greater than about ten slot heights, the agreement between the predicted and measured heat-transfer coefficients is very satisfactory; the maximum discrepancy is of the order of 10 per cent. For distances less than ten slot heights, the measured values are below the predictions. At least part of the discrepancies in this region is due to the use of the parabolic equations in the vicinity of the slot. Another feature of interest is that for velocity ratios less than 1.3, both the measured and predicted heat transfer coefficients tend towards values which are lower than the fully-developed pipe flow values (indicated by the short dashed chain-dotted line) by some 15 per cent. For velocity ratios greater than 1.3, the predicted and measured heat transfer coefficients at a distance of 50 slot heights are higher than the fully-developed pipe flow values.

A further feature is that the predictions for the heat transfer coefficient for the thick lip case ($t/y_C = 1.0$) corresponding to (i) and (m) of Fig. 6.2.3 do not differ appreciably from the prediction for the thin lip case. For run 2 ($\bar{u}_C/u_G = 0.616$) this is in good agreement with the experimental finding and for run 6 ($\bar{u}_G/u_G = 2.88$) it is a reasonable approximation. The implication of this statement is that for a given wall-heat-flux, the departure from the prevailing adiabatic-wall temperature is independent of the lip thickness.

6.4 Influence of longitudinal pressure gradient on the effectiveness of film cooling:

The cases considered so far have been those of uniform, or nearly uniform, pressure. It is interesting to examine the predictions for the case where the flow downstream of the slot is either accelerated or decelerated. Experimental data for such flows was presented in chapter 4 for three favourable and one adverse pressure gradients. The main experimental findings were that the influence of moderate pressure gradients, both favourable and adverse ($K_p = \pm 1.0 \times 10^{-6}$) and for density ratios equal or greater than unity, was quite small. Decreases in effectiveness of around ten per cent were recorded and the effect was less for velocity ratios greater than unity. For the case of the large pressure gradient ($K_p = 3.3 \times 10^{-6}$), the flow was no longer fully turbulent and the reversion towards a laminar state occurred. For this case, a larger decrease in effectiveness for velocity ratios less than unity was observed.

Predictions of impervious-wall effectiveness with initial conditions corresponding to the experiments, described in chapter 4 (Apparatus A), with a variable free stream velocity were carried out. The free stream velocity was varied to keep the value of the parameter K_p constant and equal to the nominal values existing in the experiment. These computations indicated only a small effect of the pressure gradients on the effectiveness. In particular, a small increase in effectiveness with favourable pressure gradients (about 3 per cent of local value at $x/y_C = 32.5$ and $K_p = 3.3 \times 10^{-6}$) for velocity ratios less than unity was indicated. For the higher velocity ratios, the predicted effect was less than 1 per cent. Thus, the insensitivity of the predicted effectiveness to favourable pressure gradients is in keeping with the experimental observations for the moderate pressure gradient PG1($K_p \approx 1.0 \times 10^{-6}$), though the trend for low velocity ratios is opposite to that observed. The reason for this behaviour may be found by examining the energy equation which is repeated here in Cartesian coordinates:

$$u\frac{\partial h}{\partial x} + \underset{\rightarrow o}{v\frac{\partial u}{\partial y}} = -\frac{\partial}{\partial y}\frac{\mu_{eff}}{\sigma_{eff}}\frac{\partial h}{\partial y} + \underset{\rightarrow o}{\chi\left(\frac{\partial^2 h}{\partial x^2} + \frac{\partial^2 h}{\partial y^2}\right)} + \underset{\rightarrow o}{\nu\Phi_D} \cdot$$

For an adiabatic wall in the presence of turbulent flow, the molecular transport terms may be neglected near the wall. Also, for an adiabatic wall, both $\partial h/\partial y$ and v may be expected to be small in the vicinity of the wall. Thus the predominant terms near the wall are the x-wise convection and the turbulent diffusion term. The latter may be expected to increase in a favourable pressure gradient since the (dimensional) velocity gradient increases and the eddy viscosity, given by the mixing-length theory is proportional to the velocity gradient. However, the increase in the eddy viscosity due to an increase in du/dy would be partially off-set by a decrease in the characteristic length, y_G. The gradient of h in the y-direction is unlikely to be sensitive to the pressure gradient, since dp/dx does not appear in the energy equation. Thus, it follows that an increase in the diffusion term is compensated by an increase in u on the left-hand side, leaving $\partial h/\partial x$ relatively unaltered near the wall. The effectiveness is of course directly influenced by $\partial h/\partial x$.

For the large pressure gradient, PG3 ($K_p \approx 3.3 \times 10^{-6}$) the predictions are at greater variance with the experimental observations; the latter indicate a deerease in effectiveness of the order of 20 percent of the local value at a distance of 32.5 slot-heights. For such values of K_p, the flow is no longer fully turbulent and, in fact, is undergoing reverse transition to laminar flow. The use of the mixing length hypothesis in the manner used for fully turbulent flow in this situation is incorrect and undoubtedly is the major cause of thes discrepancy between prediction and experiment. The transport hypothesis valid for such flows is not fully known. It is to be expected that the laminar viscosity and the laminar Schmidt number will play an increasing role as the reverse transition progresses. It should ne noted that the laminar Schmidt number for helium (which was used as a tracer in the experiments) is around 0.22 and so the effective Schmidt number could have been significantly lower than unity for the low Reynolds numbers prevailing in such flows. This would explain tha fact that the predictions using an effective Schmidt nuber of unity over estimate the effectiveness for the strong favourable pressure gradient case. Thus satisfactory prediction of film cooling with strong favourable pressure gradients would appear to be possible only after a fuller understanding of the process of relaminarisation and a realistic exchange hypothesis for such phenomena is available. The flow downstream of a film cooling slot is not a suitable one for a fundamental study of this phenomenon since the distribution of velocity and shear stress across the layer are complex. Such a study is best carried out in a simple boundary layer flow of the equilibrium type (33).

The predictions for the adverse pressure gradient ($K_p \approx -1.0 \times 10^{-6}$) indicate a small decrease (about 2 percent at x/y_C of 32.5) in effectiveness for velocity ratios less than unity. For velocity ratios greater than unity, the decrease in effectiveness is less than one percent. Thus the predicted trends are in accord with experimental observations, though the predicted effect of adverse pressure gradient is lower than the measured one for low velocity ratios. On the above basis, the present procedure appears to be satisfactory for predicting the effectiveness of film cooling in the presence of moderate favourable or adverse pressure gradients. It is not, however, in its present form suitable for flows with favourable pressure gradients which are strong enough to cause retransition to laminar flow.

6.5 Review of predicted trends.

A number of aspects of film cooling with two dimensional slots operating under controlled conditions have now been dealt with. It is appropriate to review the contents of the thesis so far, before proceedigg to an examination of practical applications of film cooling. The modified Patankar-Spalding prediction procedure has been used for predicting the flow development starting from the slot exit. The Prandtl mixing-length hypothesis has been used, taking the width of the whole layer as the characteristic length and a bridging procedure for the eddy diffusivity, to overcome the unrealsitic result of zero eddy diffusivity at a zero-velocity-gradient location. Integration of the momentum and species (or enthalpy) conservation equations was commenced from the slot exit, using realisitic profiles of velocity and mass fraction (or enthalpy). The appropriate boundary conditions were imposed: these comprised an adiabatic or a heated wall on one side and a free stream with constant or varying fluid-velocity on the other. Density variations within the flow, resulting either from temperature or mass fraction variations were taken into account. The downstream development of the flow was computed and in particular, predictions of the impervious- or adiabatic- wall effectiveness and the heat-transfer coefficient (based on the adiabatic-wall temperature) were made. Comparison of predictions with available data for these quantities was carried out in order to asses the utility of the procedure using the mixing-length constants selected in chapter 5. A summary of this exercise follows presently.

A representative selection of predictions and relevant experimental data are cross plotted in Fig.6.5.1 to show the influence of the variables considered in this chapter. Fig.6.5.1 (a) shows the predicted and measured influence of velocity ratio on the impervious-wall effectiveness for three values of the distance from the slot. The data shown are present measurements for air injection through a plane two-dimensional slot (apparatus A). The smallest value of x/y_C shown in the figure (x/y_C of 32.5) corresponds to a measuring station and the largest distance that is likely to be of interest in gas turbine practice. The agreement between the predictions and the measurements is good throughout except for velocity ratios greater than about two, where predictions tend to over estimate the effectiveness. The predictions for velocity ratios in the vicinity of unity are also satisfactory.

Fig. 6.5.1 (b) indicates the influence of the slot to mainstream density ratio on the effectiveness for density ratios varying from 0.069 to 4.17. and for a velocity ratio of 0.8. The predicted trends agree well with the present measurements. There is however a tendency for the predictions to under estimate the effectiveness for large density ratios.

Fig. 6.5.1 (c) shows the effect of favourable and adverse pressure gradients for constant density flows: the ratio of effectiveness in the presence of pressure gradients to the zero-pressure- gradient-value is plotted against the velocity ratio for a value of x/y_C of 32.5. The predictions are essentially insensitive to the pressure gradients: for velocity ratios less than unity, a small increase (about 2 per cent) in effectiveness is predicted for favourable pressure gradients ($K_p \leqslant 3.3 \times 10^{-6}$) and a small decrease of the same order for the adverse pressure gradient ($K_p \approx -1 \times 10^{-6}$) is indicated. The predicted trend is thus in accord with with the present experimental data for adverse pressure gradient, though the predicted effect is smaller than the observed one for velocity raios less than unity. For moderate favourable pressure gradients ($K_p \leqslant 1 \times 10^{-6}$), the insensitivity of the predicted effectiveness is again in agreement with the measurements, but for the strong pressure gradients ($K_p > 2 \times 10^{-6}$), the predictions on the basis of turbulent flow are inadequate.

Fig. 6.5.1 (d) shows the influence of lip thickness on the impervious-wall effectiveness at a density ratio of unity and a velocity ratio of 0.8. The data points correspond to the measurenents of Kacker and Whitelaw (30), interpolated for the values of the velocity ratio and x/y_C shown. The predictions were obtained with an empirical procedure to enhance the eddy diffusivity behind the lip in relation to lip thickness. to slot height ratio. Briefly, the diffusivity was augmented with a value obtained from Prandtl's formula for mixing layers (eq.6.2.1). The multiplying coefficient in this expression was empirically related to the lip thickness (eq.6.2.2) so as to give good predictions of effectiveness for a particular set of experimental data (30), which covered a useful range of velocity ratios and lip thicknesses. Prediction of data from other sources yielded mixed results: the present data with a plane slot and a tapered lip (assumed to have a nominally zero effective lip thickness) as well as present data with the axisymmetric slot configuration with a lip thickness ratio of 0.35 and 1.0 are well predicted, except for the lowest and the highest velocity ratios. Prediction of the data of Burns and Stollery (5), (6), for a plane slot with a tapered lip and a density ratio of 1.38 and 4.17 respectively are satisfactory, and so are the predictions for the data of Seban (60), Samuel and Joubert (56). However, the predictions for the recent data of Burns and Stollery (6) for a density ratio of 4.17 and a lip thickness ratio of unity are poorly predicted. This suggests that the present procedure would have to be modified for the case of high density and velocity ratios. Sufficient data to place upper limits of the velocity, density and lip thickness ratio for the present procedure do not exist.

Fig.6.5.1 (e) shows the predicted and measured influence of velocity ratio on the heat transfer coefficient (expressed as a Nusselt number based on the slot height and the conductivity at slot temperature) for the values of x/y_C. The data are present measurements obtained with the axisymmetric flow configuration (apparatus B) with a heated wall. Again, the agreement between the prediction and experiment is very satisfactory, the largest discrepancy being of the order of 10 percent. The predictions are insensitive to an increase of the lip thickness, a fact which is borne out by the experiments.

Fig.6.5.1 (f) shows the influence of the thickness of the boundary layer on the outer surface of the lip ($y_{G,C}$) for a velocity ratio of 0.8 and a density ratio close to unity for three values of x/y_C. The predictions indicate that the effect of the boundary layer thickness $y_{G,C}$ diminishes for ($y_{G,C}/y_C$) greater than about 3, and is significant for values of this ratio below about 2.5. The present data with apparatus A, the data of references (30)($t/y_C = 0.128$), (60) and (56) support the predicted trends for a range of $y_{G,C}/y_C$ from 0.8 to 7.0. These data correspond to relatively thin lip configurations, and the agreement with the present predictions seems to suggest that the thickness of the boundary layer is significant for such geometries.

6.6 Film cooling in gas turbines.

The discussion so far has mainly been concerned with film cooling through unobstructed two-dimensional slots in low turbulence wind tunnels and in the absence of combustion. It is important however, to examine the conditions under which film cooling slots have to operate in practice, for example in gas turbine combustion chambers or reheat nozzles of aircraft engines. The object of the present discussion is two-fold. First, to place the thermal aspects of film cooling in perspective by identifying the importance of the various parameters involved, and second, to define the relevance of the prediction procedures of the type discussed in the previous section.

The flow inside a flame tube of a gas turbine combustion chamber is characterised by the following features, not normally present in wind tunnels in which film cooling slots are tested:

a) large radiative heat-fluxes,

b) three-dimensional flow resulting form assymetry and irregularities in the geometries and pressure field,

c) periodicity in the flow caused by instabilities in the recirculating-flow pattern,

d) large gradients of temperature and concentration in the radial direction due to combustion and mixing in the primary and dilution streams.

Thus the flow is of a very complex nature and, particularly in view of (c) above, any time averaged quantity has to be regarded with caution. Although the solution of the flow 'in toto' is unlikely to be accomplished in the near future, the prediction of the mean wall-temperature and other time-mean properties is a feasible and challenging task.

The temperature assumed by the flame tube is such that the heat received by it through radiation and convection from the interior of the chamber is balanced by the heat loss to the surroundings by convection and radiation. For practical purposes the following equation represents this heat balance:

$$\underbrace{\sigma_B\left(\frac{1+\epsilon_W}{2}\right)\ \epsilon_G T_G^{1.5}\left(T_G^{2.5}-T_W^{2.5}\right)}_{R_1} + \underbrace{h_1(T_{a,W}-T_W)}_{C_1}$$

$$= \underbrace{\sigma_B\left(\frac{1}{\frac{2}{\epsilon_W}-1}\right)\ (T_W^{4}-T_C^{4})}_{R_2} + \underbrace{h_2(T_W-T_C)}_{C_2} \qquad 6.6.1$$

The major empiricism and simplification in the above equation is involved in the gas radiation term, R1. The derivation of this term is discussed in reference (34) and assumes, among other things, that

$$\frac{\alpha_W}{\epsilon_G} = \left(\frac{T_G}{T_W}\right)^{1.5} \quad ,$$

where ϵ_G is the flame emissivity at flame temperature and α_W is the flame absorptivity at wall temperature. The effects of reflection and re-radiation at the wall are approximately allowed for by terms$(1+\epsilon_W)/2$. For simplicity, equation 6.6.1 assumes the equality of the emissivities of the flame tube and the outer casing (ϵ_W) and that the outer casing is at a temperature T_C.

It is convenient to consider the wall-temperature (T_W) as being directly determined by the seven quantities appearing in equation 6.6.1, viz. the adiabatic-wall temperature, $T_{a,W}$ (determined by the adiabatic-wall effectiveness, η), the flame and coolant temperatures (T_G and T_C), the two convective heat-transfer coefficients (h_1 and h_2) and the two emissivities (ϵ_G and ϵ_W). Some idea of the relative importance of these quantities can be obtained from Fig. 6.6.1, which shows the variation of the wall temperature as each of these quantities is varied in turn from a set of datum values indicated in the same figure. The abscissa at the bottom of the figure indicates the values of these variables as a fraction of the datum, and the corresponding dimensional values are shown by the scales at the top. The datum values chosen may be considered representative of conditions existing at some point within a modern high-compression-ratio aero engine. The wall temperature was computed from equation 6.6.1 by an iterative solution procedure.

It can be seen from Fig. 6.6.1 that the wall temperature is strongly dependent on the gas temperature, T_G, and the adiabatic-wall effectiveness, η. The least important factor appears to be the emissivity of the wall, while the influence of the two heat-transfer coefficients and the flame emissivity are comparable in magnitude and on a percentage basis, equal to about a fourth of the influence of the effectiveness and gas temperatures. If one assumes an error of $\pm$ 10 per cent in each of the quantities, the worst resulting error in the wall temperature would be about $\pm 155^{\circ}C$ (i.e. about 16 per cent of datum value). Conversely, if one wishes to predict the wall temperature to say within $\pm 20^{\circ}C$ (i.e. 2 per cent of datum), all the controlling quantities (except the emissivity of the wall) need to be known to an accuracy better than 2 per cent. This is undoubtedly a stringent requirement.

It should be noted that the trends shown in Fig. 6.6.1 refer to a particular set of datum conditions. Trends for other datum conditions are likely to be similar, except for a particular case when the effectiveness is close to unity and a large radiation flux is present. In such a case, the direction of the convective heat flux inside the flame tube can be reversed (i.e. into the main stream) and a high heat-transfer coefficient in fact decreases the wall temperature.

The computational or experimental uncertainties in these seven factors will now be briefly discussed. The adiabatic-wall effectiveness and the two convective heat transfer coefficients can, in principle, be obtained from the prediction procedure described earlier in this chapter. As mentioned previously, the adiabatic-wall effectiveness is influenced by a number of factors including the velocity and density ratio, the geometry of the injection region and to a lesser extent, by pressure gradients. The prediction procedure described earlier has been shown to provide reasonably good predictions for two-dimensional slots with and without density and pressure gradients, and to a limited extent, the effect of the slot lip thickness to height ratio. However, slots used in practice are not two-dimensional and have a significant and complex effect of geometry. The present procedure, without modification, is therefore unlikely to provide satisfactory predictions for such geometries. The deficiencies of the present procedure may be judged from the example given later in this section. The film-heat-transfer coefficient,on the other hand, appear to be a weak function of the lip thickness, at least for the case of unobstructed slot described in chapter 4. Thus, predictions of the heat-transfer coefficients on the film-cooled surface obtained with the present procedure, can probably be used, unless three-dimensional effects are dominant. The heat-transfer coefficient on the outer surface of the flame-tube can also be obtained as a first approximation from the boundary-layer prediction procedure. Here a suitable boundary condition which does not differ a great deal from the actual one would have to be assumed. Of course the flow in the annulus between the flame tube and outer casing is not strictly two-dimensional, especially for tubo-annular arrangements and near dilution holes.

The next important factor is the flame emissivity. There is considerable uncertainty in its value, especially at high pressures (say thirty atmospheres). The gas emissivity is a function of the pressure, temperature, the fuel and its burning characteristics. The current industrial practice seems to be its evaluation from an empirical formula due to Reeves, referenced in (34). However, reliable experimental data for this quantity at typical engine conditions is urgently needed. It is conceivable that the value given by the empirical expression may be in error by as much as 100 per cent, the resulting error in the wall temperature being about 55°C for the datum conditions shown in Fig. 6.6.1.

Finally, the two gas temperatures, the mainstream and coolant temperatures need to be known accurately for the wall temperature to be computed. The compressor delivery temperature is probably a good approximation to the coolant temperature at least for the cooling strips near the primary zone. Estimation of the flame temperature,on the other hand, is fraught with uncertainties. The practice of obtaining the flame temperature from the overall fuel-air ratio and an assumption of the combustion efficiency is probably too crude. The best procedure at present seems to be the use of experimentally determined values using, for example, an aspirated probe. Again such data is scarce and generally of a restricted nature. Even if such data were available, the problem still remains as to the radial station at which the gas temperature should be measured. It would be reasonable to expect that since the layer near the wall is transparent to radiation, the flame temperature used in the radiation term of equation 6.6.1 should correspond to the core of the flame tube, whereas the gas temperature for the convection term should correspond to the temperature at the edge of the boundary layer (i.e. the film).

A sample calculation was conducted corresponding to a practical combustion chamber with a wiggle strip geometry. The adiabatic-wall effectiveness and the heat transfer coefficient were computed using the prediction procedure mentioned earlier in the chapter. The slot height was taken equal to the maximum opening of the wiggle strip gap, and the lip thickness equal to that of the wiggle strip material. The predicted wall temperatures were some 300°C lower than the thermal paint results of Rolls Royce Ltd. (54). This is not surprising, as the predicted values of effectiveness correspond to unobstructed slots, whereas wiggle strips are known to yield much lower values of effectiveness. Further, the flame temperatures were calculated on the basis of overall fuel-air ratio and assumed combustion efficiency. These could be significantly in error: no direct measurements of the flame temperature were available.

6.7 Suggestions for future research in film cooling

The example above serves to stress the point that there is still a big gap before the prediction of mean wall temperatures of a film-cooled surface, such as the flame tube of a combustion chamber, can be achieved with any degree of confidence. The two main regions of uncertainty are (a) the effectiveness of practical slot geometries under operating-engine conditions, and (b) the gas conditions existing inside the combustion chamber. Future research should be mainly directed towards the examination of these two aspects. The present state of knowledge with two-dimensional slots in laboratory conditions is a useful starting point for the above goal, but is not the end in itself.

The two items mentioned above will now be discussed in turn. First, the question of the adiabatic-wall effectiveness for practical geometries. Fig. 6.6.1 indicates that there is considerable incentive for achieving high values of effectiveness, as the wall temperature varies almost linearly with effectiveness. The problem here is not so much the acquisition of experimental data (although even this is hard to come by) but to devise a method of predicting the performance of practical devices. This can be done from first principles only when a solution procedure for time-dependent elliptic equations in three dimensions becomes available. Until such time, one would need to use considerable empiricism in any prediction procedure. In chapter 6.2 it was shown that it is possible to allow for one geometrical variable viz. the slot lip thickness to height ratio within the framework of the present prediction procedure for two-dimensional flows. It may be possible to extend this procedure to practical geometries by introducing the concept of an equivalent two-dimensional slot. Thus, for a given practical slot geometry, a value of y_C and t/y_C corresponding to a two-dimensional slot of similar performance would have to be found. The effectiveness for the two-dimensional slot with a finite lip thickness can be found using, for example, the procedure outlined in chapter 6.2.

There is some similarity between the performance of practical slots and two-dimensional slots with thick lips ($t/y_C \geqslant 0.5$). For example, neither show a decrease in effectiveness for velocity ratios greater than unity. It is probably worth investigating this similarity further by comparing the performance of a specific practical slot and 2-D slots with varying lip thickness ratio. A design change in the practical device would be reflected in a change in the values of the 'equivalent clean slot' but the extent of the change cannot be predicted without experience. For example, if the pitch of a wiggle strip is altered, fresh data for the new design would be needed to determine the new value of the equivalent clean slot. The only advantage of this concept would be that relatively few parameters would be sufficient (two if equation 6.6.2 is used, or only one if a value of ξ in equation 6.2.1 for a given geometry, is chosen directly) to characterise the performance of a practical cooling strip over a range of velocity and density ratios. This is an attractive proposition and should, in the author's opinion, be explored further. Plots of the type shown in Fig. 6.5.1(d) (i.e. effectiveness plotted against t/y_C for constant values of x/y_C) would aid in the determination of the equivalent t/y_C. It should be a relatively straightforward procedure to check if the value of ξ (equation 6.2.1) chosen is satisfactory for the desired range of velocity and density ratios, provided reliable experimental data for the practical geometry are available.

The other aspect of the effectiveness of film cooling which needs investigation is the observation (by personnel of the Rolls Royce Ltd., Derby and Bristol) that the effectiveness of cooling strips under 'engine conditions' is different (worse) than in rig tests. It would be worthwhile to perform cold tests with a modified practical combustion chamber to determine the causes of this discrepancy. In particular, realistic density gradients could be achieved for the cold test by foreign gas injection in the secondary stream (the flow splitter at the inlet to the combustion chamber would have to be blanked off to permit independent control of the primary and secondary streams) and the impervious-wall effectiveness of the cooling strips determined by gas samples drawn through static-pressure holes drilled in the wall of the flame tube. Further, such cold tests would permit a better estimation of the flow pattern within the chamber and, in particular, the velocity ratio prevailing at the cooling strip could be measured accurately. Such a test will provide the much-needed information about the performance of cooling strips under realistic conditions and in the absence of radiation. It would then be possible to assess the effects due to the radiation term independently: at present one of the major difficulties is to determine the proportion of the discrepancy between measured and predicted wall temperatures which is due to error in the prediction of effectiveness and that due to incorrect gas temperatures and emissivities.

Another item which needs further investigation is the determination of the flow properties inside the combustion chamber. In particular, more accurate methods for measuring the gas temperatures and gas emissivity need to be devised and the spatial variations of these quantities within the chamber need to be measured. It also seems worthwhile to attempt to use the solution procedure of reference (19) to determine the temperature and velocity field on an analytical basis. This would probably be more accurate than the current practice of obtaining the gas temperatures from the overall fuel-air ratio and an assumed combustion efficiency.

The task of predicting the wall temperatures of a practical film-cooled surface should become more hopeful when the distributions of the gas temperature, velocity and emissivity within the chamber are known more accurately, and the science of predicting the effectiveness of practical devices, perhaps on the lines indicated here, is more advanced.

REFERENCES.

1. BADRINARAYANAN, M.A. and RAMJEE, V. : On the criteria for reverse transition in a two-dimentional boundary layer flow. J. Fluid Mech. 35, 2 (1969).

2. BAKER, P.J. : Heat tranfer in a supersonic parallel diffuser. J. of Mech. Eng. Sci. 7, 1 (1965).

3. BLOM, J and deVRIES, D.A. : On the value of the Turbulent Prandtl number. Proc. of the 3rd All Union Heat and Mass Transfer Conference, Minsk. Paper No. 1.8 (1968).

4. BRADSHAW, P and GEE, M.T. : Turbulent wall jets with and without an external stream. A.R.C., R & M 3252,(1962).

5. BURNS,K and STOLLERY,J.L. : Film cooling: The influences of foreign gas injection and slot geometry on impervious-wall effectiveness. Imperial College, Dept. of Aero., Rep. EHT/TN/12 (1968).

6. BURNS, W.K. and STOLLERY, J.L. : The influence of lip thickness on the impervious-wall effectiveness of a wall jet with foreign gas injection. Imperial Coll. Dept. of Aero. , EHT/TN/19, (1969).

7. CARLSON, L.W. and TALMOR, E. : Gaseous film cooling at various degrees of hot gas acceleration and turbulence levels. Int. J. of Heat and Mass Transfer, 11, 1695, (1968).

8. CHIN, J.H., SKIRVIN, S.C., HAYES, L.E. and SILVER, A.H. : Adiabatic wall temperatures downstream of a single, tangential injection slot. A.S.M.E., Paper 58-A-107 (1958).

9. CLAUSER, F.H. : The turbulent boundary layer. Advances in App. Mech., IV, 1. Academic Press, N.York (1956).

10. COLE,E.H., SPALDING, D.B. and STOLLERY, J.L. : Film cooling effectiveness calculated by a finite-difference procedure. Imperial Col. Rep. EHT/TN/3 (1967).

11. DEDMAN, deFORGE, A.S. and MARTIN, B.W. : Effects of secondary injection on the characteristics of a supersonic parallel diffuser. J. of Mech. Eng. Sci. 10, 5 (1968).

12. ECKERT, E.R.G. and DRAKE R.M. (Jr): Heat and Mass Transfer. McGraw-Hill, (1959).

13. ECKERT, E.R.G. and BIRKEBACK, R.C. : Effects of slot geometry on film cooling. Heat Transfer Thermodynamics Education (Boelter anniversary vol.) McGraw-Hill Book Co. (1964).

14. ESCUDIER, M.P. : The distribution of the mixing length in turbulent flows near walls. Imperial Coll., Dept. of Mech. Eng. Rep. TWF/TN/1 , (1965).

15. ESCUDIER, M.P. and WHITELAW,J.H. : The influence of strong adverse pressure gradients on the effectiveness of film cooling. Int. J. of Heat and Mass Transfer, 11, 1289 (1968).

16. ESKINAZI, S. and KRUKA, V. : The wall jet in a moving stream. J. Fluid Mech. 20, 555, (1964).

17. GARTSHORE, I.S. and HAWALESHKA, O. : The design of a two-dimensional blowing slot and its application to a turbulent wall-jet in still air. McGill Univ. Mech. Eng. Res. Labs., Tech Note 64-5 (1964).

18. GOLDMAN,J.B. and MARCHELLO, J.M. : Turbulent Schmidt numbers. Int. J. Heat and Mass Transfer 12, (1968).

19. GOSMAN, A.D., PUN, W.M., RUNCHAL, A.K., SPALDING, D.B. and WOLFSTEIN,W. : Heat and Mass Transfer in recirculating flows. Academic Press (1969).

20. GOLDSTEIN, R.J., ECKERT. E.R.G., TSOU, F.K. and HAJI-SHEIKH, A., : Film cooling with air and helium injection through a rearward-facing slot into a supersonic air flow. A.I.A.A., J., 4 , 6, 981 (1966).

21. HARTNETT, J.P. : Experimental distribution of the thermal-entrance length for the flow of water and oil in circular pipes. Trans. A.S.M.E., 77, 1211 (1955).

22. HARTNETT, J.P., BIRKEBACK, R.C. and ECKERT, E.R.G.: Velocity distributions, temperature distributions effectiveness and heat transfer for air injection through a tangential slot into a turbulent boundary layer. A.S.M.E., J. of Heat Transfer 83,293 (1961).

23. HARTNETT, J.P., BIRKEBACK, R.C. and ECKERT, E.R.G. : Velocity distributions, temperature distributions, effectiveness and heat transfer in cooling a surface with a pressure gradient. A.S.M.E., Int. Dev. in Heat Transfer, Part IV, 682 (1961).

24. KESTIN, J, MAEDER, P.F. and WANG, H.E. : Influence of turbulence on the transfer of heat from plates with and without a pressure gradient. Int. J. of Heat and Mass transfer 3, (1961).

25. KESTIN, J. and RICHARDSON, P.D. : Heat transfer across turbulent, incompressible boundary layers. Int. J. of Heat and Mass Transfer, 6, 147 (1963).

26. KREITH, F. : Principles of Heat Transfer. Int. Text Book Co., Scranton (1958).

27. KACKER, S.C. and WHITELAW, J.H. : The dependence of the impervious-wall effectiveness of a two-dimensional wall-jet on the thickness of the upper lip boundary layer. Int. J. of Heat and Mass Transfer, 10, 1623 (1967).

28. KACKER, S.C., And WHITELAW, J.H. : Some properties of the two-dimensional turbulent wall-jet in a moving stream. A.S.M.E., J. of App. Mech., Trans.,35,4 (1968).

29. KACKER, S.C., PAI, B.R., and WHITELAW, J.H. : The prediction of wall-jet flows with particular reference to film cooling. Prog. in Heat and Mass Transfer, Vol.2, Eckert presentation vol. Pergamon Press (1969).

30. KACKER, S.C. and WHITELAW, J.H. : An experimental investigation of the influence of slot-lip-thickness on the impervious wall effectiveness of the uniform density, two-dimensional wall jet. Imperial Coll., Dept. of Mech. Eng. Rep. EHT/TN/13 (1968). To be published in the Int. J. of Heat and Mass Transfer.

31. KACKER, S.C. and WHITELAW, J.H. : The turbulence characteristics of two dimensional wall jet and wall wake flows. Imperial Coll., Dept. of Mech. Eng. Rep. BL/TN/6 (1969).

32. KLEIN, J. and TRIBUS, M. : Forced convection from non-isothermal surfaces. Heat Transfer, a sympssium, Univ. of Michigan, Ann Arbor, Michigan (1953).

33. LAUNDER, B.E. and STINCHCOMBE, H.S. : Non-normal similar turbulent boundary layers. Imperial Coll., Dept. of Mech. Eng., Rep. TWF/TN/21 (1967).

34. LEFEBVRE, A.H. and HERBERT, M.V. : Heat Transfer Process in Gas-Turbine combustion chambers. Proc. Inst. of Mech. Engrs. 174, 12 (1960).

35. LOCKWOOD, F.C. : Equilibrium-turbulent boundary layer prediction for a proposed Prandtl mixing length distribution. J. of Mech. Eng. Sci., 10, 5, (1968).

36. LUCAS GAS TURBINE EQUIPMENT, Res. Rep. B.48016 : The skin cooling process and flame tube temperatures.

37. McMILLAN, F.A. : Experiments on Pitot tubes in shear flow. A.R.C., R.&M. No. 3028 (1957).

38. METZGER, D.E., CARPER, H.J. and SWANK, L.R. : Heat transfer with film cooling near non-tangential injection slots. Trans., A.S.M.E., J. of Engineering for Power, Paper No. 67- WA/GT-1 (1967).

39. MUKERJEE, T. : Design and performance criteria for supersonic parallel diffuser-ejector systems. Univ. of London, Ph.D. Thesis, (1968).

40. MYERS, G.E., SCHAUER, J.J. and EUSTIS, R.H. : The plane turbulent wall-jet. Part II. Heat Transfer. Tech. Rep. 2, NSFG 9705, Thermosciences Div., Dept. of Mech. Eng. Stanford Univ. (1961)

41. NICOLL, W.B. and WHITELAW, J.H.: The effectiveness of the uniform density, two-dimensional wall jet. Int. J. Heat and Mass Transfer 10, 623 (1966).

42. NICOLL, W.B. : The turbulent wall jet: Its development and film-cooling effectiveness. Ph.D. Thesis, Univ. of London, Faculty of Engineering, (1967).

43. PAI, B.R. : Heat and Mass Transfer in Turbulent Boundary Layers - A Survey. Imperial Coll., Dept. of Mechanical Eng., Rep. TWF/TN/23 (1967).

44. PAI, B.R. and WHITELAW, J.H. : The influence of density gradients on the effectiveness of film-cooling. A.R.C., C.P. 1013 (1968).

45. PAI, B.R. : The application of the boundary-layer model to predict the influence of slot boundary conditions on film cooling. Imperial Coll., Dept. of Mech. Eng. Rep. EHT/TN/9 (1968).

46. PAI, B.R. and WHITELAW, J.H. : Simplification of the razor blade technique and its application to the measurement of wall-shear stress in wall-jet flows. To be published in the Aero-Quarterly.

47. PAI, B.R. and WHITELAW, J.H. : The influence of strong pressure gradients on film cooling. Imperial Coll. Dept. of Mech. Eng., Rep. EHT/TN/A/15.

48. PATANKAR, S.V. and SPALDING, D.B. : A calculation procedure for heat transfer by forced convection through two-dimensional uniform property turbulent boundary layer on smooth impermeable wall. Proc. of 3rd Int. Heat Transfer Conf., Chicago (A.I.Ch.E.) 11, (1966).

49. PATANKAR, S.V. and SPALDING, D.B. : Heat and Mass Transfer in Boundary Layers, Morgan-Grampian Press. (1967).

50. PATEL, R.P. and NEWMAN, J. : Self preserving, two-dimensional turbulent jets and wall jets in a moving stream. McGill Univ. Rep. Ae 5, (1961).

51. PATEL, V.C. : Calibration of the Preston tube and limitations on its use in pressure gradients. J. Fluid Mech., 23, (1965).

52. PATEL, V.C. and HEAD, M.R. : Reverse transition of turbulent to laminar flow. J. Fluid Mech. 34, 371 (1968).

53. REYNOLDS, W.C., KAYS, W.M. and KLINE, S.J. : Heat transfer in turbulent incompressible boundary layer. II - Step wall-temperature distribution. N.A.S.A. MEMO 12 - 2-58W (1958).

54. ROLLS ROYCE LTD., Aero Engine Division, Derby (Combustion Research Department): Private communication, (1969).

55. ROTTA, J. : Statische Theorie nicht homogenous Turbulenz. Z. Physik 129, 547 (1951).

56. SAMUEL, A.E. and JOUBERT, P.N. : Film cooling of an adiabatic flat plate in zero pressure gradient in the presence of a hot mainstream and cold tangential secondary injection. J. of Heat Transfer, Paper No. 64 WA/HT - 48, (1965).

57. SCHETZ, A.J. and GILREATH, H.E. : Tangential slot injection in supersonic flow. A.I.A.A., J. 5, 12 (1967).

58. SCHLICHTING, H. : Boundary layer theory. 4th Ed., McGraw Hill, N. York.

59. SEBAN, R.A., CHAN, H.W. and SCESA, S. : Heat transfer to a turbulent boundary layer downstream of an injection slot. A.S.M.E. Paper No. 57 - A- 36 (1957).

60. SEBAN, R.A. : Heat transfer and effectiveness for a turbulent boundary layer with tangential fluid injection. A.S.M.E., Journal of Heat Tranfer, 82 C, 303 (1960).

61. SEBAN, R.A. and BACK, L.H. : Velocity and temperature profiles in turbulent boundary layers with tangential injection. A.S.M.E., 84, 45-54 (1962).

62. SEBAN, R.A. and BACK, L.H. : Effectiveness and heat transfer for a turbulent boundary layer with tangential injection and variable free-stream velocity. A.S.M.E., J. of Heat Tranfer, 84 C, 235 (1962).

63. SIMPSON, R.L., WHITTEN, D.G. and MOFFAT, R,J. : An experimental study of the turbulent Prandtl number of air with injection and suction. Int. J. of Heat and Mass Transfer, 12 (1969).

64. SIVASEGARAM, S. and WHITELAW, J.H. : Film cooling slots; the importance of lip thickness and injection angle. J. of Mech, Eng. Sci. 11, 1, 22 (1969).

65. SPALDING, D.B., JAIN, V.K. and NICOLL, W.B. : Film cooling in incompressible turbulent flow: examination of experimental data for the adiabatic-wall temperature. A.R.C., REP. 25311 (1963).

66. SPALDING, D.B. : A unified theory of friction, heat transfer and mass transfer in the turbulent boundary layer and wall jet. A.R.C. CP 829 (1965).

67. SPALDING, D.B. : Lecture notes on turbulent jets, wakes and boundary layers. Imperial Col., Dept. of Mech. Eng. (1965).

68. SPALDING, D.B. : Monograph on turbulent boundary layers. Imperial Coll., Dept. of Mech. Eng., Report Nos. TWF/TN 24, 33, 34, 35, 37, 41. (1967 - 68).

69. SPALDING, D.B. : Private communication; Slip relations near boundaries. (1968).

70. SPALDING, D.B. : The calculation of the length scale of turbulence in some turbulent boundary layers remote from walls. Progress in Heat and Mass transfer, Eckert Presentation vol. 2, Pergamon Press. (1969).

71. STOLLERY, J.L. and EL-EHWANY, A.A. : On the use of a boundary-layer model for correlating film-cooling data. Int. J. of Heat and Msss transfer 10, 101 (1967).

72. STOLLERY, J.L. and EL-EHWANY, A.A. : A note on the use of a boundary-layer model for correlating film-cooling data. Int. J. of Heat and Mass Transfer, 8, 55 (1965).

73. TAILLAND, A. and MATHIEU, J. : Jet Parietal. J. de Mecanique, 6, 103, (1967).

74. van DRIEST, E.R. : On turbulent flow near a wall. J. Aero. Sci. 23, (1956).

75. WIEGHARDT, K. : On the blowing of warm air for de-icing devices. German ref. : FB No. 1900 (1944) - Zentrale f. wiss. Bericht. (ZWB).

76. WHITELAW, J.H. : Review of heat transfer literature pertaining to wall jets. Imperial Coll. Rep. IC/HRJ/25 (1965).

77. WHITELAW, J.H. : The effect of the geometry of the injection region on wall cooling processes. A.R.C. 27373, HMT. 78 (1965).

78. WHITELAW, J.H. : An experimental investigation of the two-dimensional wall jet. A.R.C. C.P. 942 (1967).

79. WHITELAW, J.H. : The effect of slot height on the effectiveness of the uniform density, two-dimensional wall-jet. Imperial Coll., Dept. of Mech. Eng., Rep. EHT/TN/4 (1967).

NOMENCLATURE.

SYMBOL	MEANING	UNITS
A_q	calibration coefficient of heat-flux meter. (Eq. A.2.1)	W/m²-deg C
c	mass-fraction of injected fluid	-
c_f	skin-friction coefficient $[2\tau_W/\rho u_G^2]$	-
C_p	specific heat at constant pressure	J/kg-deg C
E	constant in the law of the wall	-
h	specific (total) enthalpy	kcal/kg
h'	non-dimensional enthalpy $[h-h_G/h_W-h_G]$	-
h_f	convective heat transfer coefficient in the presence of film cooling	W/m²-deg C
h_1	convective heat transfer coefficient at inner surface of flame tube	W/m²-deg C
h_2	heat transfer coefficient at outer surface of flame tube	W/m²-feg C
H	shape factor; displacement to momentum thickness ratio	-
H_{32}	shape factor; kinetic energy to momentum - thickness ratio	-
J_h	diffusive enthalpy flux	W/m²
k	kinetic energy per unit mass of fluid associated with turbulent motion	-
K	constant in the law of the wall	-
K_p	pressure gradient parameter $[\nu/u_G^2 \cdot du_G/dx]$	-
ℓ	mixing length	m
ℓ_w	characterisitc length of the wake	m
m	slot to main-stream mass velocity ratio $[(\rho_C\bar{u}_C)/(\rho_G u_G)]$	-
$\dot{m}''$	mass flux	kg/s-m²
M	molecular weight	-
Ma	Mach number	-
Nu_C	Nusselt number $[h_f y_C/\kappa_C]$	-
p	static pressure	N/m²
p_o	stagnation pressure	N/m²
$\dot{q}''_W$	heat flux through the wall	W/m²
$\dot{q}''_{gen}$	heat flux generated	W/m²
R_2	momentum-thickness Reynolds number $[\delta_2 u_G/\nu]$	-
R_3	kinetic-energy thickness Reynolds number $[\delta_3 u_G/\nu]$	-

SYMBOL	MEANING	UNITS
R_C	slot-Reynolds number [$\bar{u}_C y_C/\nu$]	-
R_x	Reynolds number [$x u_G/\nu$]	-
R_j	rate of generation of species j	kg/ft²-s
$\bar{R}$	universal gas law constant	m²/s²-deg C
$\bar{s}$	shear work integral $\int_0^{y_G}(\tau/\rho u_G^2)\cdot(\partial u/\partial y)\cdot dy$	-
S	Stanton number (eq. A.2.2)	-
t	slot-lip thickness	m
T	absolute temperature	^oK
u	mean velocity in x-direction	m/s
u'	fluctuating component of velocity in the x-direction	m/s
u_W	characterisitc velocity of the wake	m/s
$\bar{u}_C$	mean velocity at slot exit $1/y_C\cdot\int_0^{y_C} u\cdot dy$	m/s
u_G	free stream velocity	m/s
u_{MAX}	velocity maximum	m/s
v	mean velocity in the y-direction	m/s
v'	fluctuating component of velocity in the y-direction	m/s
x	distance from the slot exit	m
X	correlating parameter, eqns. (2.2.1) and (2.2.2)	-
y	distance normal to the wall	m
y_{HALF}	distance from the wall where $(u-u_G)$ has half its maximum value	m
y_{MAX}	distance from the wall to the location where u is a maximum	m
y_C	slot height	m
y_G	velocity-boundary layer thickness	m
y_ℓ	characteristic width of boundary layer	m
Γ_o	effective diffusivity (Fig.6.2.1)	kg/m-s
Γ_{add}	additive diffusivity (Eq. 6.2.1)	kg/m-s
δ_1	displacement thickness $\equiv\int_0^{y_G}(1-\rho u/\rho_G u_G)\cdot dy$	m
δ_2	momentum thickness $\equiv\int_0^{y_G}\frac{(\rho u)}{(\rho_G u_G)}\left(1-\frac{u}{u_G}\right)\cdot dy$	m

SYMBOL	MEANING	UNITS
δ_3	kinetic energy thickness $\equiv \int_0^{y_G} \left(\frac{\rho u}{\rho_G u_G}\right)\left\{1 - \left(\frac{u}{u_G}\right)^2\right\} dy$	m
Δ_p	pressure gradient parameter $[-K_p (c_f/2)^{-3/2}]$	-
ϵ_G	emissivity of the flame	-
ϵ_o	emissivity of the combustion-chamber casing	-
ϵ_W	emissivity of flame-tube wall	-
η	effectiveness based upon the general conserved property φ	-
η_I	impervious-wall effectiveness	-
κ	thermal conductivity	W/m-deg C
λ	mixing length constant (eq. 5.1.1)	-
Λ	a measure of deviation (eq. 5.2.1)	-
$\overline{\Lambda}$	a mean value of Λ (eq. 5.2.2)	-
μ	laminar viscosity	Ns/m^2
μ_{eff}	effective viscosity	Ns/m^2
ν	kinematic viscosity	m^2/s
ξ	coefficient in eq. 6.2.1	-
ρ	fluid density	kg/m^3
σ	laminar Schmidt number	-
σ_B	Stefan-Boltzman constant	$W/m^2\text{-}^oK^4$
τ	shear-stress in fluid	N/m^2
φ	a conserved property	-
Φ	dissipation function (eq. 3.2.4)	-
ψ	stream function(defined by eq.3.4.3)	-
ω	non-dimensional stream function (eq.3.4.4)	-

SUBSCRIPTS.

W	pertaining to the wall
G	pertaining to the free stream
C	pertaining to the slot exit
a,W	pertaining to an adiabatic wall
I	inner edge
E	external edge
U	upstream station
D	downstream station; pertaining to pipe diameter
eff	effective (ie. laminar + turbulent)
t	turbulent

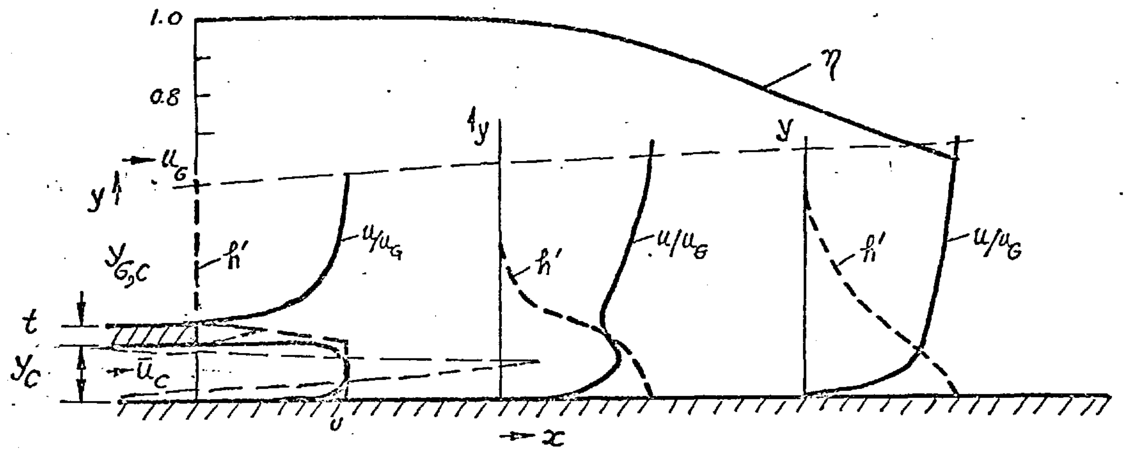

FIG. 3.1.1. THE FLOW DOWNSTREAM OF A FILM COOLING SLOT.

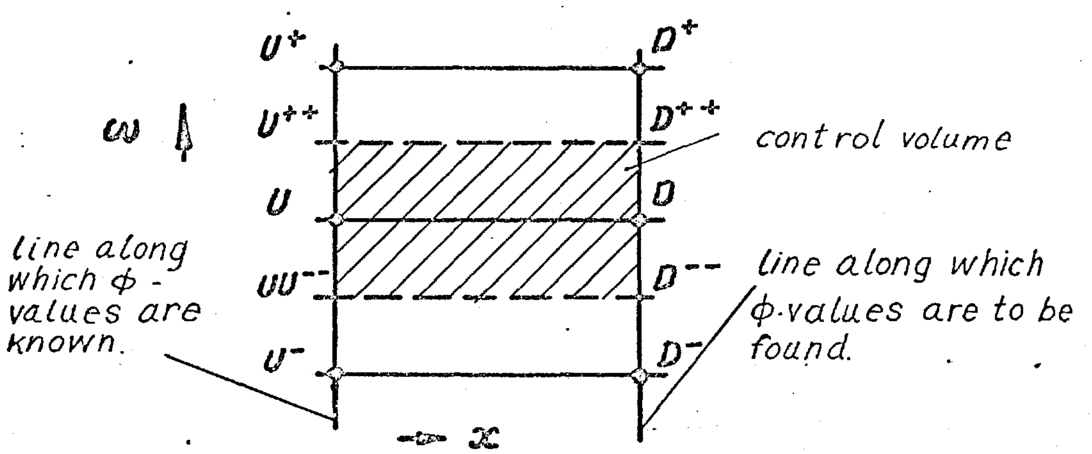

FIG. 3.4.1 THE $x-\omega$ GRID.

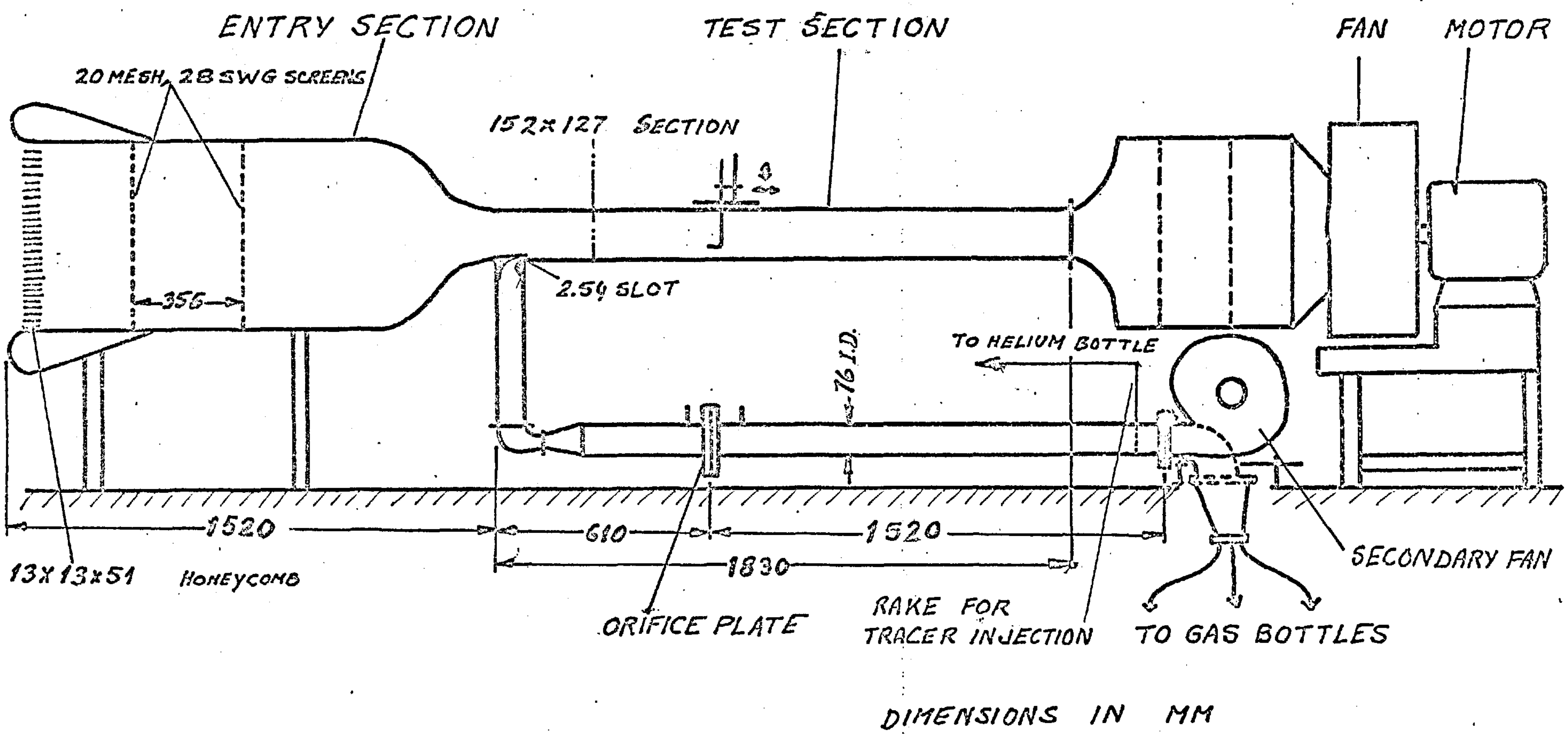

FIG 4.1.1. SCHEMATIC DIAGRAM OF APPARATUS-A

Fig. 4.1.2 (a) Entry section, apparatus A.

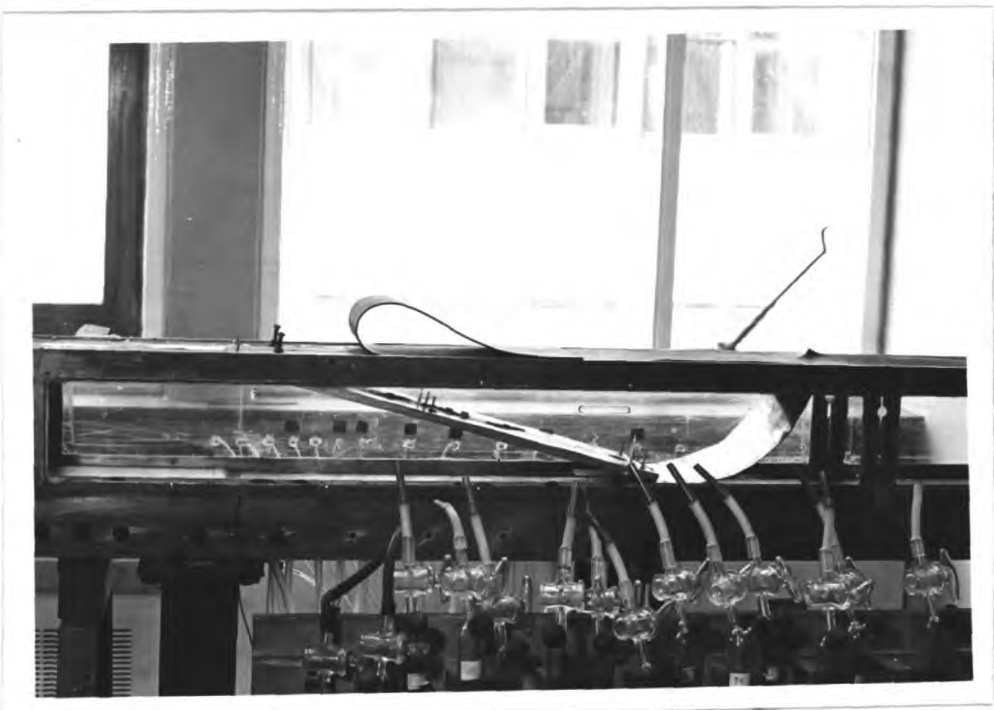

Fig. 4.1.2 (b) Test Section , apparatus A.

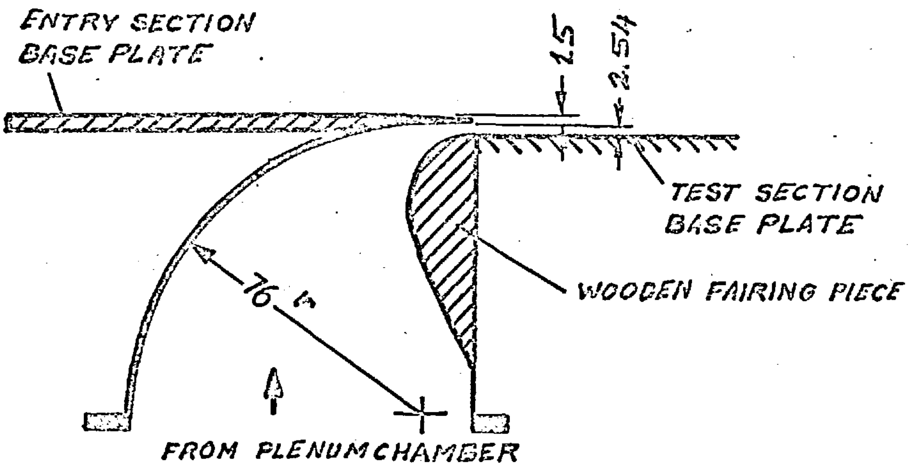

4.1.3. THE INJECTION SLOT

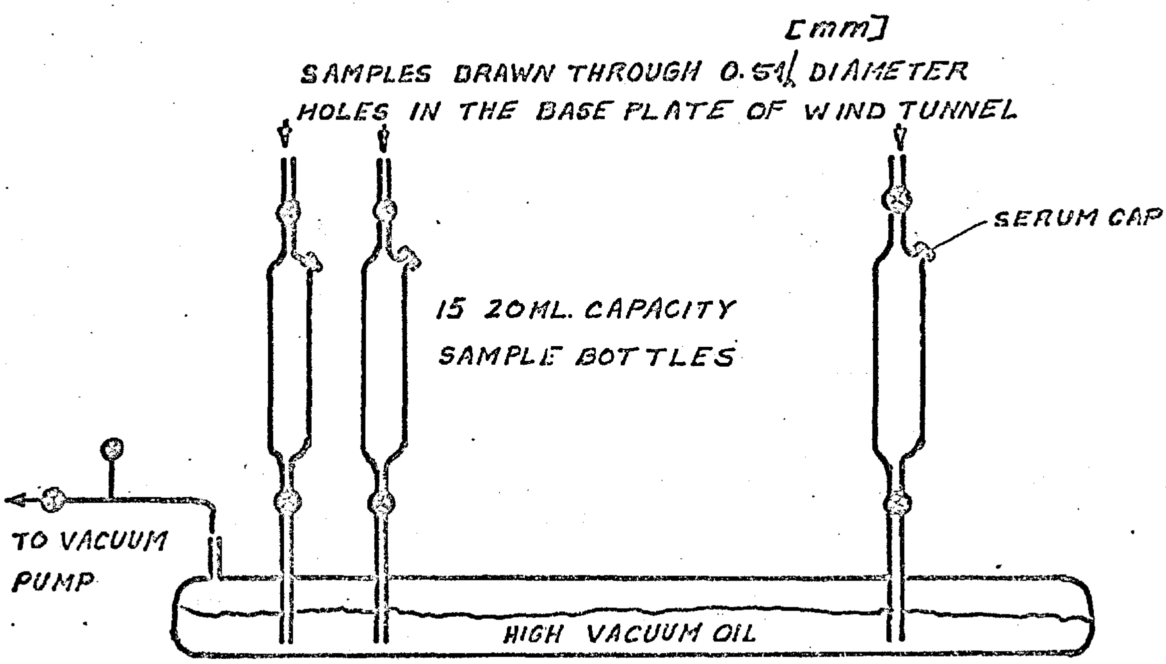

FIG.4.1.4. SAMPLING SYSTEM

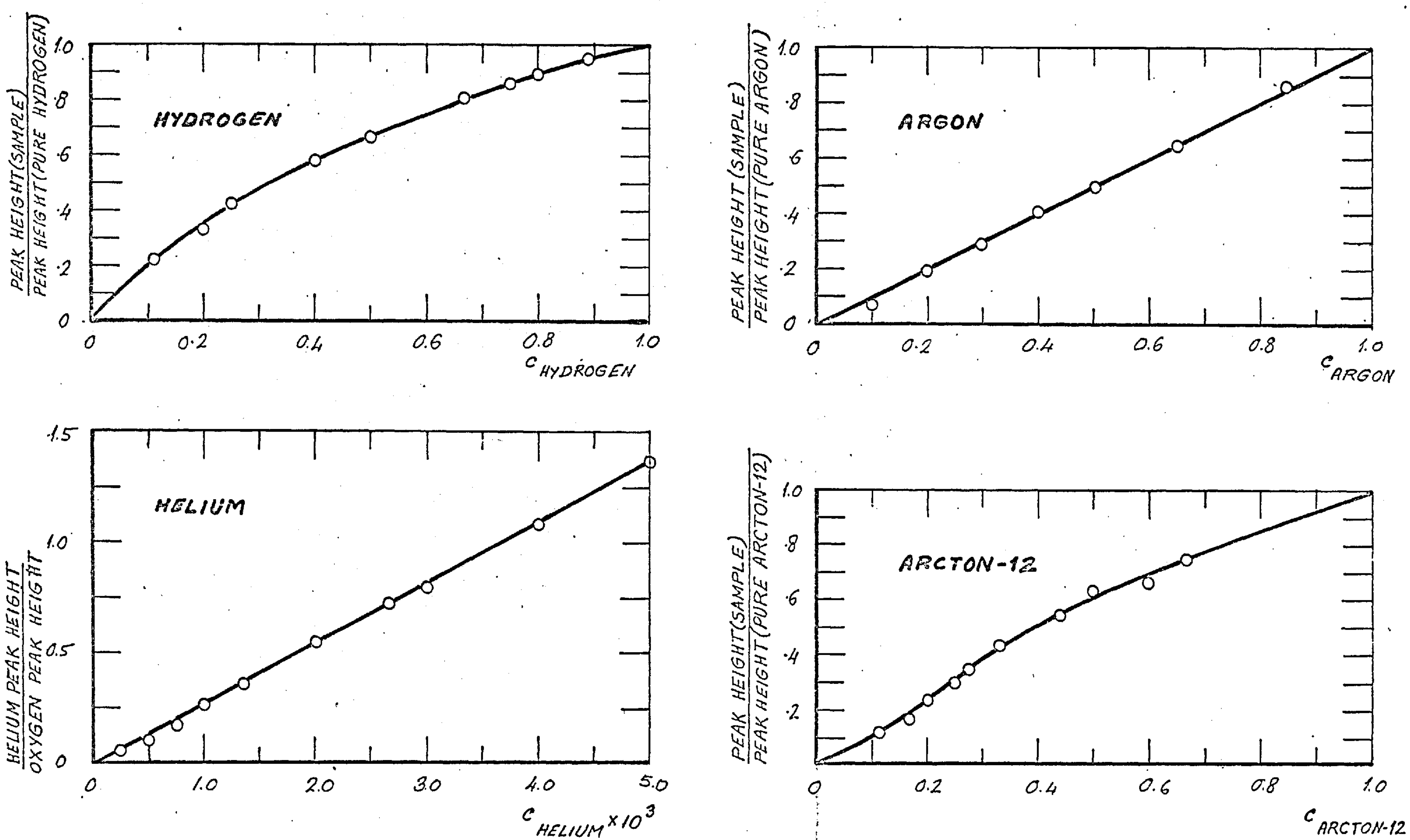

FIG. 4.1.5. TYPICAL CALIBRATIONS OF THE CHROMATOGRAPH. FOR ALL CALIBRATIONS, THE CARRIER GAS WAS NITROGEN, COLUMN TEMPERATURE - 55°C, FLOW RATE SETTING 38 (ON ROTAMETER), BRIDGE CURRENT - 130 mA.

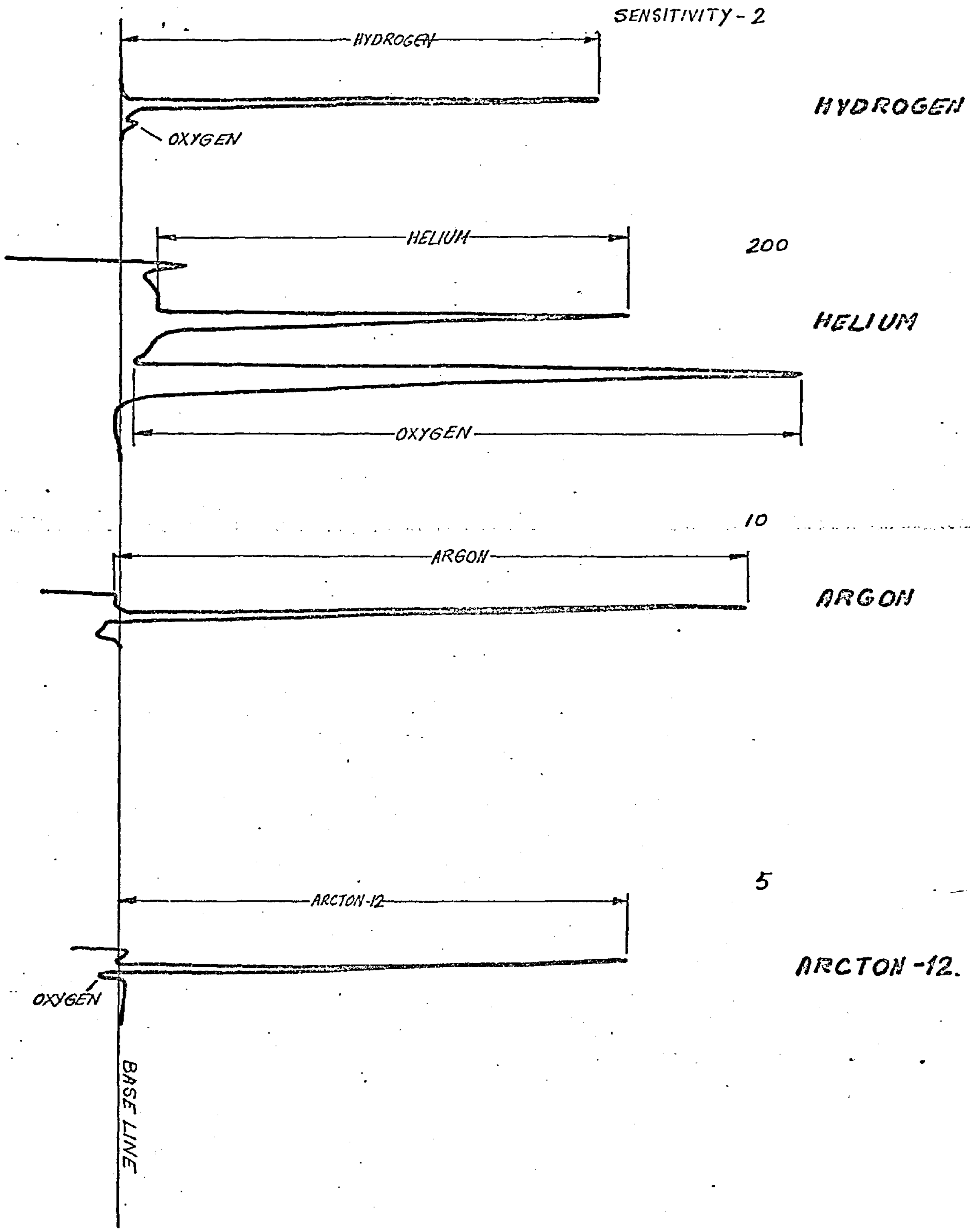

FIG. 4.1.6 TYPICAL CHROMATOGRAMS

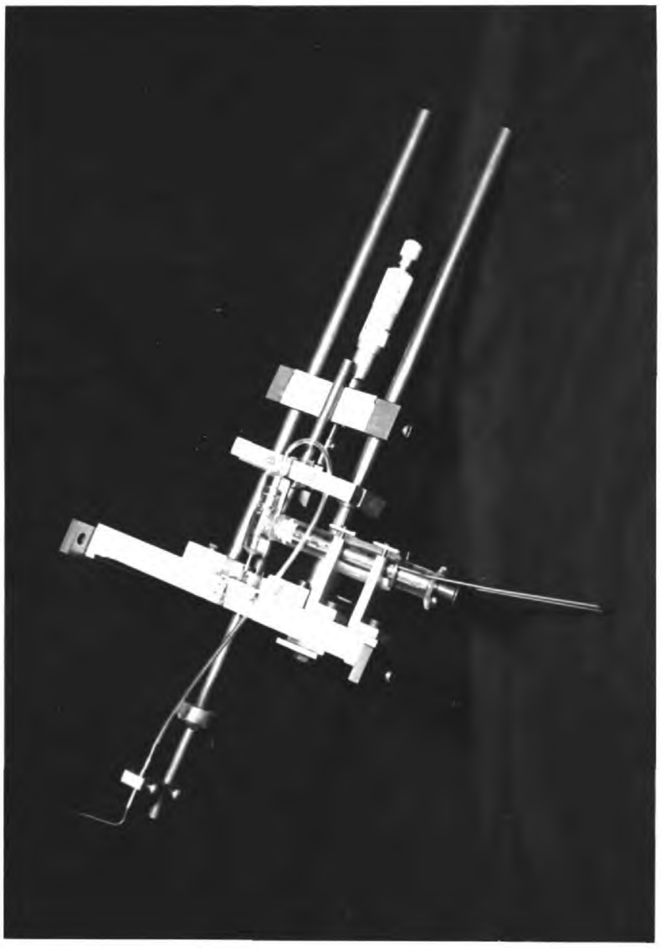

Fig. 4.1.7 The Traverse Gear.

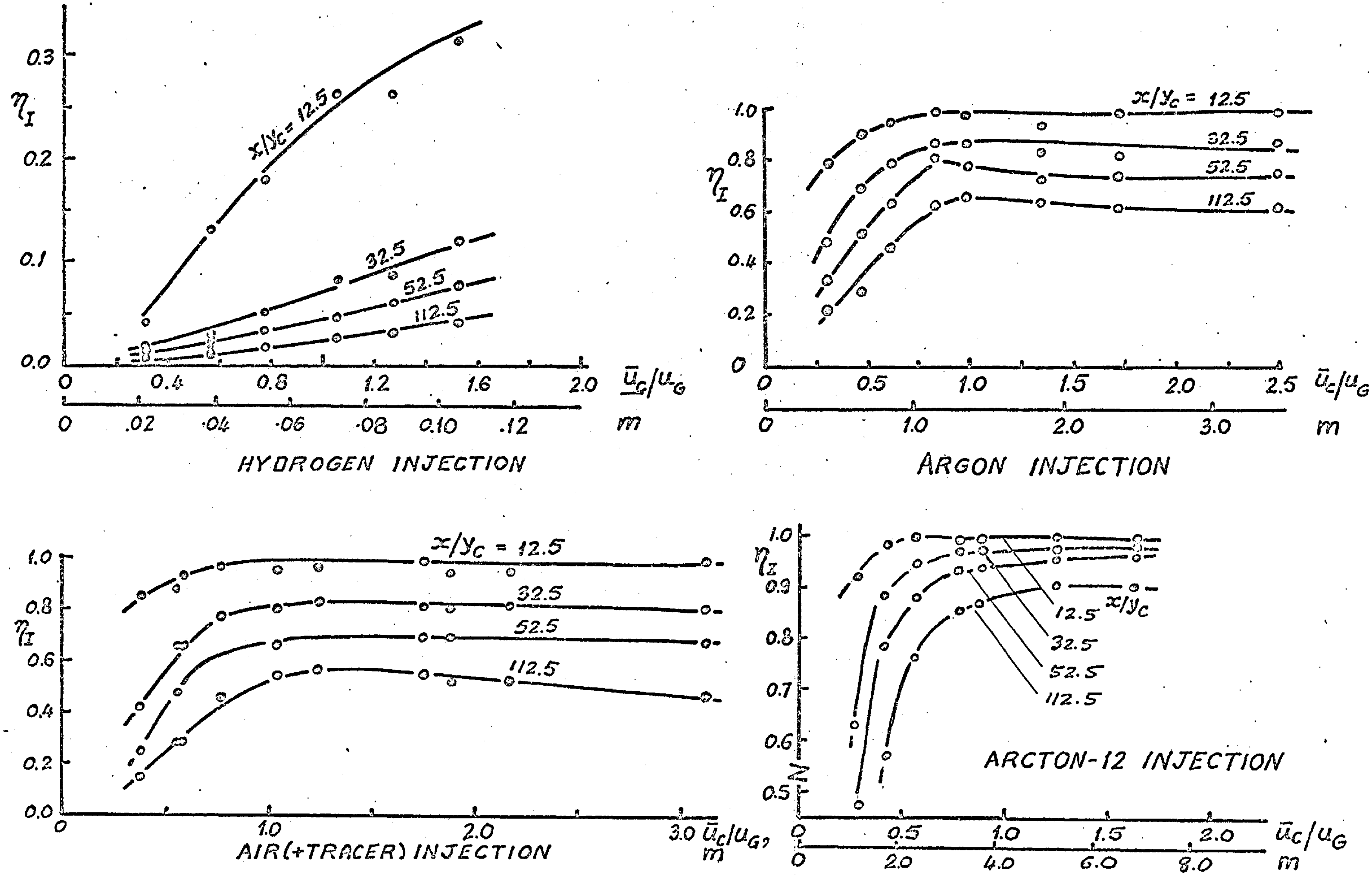

FIG. 4.2.1. MEASURED VALUES OF IMPERVIOUS WALL EFFECTIVENESS – η_I AGAINST $\bar{u}_c/u_G$

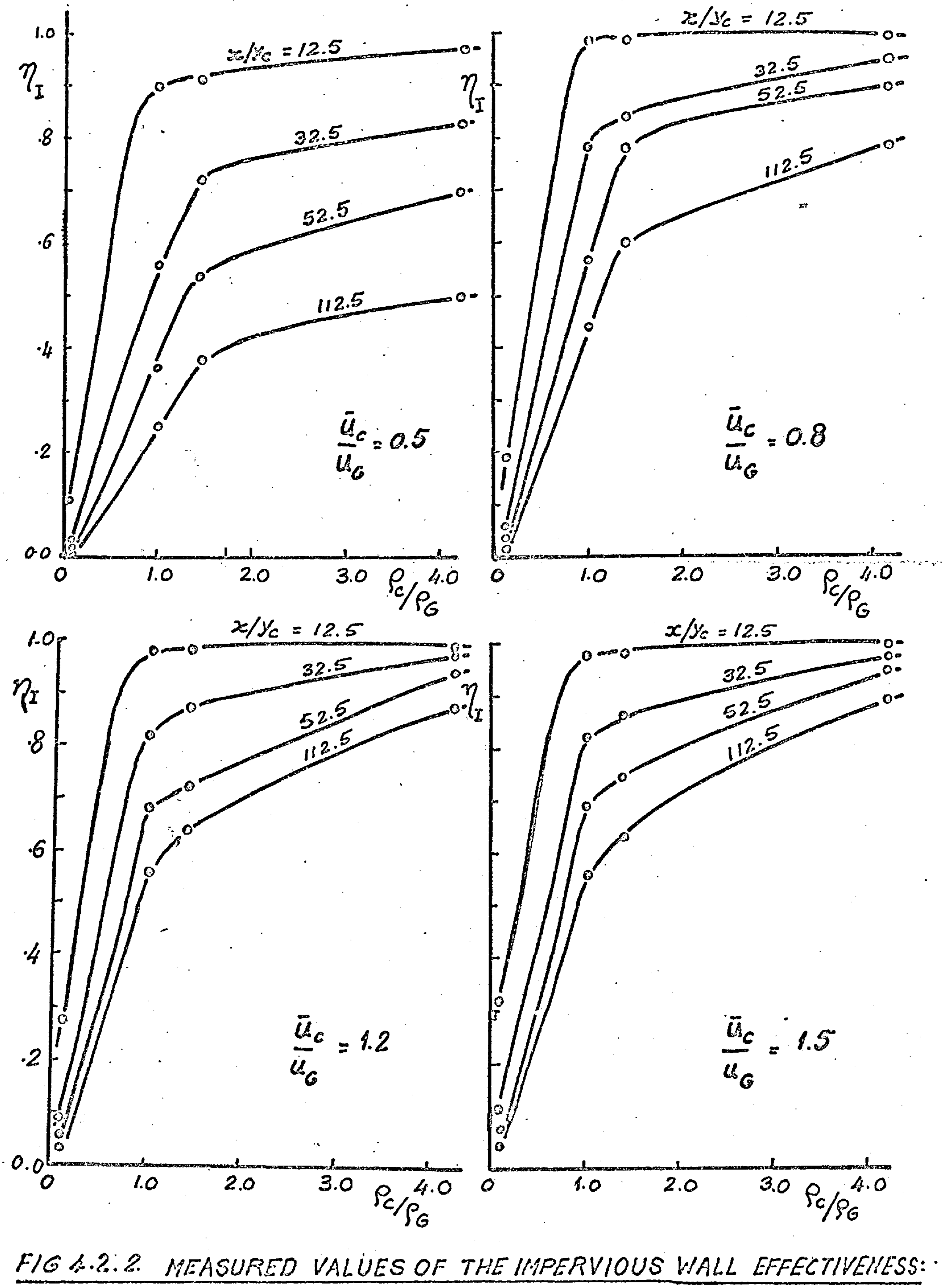

FIG 4.2.2. MEASURED VALUES OF THE IMPERVIOUS WALL EFFECTIVENESS: η_I AGAINST ρ_c/ρ_G

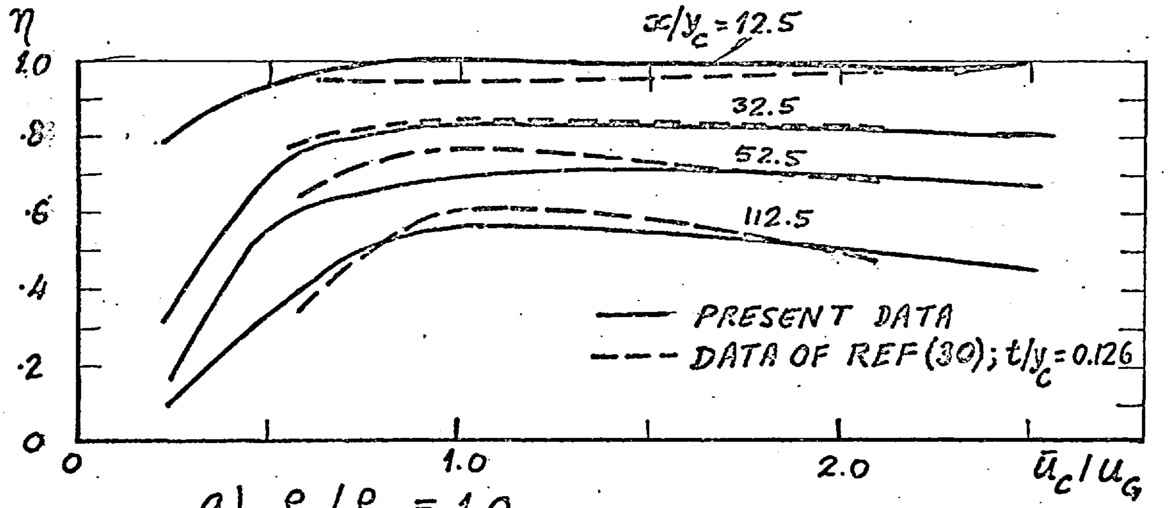

a) $\rho_c/\rho_G = 1.0$

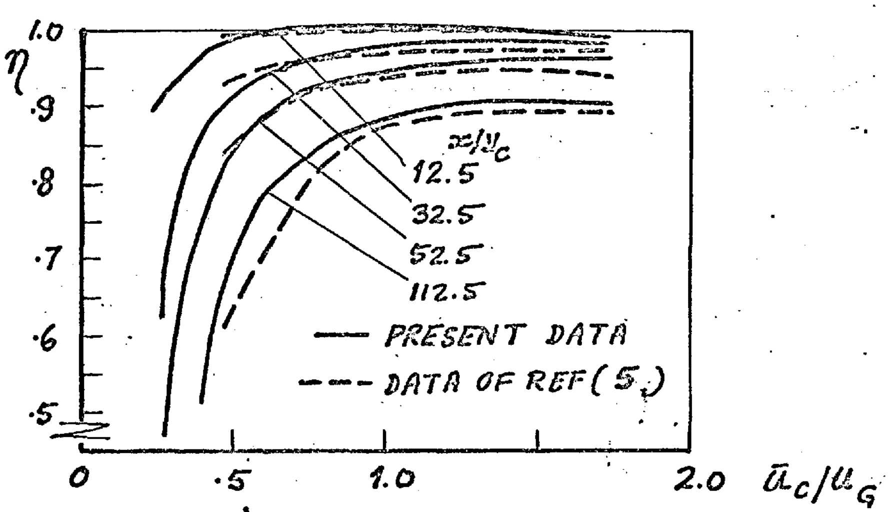

b) $\rho_c/\rho_G = 4.17$

FIG. 4.2.3 COMPARISON OF PRESENT MEASUREMENTS OF THE IMPERVIOUS WALL EFFECTIVENESS WITH DATA OF REFERENCES (30) AND (5).

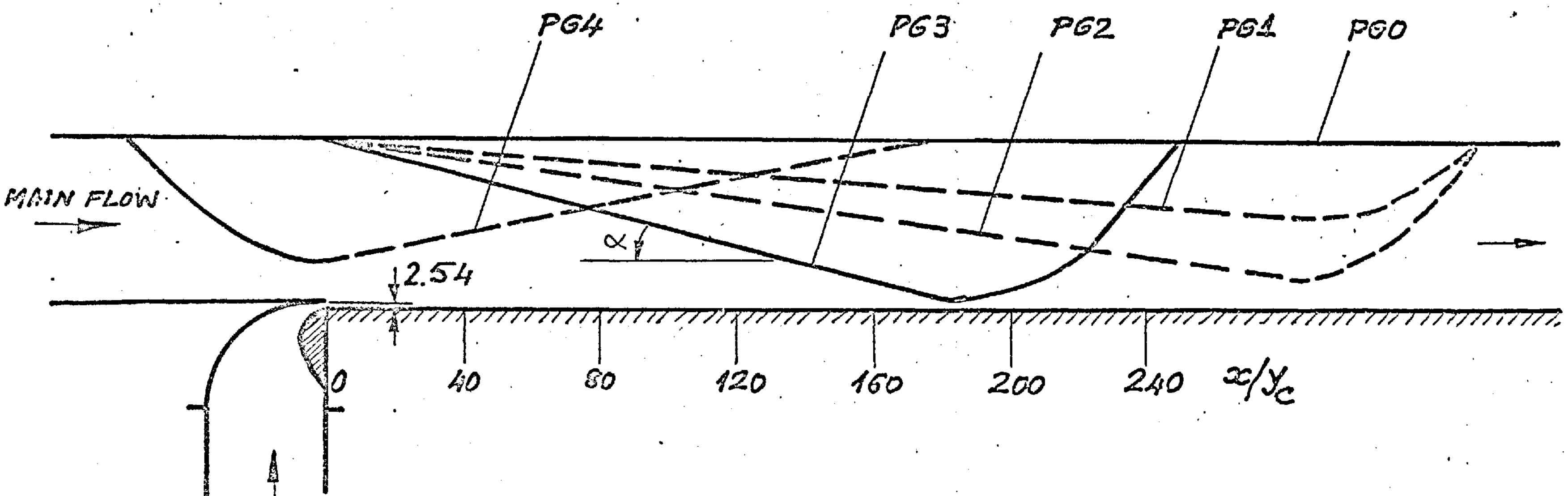

PRESSURE GRADIENT	$K_{p:NOML} \times 10^6$	$\alpha(°)$	SYMBOL
PG0	0.	0	○
PG1	1.00	4.65	⊡
PG 2	1.82	8.3	+
PG3	3.30	14.7	△
PG4	-1.0	-7.2	▽

FIG.4.2.4 SCHEMATIC DIAGRAM OF TEST SECTION WITH PRESSURE GRADIENTS

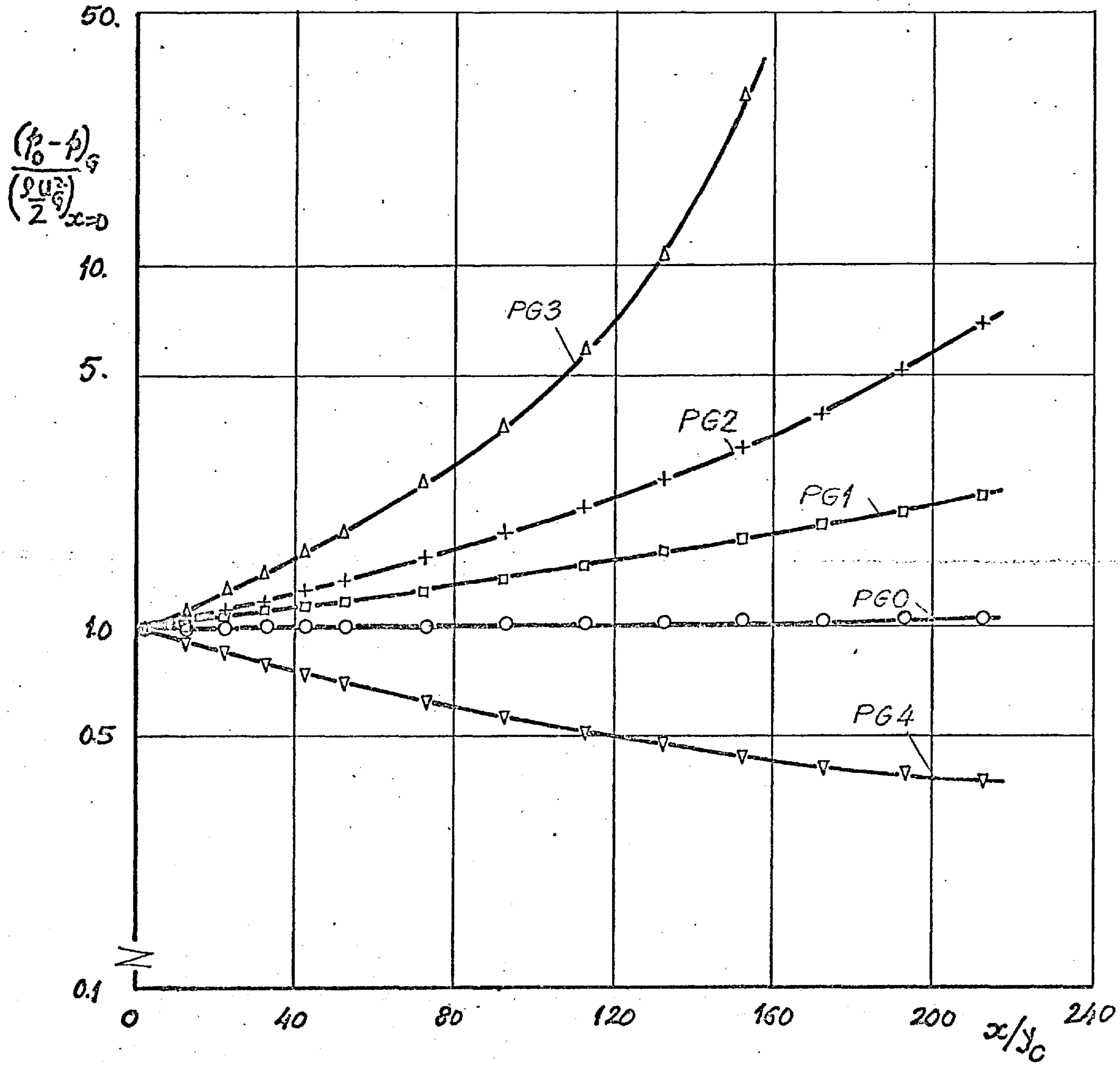

FIG.A.2.5. FREE-STREAM STATIC PRESSURE DISTRIBUTIONS.

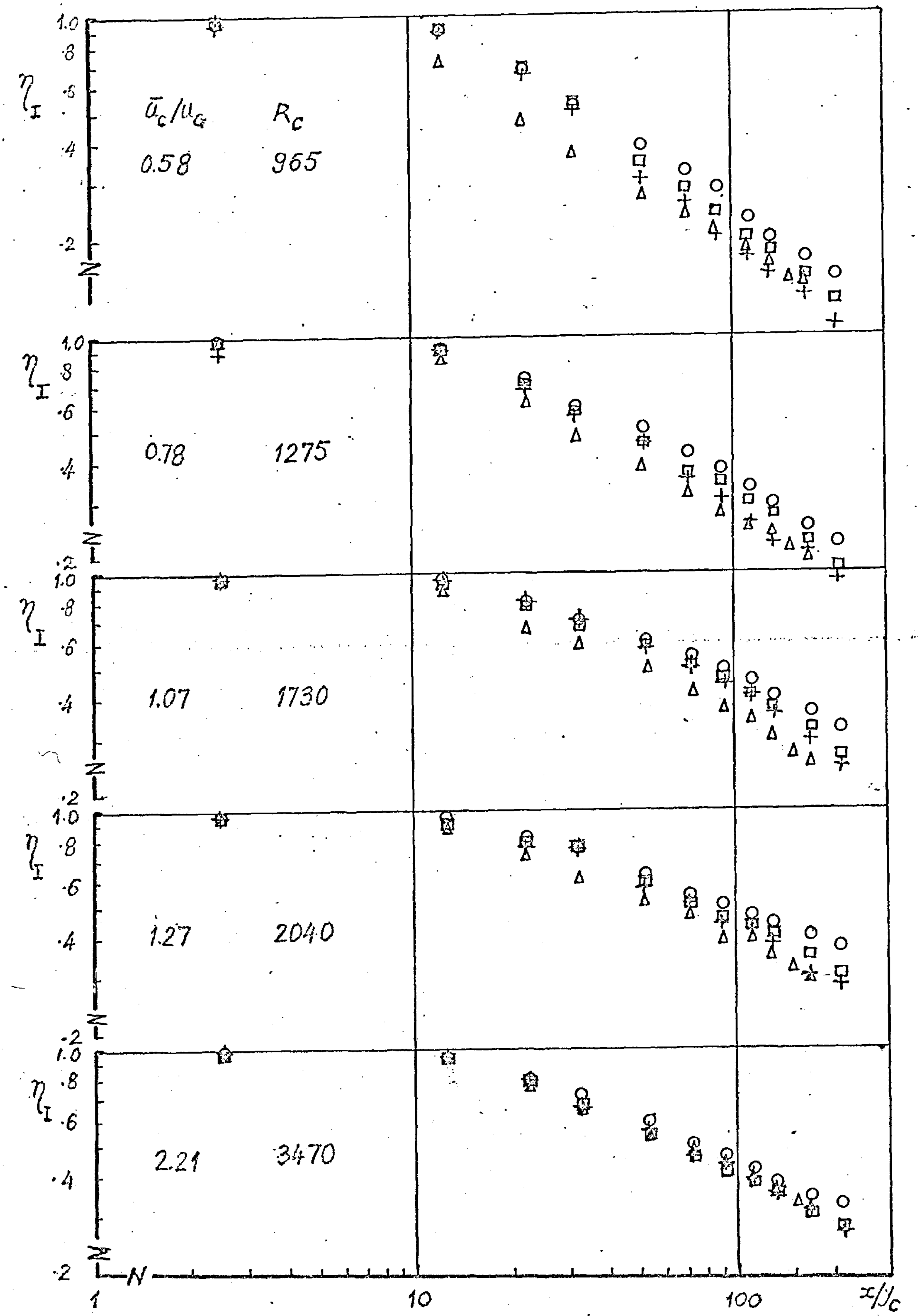

FIG.4.2.6(a) MEASURED VALUES OF IMPERVIOUS WALL EFFECTIVENESS IN PRESENCE OF FAVOURABLE PRESSURE GRADIENTS: $\frac{\rho_c}{\rho_G} = 1.0$

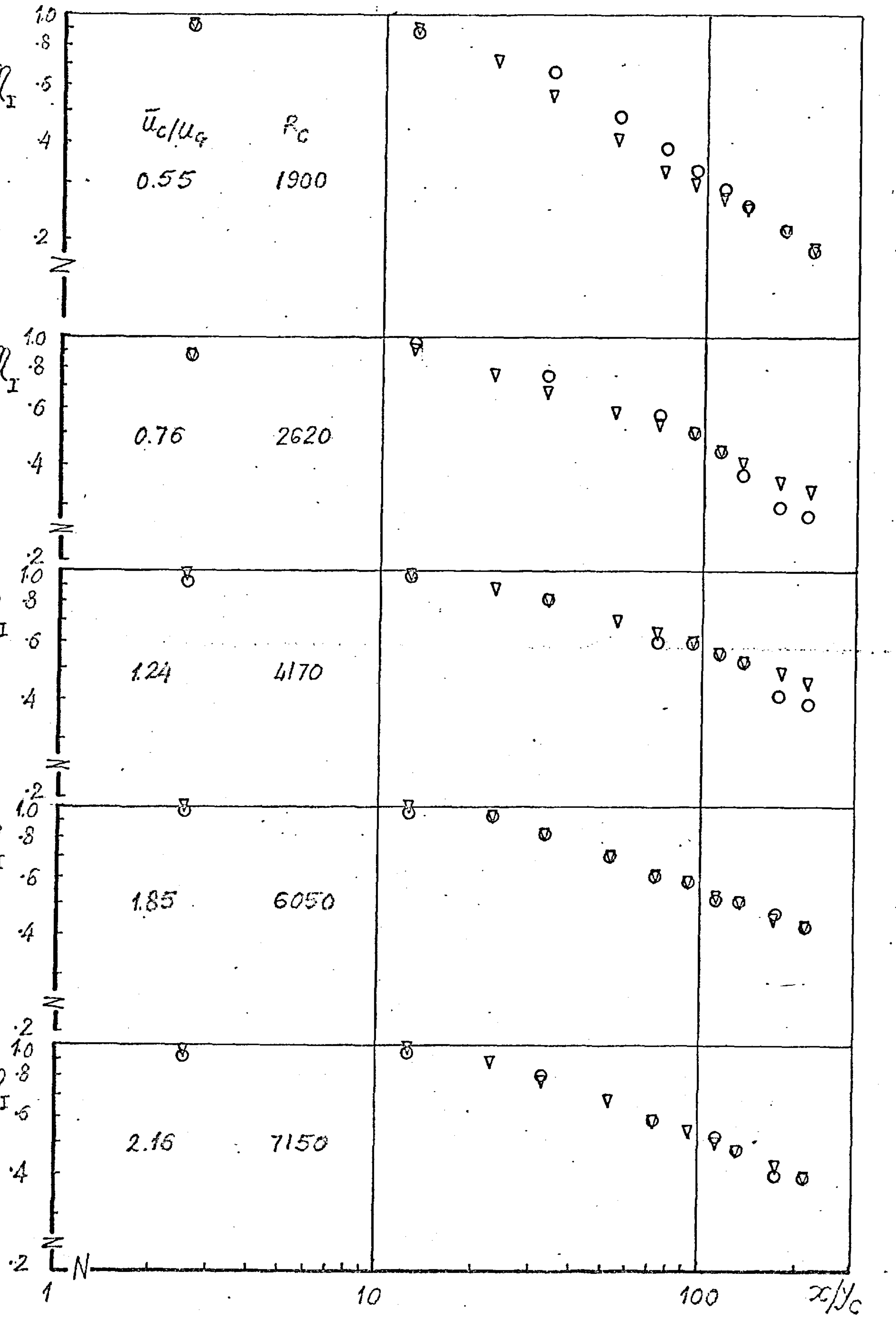

FIG. 4.2.6 (b) MEASURED VALUES OF IMPERVIOUS WALL EFFECTIVENESS IN PRESENCE OF ADVERSE PRESSURE GRADIENT: $\rho_c/\rho_G = 1.0$.

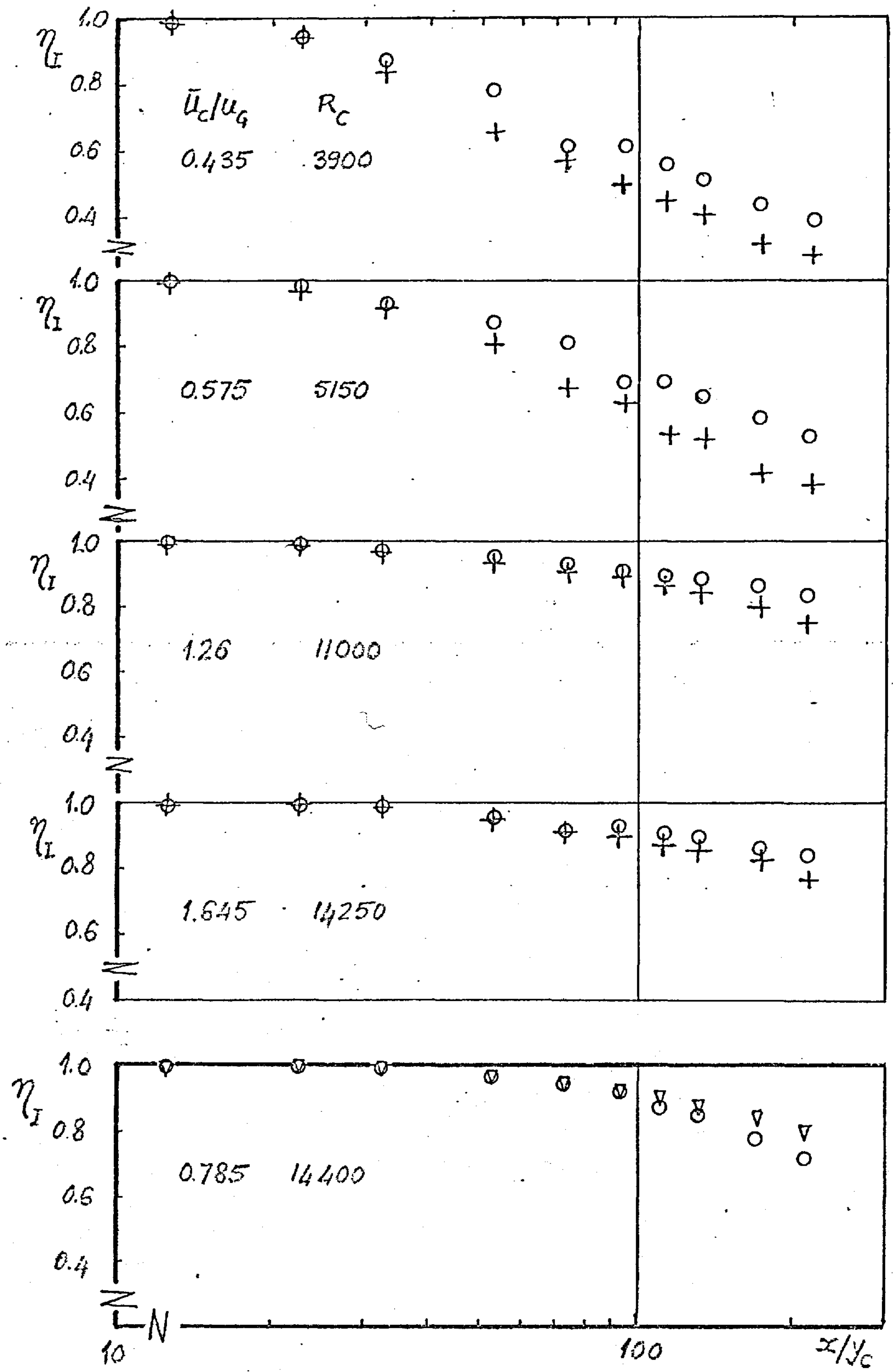

FIG.4.2.7(a) MEASURED VALUES OF IMPERVIOUS WALL EFFECTIVENESS IN PRESENCE OF PRESSURE GRADIENTS: $\rho_c/\rho_G = 4.17$

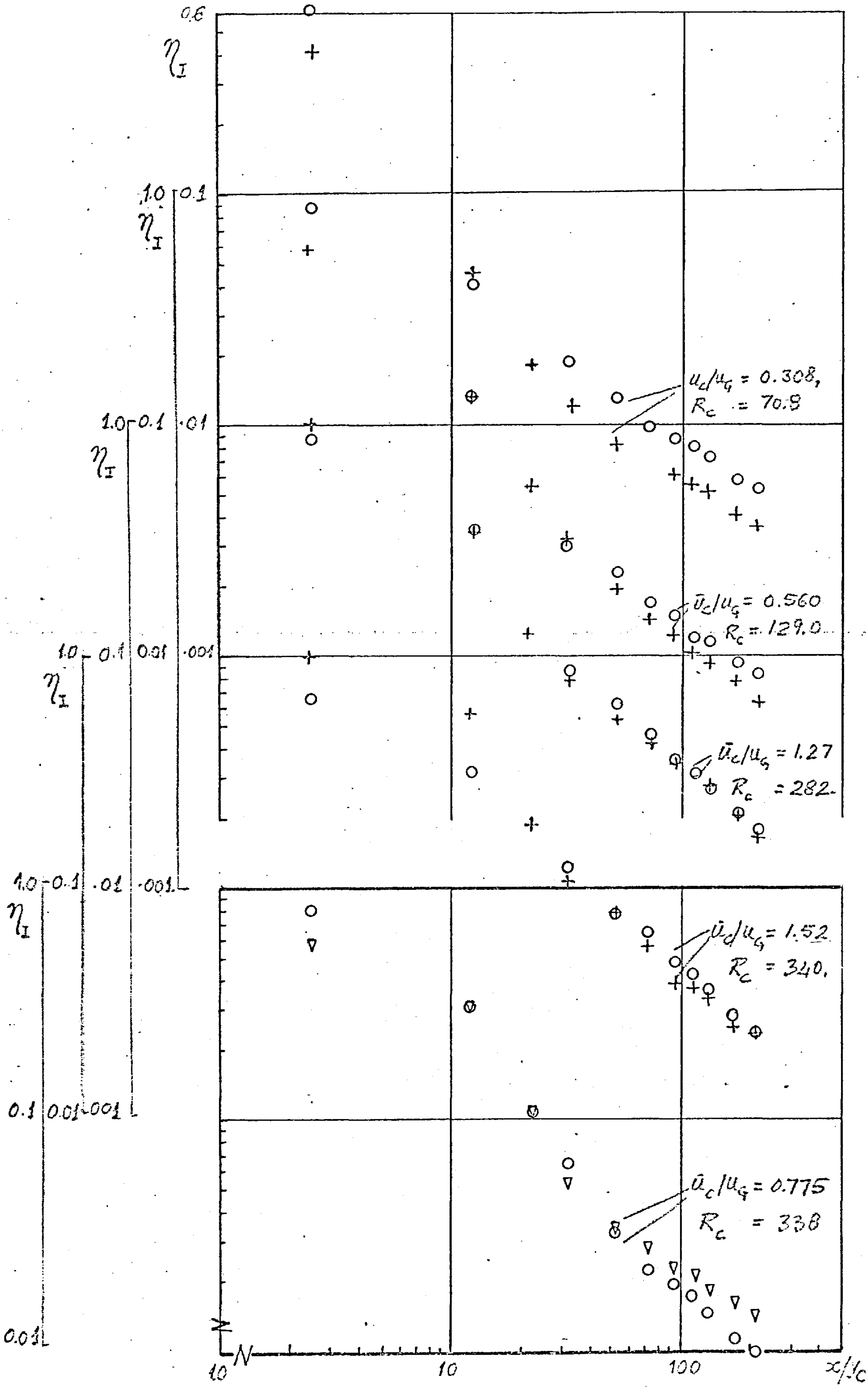

FIG. 4.2.7(b) MEASURED VALUES OF IMPERVIOUS WALL EFFECTIVENESS IN PRESENCE OF PRESSURE GRADIENTS : $\rho_c/\rho_G = 0.069$

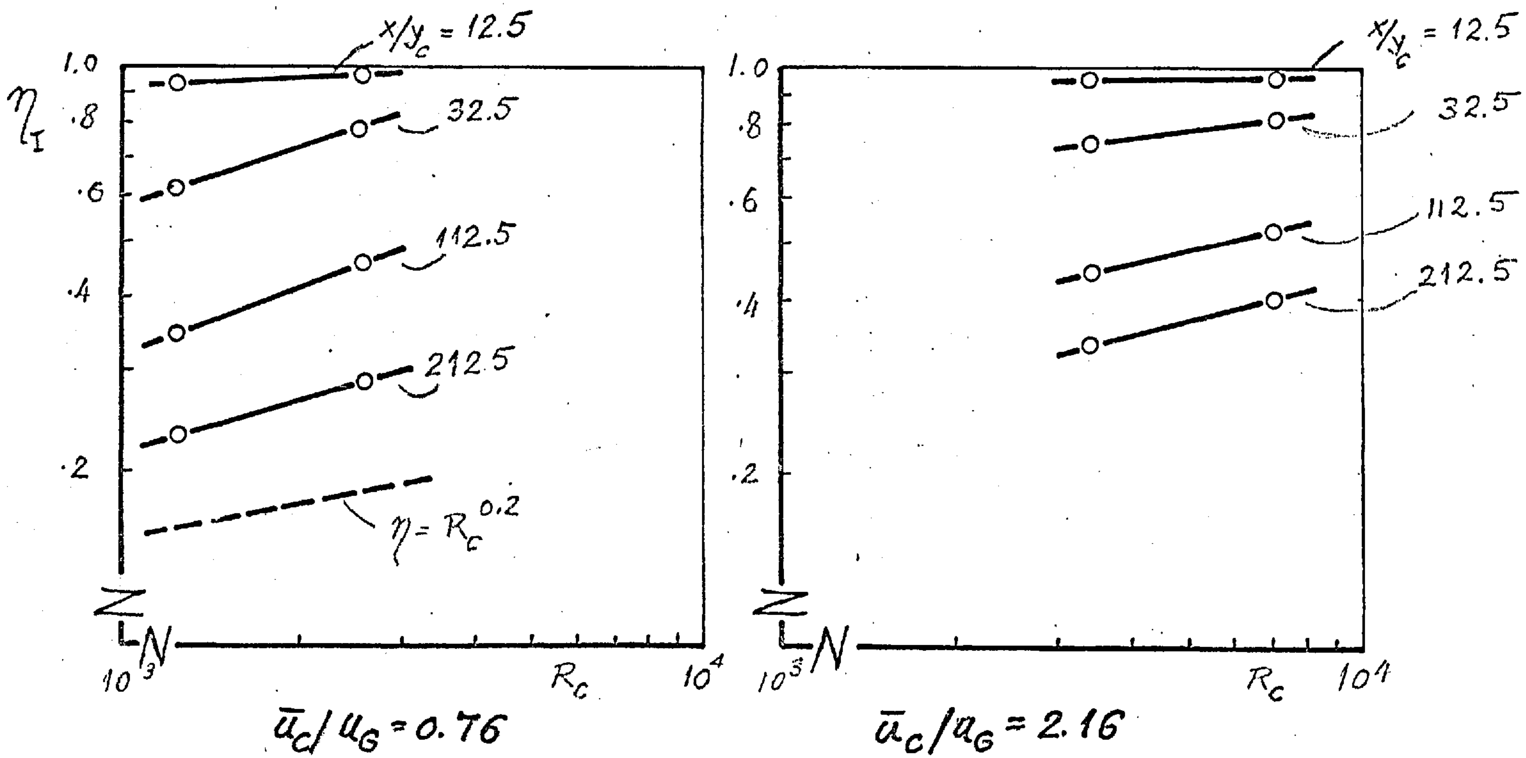

FIG. 4.2.8 . EFFECT OF SLOT REYNOLDS NUMBER ON EFFECTIVENESS: $\rho_c/\rho_G = 1.0$

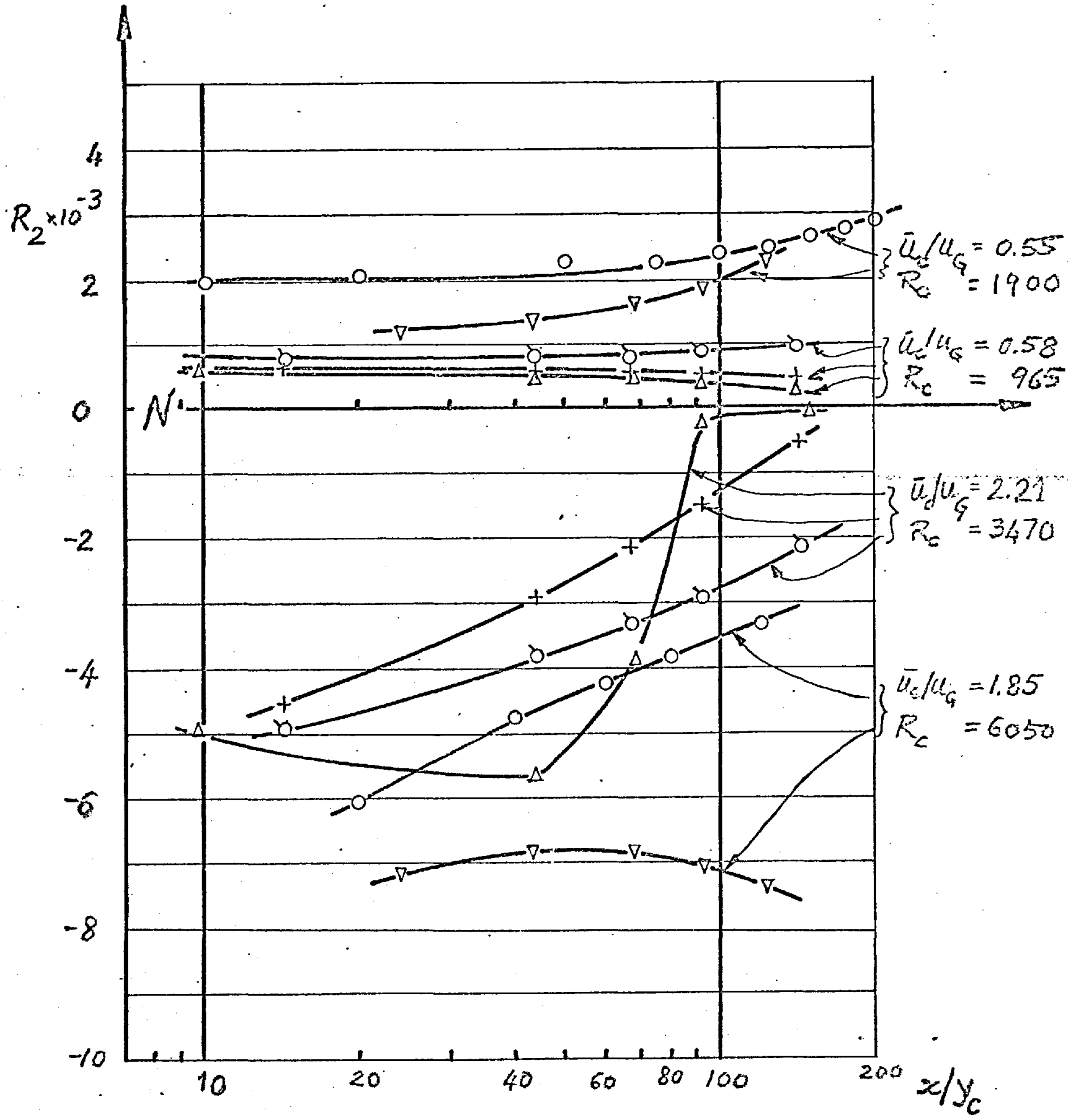

FIG. 4.2.9 INFLUENCE OF PRESSURE GRADIENT ON THE MOMENTUM THICKNESS REYNOLDS NUMBER.

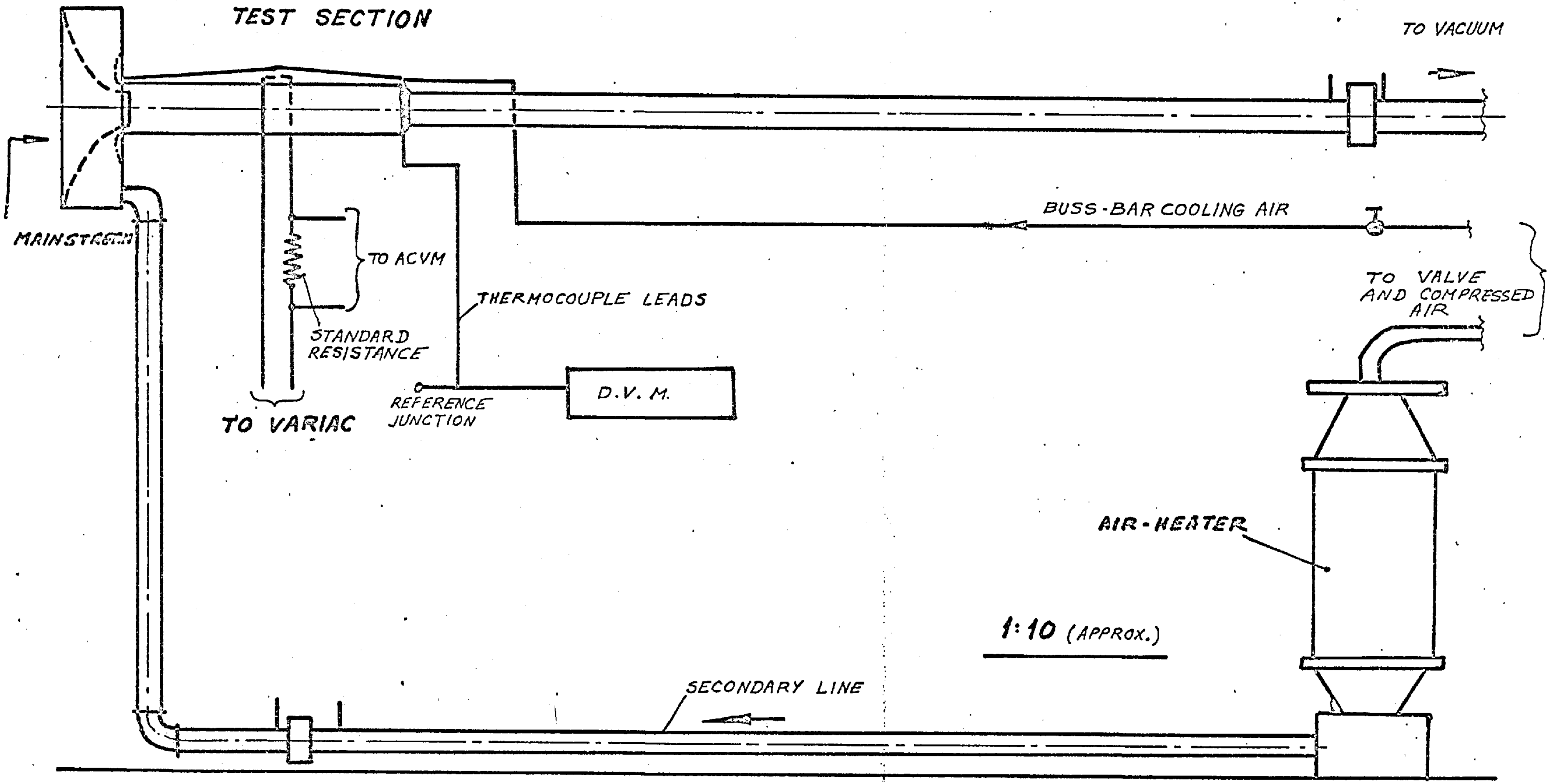

FIG. 4.3.1 SCHEMATIC DIAGRAM OF APPARATUS 'B'

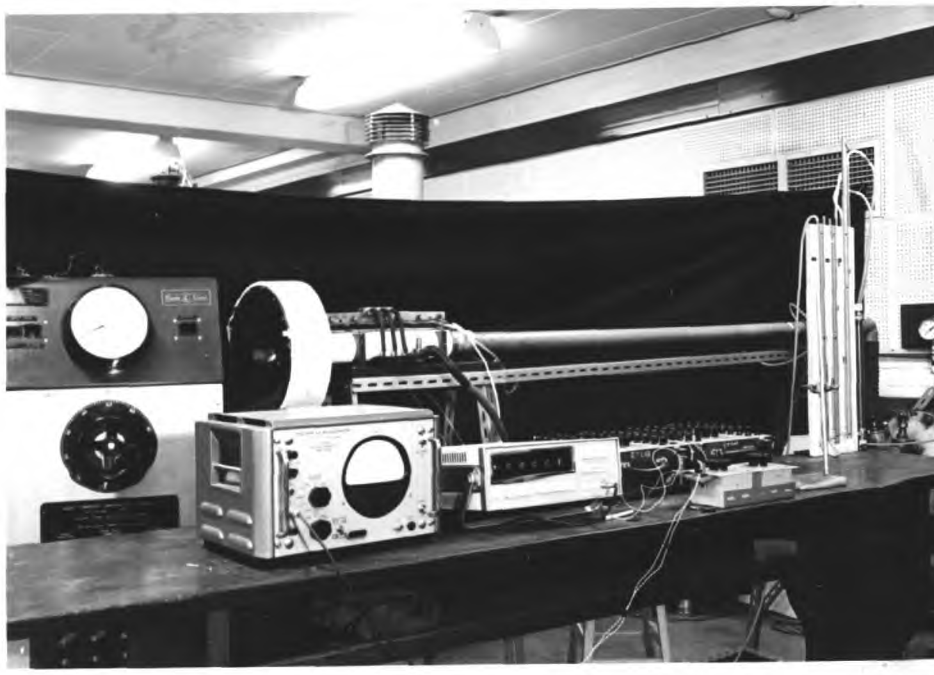

Fig. 4.3.2 (a) General view of apparatus B.

Fig. 4.3.2 (b) Test Section, apparatus B.

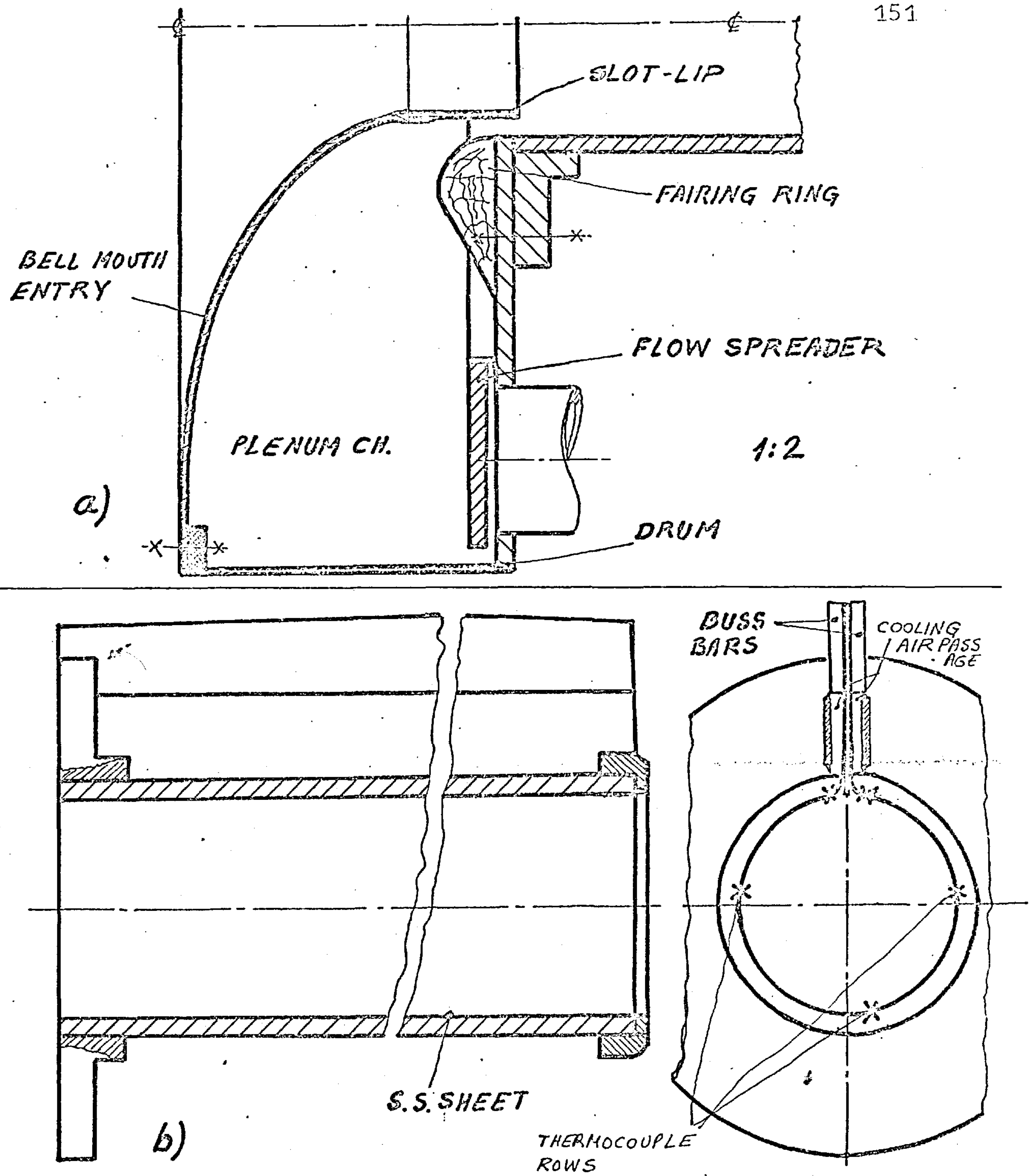

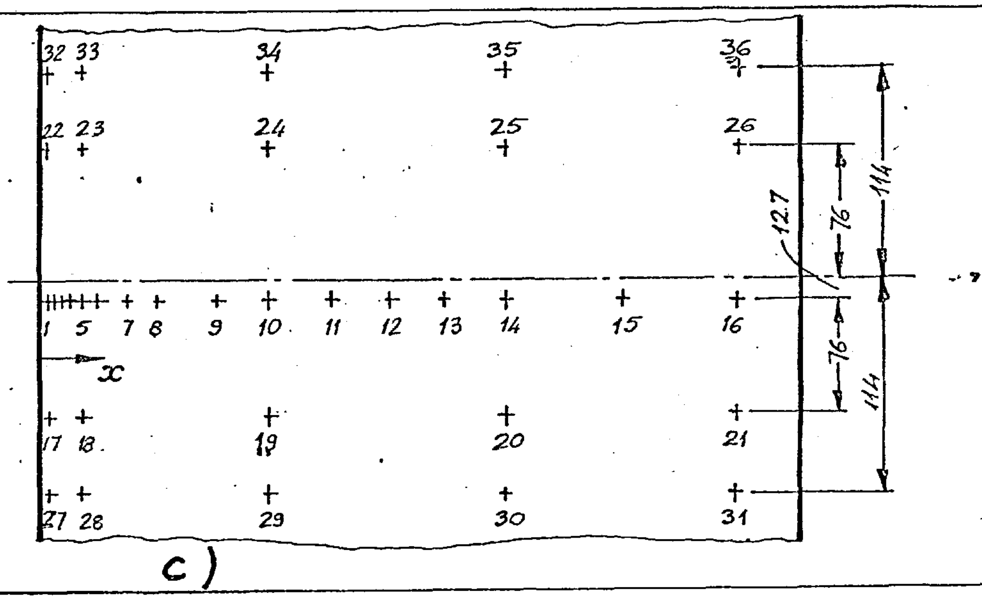

NO.	x(mm)
1	4.9
2	9.8
3	14.9
4	19.5
5	29.2
6	39.0
7	58.5
8	78.0
9	111.7
10	156.1
11	195.0
12	234.0
13	274.0
14	313.0
15	390.0
16	470.0

FIG.4.3.3. DETAILS OF APPARATUS 'B'.

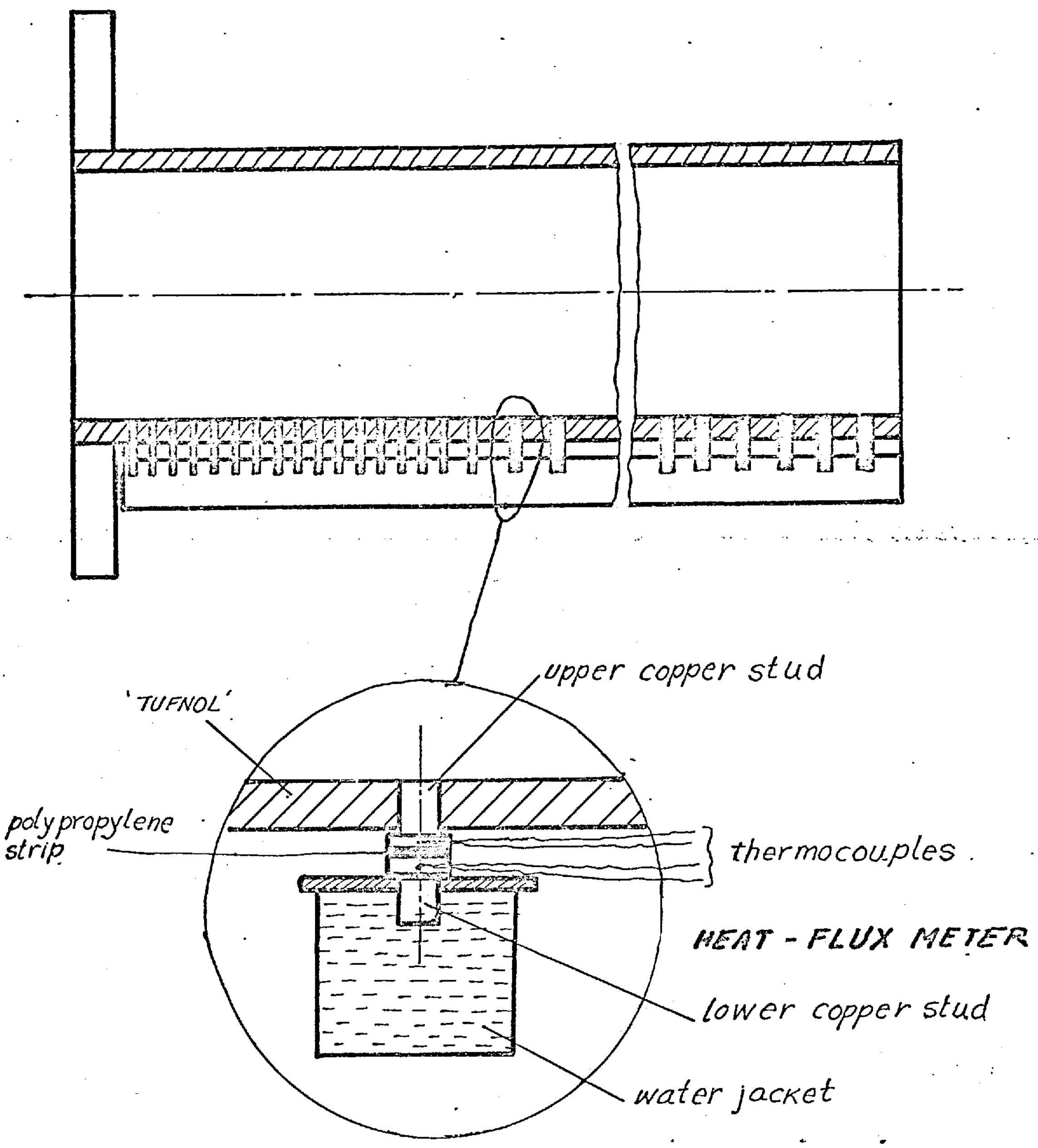

FIG. 4.3.4 TEST SECTION OF REFERENCE (39).

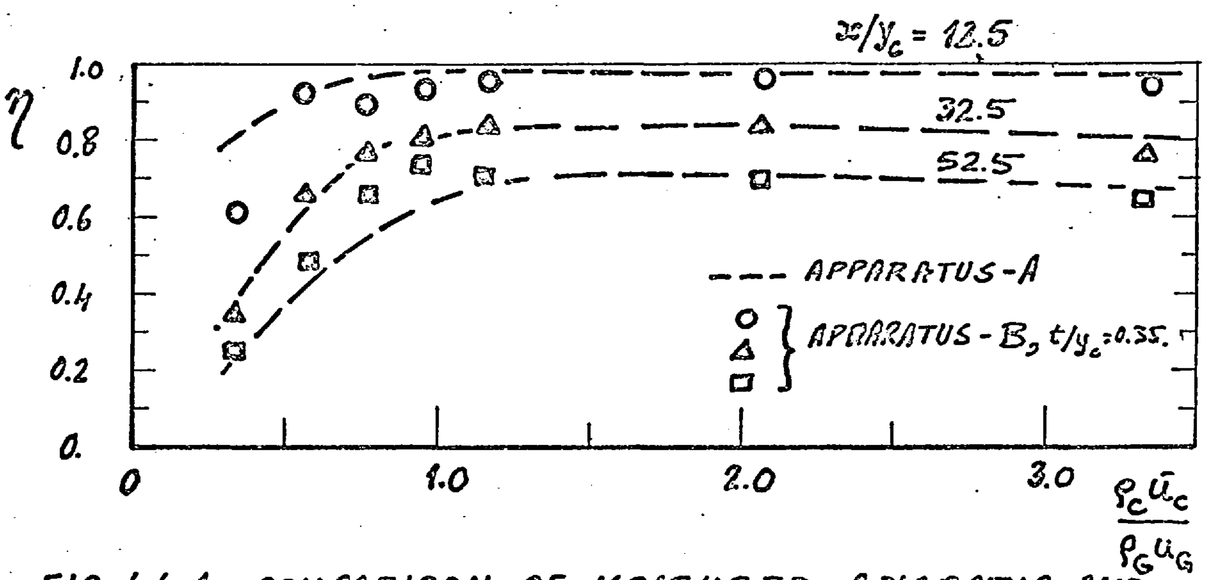

FIG. 4.4.1. COMPARISON OF MEASURED ADIABATIC AND IMPERVIOUS-WALL EFFECTIVENESS : APPARATUS-B AND APPARATUS-A.

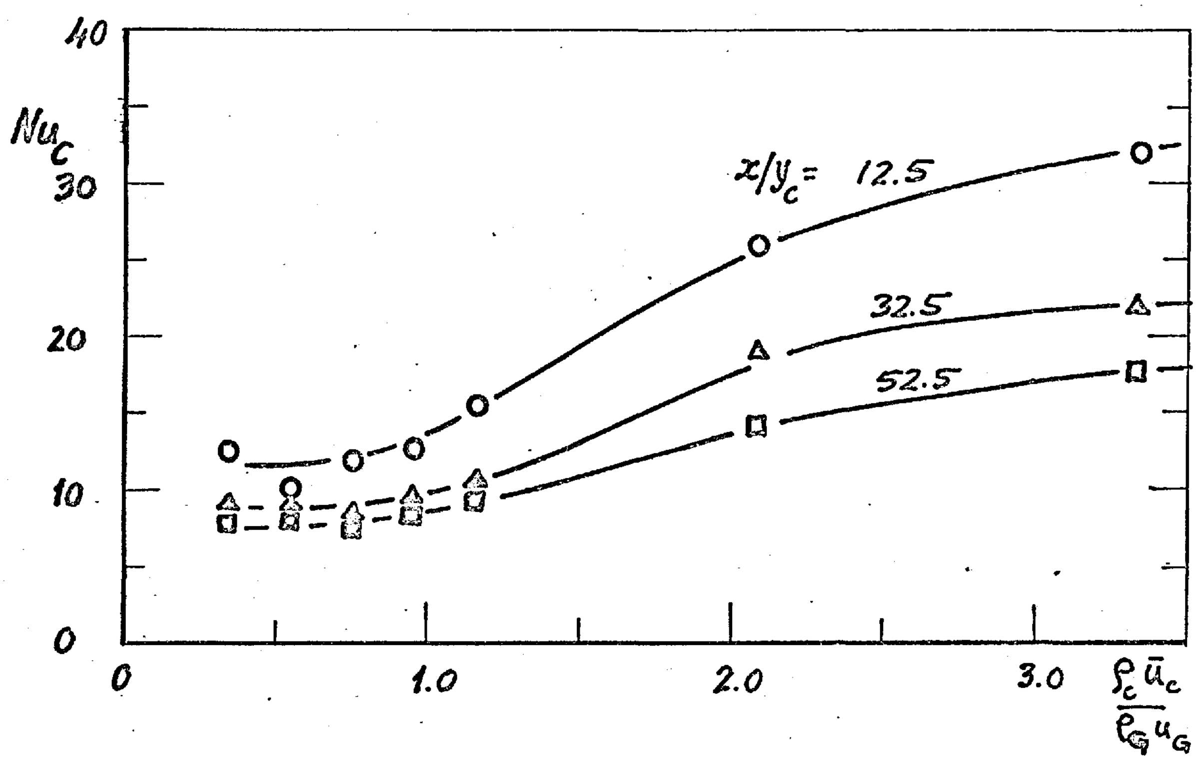

FIG. 4.4.2. INFLUENCE OF THE MASS-VELOCITY RATIO ON THE MEASURED HEAT-TRANSFER COEFFICIENT: APPARATUS-B, t/y_c = 0.35.

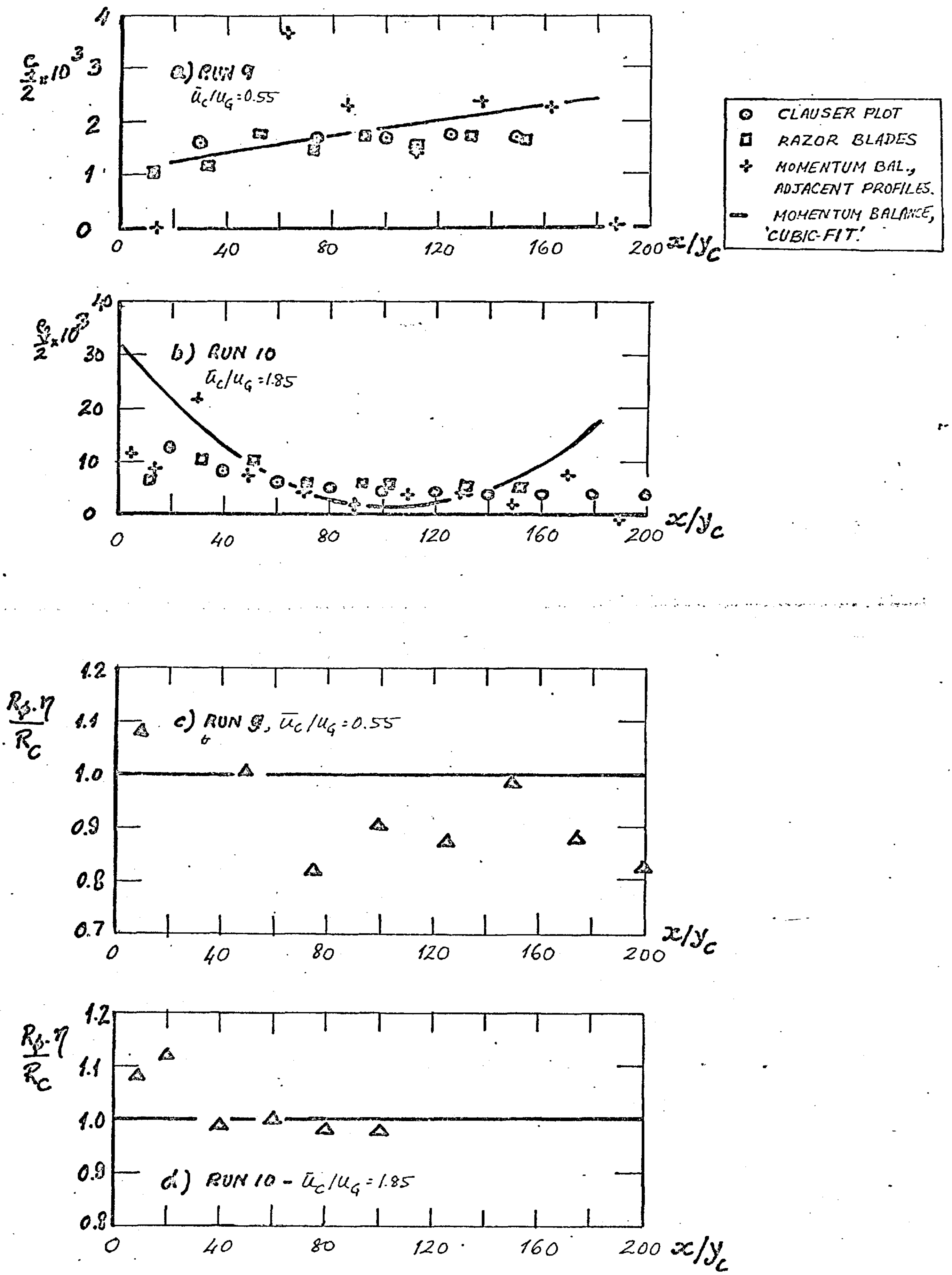

FIG. 5.1.1 MOMENTUM AND MASS BALANCE FROM MEASURED PROFILES.

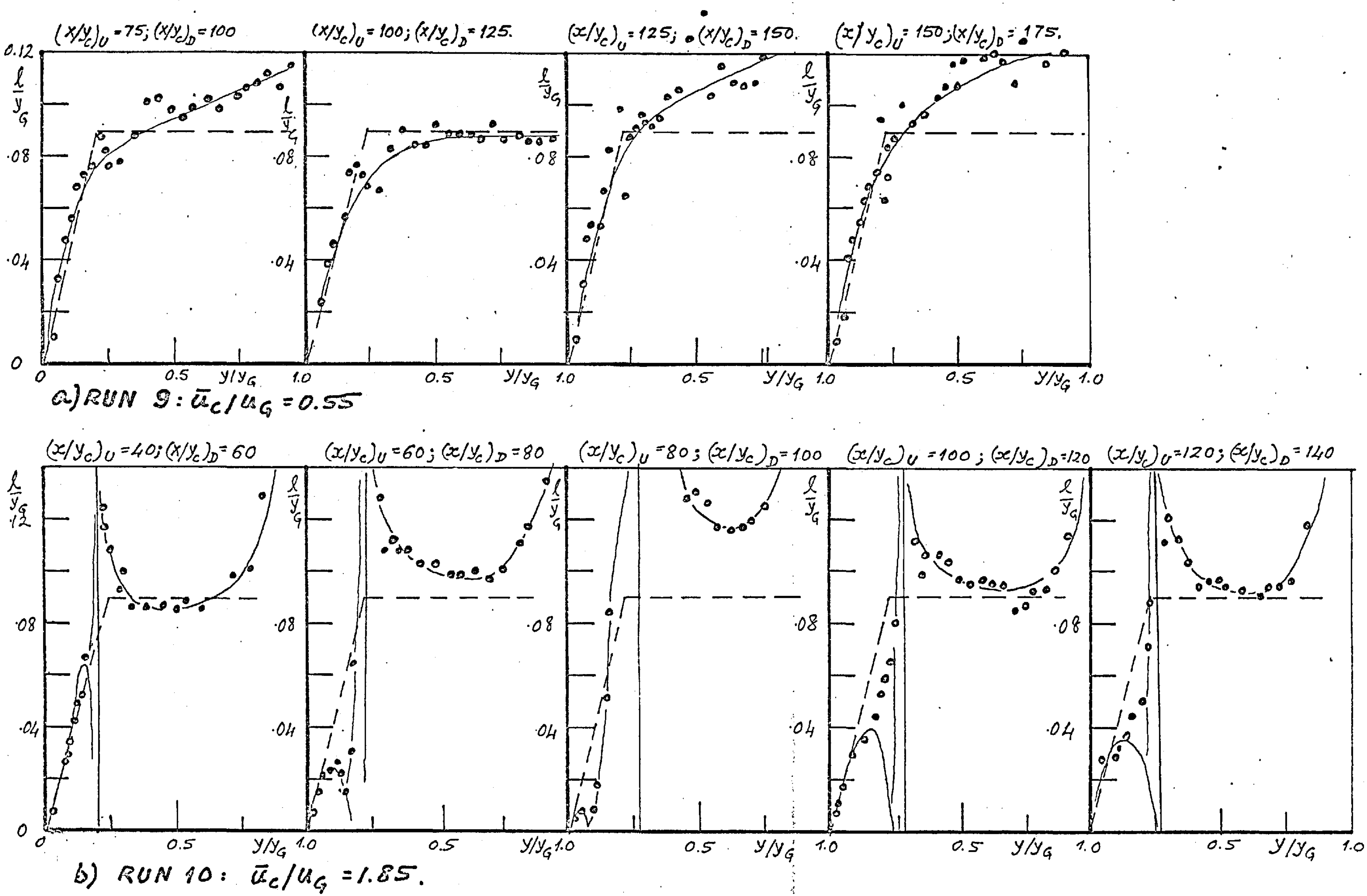

FIG. 5.1.2 MIXING LENGTH DISTRIBUTIONS DERIVED FROM PRESENT DATA (APPARATUS 'A')

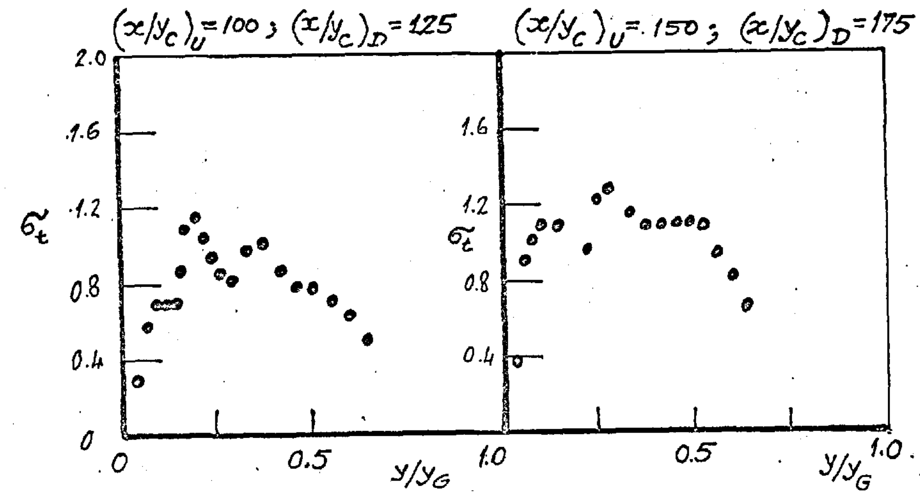

a) RUN 9 ; $\bar{u}_c / u_G = 0.55$.

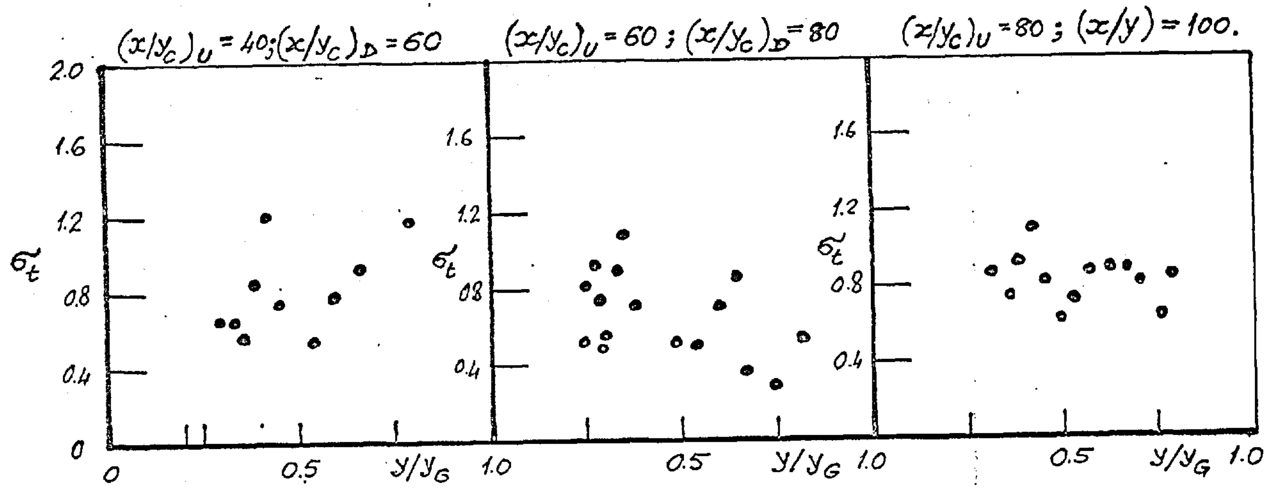

b) RUN 10 ; $\bar{u}_c / u_G = 1.85$.

FIG. 5.1.3. TURBULENT SCHMIDT NUMBERS DERIVED FROM PRESENT DATA.

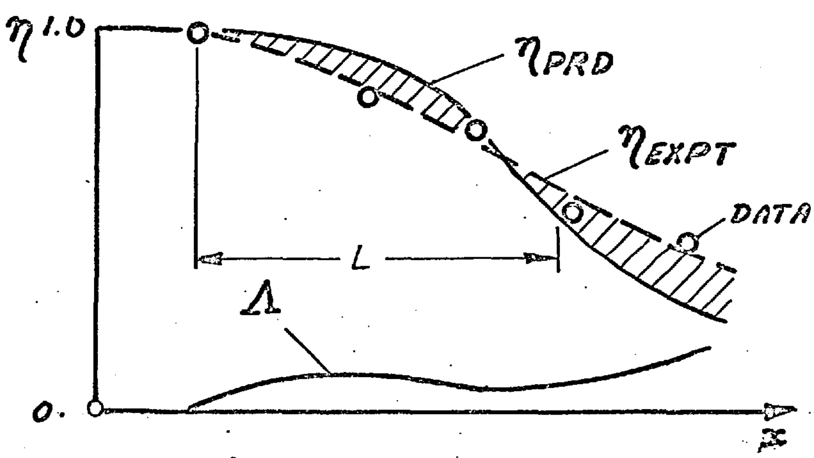

FIG. 5.2.1. Λ, A MEASURE OF AGREEMENT BETWEEN PREDICTED AND MEASURED EFFECTIVENESS.

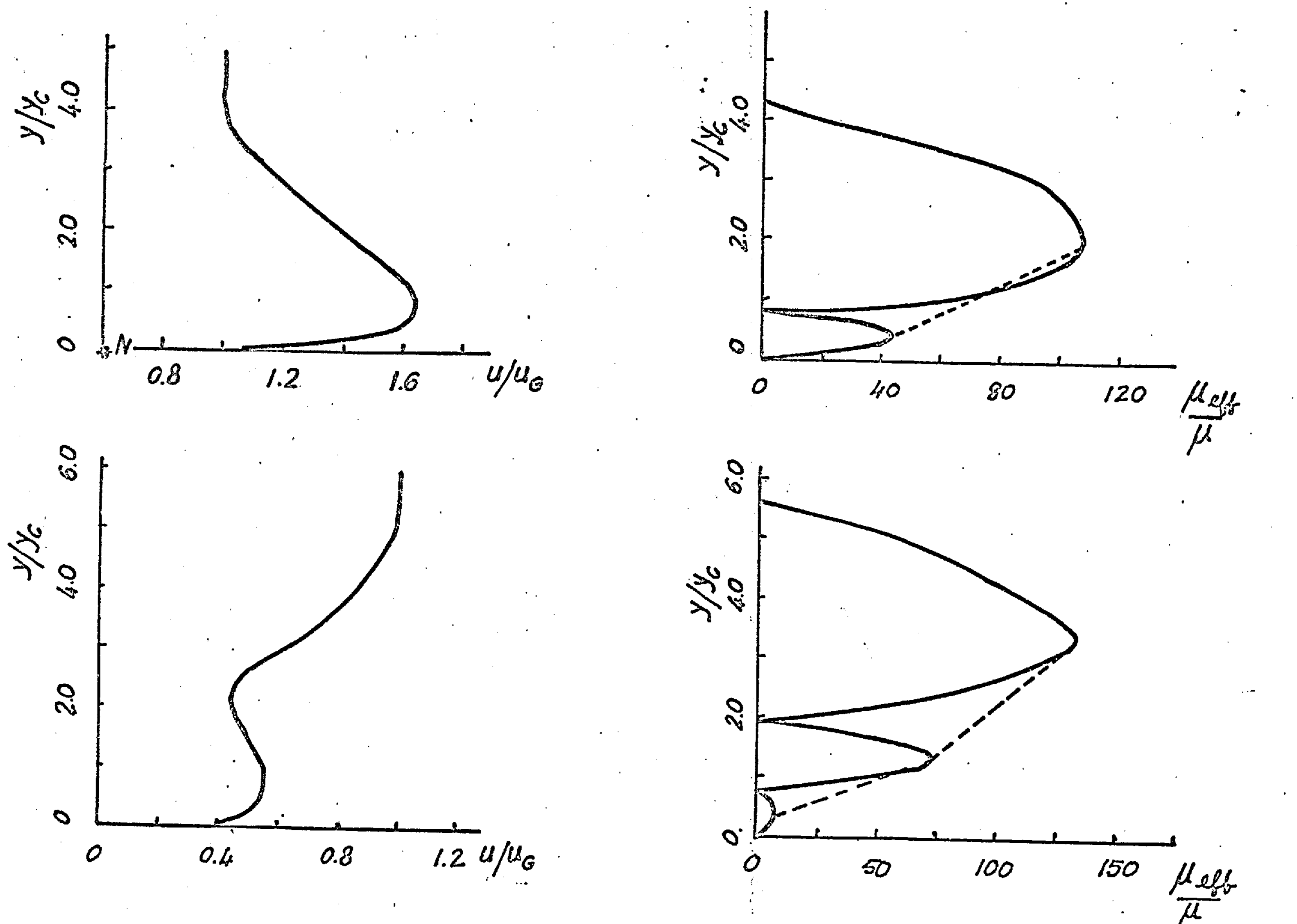

FIG.5.2.2. EDDY VISCOSITY PROFILES RESULTING FROM A RAMP MIXING-LENGTH DISTRIBUTION.

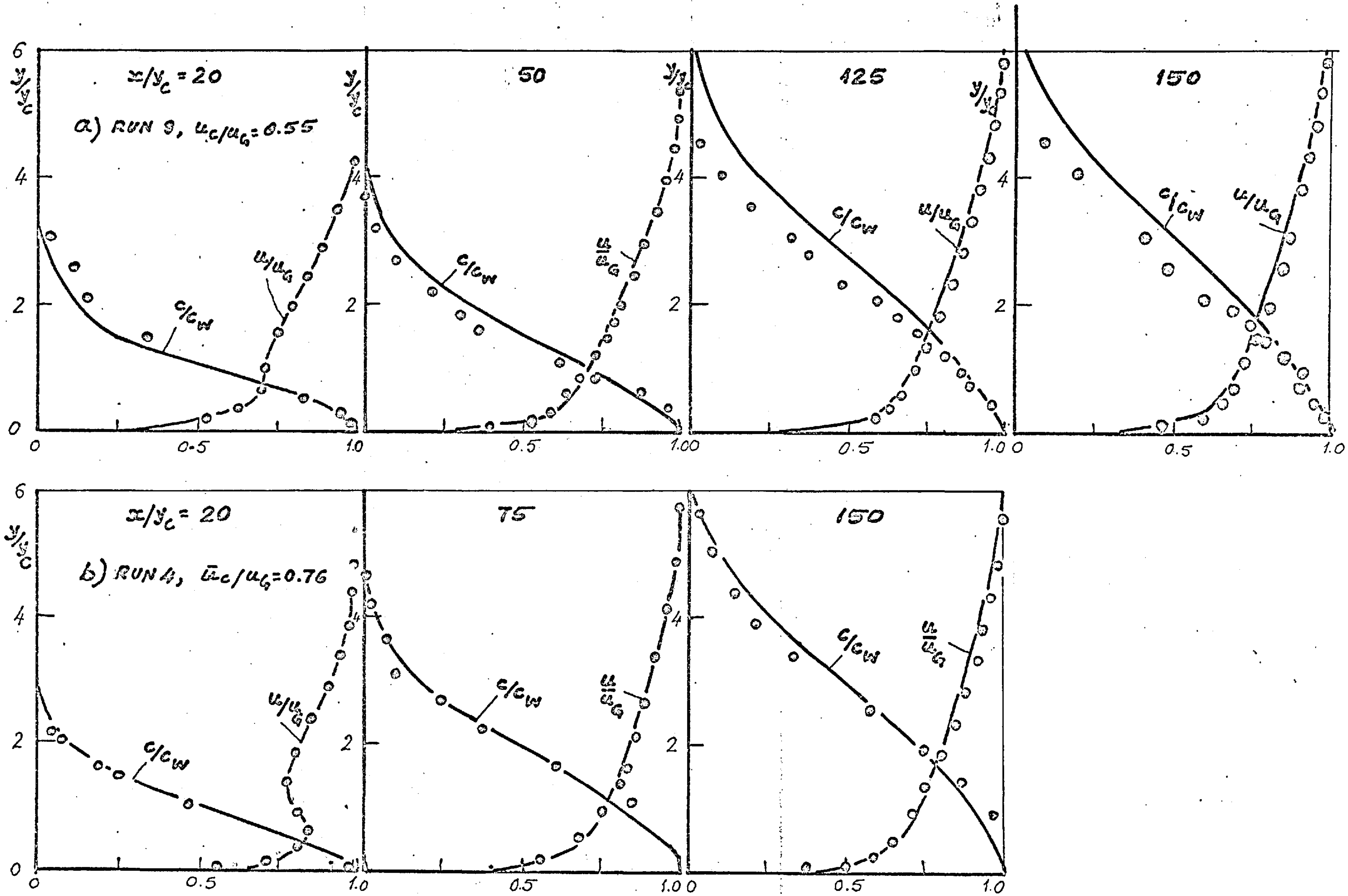

FIG. 5.2.3 PREDICTED AND MEASURED PROFILES OF VELOCITY AND CONCENTRATION: PRESENT DATA, $dP/dx = 0$, $\rho_C/\rho_G = 1.0$, $\bar{u}_C/u_G < 1.0$.

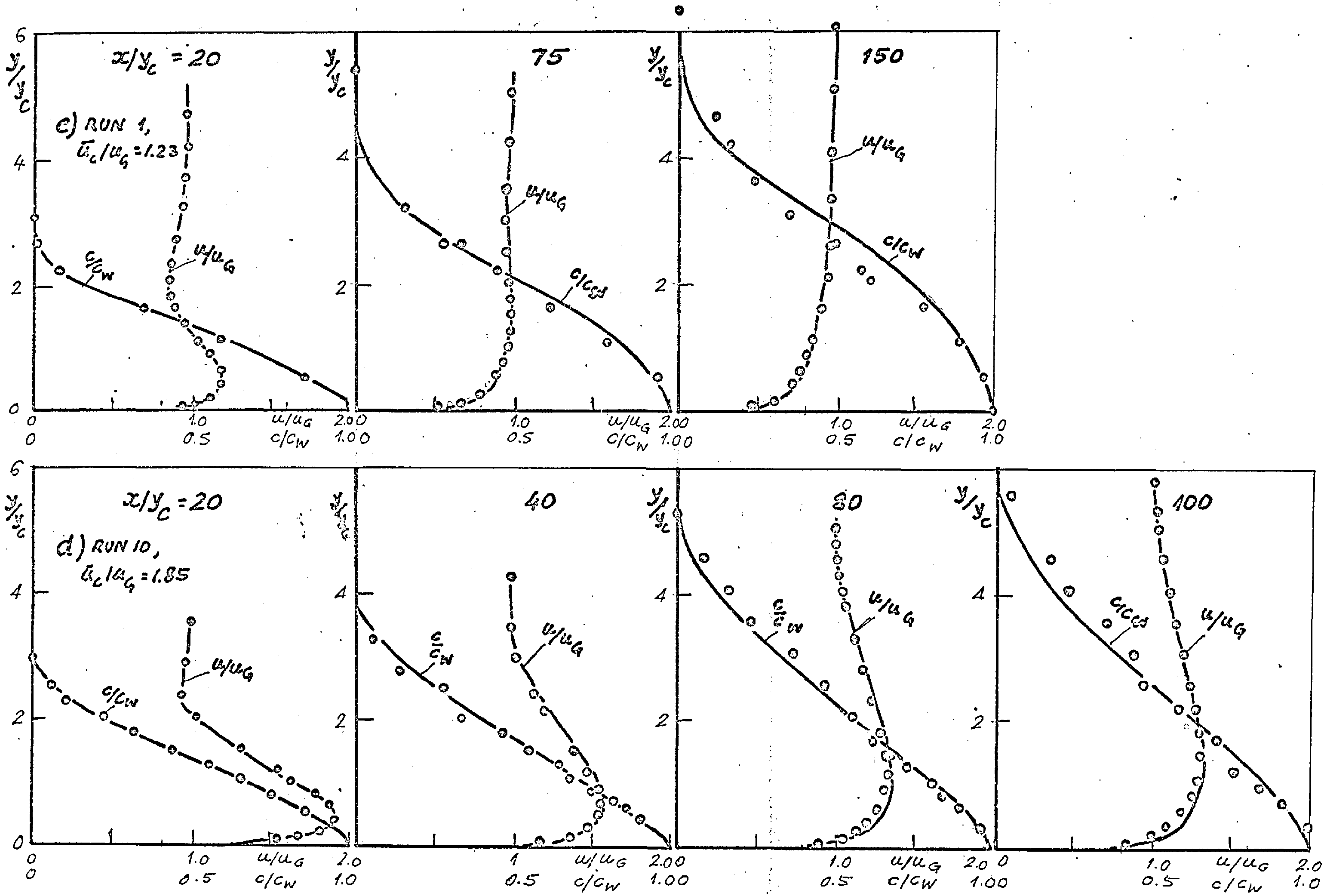

FIG. 5.2.3 (CONTD.) : PRESENT DATA, $dp/dx = 0$, $\rho_c/\rho_G = 1.0$, $\bar{u}_c/u_G > 1.0$

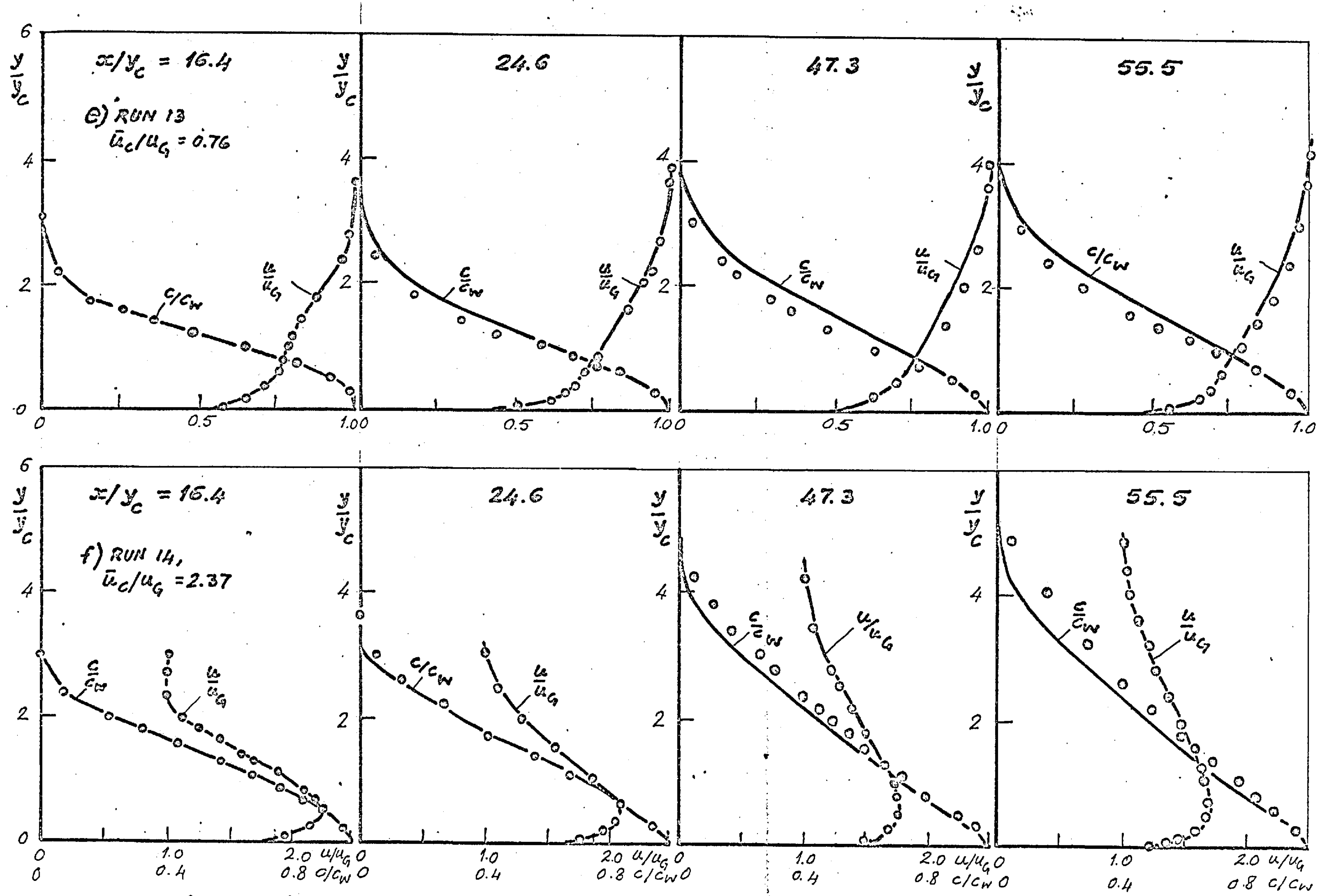

FIG. 5.2.3 (CONTD): DATA OF REF(29); $\rho_c/\rho_G = 1.0$.

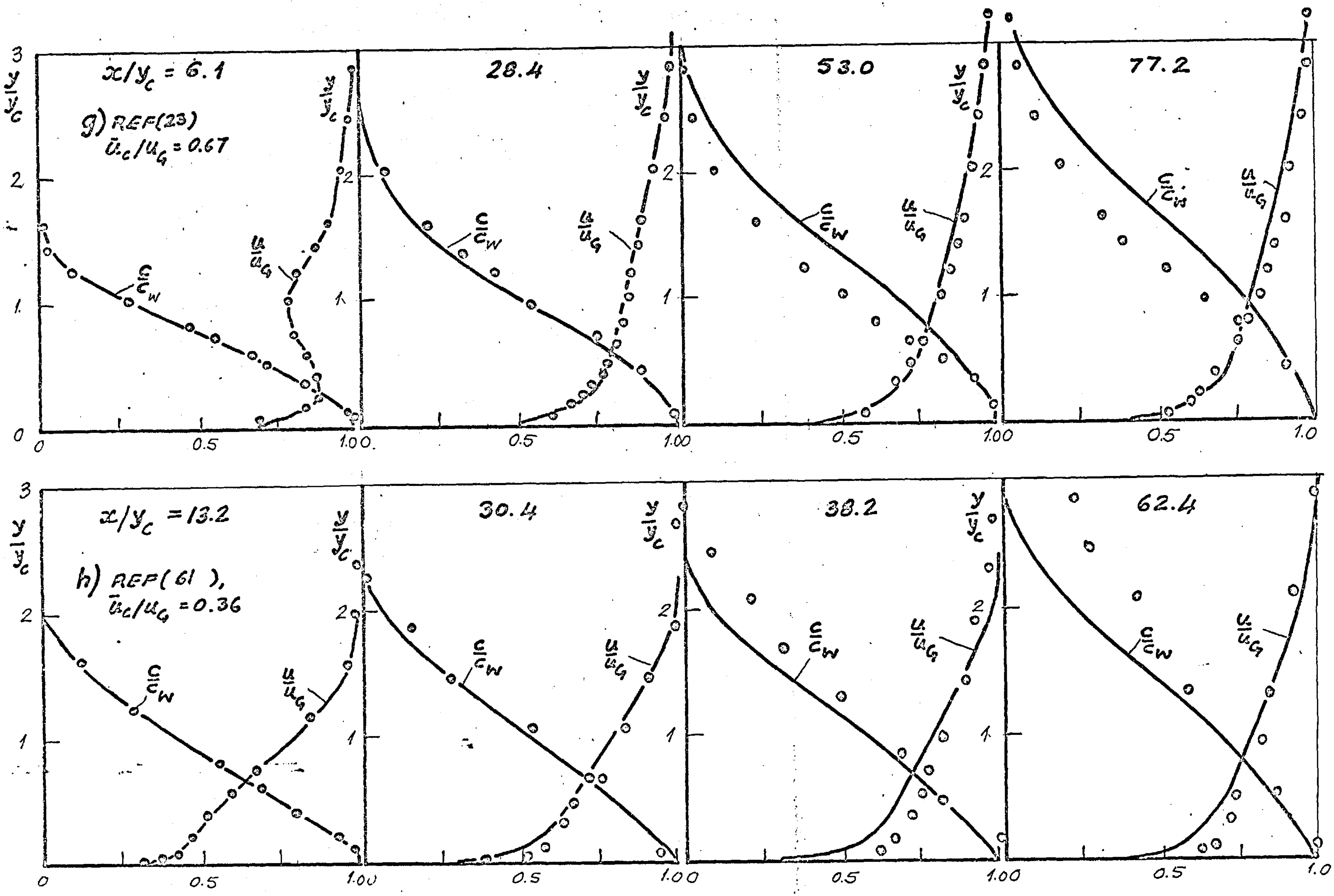

FIG. 5.2.3 (CONTD): DATA OF REFS.(23), (61).

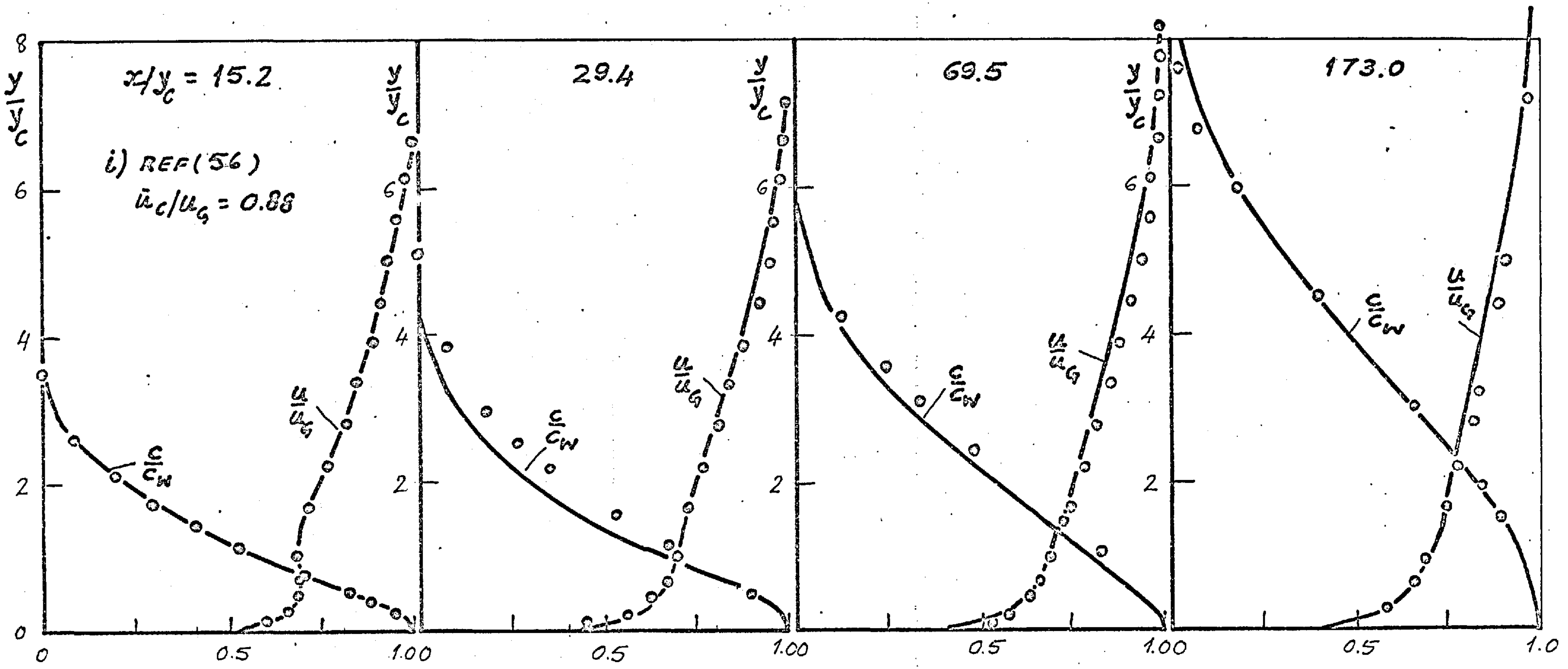

FIG. 5.2.3 (CONTD) DATA OF REF (56).

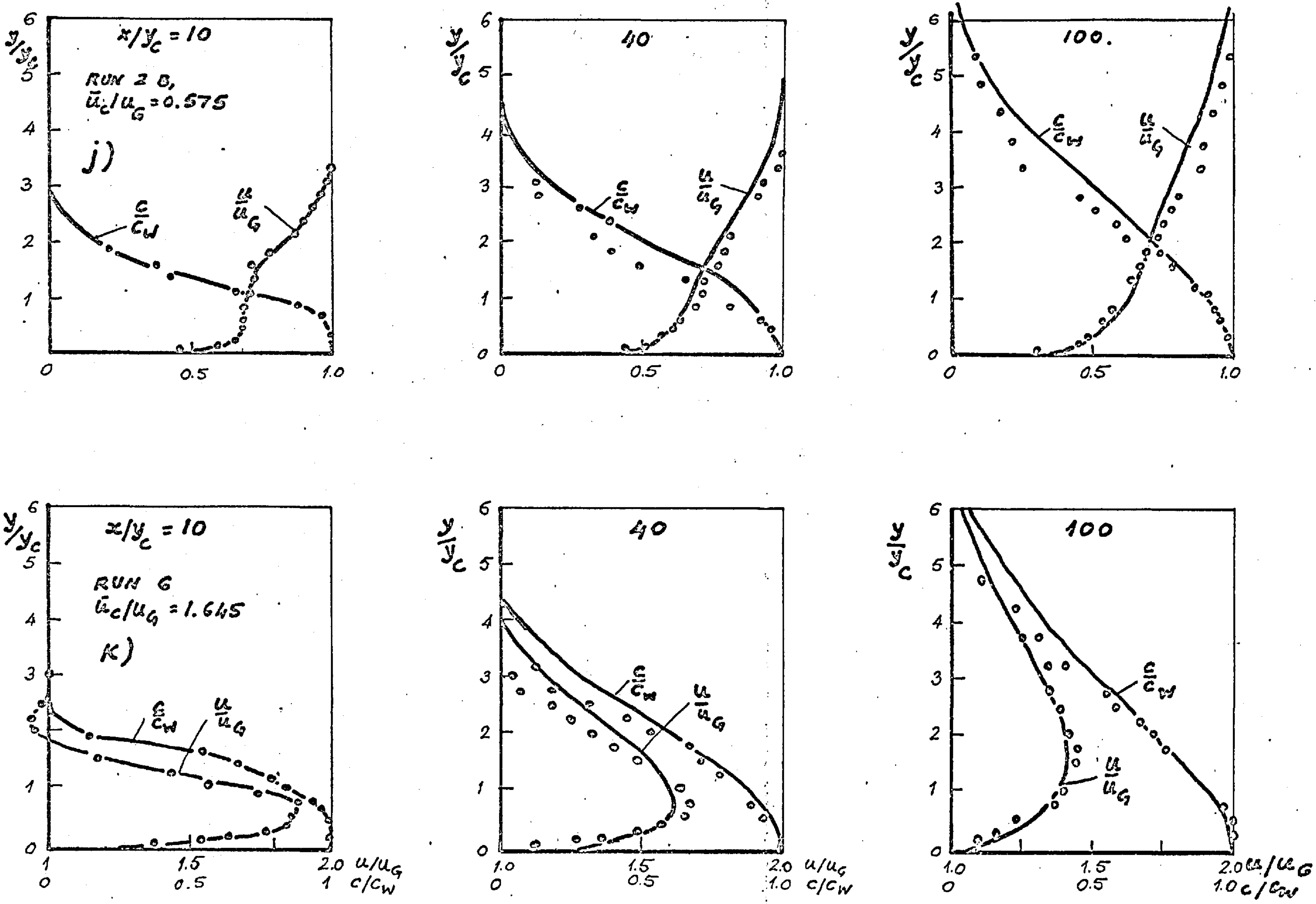

FIG. 5.2.3 (CONTD) PRESENT DATA, $\rho_C/\rho_G = 4.17$.

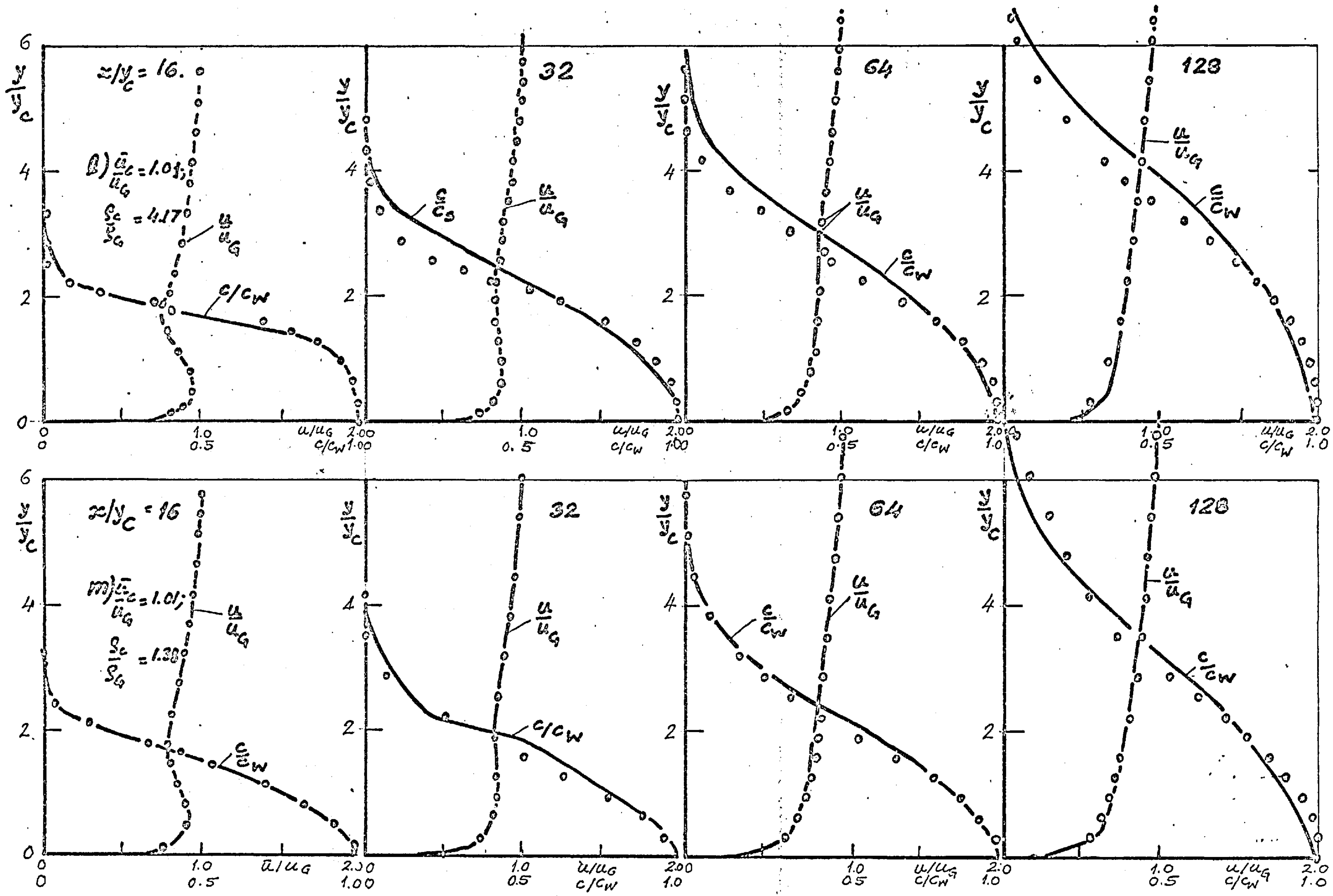

FIG. 5.2.3 (CONCLUDED): DATA OF REF (5); ρ_c/ρ_G = 4.17 & 1.38.

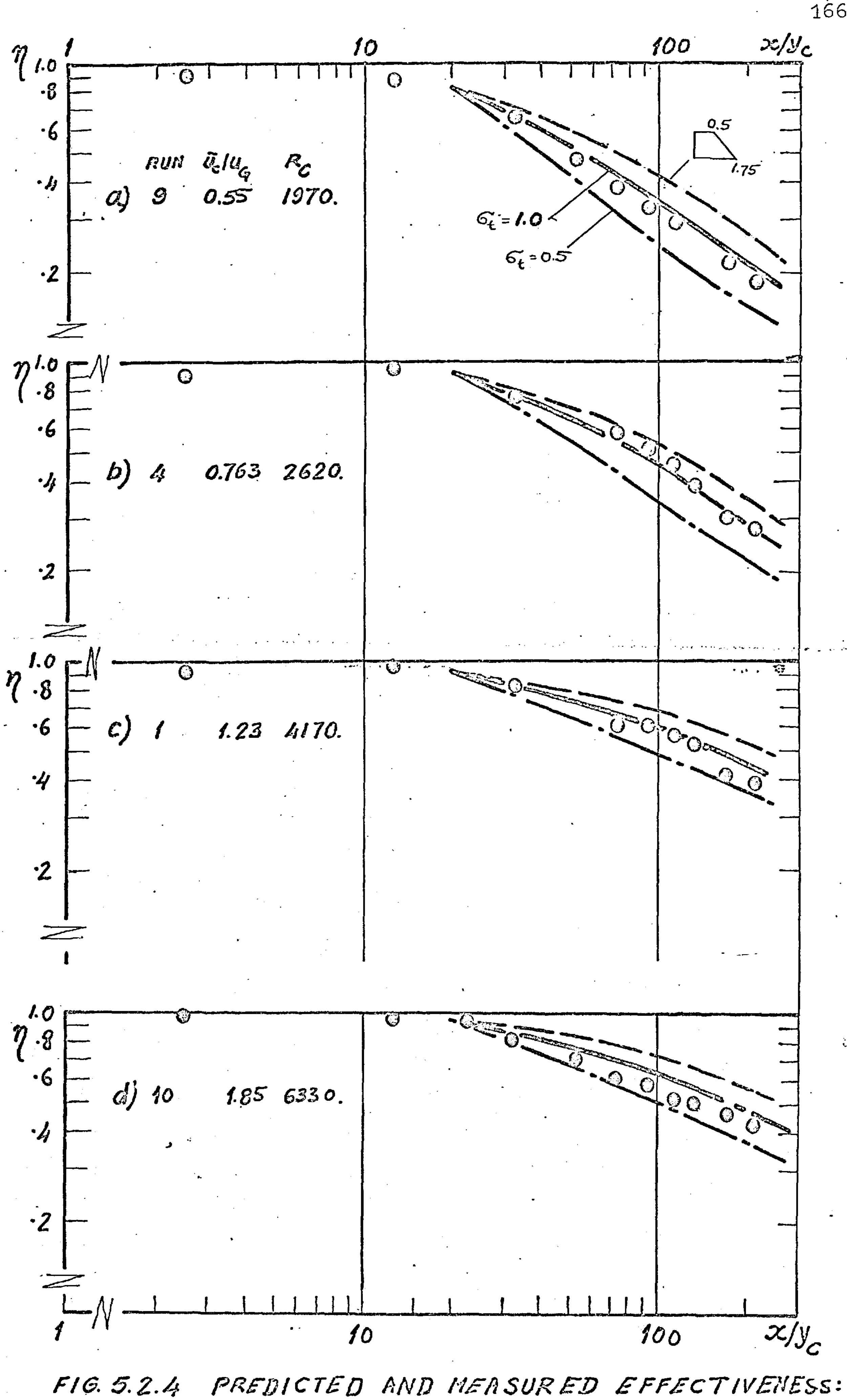

FIG. 5.2.4 PREDICTED AND MEASURED EFFECTIVENESS: PRESENT DATA; $dp/dx = 0$, $\rho_c/\rho_G = 1.0$

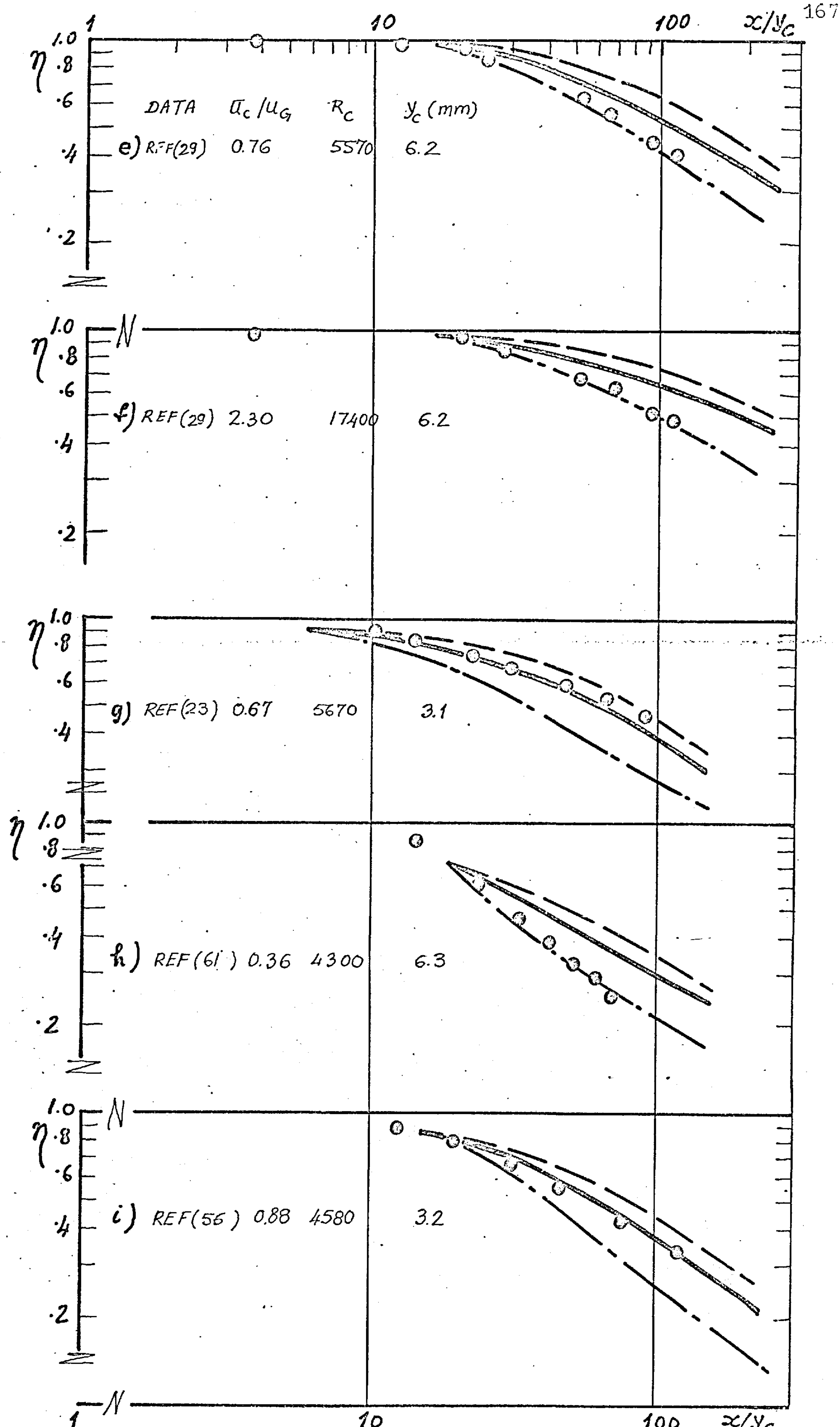

FIG. 5.2.4 (Contd). DATA OF REFS(29) (23) (61) (56); dp/dx=0;

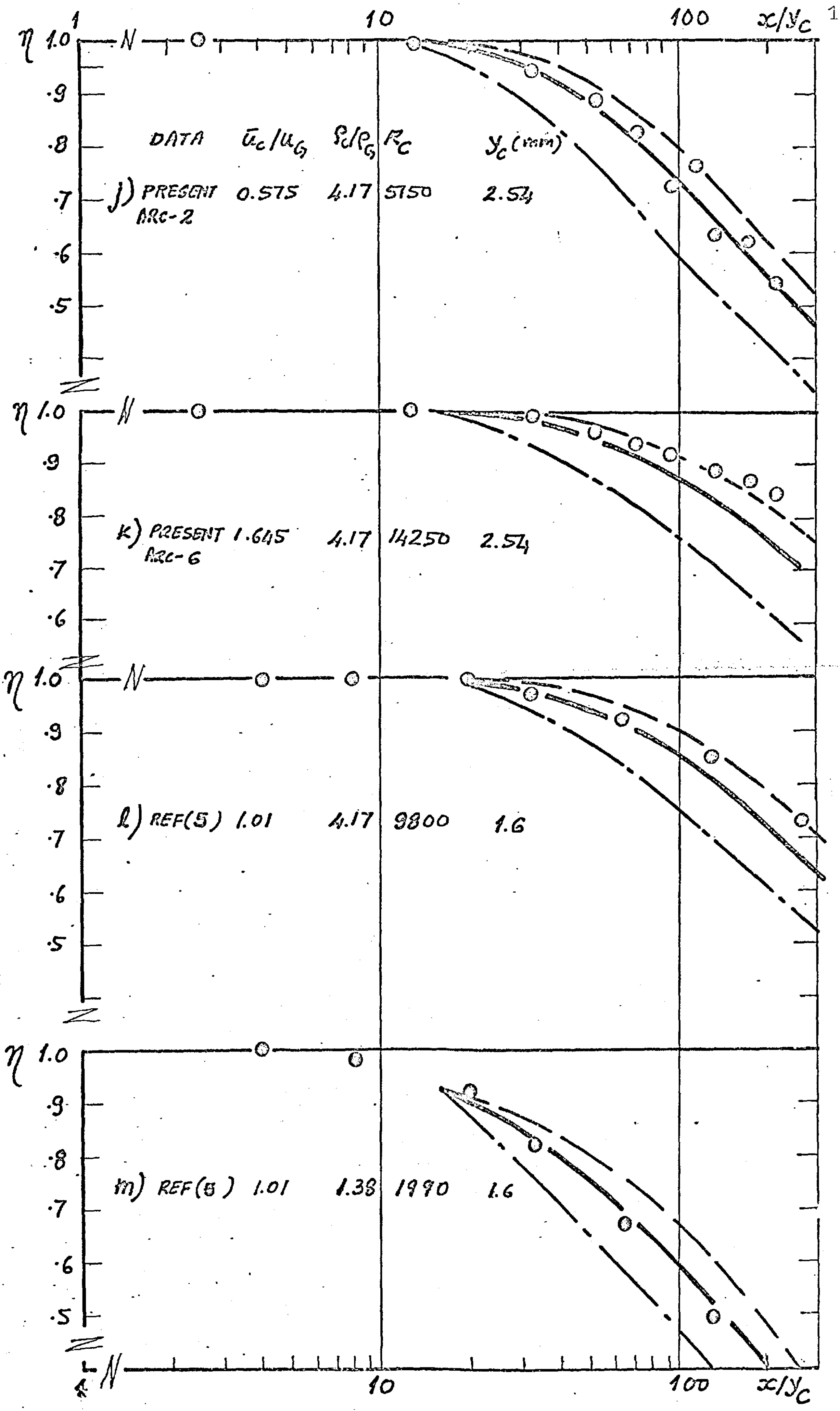

FIG. 5.2.4.(CONCLUDED): PRESENT DATA AND DATA OF REFS (5) : $dp/dx = 0$; $\rho_C/\rho_G > 1$.

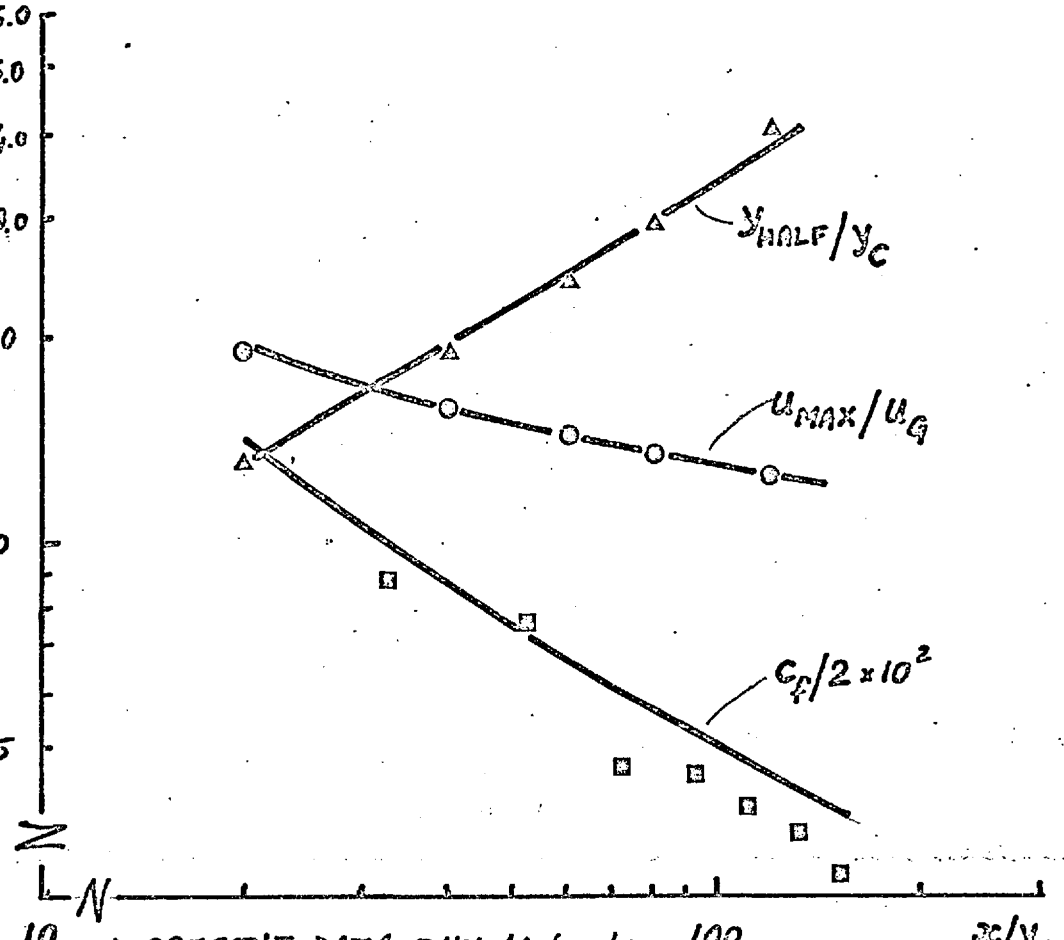

a) PRESENT DATA, RUN 10 (u_c/u_G = 1.85, ρ_c/ρ_G = 1.0)

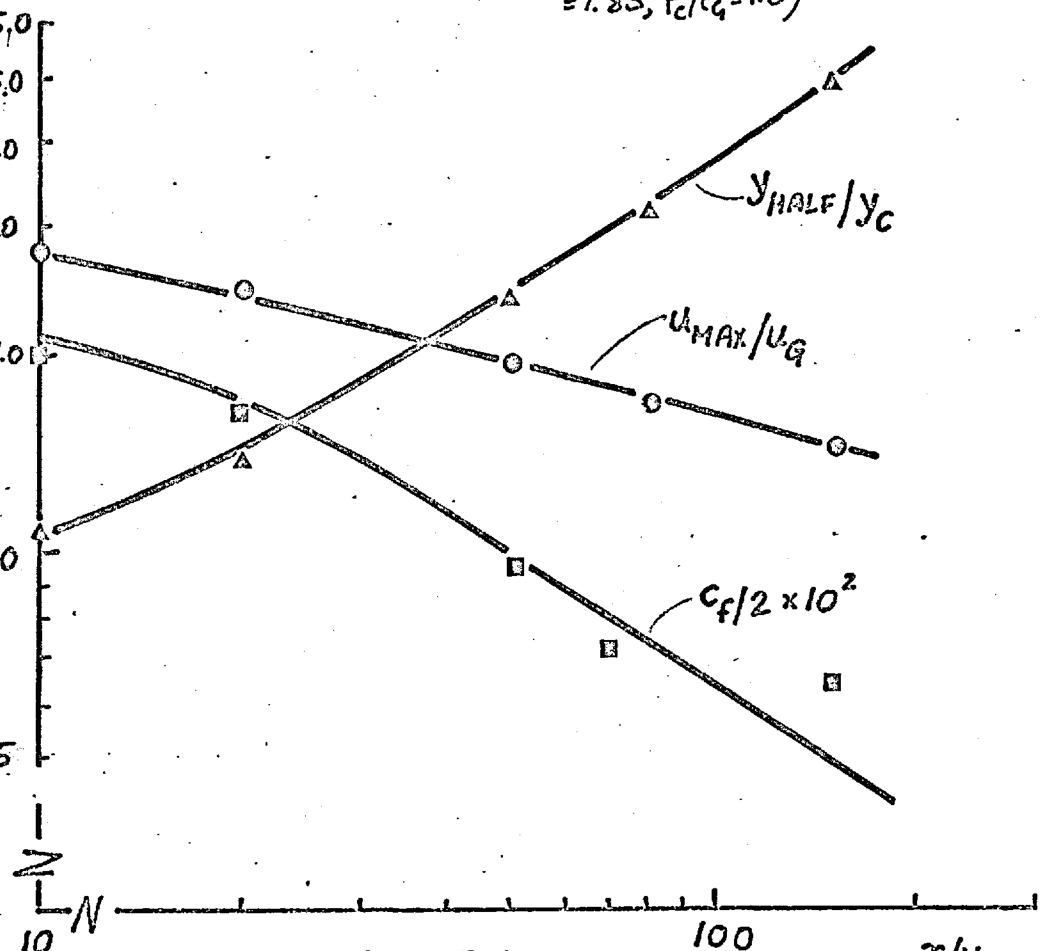

b) DATA OF REF. (28), $\bar{u}_c/u_G$ = 2.74.

FIG. 5:2.5. MEASURED AND PREDICTED WALL JET DEVELOPMENT AND WALL SHEAR STRESS: $\bar{u}_c/u_G > 1.0$, $\rho_c/\rho_G = 1.0$.

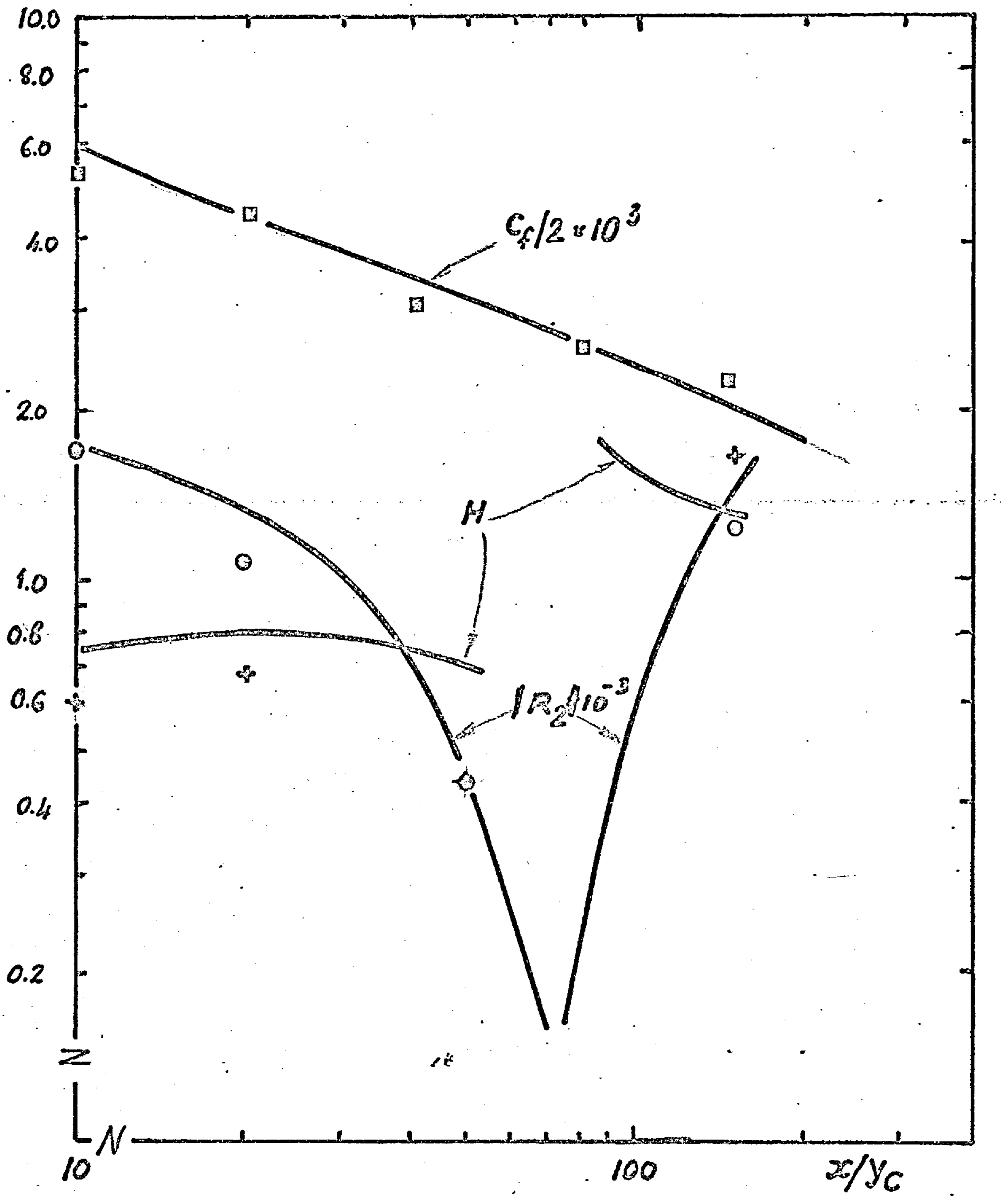

FIG. 5.2.5 (e): MEASURED AND PREDICTED INTEGRAL PROPERTIES AND WALL SHEAR STRESS: $\bar{u}_c/u_G = 1.33$, $\rho_c/\rho_G = 1.0$. (DATA OF REF. (28)).

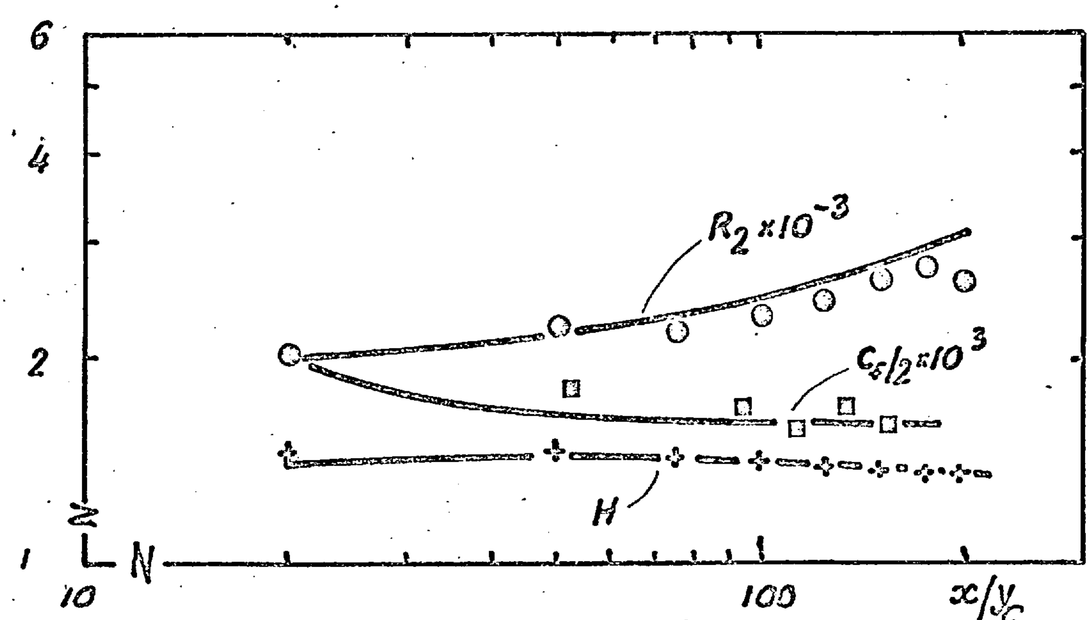

(d) PRESENT DATA (RUN 9) $\bar{u}_c/u_G = 0.55$, $\rho_c/\rho_G = 1.0$

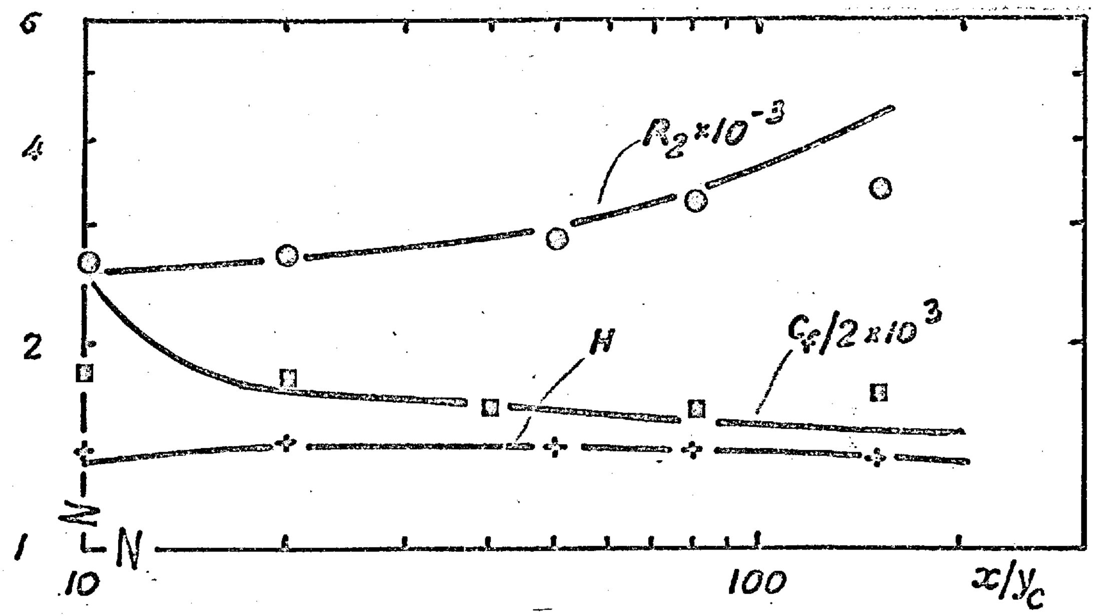

(e) DATA OF REF(28), $\bar{u}_c/u_G = 0.745$

FIG. 5.2.5 (CONCLUDED) MEASURED AND PREDICTED INTEGRAL PROPERTIES AND WALL SHEAR STRESS: $\bar{u}_c/u_G < 1.0$, $\rho_c/\rho_G = 1.0$

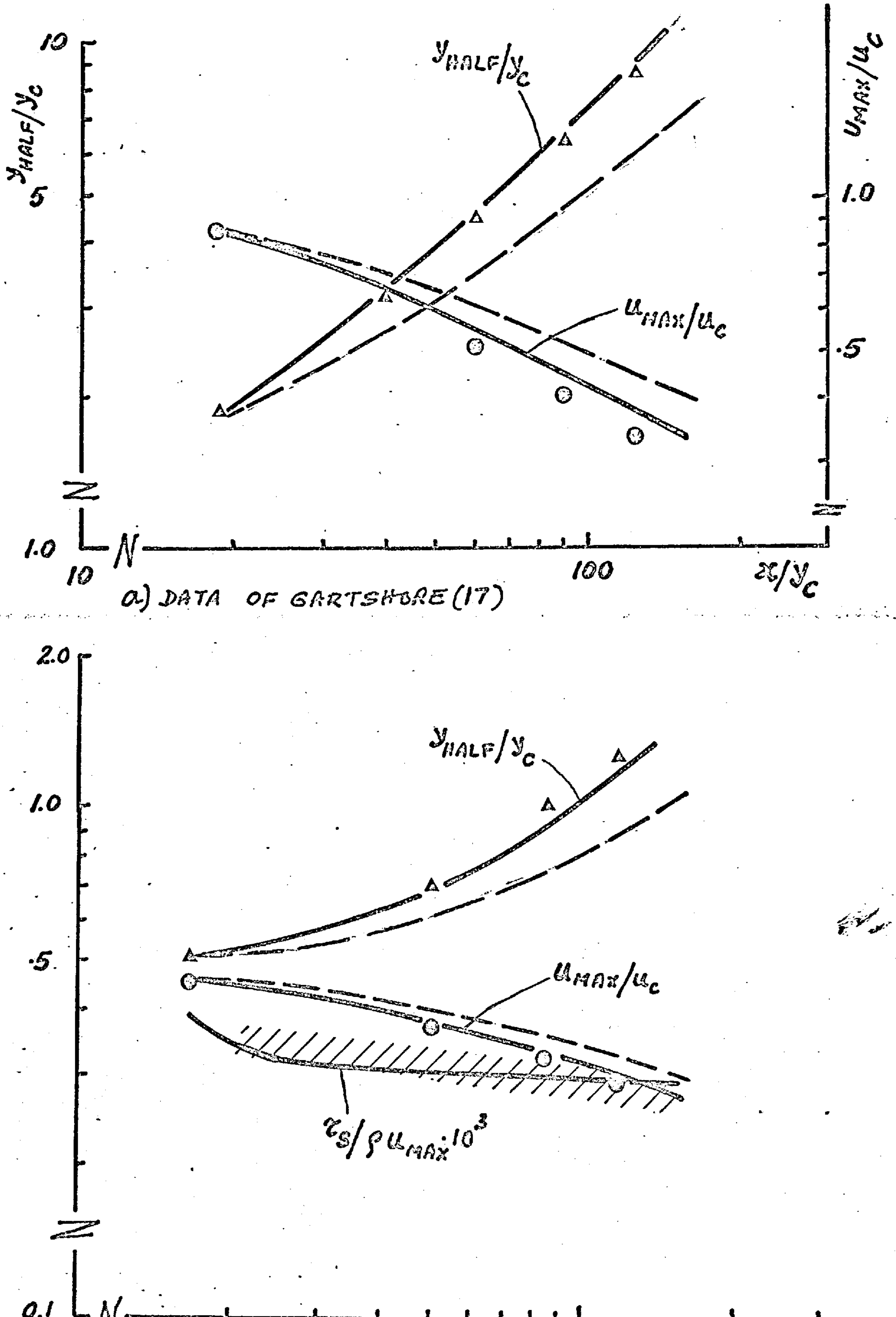

a) DATA OF GARTSHORE (17)

b) DATA OF TAILLAND & MATHIEU (73)

FIG. 52.6. PREDICTION OF WALL JET DEVELOPMENT, $\bar{u}_c/u_g \to \infty$

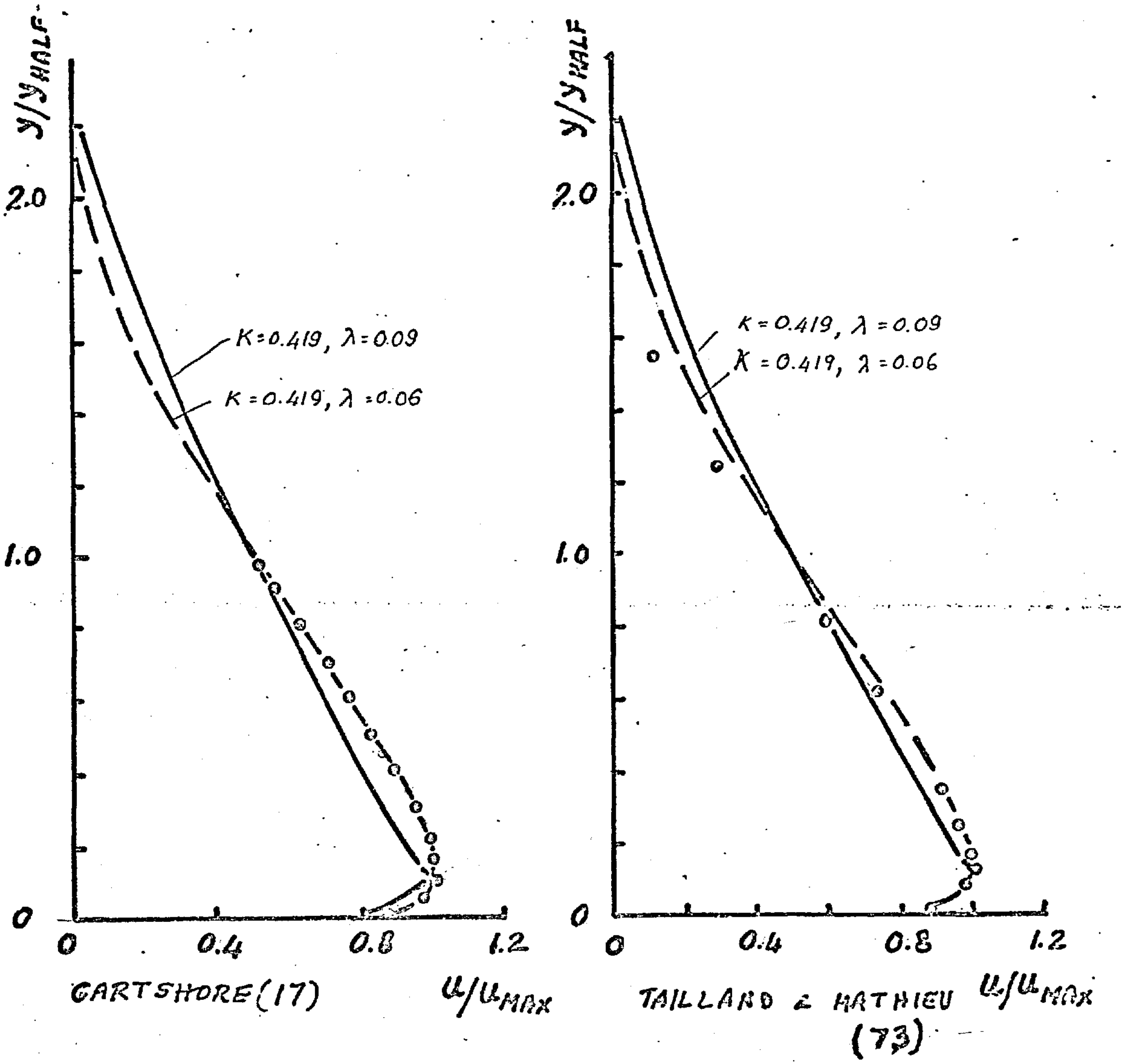

FIG. 5.2.7 PREDICTION OF MEAN VELOCITY PROFILES: $\overline{U}_c/U_G \to \infty$

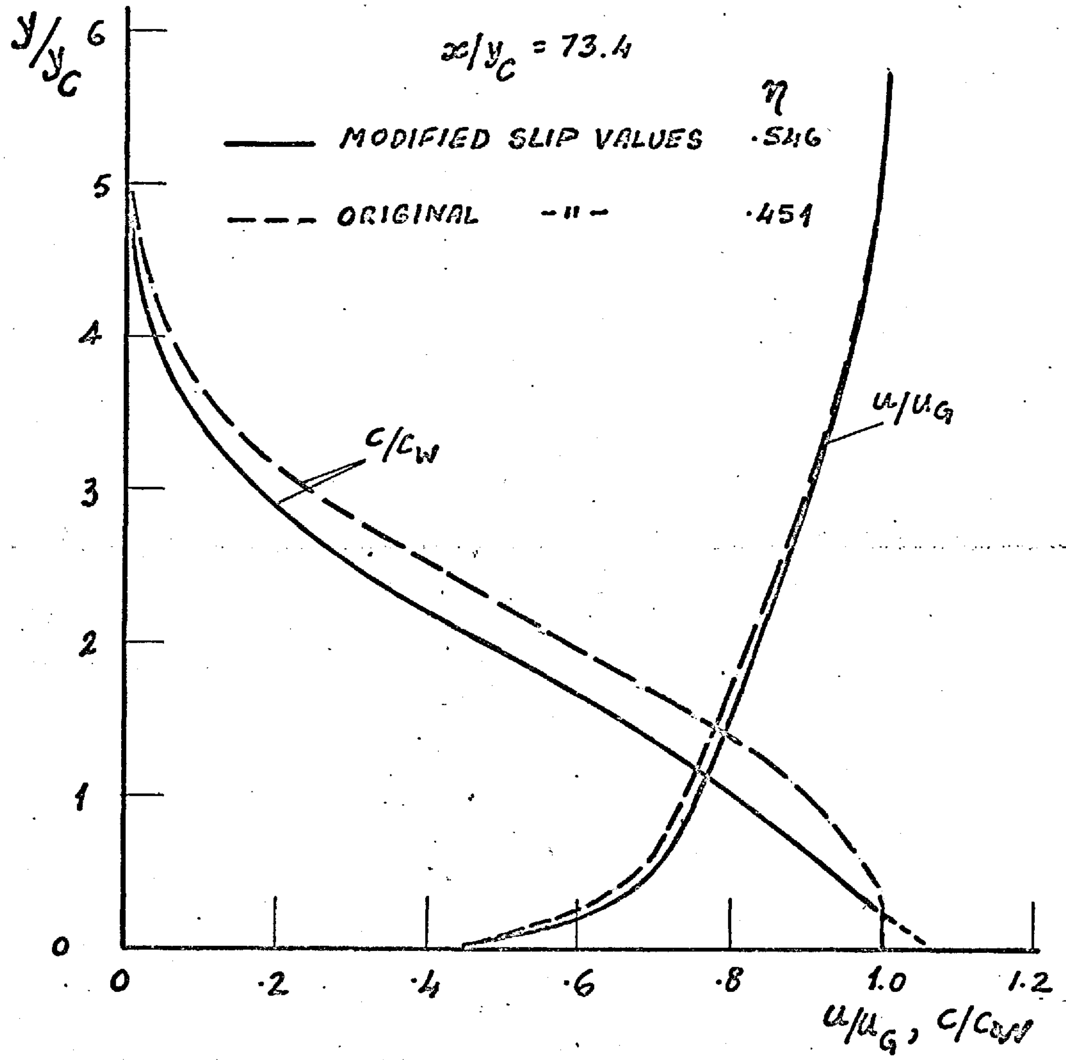

FIG. 5.2.8. INFLUENCE OF MODIFIED SLIP-RELATIONS ON PREDICTED PROFILES OF MEAN VELOCITY AND MASS-FRACTION.

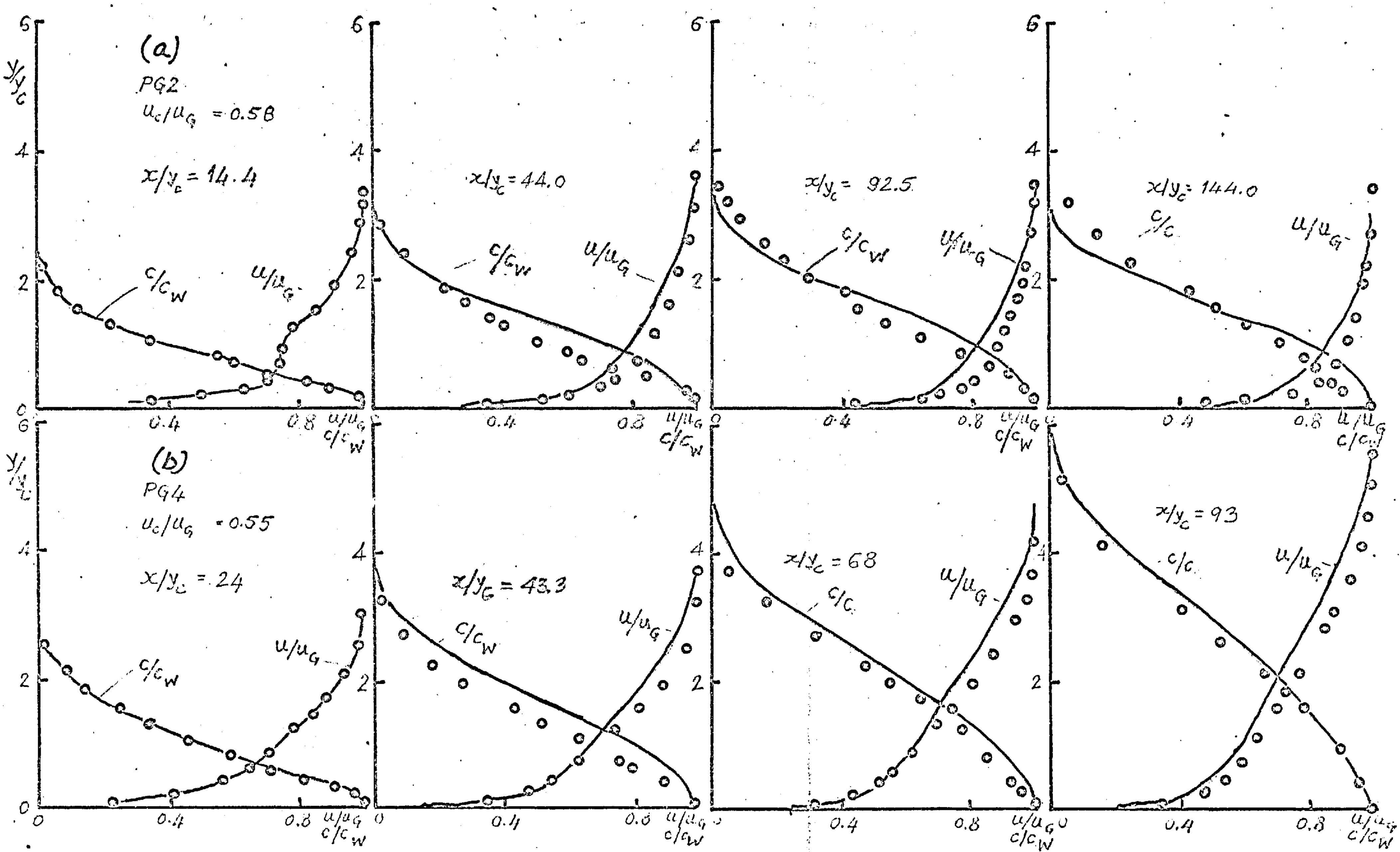

FIG.5.2.9 MEASURED AND PREDICTED PROFILES OF VELOCITY AND CONCENTRATION IN PRESENCE OF PRESSURE-GRADIENTS : $\bar{u}_c/u_G < 1.0$; $\rho_c/\rho_G = 1.0$

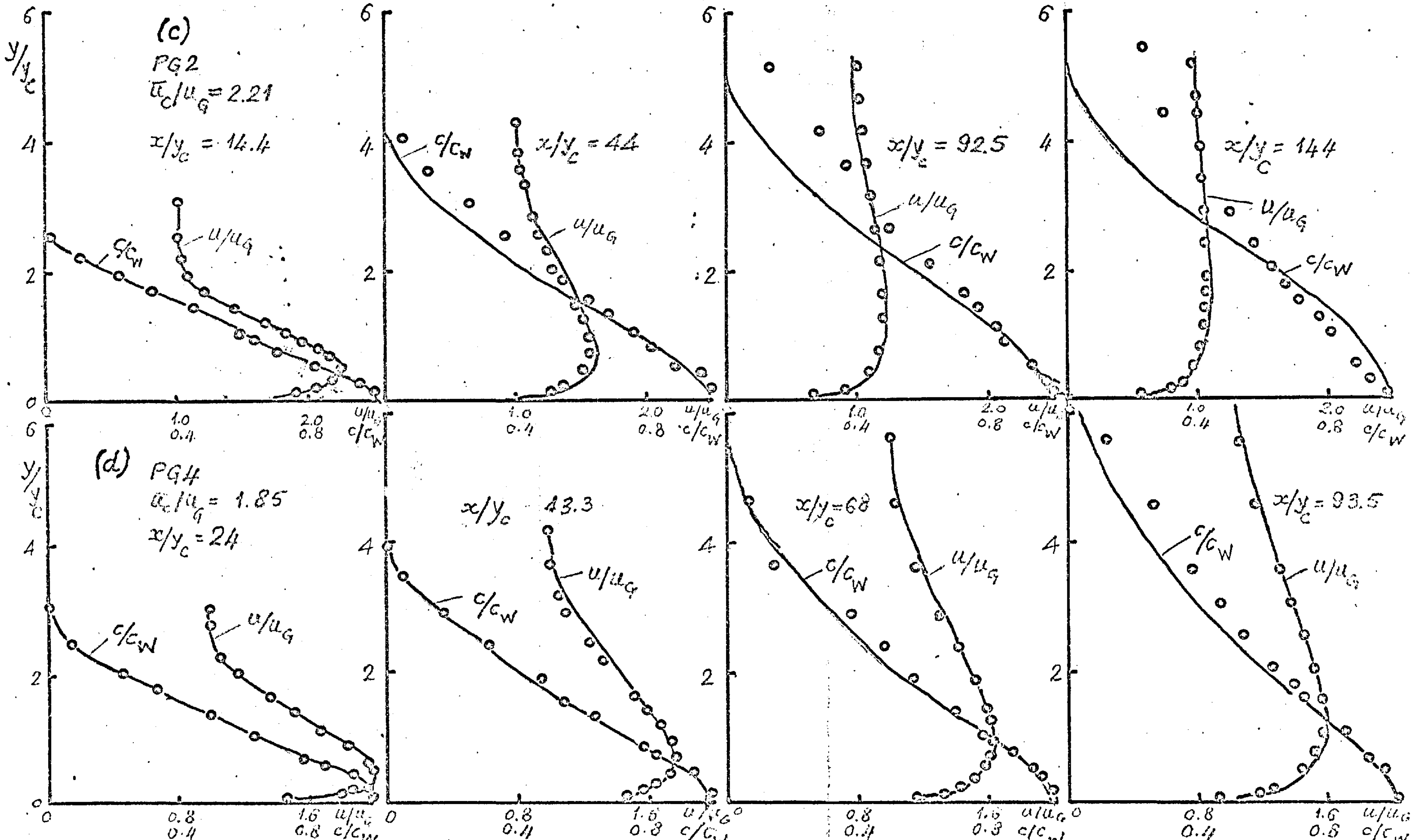

FIG. 5.2.9 (CONTD): $\bar{u}_c/u_G > 1.0$.

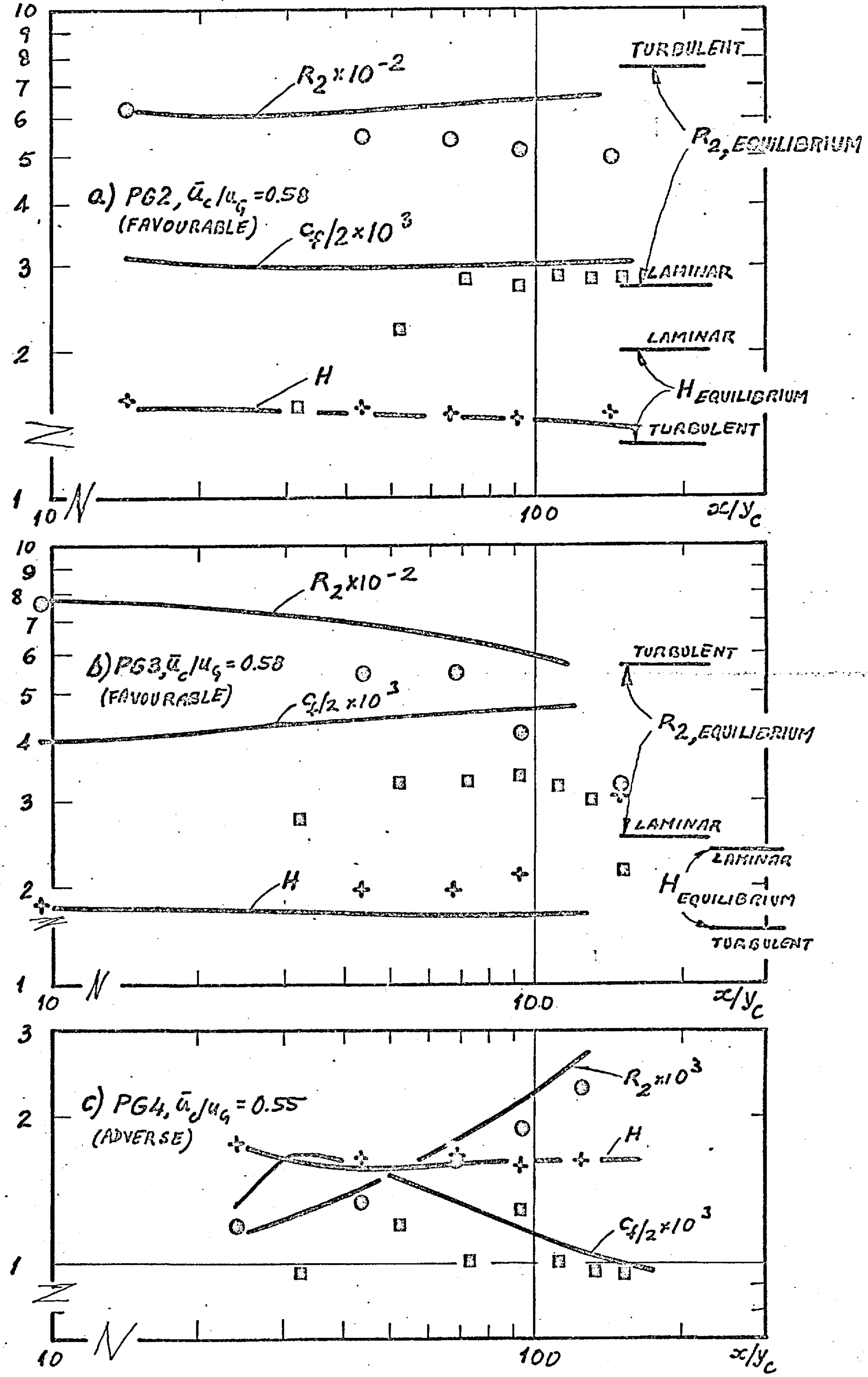

FIG. 5.2.10. PREDICTED AND MEASURED VALUES OF R_2, H AND $C_f/2$ IN PRESSURE GRADIENTS : $\bar{u}_c/u_G < 1.0$.
(○ – R_2; ✢ – H ; □ – $c_f/2$ DATA)

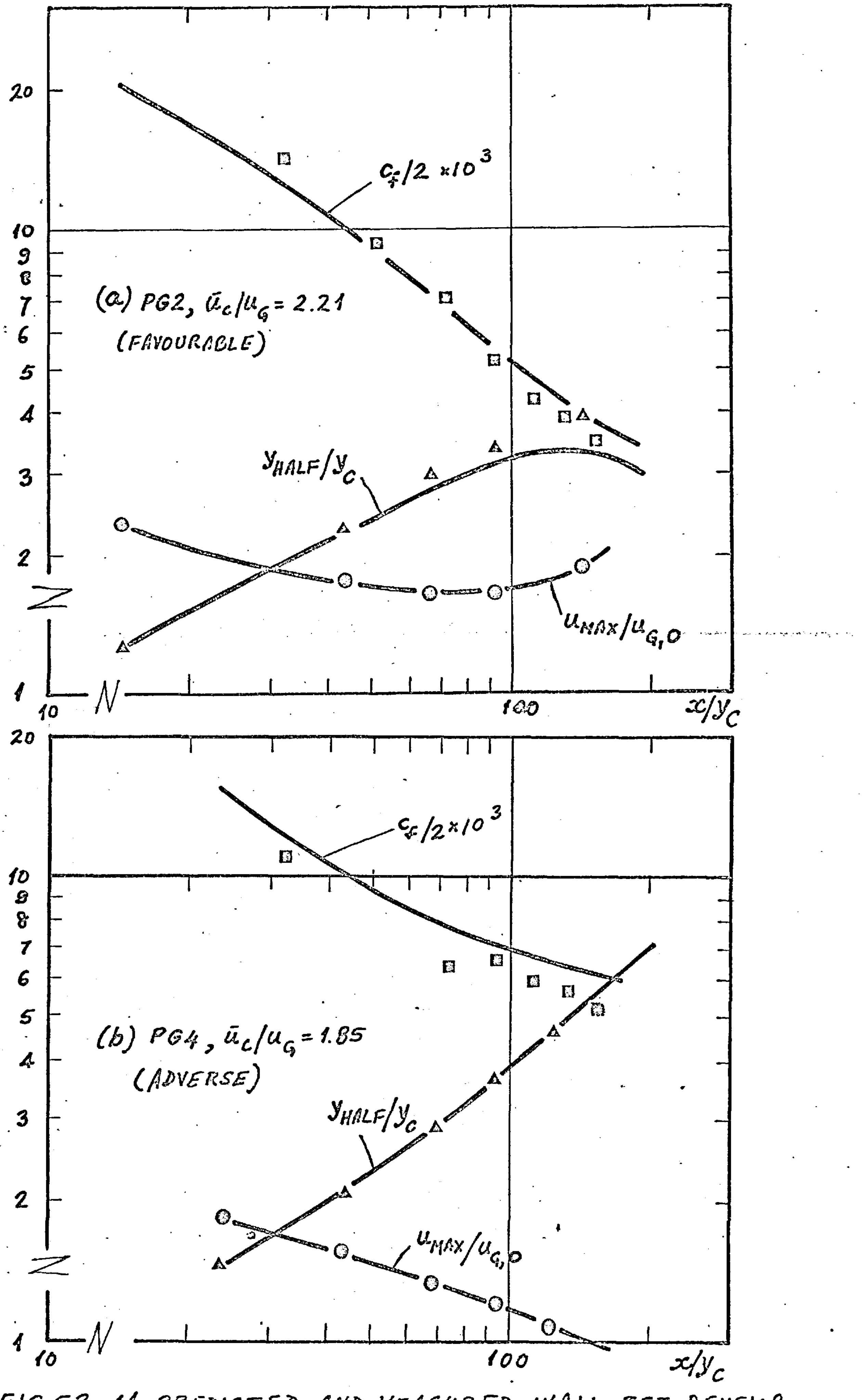

FIG. 5.2.11 PREDICTED AND MEASURED WALL-JET DEVELOPMENT IN FAVOURABLE AND ADVERSE PRESSURE GRADIENTS.

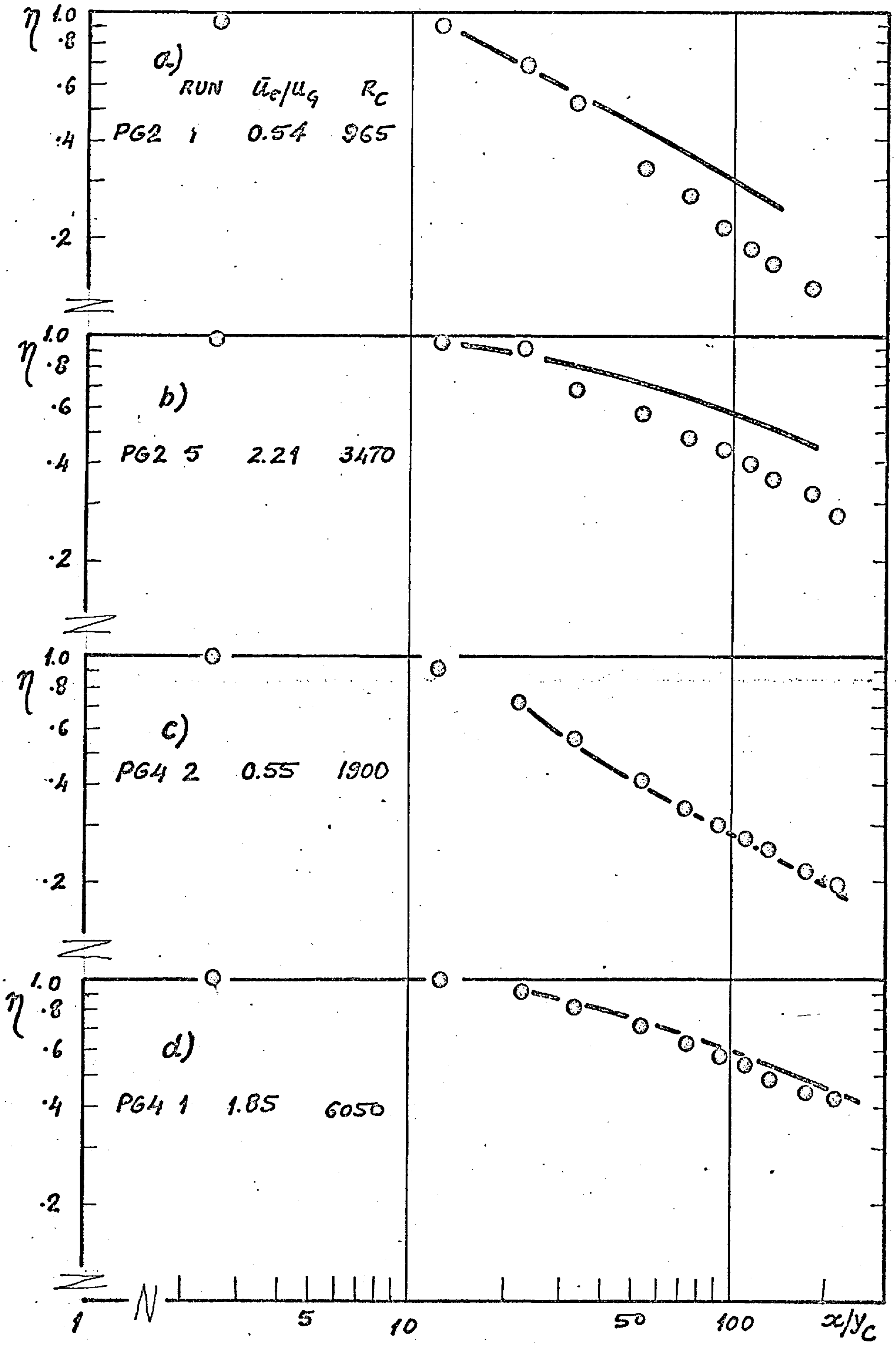

FIG.5.2.12. PREDICTED AND MEASURED IMPERVIOUS WALL EFFECTIVENESS IN PRESENCE OF PRESSURE GRADIENTS.

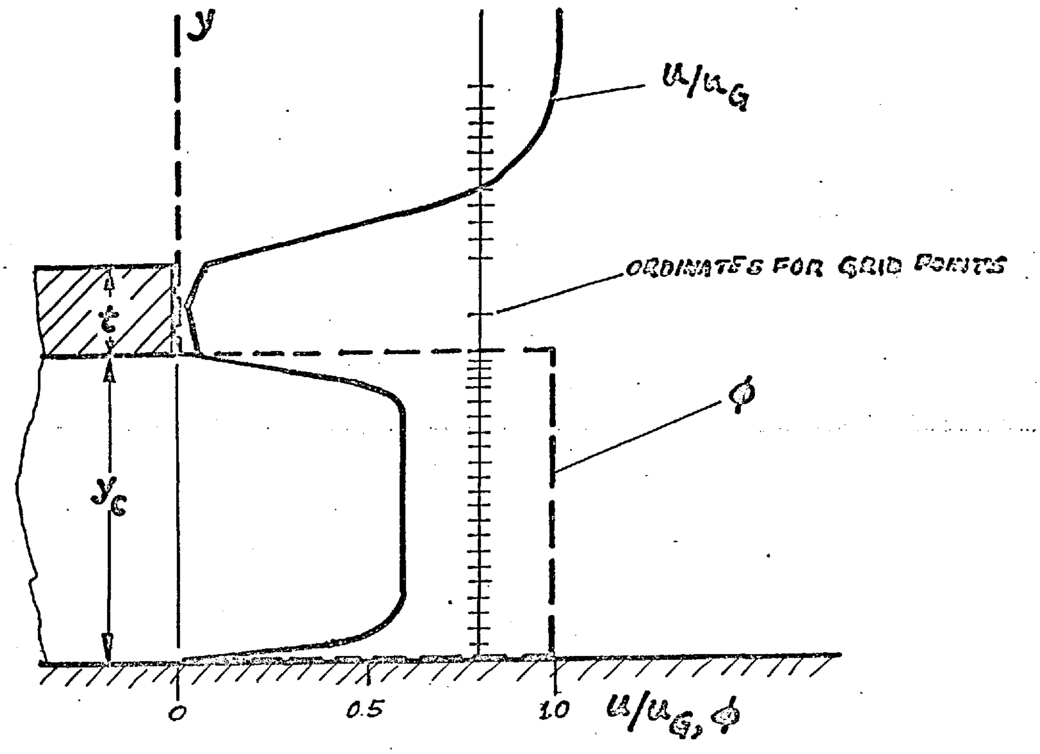

FIG. 6.1.1 TYPICAL PROFILES AND FINITE DIFFERENCE GRID AT SLOT EXIT.

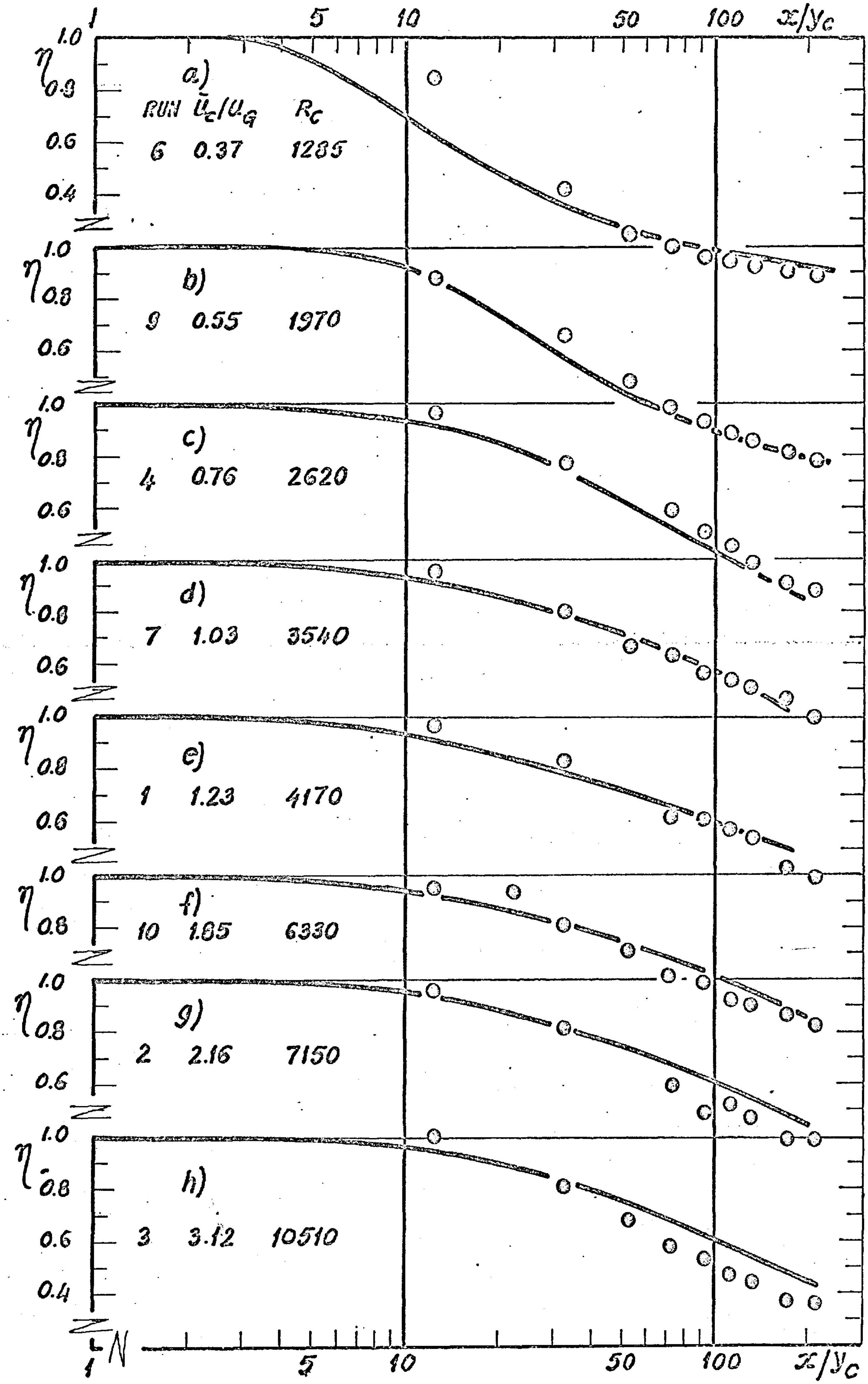

FIG. 6.1.2. PREDICTED AND MEASURED IMPERVIOUS WALL EFFECTIVE-NESS: PRESENT MEASUREMENTS (APPARATUS A), y_c = 2.54 mm ρ_c/ρ_G = 1.0 (AIR + TRACER INJECTION).

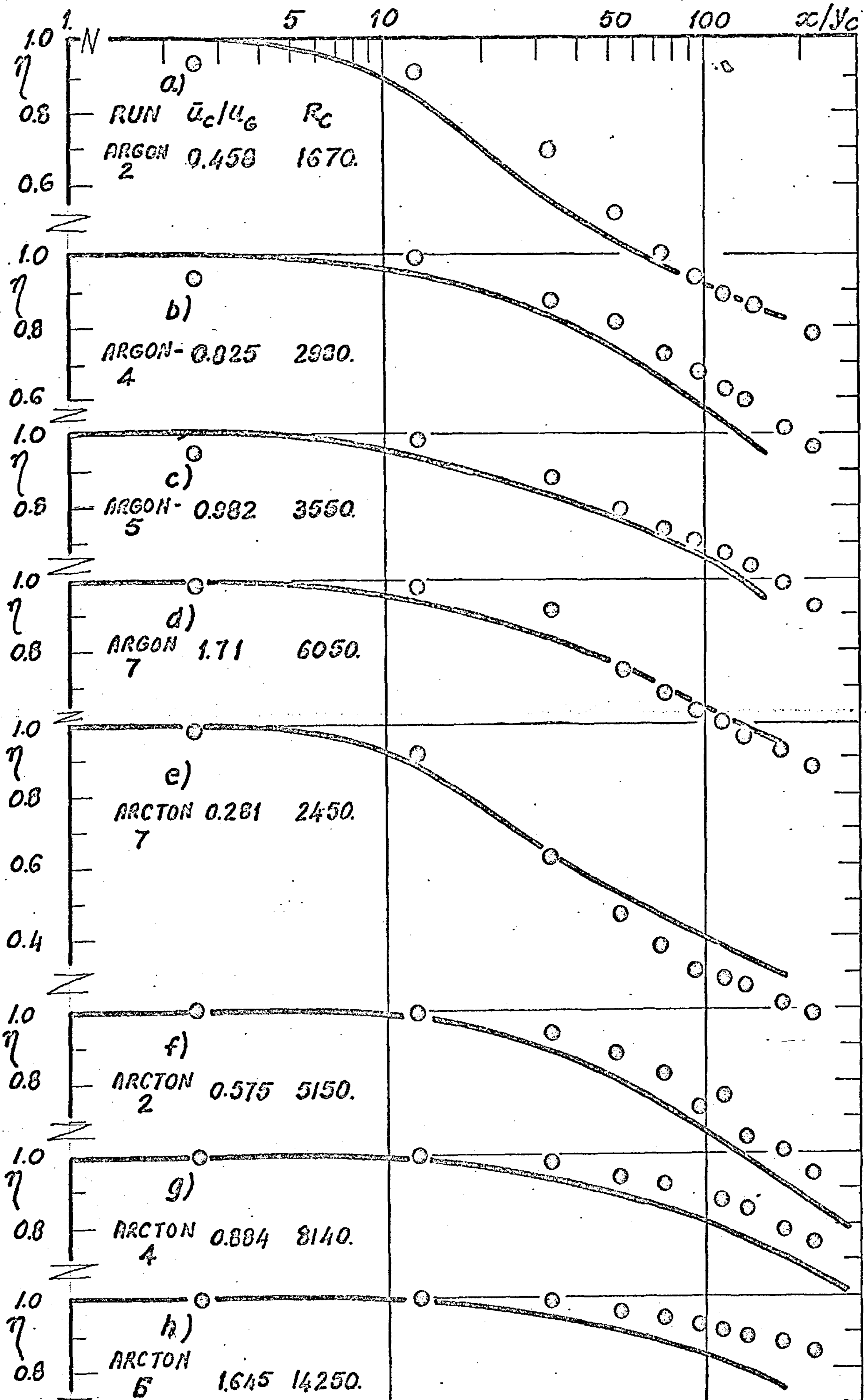

FIG. 6.1.3. PREDICTED AND MEASURED IMPERVIOUS WALL EFFECTIVE-NESS: PRESENT MEASUREMENTS (APPARATUS A), $y_c = 2.54$ mm, $\rho_c/\rho_G > 1.0$ (ARGON AND ARCTON-12 INJECTION).

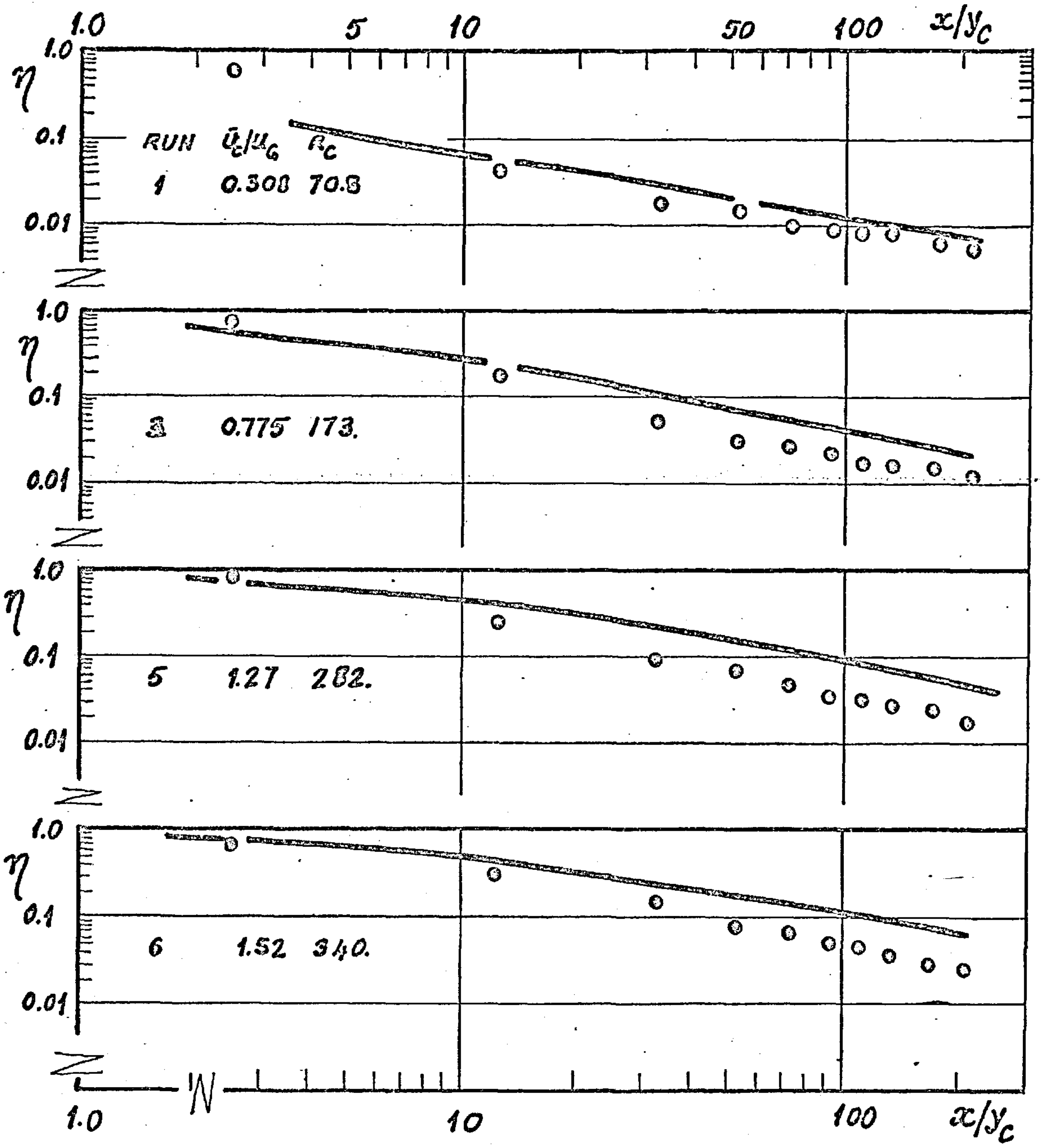

FIG. 6.1.4. PREDICTED AND MEASURED IMPERVIOUS WALL EFFECTIVENESS: PRESENT MEASUREMENTS FOR HYDROGEN INJECTION ($\rho_c/\rho_G = 0.069$).

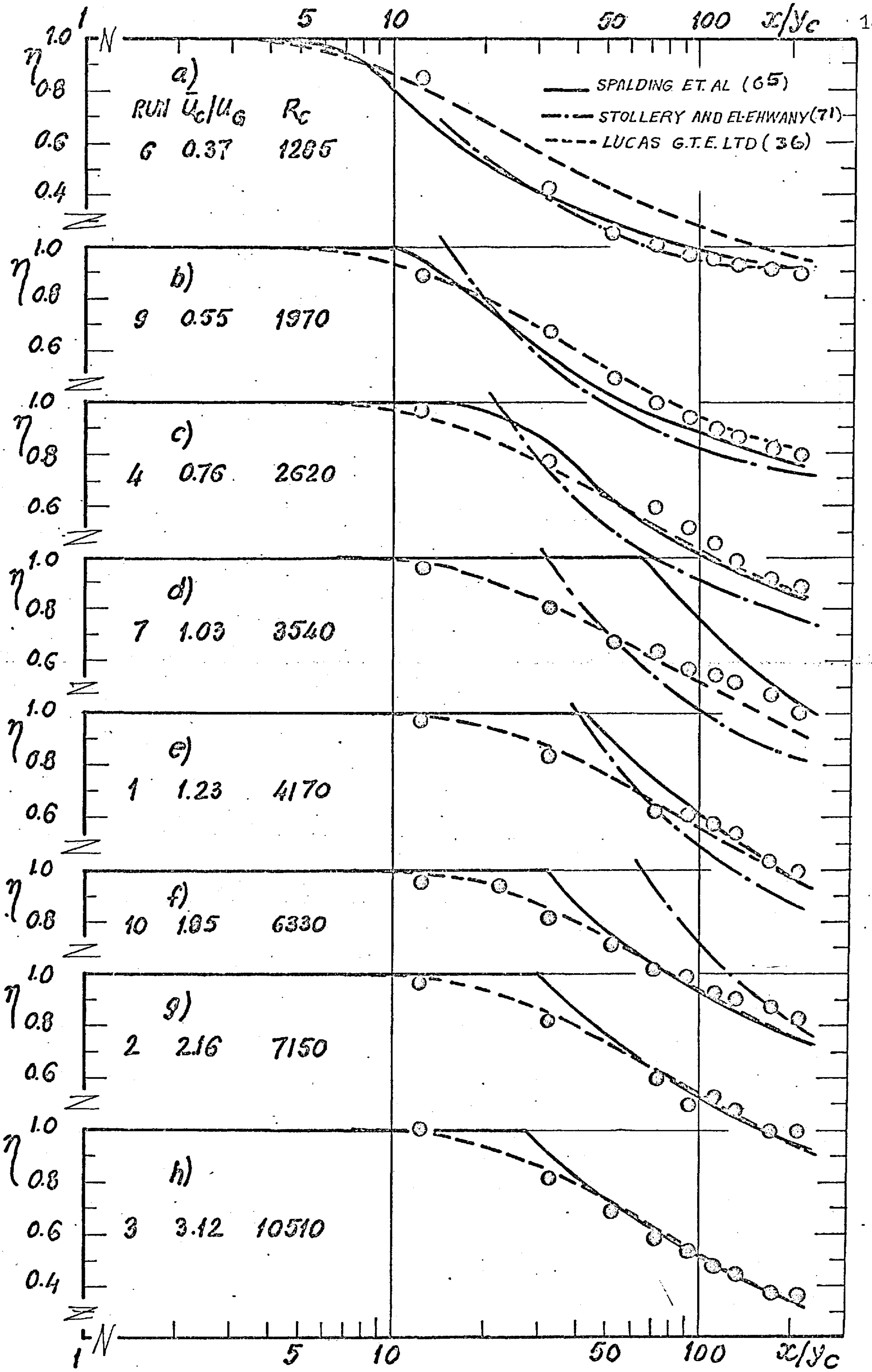

FIG. 6.1.5. PREDICTIONS OF PRESENT DATA FROM CORRELATIONS OF REFERENCES (65), (71), (36): $\rho_c/\rho_G = 1.0$.

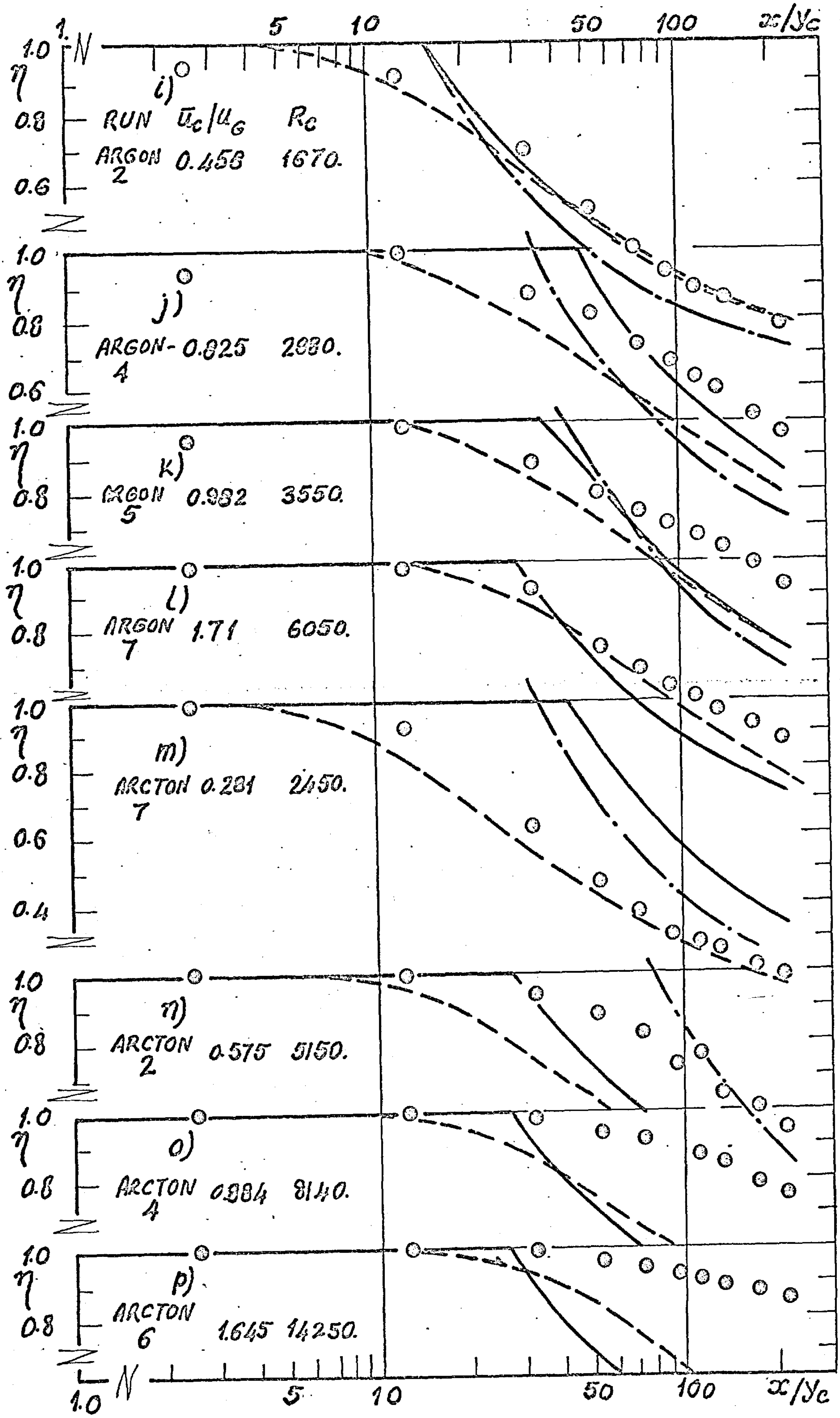

FIG. 6.1.5. (CONTD.) DENSITY RATIO. $\rho_c/\rho_G > 1.0$.

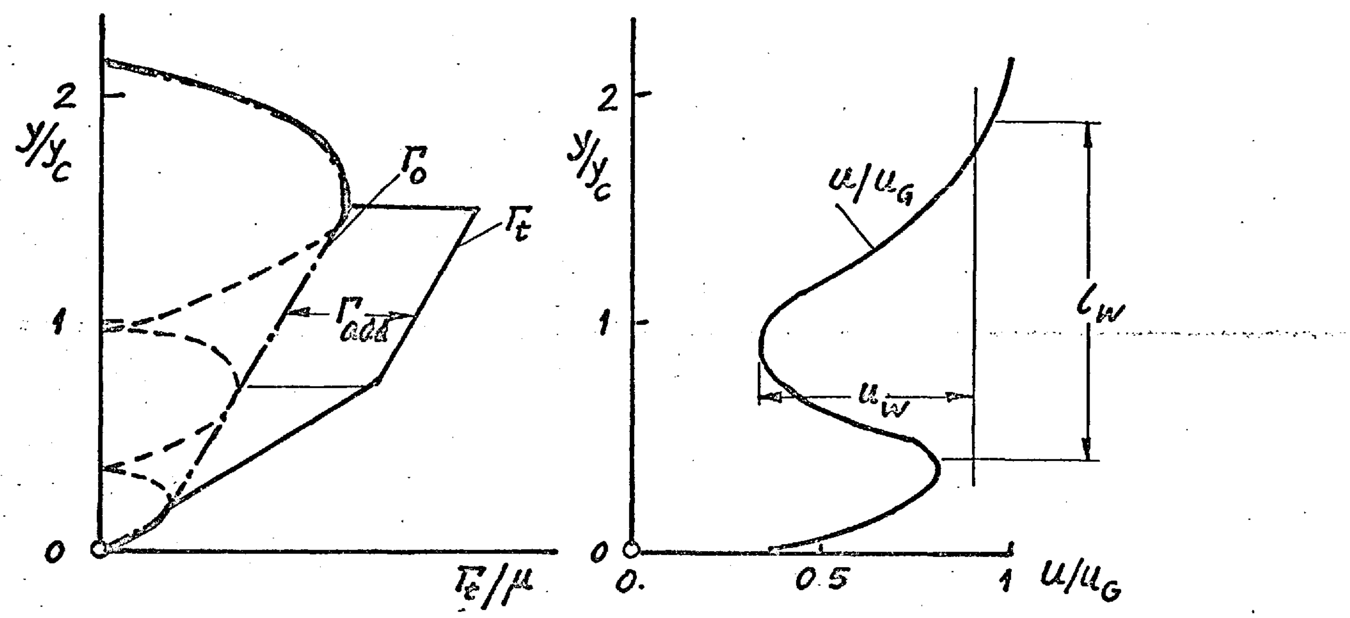

FIG.6.2.1. EDDY DIFFUSIVITY PROFILE USED FOR PREDICTION OF THE INFLUENCE OF LIP THICKNESS ON EFFECTIVENESS.

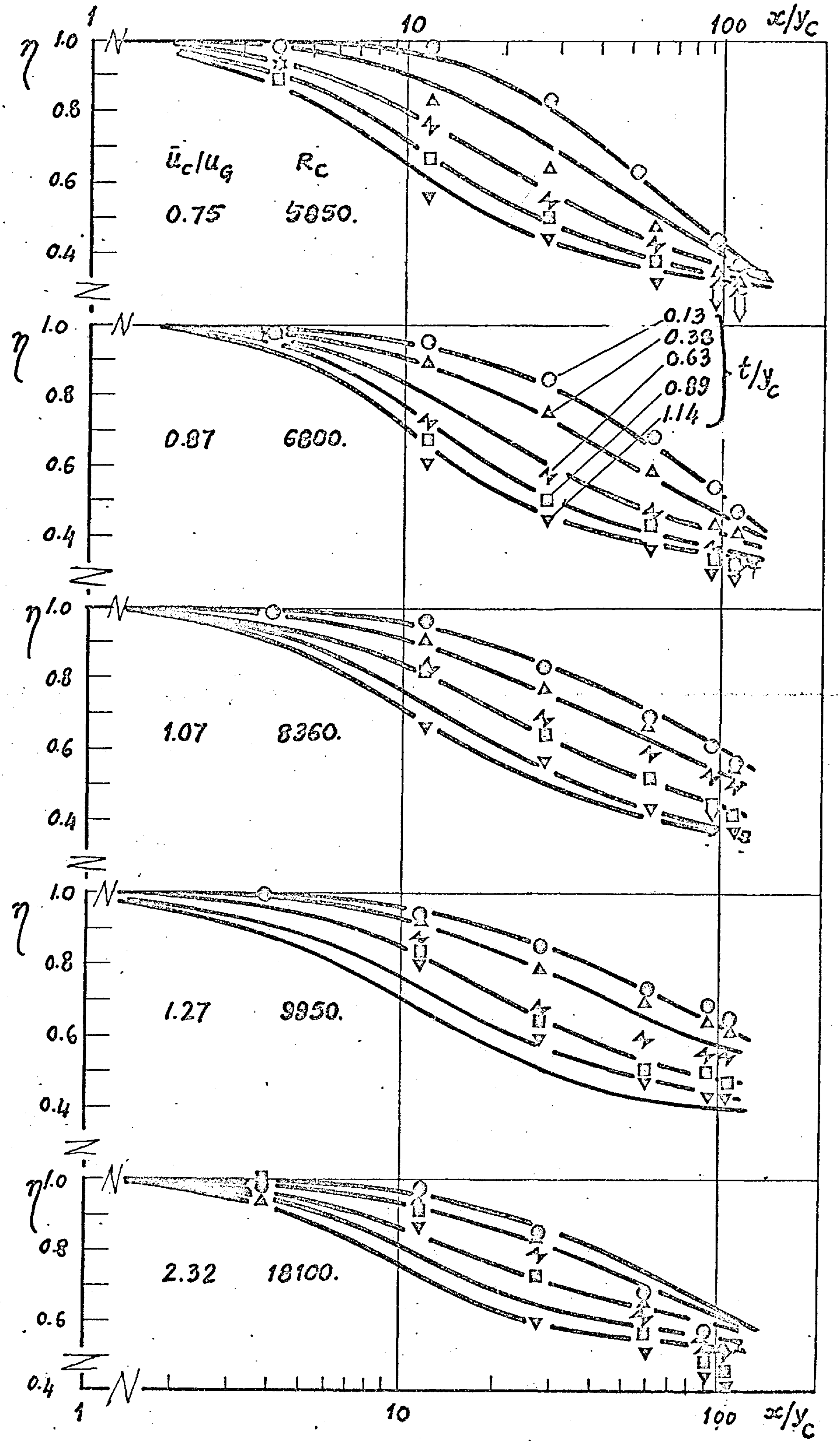

FIG.6.2.2. PREDICTED AND MEASURED IMPERVIOUS WALL EFFECTIVENESS: INFLUENCE OF SLOT LIP THICKNESS: DATA OF REFERENCE(30), $\rho_c/\rho_G = 1.0$, $y_c = 6.2$ mm

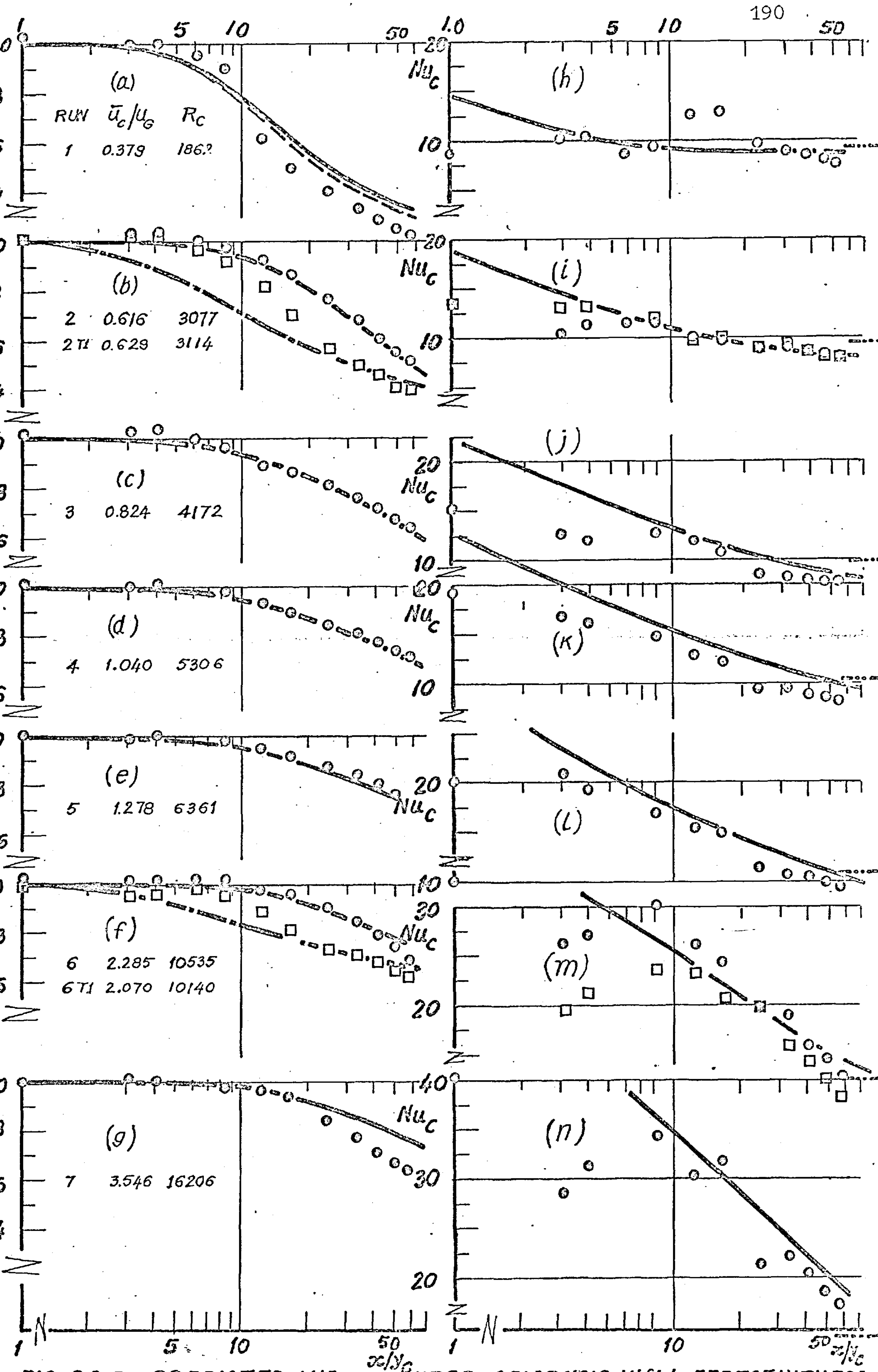

FIG. 6.2.3. PREDICTED AND MEASURED ADIABATIC WALL EFFECTIVENESS AND HEAT TRANSFER COEFFICIENT : PRESENT MEASUREMENTS (APPARATUS B), $y_c = 4.7$ mm , $\rho_c/\rho_G = 0.93$, $t/y_c = 0.35$ AND 1.0.

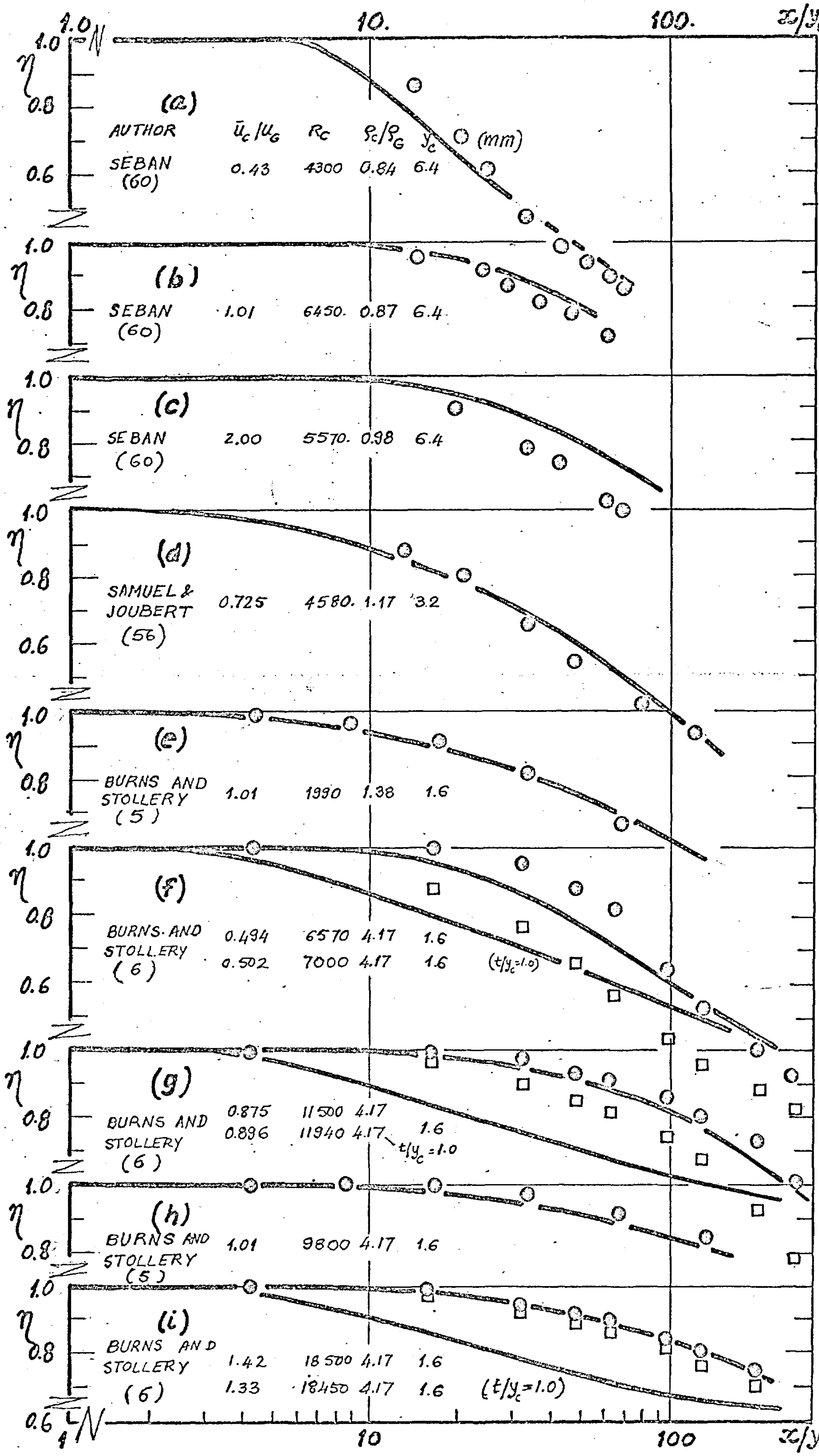

FIG.6.2.4 PREDICTED AND MEASURED EFFECTIVENESS: DATA OF REFS (60), (56), (5) AND (6).

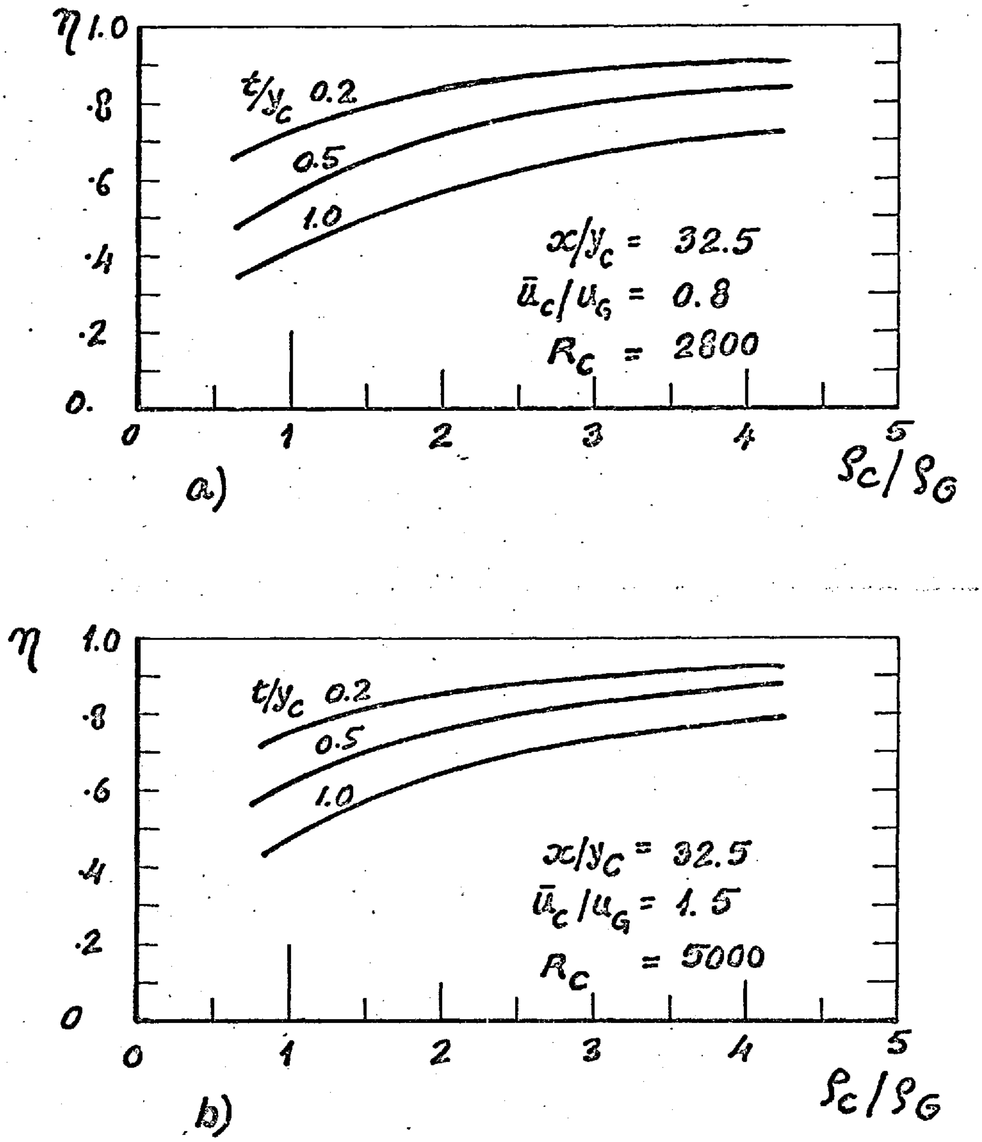

FIG. 6.2.5. PREDICTED INFLUENCE OF DENSITY AND LIP THICKNESS RATIO ON EFFECTIVENESS.

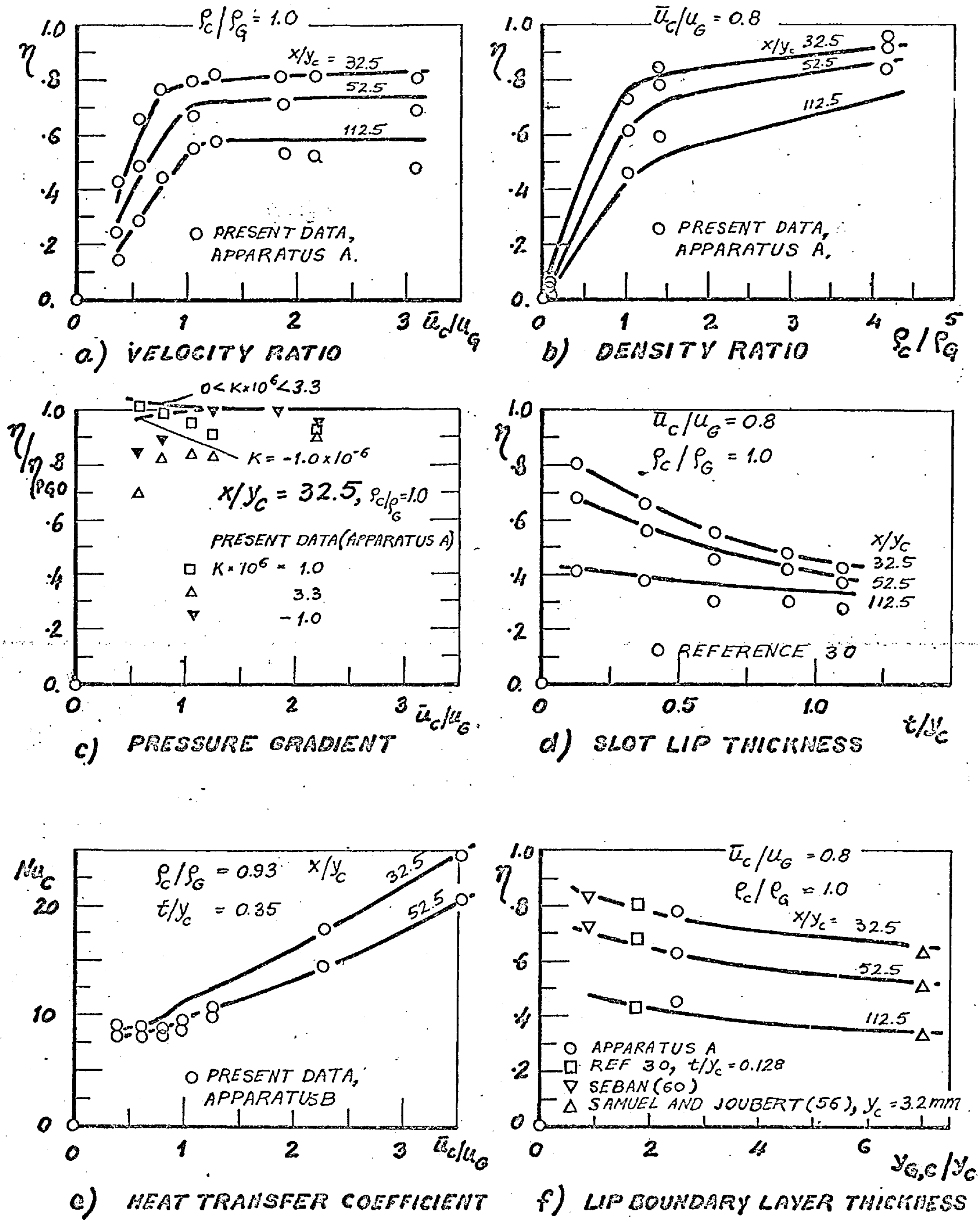

FIG. 6.5.1. SUMMARY OF COMPARISONS OF PREDICTIONS AND EXPERIMENTAL DATA FOR EFFECTIVENESS AND HEAT TRANSFER COEFFICIENT.

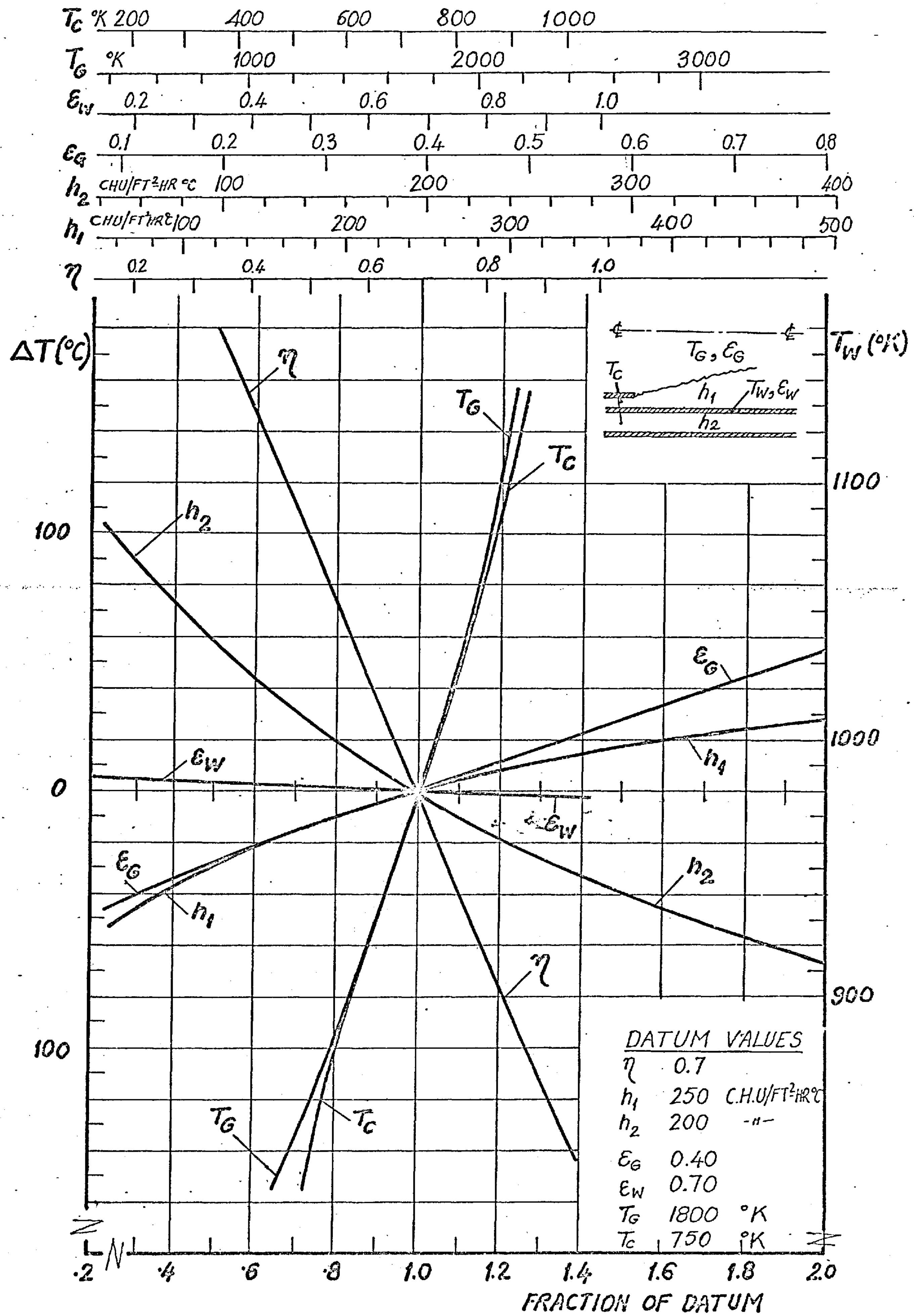

FIG. 6.6.1. INFLUENCE OF η, h_1, h_2, ε_G, ε_W, T_G AND T_C ON THE TEMPERATURE OF A FILM-COOLED SURFACE.

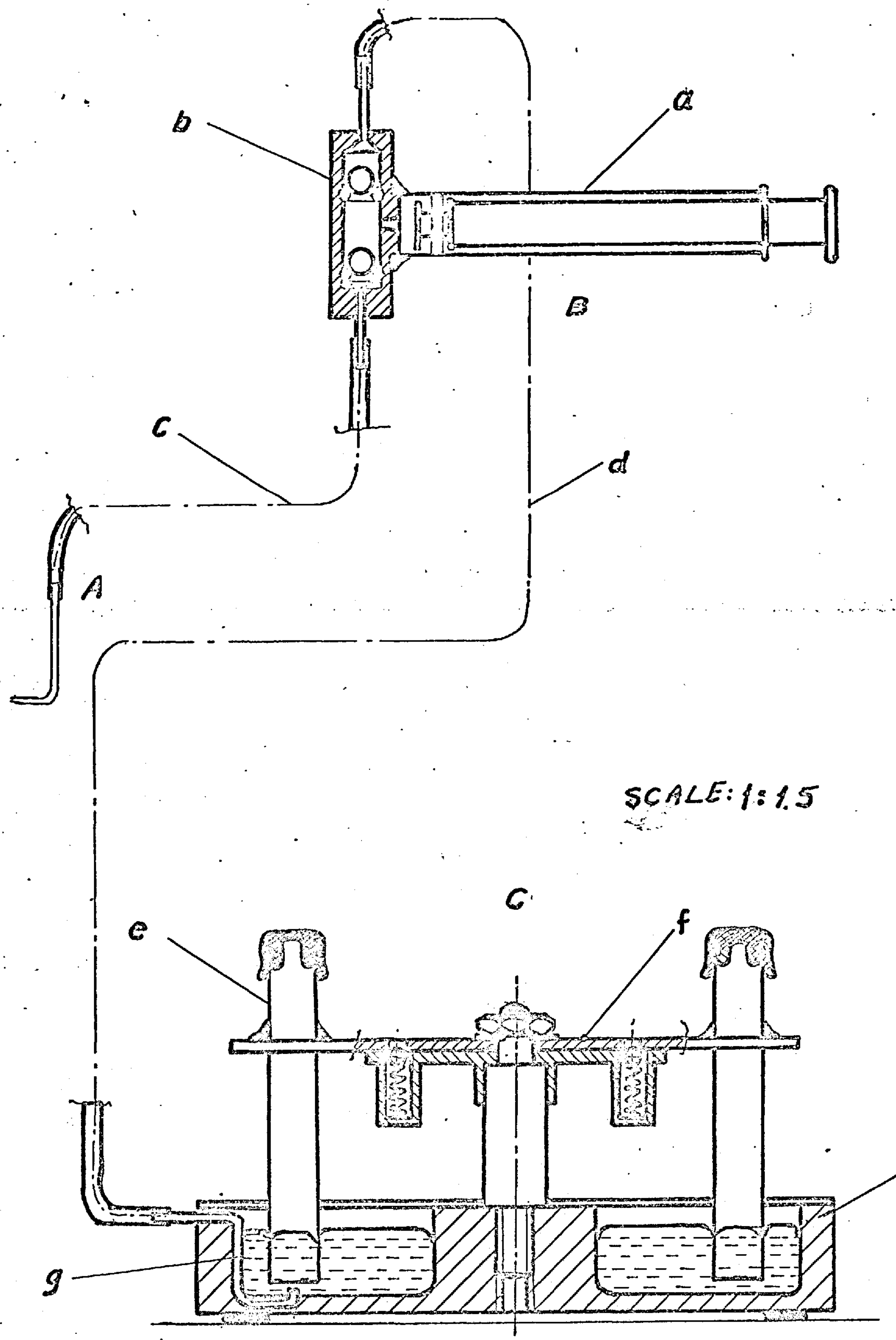

FIG. A.1-1 GAS SAMPLING SYSTEM.

Fig.A.1.2 Bank of Sample Bottles.

Fig. A.1.3 Rotary Pressure Switch.

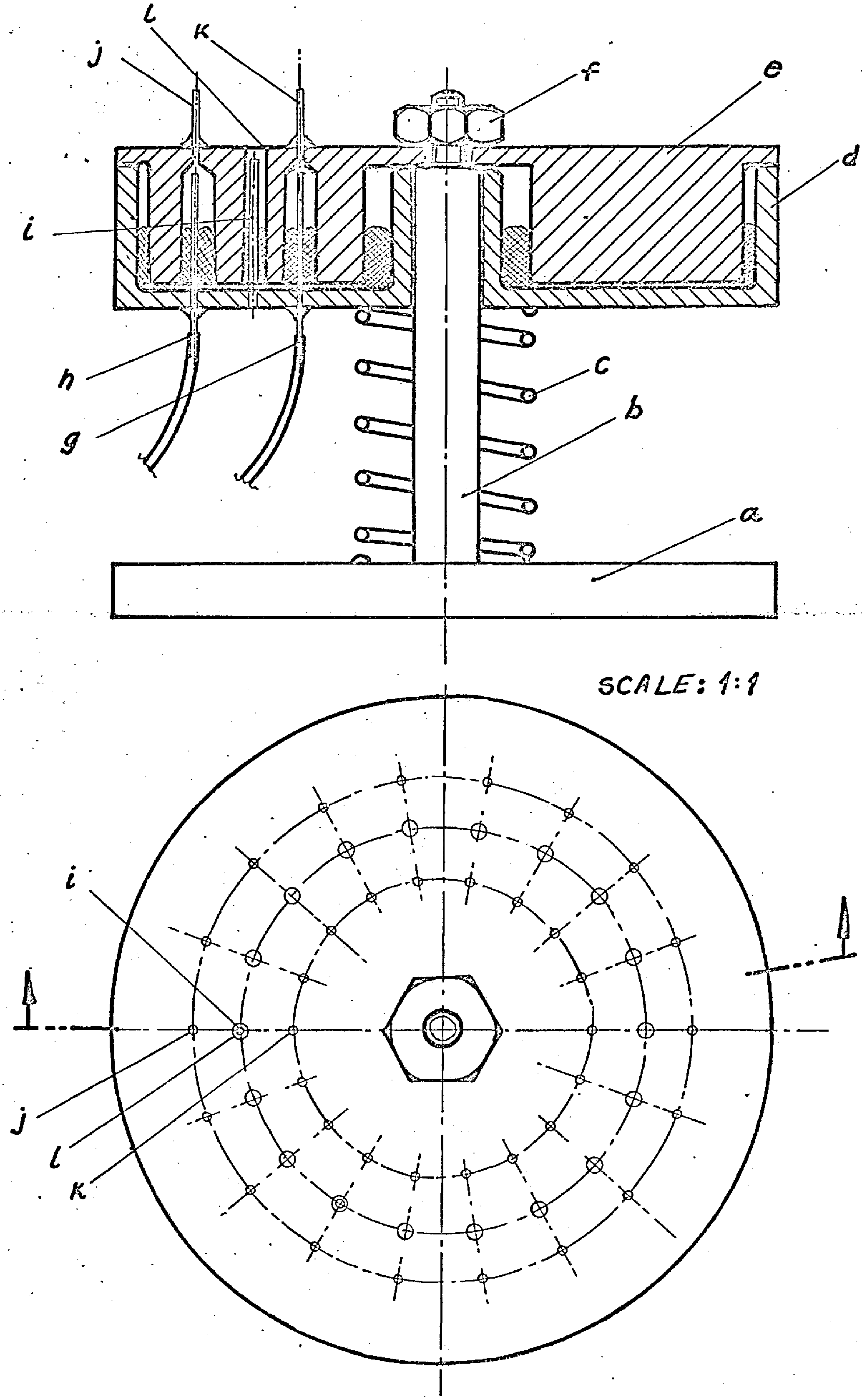

FIG. A.1.-4 : A ROTARY PRESSURE SWITCH.

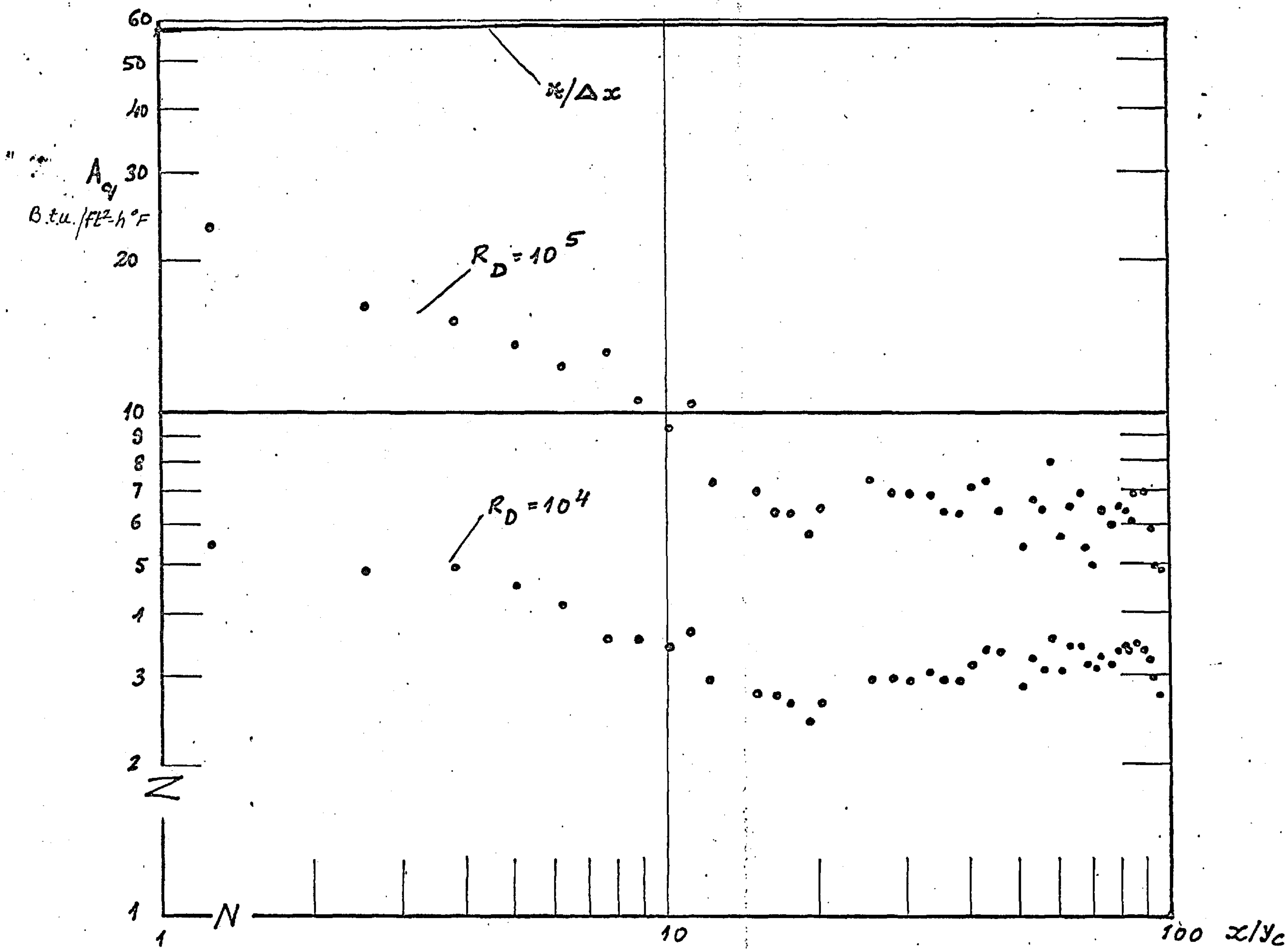

FIG. A.2.1 HEAT-METER CALIBRATION CONSTANTS.

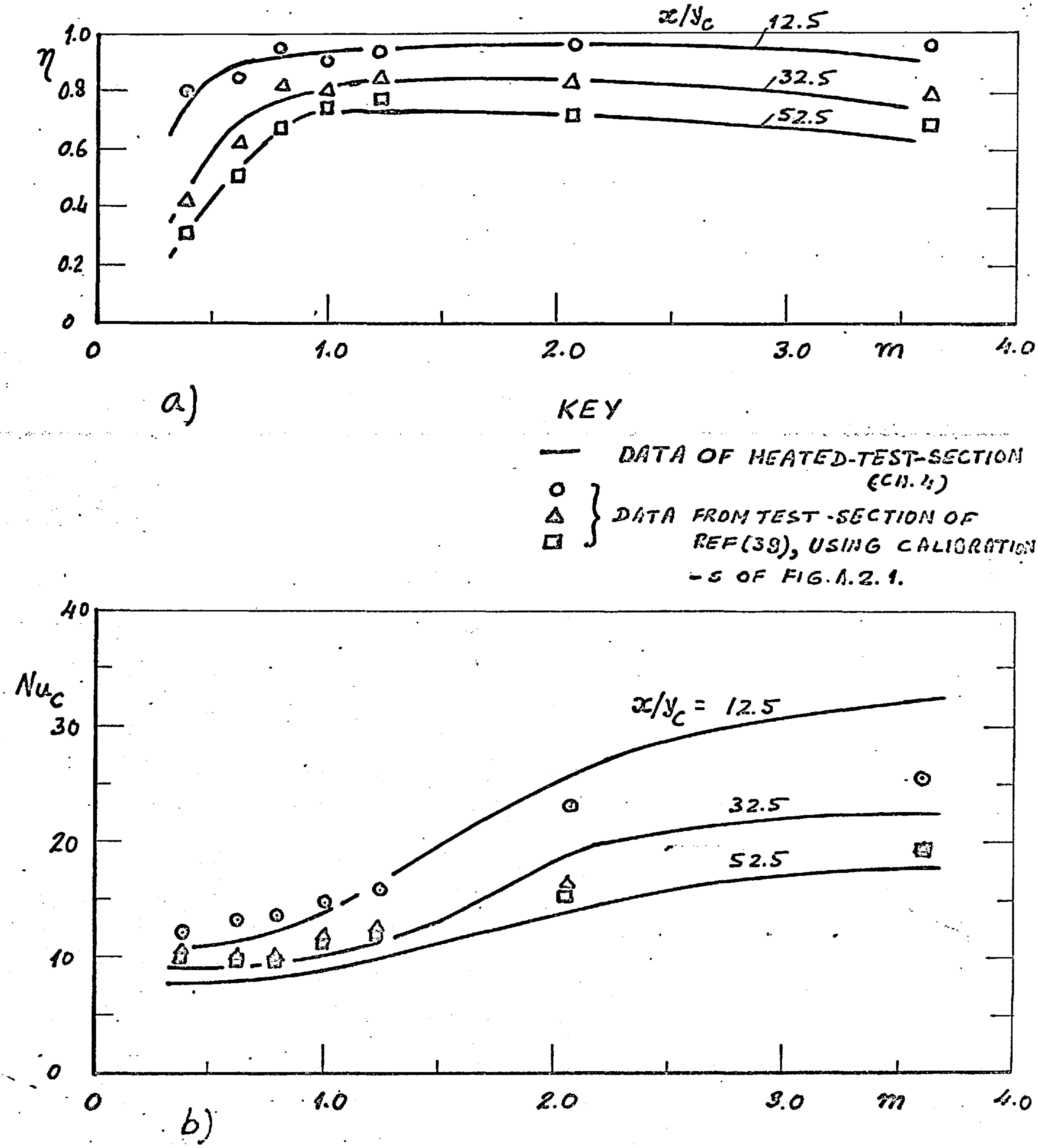

FIG. A.2.2. COMPARISON OF MEASURED VALUES OF EFFECTIVENESS AND HEAT-TRANSFER COEFFICIENT OBTAINED WITH HEATED-TEST SECTION AND TEST-SECTION OF REF (39).

APPENDIX A.1

A.1 Details of some auxiliary apparatus

A.1-1 A gas-sampling system

The gas sampling system shown in Fig. A.1-1 was designed and developed to obtain concentration profiles across the boundary layer at any desired streamwise location. It enabled gas samples to be rapidly withdrawn and collected in sample bottles from successive locations of the sampling probe across the boundary layer.

The sampling system comprised (see Fig. A.1-1) a sampling probe 'A', a hand-pump 'B' and a bank of sample bottles 'C'. A photograph of the hand-pump appears in Fig. 4.1.7, while that of the bank of sample bottles in Fig. A.1-2.

The probe 'A' was connected to one of the non-return valves by means of a 2 mm-bore neoprene tube 'C' about 30 cm long. A similar neoprene tube 'd' connected the other non-return valve to the inlet of the bank of sample-bottles.

The bank of sample bottles 'C' comprised eighteen sample bottles 'e', a pivoted disc 'f', a perspex dish 'h' and a discharge spout 'g'. Each sample bottle was a length of pyrex tube, 10.5 mm inside diameter and 79 mm long, with a serum cap plugged in its upper end. The sample bottles were mounted on the periphery of the disc 'f', which could be rotated manually and was indexed to click at 36 preferred positions. The discharge spout 'g' was a bent hypodermic tube, 1.6 mm I.D., and was arranged to be either vertically below or in between two sample tubes, as the disc 'f' was rotated through successive indexed positions. The perspex dish 'h' was filled with mercury so that the lower ends of the sample bottles were always immersed.

Operation: The operation of the system is best explained by describing the sequence of obtaining a concentration profile across the boundary layer. First, the sample bottles 'e' were completely filled with mercury, by withdrawing the air in the bottles with a hypodermic needle, coupled to a vacuum pump, and pierced through the serum caps. Next, the plate 'f' was rotated so that the spout 'g' was in between two sample bottles. The sampling probe was placed in its first desired position and the tubes 'c' and 'd' and the syringe 'a' flushed by the operation of the plunger. Next, the plate 'f' was indexed to its next preferred position, so that one of the sample bottles was vertically over the discharge spout. The sample was then collected in the sample bottle by activation of the plunger. The sampling probe was then moved to its next position in the boundary layer and the tube-bank advanced to its next preferred position for which the spout was in between a pair of sample bottles. The procedure of flushing the line, collecting the sample and advancing the sampling probe was repeated until the traverse was completed. The samples were later withdrawn in turn through the self-sealing serum caps by means of a 1 ml gas-tight syringe and injected into a gas chromatograph. A single stroke of the syringe was sufficient to fill a sample bottle of about 7 ml capacity. Further, the volumes of the connecting tubes 'c' and 'd' were kept to a minimum to reduce the dead space which had to be flushed. The time required for a traverse with eighteen points was approximately two and a half minutes.

A.1-2 A rotary pressure switch.

A rotary pressure switch was designed by the author to enable successive pairs of static-pressure holes in a wind tunnel to be conveniently connected to a differential micromanometer. Mercury was used as a seal between the moving parts and the device was suitable for gauge pressures up to ± 100 mm of water. The design and dimensions of the device implied that no great precision was required in the manufacture of any of its components.

Construction: Fig. A.1-4 shows a cross-section and plan view of the rotary pressure switch. A photograph of the same appears in Fig. A.1-3. It comprised a base 'a', an arbor 'b', a compression spring 'c', a sliding perspex dish 'd', a stationary perspex disc 'e' and a lock nut 'f'.

The dish 'd' had a central bore which permitted it to slide and rotate freely on the arbor 'b'. It carried along one of its radii, two hypodermic tubes 'g' and 'h' of 1.6 mm O.D. and a locating pin 'i', 1.6 mm O.D. The tubes 'g' and 'h' protruded 21 mm over the inner surface of the dish 'd' and the locating pin 23 mm. The stationary disc 'e' carried 18 pairs of hypodermic tubes (such as 'j' and 'k'), each 1.6 mm O.D., at

20-degree intervals; the radial location of each pair corresponded to that of the tubes 'g' and 'h' on the sliding dish 'd'. The disc 'e' also had 18 holes (such as 'l'), each of 2.4 mm diameter along a radius corresponding to the locating pin 'i' and along angular positions corresponding to the tubes 'g' and 'h'. The stationary disc 'e' was fixed to the arbor 'b' by the lock-nut 'f'.

The dish 'd' contained mercury to a depth of approximately 10 mm, when the dish was at its highest position on the arbor 'b'.

Operation: The pairs of tubes 'j' and 'k' were connected to the static-pressure holes in the test section of the wind tunnel through neoprene tubing, 2 mm I.D.; the tubes 'g' and 'h' were connected to a differential micromanometer through similar tubing.

To connect the micromanometer to the desired pair of static-pressure holes, the dish 'd' was lowered and rotated until the tubes 'g' and 'h' were directly below the desired pair of 'k' - 'l' tubes. The dish was then released, which caused it to be raised due to the compression spring 'c'. The chamfer at entry and an easy clearance between the hole 'l' and the locating pin 'i', as well as a fiducial on the outside of the dish, ensured that the process of aligning the dish against the required tube pair was a simple matter.

The use of mercury ensured reliable sealing and also that the tube pairs not connected to the manometer were sealed from the atmosphere. The range of the device could be altered to some extent by changing the amount of mercury in the dish 'd'. For instance, if all the static pressures were subatmoshperic, a lower level of the mercury would permit a larger range of operating pressures. The design for a larger range of pressure can of course be obtained by increasing the vertical dimensions of the device.

APPENDIX A-2 .

A.2 Experiments with apparatus B- Test section of ref (39).

The test section reported in (39) has been briefly described in chapter 4.2.2. In the present section, the experimental procedure and results for the adiabatic-wall effectiveness and the heat transfer coefficient, are discussed.

Experimental procedure. The desired velocities and temperatures of the main and secondary streams were set in the tunnel, as described in section 4.3.3.

The value of the heat-flux through each of the forty seven heat- flux meters (see Fig,4.2.4) could be altered by changing the temperature of the water flowing through the jacket enclosing the lower set of copper studs. For each flow condition, the steady-state temperatures of all the copper studs, corresponding to three different values of the water temperature in the jacket, were recorded. This permitted the evaluation of the adiabatic-wall effectiveness and heat-tranfer coefficient as described below.

Evaluation of the adiabatic-wall effectiveness and the heat-transer coefficient.

The steady-state heat flux through each of the heat-flux meters could be infereed from the following equation:

$$\dot{q}''_W = A_q \ (T_W - T_B) \quad , \qquad A.2\text{-}1$$

where A_q is a calibration coefficient of the heat flux meter, T_W is the temperature of the upper copper stud, assumed to be equal to the local wall temperature, and T_B is the temperature of the lower copper stud. Since the wall-temperatures corresponding to three values of $\dot{q}''_W$ were measured, the adiabatic-wall temperature and the heat-tranfer coefficient was obtained by a linear fit between the $\dot{q}''_W$'s and T_W's for each of the heat-flux meters - a least squares procedure was used for this purpose.

If the heat-transfer coefficient was completely independent of the boundary conditions, and the contact between the copper studs and the polypropylene sheet of each heat-flux meter was perfect, the value of the coefficient A_q should equal $(k/\Delta x)$, where k is the thermal conductivity of the polypropylene sheet and Δx its thickness. However, values of the heat-tranfer coefficient obtained o n this basis were found to be higher than expected, by a factor of about seven; the reasons for this discrepancy are outlined in chapter 4.2.2. Consequently an 'in situ' calibration was arranged - the drum assembly upstream of the test section was replaced by a 3.6 m length of 73 mm inside diameter Dural pipe section, so that a fully developed pipe flow was established at the test section, for which the teat tranfer coefficient could be obtained from the well known Colburn relation (26):

$$St = 0.023\ R_D^{-0.2}\ Pr^{-2/3} \qquad A.2.2$$

The calibration coefficient A_q for each heat-flux meter was obtained by equating the heat flux through the meter (as given by eq. A.2.1) to the product of the pipe-flow value of the heat tranfer coefficient (eq. A.2.2) and the local wall-to-mainstream temperature difference. It was found that values of the coefficent A_q determined in this manner were a function of the pipe-Reynolds number, R_D. In the range of the experiments, a power-law relat n of the type

$$A_q = C\ R_D^{\ m} \quad ,$$

was found to be appropriate to describe this relationship. Consequently, C and m were obtained by a least-squares linear fit between log A_q and R_D for each of the heat-flux meters. Values of A_q corresponding to two values of R_D ($R_D = 10^4$ and 10^5) are shown in Fig. A.2.1. It is evident that values of A_q are much below $(k/\Delta x)$, the value corresponding to the 'ideal' case; the large scatter in the values of A_q for the different heat-flux meters is indicative of their variable characteristics.

<u>Results and discussion.</u>

Values of the adiabatic-wall effectiveness and the heat transfer coefficient obtained in conjunction with the A_q's obtained with the above calibration procedure are shown in Fig. A.2.2 (a) and (b) respectively, for three values of x/y_C, plotted against the mass-velocity ratio. The symbols represent the data in question, and the lines are mean curves through corresponding data obtained with the electrically heated test section, presented in chapter 4.4.1.

It is evident from Fig. A.2.2 (a) that values of the adiabatic-wall effectiveness measured with the two test-sections are in good agreement (within 5 percent of unity) with one another. This was to be expected, since the same slot assembly was used for both the test sections.

Values of the heat tranfer coefficients, Fig. A.2.2 (b) obtained with the two test sections are in good qualitative agreement with one another. Discrepancies of upto 18 percent are noticeable for large values of m. The agreement between the two sets of data may be considered to be satisfactory, in view of the differences in the boundary conditions, experimental uncertainties and the limited validity of the calibration procedure for the heat-flux meters.

The present experience with the test-section of reference (39) indicates that an 'in situ' calibration of the heat flux meters is essential. However, the fact that the calibration coefficients are a function of the Reynolds number, makes its application problematic, since Reynolds number, based on a bulk-velocity may not be appropriate to a film cooling problem. Further, the use of an adiabatic wall with intermittent heat sinks or sources does not appear to be a desirable boundary condition for the measurement of the heat-transfer coefficient.

A.3.1 IMPERVIOUS-WALL EFFECTIVENESS

CONTENTS

TABLE 3.1-1 IMPERVIOUS WALL EFFECTIVENESS

PRESSURE GRADIENT PGO KP 10**6 (NOM) = 0.0
INJECTED GAS HYDROGEN DENSITY RATIO = 0.069
SLOT HEIGHT (MM) = 2.54

	RUN 1	RUN 2	RUN 3	RUN 4	RUN 5	RUN 6	RUN 7
UC/UG	0.308	0.560	0.775	1.05	1.270	1.52	0.775
M	0.021	0.039	0.054	0.073	0.088	0.105	0.035
RC	70.8	129.0	173.0	233.0	282.0	340.0	338.0
X/YC							
2.5	0.612	0.8720	0.774	1.00	0.870	0.655	0.800
12.5	0.0403	0.1310	0.1795	0.2640	0.2640	0.3160	0.300
32.5	0.0186	0.0295	0.0505	0.0825	0.0855	0.1208	0.064
52.5	0.0130	0.0229	0.0328	0.0462	0.0612	0.0778	0.032
72.5	0.0097	0.0169	0.0256	0.0374	0.0458	0.0640	0.022
92.5	0.0085	0.0147	0.0214	0.0268	0.0344	0.0480	0.019
112.5	0.0079	0.0119	0.0178	0.0255	0.0304	0.0417	0.017
132.5	0.0071	0.0115	0.0168	0.0209	0.0256	0.0352	0.014
172.5	0.0057	0.0092	0.0130	0.0181	0.0206	0.0270	0.011
212.5	0.0052	0.0081	0.0111	0.0160	0.0177	0.0230	0.010

TABLE 3.1-2 IMPERVIOUS-WALL EFFECTIVENESS

PRESSURE GRADIENT PGO KP 10**6 (NOM) = 0.0
INJECTED GAS AIR DENSITY RATIO = 1.0
SLOT HEIGHT (MM) = 2.54

	RUN 6	RUN 9	RUN 5	RUN 4	RUN 7
UC/UG	0.37	0.55	0.575	0.763	1.035
M	0.37	0.55	0.575	0.763	1.035
RC	1285.	1970.	1990.	2620.	3540.
X/YC					
2.5	0.806	0.910	0.725	0.879	0.770
12.5	0.842	0.880	0.930	0.966	0.955
22.5					
32.5	0.418	0.660	0.655	0.770	0.800
52.5	0.244	0.480			0.661
72.5	0.205	0.385	0.405	0.587	0.635
92.5	0.167	0.330	0.318	0.510	0.565
112.5	0.150	0.290	0.288	0.455	0.540
132.5	0.128	0.260	0.244	0.384	0.511
172.5	0.108	0.215	0.210	0.303	0.461
212.5	0.092	0.185	0.170	0.283	0.394

A312
$EOF

TABLE 3.1-2 (CONTD) IMPERVIOUS-WALL EFFECTIVENESS

PRESSURE GRADIENT PGO KP 10**6 (NOM) = 0.0
INJECTED GAS AIR DENSITY RATIO = 1.0
SLOT HEIGHT (MM) = 2.54

	RUN 1	RUN 8	RUN 10	RUN 2	RUN 3
UC/UG	1.23	1.74	1.85	2.16	3.12
M	1.23	1.74	1.85	2.16	3.12
RC	4170.	5700.	6330.	7150.	10510.
X/YC					
2.5	0.920	0.920	0.972	0.929	1.00
12.5	0.965	0.994	0.954	0.950	1.00
22.5			0.938		
32.5	0.825	0.818	0.807	0.815	0.805
52.5		0.694	0.705		0.680
72.5	0.610	0.636	0.608	0.594	0.587
92.5	0.605	0.587	0.594	0.493	0.525
112.5	0.562	0.555	0.520	0.521	0.473
132.5	0.530	0.476	0.505	0.479	0.442
172.5	0.416	0.456	0.461	0.394	0.370
212.5	0.394	0.412	0.425	0.398	0.366

TABLE 3.1-2 (CONTD) IMPERVIOUS-WALL EFFECTIVENESS

PRESSURE GRADIENT PGO KP 10**6 (NOM) = 0.0
INJECTED GAS AIR DENSITY RATIO = 1.0
SLOT HEIGHT (MM) = 2.54

	RUN 15	RUN 16	RUN 17	RUN 18	RUN 19
UC/UG	0.583	0.780	1.070	1.268	2.210
M	0.583	0.780	1.070	1.268	2.210
RC	965.	1275.	1730.	2040.	3470.
X/YC					
2.5	0.970	0.985	0.974	0.950	0.975
12.5	0.932	0.940	0.940	0.982	0.954
22.5	0.710	0.742	0.825	0.845	0.820
32.5	0.557	0.610	0.725	0.768	0.735
52.5	0.414	0.522	0.624	0.640	0.610
72.5	0.345	0.440	0.559	0.551	0.517
92.5	0.304	0.393	0.513	0.520	0.478
112.5	0.243	0.345	0.470	0.482	0.434
132.5	0.224	0.308	0.421	0.455	0.397
172.5	0.187	0.258	0.378	0.415	0.358
212.5	0.165	0.230	0.338	0.380	0.338

A313
$EOF

TABLE 3.1-3 IMPERVIOUS-WALL EFFECTIVENESS

PRESSURE GRADIENT PGO   KP 10**6 (NOM) = 0.0
INJECTED GAS ARGON   DENSITY RATIO = 1.38
SLOT HEIGHT (MM) = 2.54

	RUN 1	RUN 2	RUN 3	RUN 4
UC/UG	0.292	0.458	0.600	0.825
M	0.403	0.632	0.830	1.140
RC	1065.	1670.	2180.	2980.
X/YC				
2.5	0.935	0.910	0.910	0.935
12.5	0.785	0.905	0.951	0.991
32.5	0.478	0.688	0.785	0.865
52.5	0.331	0.510	0.628	0.810
72.5	0.273	0.396	0.545	0.720
92.5	0.245	0.329	0.478	0.667
112.5	0.218	0.288	0.457	0.620
132.5	0.194	0.254	0.368	0.580
172.5	0.171	0.207	0.332	0.498
212.5	0.153	0.175	0.266	0.446

TABLE 3.1-3 (CONTD) IMPERVIOUS-WALL EFFECTIVENESS

	RUN 5	RUN 8	RUN 7	RUN 6
UC/UG	0.982	1.340	1.710	2.480
M	1.357	1.850	2.36	3.42
RC	3550.	4800.	6050.	8720.
X/YC				
2.5	0.950	0.919	0.986	0.999
12.5	0.975	0.935	0.986	0.998
32.5	0.866	0.830	0.918	0.877
52.5	0.775	0.730	0.745	0.756
72.5	0.720	0.685	0.690	0.690
92.5	0.690	0.660	0.638	0.639
112.5	0.660	0.633	0.617	0.616
132.5	0.620	0.607	0.570	0.575
172.5	0.562	0.558	0.529	0.525
212.5	0.500	0.532	0.480	0.482

A314
$EOF

TABLE 3.1-4 IMPERVIOUS-WALL EFFECTIVENESS

PRESSURE GRADIENT PGO KP 10**6 (NOM) = 0.0
INJECTED GAS ARCTON-12 DENSITY RATIO = 4.17
SLOT HEIGHT (MM) = 2.54

	RUN 7	RUN 1	RUN 2	RUN 3
UC/UG	0.281	0.435	0.575	0.782
M	1.17	1.815	2.40	3.26
RC	2450.	3900.	5150.	7000.
X/YC				
2.5	0.985	0.998	1.00	0.998
12.5	0.915	0.979	0.995	0.997
32.5	0.630	0.880	0.945	0.973
52.5	0.473	0.780	0.886	0.930
72.5	0.382	0.646	0.828	0.910
92.5	0.316	0.630	0.722	0.885
112.5	0.304	0.568	0.761	0.857
132.5	0.278	0.512	0.635	0.815
172.5	0.224	0.442	0.613	0.802
212.5	0.197	0.394	0.540	0.745

TABLE 3.1-4 (CONTD) IMPERVIOUS-WALL EFFECTIVENESS

	RUN 4	RUN 5	RUN 6	RUN 8
UC/UG	0.884	1.26	1.645	0.785
M	3.68	5.25	6.87	3.30
RC	8140.	11000.	14250.	14400.
X/YC				
2.5	0.995	1.00	0.996	0.975
12.5	1.000	1.00	0.996	0.995
32.5	0.975	0.985	0.990	0.990
52.5	0.936	0.960	0.960	0.960
72.5	0.920	0.940	0.940	0.945
92.5	0.885	0.925	0.922	0.920
112.5	0.870	0.908	0.905	0.898
132.5	0.840	0.897	0.890	0.870
172.5	0.785	0.870	0.870	0.840
212.5	0.752	0.835	0.845	0.788

A315
$EOF

TABLE 3.1-5 IMPERVIOUS-WALL EFFECTIVENESS

PRESSURE GRADIENT PG1 — KP 10**6 (NOM) = 1.0
INJECTED GAS AIR — DENSITY RATIO = 1.0
SLOT HEIGHT (MM) = 2.540

	RUN 1	RUN 2	RUN 3	RUN 4	RUN 5
UC/UG	0.583	0.780	1.070	1.27	2.21
M	0.583	0.780	1.070	1.27	2.21
RC	965.	1275.	1730.	2040.	3470.
X/YC					
2.5	0.955	0.940	0.960	0.965	0.951
12.5	0.950	0.930	0.950	0.942	0.965
22.5	0.745	0.738	0.798	0.820	0.800
32.5	0.570	0.600	0.687	0.695	0.680
52.5	0.362	0.462	0.606	0.603	0.554
72.5	0.306	0.387	0.530	0.520	0.470
92.5	0.251	0.363	0.488	0.478	0.422
112.5	0.216	0.310	0.429	0.448	0.394
132.5	0.198	0.287	0.399	0.422	0.365
172.5	0.164	0.234	0.338	0.363	0.314
212.5	0.139	0.190	0.279	0.312	0.288

TABLE 3.1-6 IMPERVIOUS-WALL EFFECTIVENESS

PRESSURE GRADIENT PG2 — KP 10**6 (NOM) = 1.82
INJECTED GAS AIR — DENSITY RATIO = 1.0
SLOT HEIGHT (MM) = 2.54

	RUN 1	RUN 2	RUN 3	RUN 4	RUN 5
UC/UG	0.583	0.780	1.070	1.27	2.21
M	0.583	0.780	1.070	1.27	2.21
RC	965.	1275.	1730.	2040.	3470.
X/YC					
2.5	0.941	0.887	0.995	0.984	0.986
12.5	0.905	0.913	0.985	0.967	0.970
22.5	0.682	0.690	0.845	0.780	0.810
32.5	0.525	0.570	0.710	0.680	0.679
52.5	0.324	0.469	0.596	0.590	0.574
72.5	0.274	0.360	0.520	0.525	0.478
92.5	0.216	0.316	0.460	0.454	0.444
112.5	0.187	0.264	0.420	0.438	0.400
132.5	0.165	0.229	0.372	0.398	0.364
172.5	0.140	0.218	0.308	0.318	0.325
212.5	0.115	0.178	0.255	0.295	0.278

A316
$EOF

TABLE 3.1-7 IMPERVIOUS-WALL EFFECTIVENESS

PRESSURE GRADIENT PG3 KP 10**6 (NOM) = 3.30
INJECTED GAS AIR DENSITY RATIO = 1.0
SLOT HEIGHT (MM) = 2.54

	RUN 1	RUN 2	RUN 3	RUN 4	RUN 5
UC/UG	0.583	0.780	1.070	1.27	2.21
M	0.583	0.780	1.070	1.27	2.21
RC	965.	1275.	1730.	2040.	3470.
X/YC					
2.5	1.000	0.970	0.975	0.985	1.000
12.5	0.753	0.840	0.872	0.900	0.945
22.5	0.498	0.625	0.678	0.735	0.775
32.5	0.390	0.498	0.605	0.630	0.660
52.5	0.288	0.397	0.513	0.540	0.550
72.5	0.252	0.334	0.440	0.481	0.501
92.5	0.227	0.283	0.398	0.410	0.466
112.5	0.195	0.260	0.363	0.414	0.422
132.5	0.177	0.250	0.328	0.360	0.383
172.5	0.160	0.220	0.280	0.330	0.340
212.5	0.152	0.204	0.268	0.310	0.304

TABLE 3.1-8 IMPERVIOUS-WALL EFFICTIVENESS

PRESSURE GRADIENT PG4 KP 10**6 (NOM) = -1.0
INJECTED GAS AIR DENSITY RATIO = 1.0
SLOT HEIGHT (MM) = 2.54

	RUN 2	RUN 3	RUN 4	RUN 1	RUN 5
UC/UG	0.55	0.760	1.24	1.85	2.1
M	0.55	0.760	1.24	1.85	2.16
RC	1970.	2620.	4200.	6330.	7150.
X/YC					
2.5	0.910	0.890	0.980	1.020	0.974
12.5	0.905	0.890	0.990	1.010	0.965
22.5	0.718	0.770	0.895	0.926	0.885
32.5	0.556	0.683	0.825	0.822	0.790
52.5	0.412	0.600	0.712	0.715	0.676
72.5	0.335	0.540	0.662	0.631	0.596
92.5	0.300	0.523	0.605	0.590	0.545
112.5	0.272	0.462	0.560	0.545	0.500
132.5	0.251	0.422	0.545	0.496	0.478
172.5	0.216	0.371	0.490	0.455	0.422
212.5	0.198	0.348	0.456	0.428	0.396

A317
$EOF

TABLE 3.1-9 IMPERVIOUS-WALL EFFICTIVENESS

PRESSURE GRADIENT PG2 KP 10**6 (NOM) = 1.82
INJECTED GAS HYDROGEN DENSITY RATIO = 0.069
SLOT HEIGHT (MM) = 2.54

	RUN 1	RUN 2	RUN 3	RUN 4
UC/UG	0.308	0.560	1.27	1.52
M	0.021	0.0388	0.088	0.105
RC	70.8	129.0	282.0	340.0
X/YC				
2.5	0.4050	0.5680	1.00	1.00
12.5	0.0460	0.1325	0.3350	0.5680
22.5	0.0180	0.0540	0.1240	0.1870
32.5	0.0120	0.0320	0.0778	0.1072
52.5	0.0080	0.0190	0.0520	0.0695
72.5		0.0140	0.0410	0.0552
92.5	0.0060	0.0120	0.0334	0.0380
112.5	0.0055	0.0100		0.0362
132.5	0.0050	0.0090	0.0273	0.0330
172.5	0.0040	0.0076	0.0200	0.0250
212.5	0.0035	0.0060	0.0160	0.0238

TABLE 3.1-10 IMPERVIOUS-WALL EFFICTIVENESS

PRESSURE GRADIENT PG2 KP 10**6 (NOM) = 1.82
INJECTED GAS ARCTON-12 DENSITY RATIO = 4.17
SLOT HEIGHT (MM) = 2.54

	RUN 1	RUN 2	RUN 3	RUN 4
UC/UG	0.435	0.575	1.26	1.645
M	1.815	2.40	5.25	6.87
RC	3900.	5150.	11000.	14250.
X/YC				
2.5	0.985	0.995	0.995	1.00
12.5	0.998	1.000	1.000	1.00
22.5	0.946	0.972	0.997	1.00
32.5	0.840	0.915	0.980	0.990
52.5	0.657	0.800	0.940	0.946
72.5	0.564	0.675	0.910	0.920
92.5	0.495	0.622	0.890	0.895
112.5	0.440	0.533	0.865	0.875
132.5	0.400	0.520	0.845	0.860
172.5	0.315	0.415	0.796	0.817
212.5	0.280	0.380	0.740	0.760

A318
$EOF

TABLE 3.1-11 IMPERVIOUS-WALL EFFECTIVENESS

PRESSURE GRADIENT PG4 KP 10**6 (NOM) = -1.0
INJECTED GAS HYDROGEN DENSITY RATIO = 0.069
SLOT HEIGHT (MM) = 2.54

	RUN 1
UC/UG	0.775
M	0.053
RC	338.0
X/YC	
2.5	0.575
12.5	0.306
22.5	0.107
32.5	0.057
52.5	0.034
72.5	0.028
92.5	0.023
112.5	0.021
132.5	0.018
172.5	0.016
212.5	0.014

TABLE 3.1-12 IMPERVIOUS-WALL EFFECTIVENESS

PRESSURE GRADIENT PG4 KP 10**6 (NOM) = -1.0
INJECTED GAS ARCTON-12 DENSITY RATIO = 4.17
SLOT HEIGHT (MM) = 2.54

	RUN 1
UC/UG	0.785
M	3.3
RC	14400.
X/YC	
2.5	0.985
12.5	1.000
22.5	1.00
32.5	0.99
52.5	0.965
72.5	0.945
92.5	0.915
112.5	0.875
132.5	0.840
172.5	0.775
212.5	0.710

A319
$EOF

A 3.2 VELOCITY PROFILES

TABLE NO	RUN	UC/UG	RC	PRESSURE GRADIENT	INJECTED GAS	PAGE
1	9	0.550	1970.	PG0	AIR	A32 1
2	4	0.760	2620.	PG0	AIR	A32 3
3	1	1.230	4170.	PG0	AIR	A32 4
4	10	1.850	6330.	PG0	AIR	A32 5
5	2	0.575	5150.	PG0	ARCTON-12	A32 7
6	6	1.645	14250.	PG0	ARCTON-12	A32 8
7	1	0.583	965.	PG2	AIR	A32 9
8	5	2.210	3470.	PG2	AIR	A3211
9	1	0.583	965.	PG3	AIR	A3213
10	5	2.210	3470.	PG3	AIR	A3214
11	2	0.550	1970.	PG4	AIR	A3215
12	1	1.850	6330.	PG4	AIR	A3216

A 32 0

END

TABLE 3.2- 1 RUN 9, UC/UG= 0.55, RC= 1970., PG0, AIR INJECTION

X/YC	0.0		10.0		20.0		50.0		75.0
UG M/S	21.0		21.0		21.0		21.4		21.1
Y/YC	U/UG	Y/YC	U/UG	Y/YC	U/UG	Y/YC	U/UG	Y/YC	U/UG
.00	0.000	0.00	0.000	0.00	0.000	0.00	0.000	0.00	0.000
.10	0.508	0.10	0.430	0.10	0.354	0.10	0.394	0.10	0.415
.13	0.565	0.16	0.539	0.16	0.531	0.16	0.528	0.16	0.552
.16	0.597	0.22	0.627	0.22	0.565	0.22	0.546	0.22	0.572
.19	0.649	0.28	0.674	0.28	0.631	0.34	0.586	0.34	0.614
.22	0.706	0.34	0.716	0.34	0.653	0.47	0.614	0.47	0.634
.28	0.729	0.47	0.727	0.47	0.690	0.59	0.639	0.59	0.657
.34	0.734	0.59	0.718	0.59	0.706	0.72	0.661	0.72	0.674
.59	0.735	0.72	0.702	0.72	0.710	0.84	0.682	0.84	0.688
.84	0.733	0.84	0.692	0.84	0.710	0.97	0.702	0.97	0.708
.91	0.722	0.97	0.686	0.97	0.713	1.09	0.718	1.09	0.723
.97	0.645	1.09	0.685	1.09	0.718	1.22	0.735	1.22	0.733
1.00	0.514	1.22	0.694	1.22	0.729	1.34	0.751	1.34	0.748
1.03	0.443	1.34	0.708	1.34	0.736	1.47	0.767	1.47	0.762
1.06	0.336	1.47	0.722	1.47	0.748	1.59	0.781	1.59	0.775
1.09	0.320	1.59	0.744	1.59	0.755	1.72	0.789	1.84	0.801
1.13	0.408	1.72	0.759	1.72	0.763	1.84	0.796	2.09	0.823
1.16	0.447	1.84	0.780	1.84	0.781	1.97	0.809	2.34	0.844
1.22	0.529	1.97	0.797	1.97	0.797	2.22	0.827	2.59	0.859
1.28	0.569	2.09	0.822	2.09	0.811	2.47	0.850	2.84	0.876
1.34	0.608	2.34	0.857	2.34	0.842	2.72	0.870	3.09	0.894
1.41	0.632	2.59	0.883	2.59	0.870	2.97	0.885	3.34	0.909
1.53	0.676	2.84	0.908	2.84	0.894	3.22	0.899	3.59	0.928
1.66	0.716	3.09	0.930	3.09	0.918	3.47	0.922	3.84	0.940
1.91	0.770	3.34	0.951	3.34	0.938	3.72	0.939	4.09	0.952
2.16	0.807	3.59	0.966	3.59	0.960	3.97	0.957	4.35	0.968
2.41	0.840	3.84	0.977	3.84	0.973	4.22	0.971	4.59	0.976
2.66	0.868	4.09	0.985	4.09	0.985	4.47	0.980	4.84	0.984
2.91	0.898	4.35	0.994	4.35	0.992	4.72	0.989	5.09	0.991
3.41	0.947	4.59	0.998	4.59	0.997	4.97	0.993	5.35	0.995
3.91	0.977	4.84	0.999	4.84	1.000	5.22	0.996	5.60	0.997
4.41	0.994	5.09	0.999	5.09	1.000	5.47	0.996	5.84	0.999
4.91	0.999	5.35	0.999	5.35	1.000	5.72	0.997	6.09	1.000
5.41	1.000	5.60	1.000	5.60	1.000	5.97	0.997	6.34	1.000
5.91	1.000	5.84	1.000	5.84	1.000	6.22	0.999	6.60	1.000
*****	*****	6.09	1.000	6.09	1.000	6.47	0.999	6.85	1.000
*****	*****	6.34	1.000	6.34	1.000	6.72	1.000	7.09	1.000

TABLE 3.2- 1 RUN 9. UC/UG= 0.55. RC= 1970.. PGO. AIR INJECTION

X/YC	100.0		125.0		150.0		175.0		200.0
UG M/S	21.2		21.4		21.5		21.6		21.6
Y/YC	U/UG	Y/YC	U/UG	Y/YC	U/UG	Y/YC	U/UG	Y/YC	U/UG
.00	0.000	0.00	0.000	0.00	0.000	0.00	0.000	0.00	0.000
.10	0.422	0.10	0.441	0.10	0.459	0.10	0.430	0.10	0.469
.22	0.576	0.22	0.588	0.22	0.596	0.22	0.588	0.22	0.604
.34	0.617	0.34	0.631	0.34	0.630	0.34	0.629	0.34	0.645
.47	0.645	0.47	0.653	0.47	0.655	0.47	0.654	0.47	0.670
.59	0.664	0.59	0.669	0.59	0.671	0.59	0.675	0.59	0.690
.72	0.682	0.72	0.685	0.72	0.694	0.72	0.689	0.72	0.703
.84	0.696	0.84	0.707	0.84	0.706	0.84	0.705	0.84	0.719
.97	0.707	0.97	0.717	0.97	0.721	0.97	0.719	0.97	0.727
1.09	0.717	1.09	0.730	1.09	0.729	1.09	0.732	1.09	0.739
1.22	0.731	1.22	0.737	1.22	0.724	1.22	0.739	1.22	0.752
1.34	0.744	1.34	0.748	1.34	0.750	1.34	0.749	1.34	0.765
1.47	0.756	1.47	0.761	1.47	0.758	1.47	0.760	1.47	0.774
1.59	0.770	1.59	0.773	1.59	0.767	1.59	0.773	1.59	0.784
1.84	0.795	1.84	0.790	1.72	0.778	1.84	0.786	1.84	0.801
2.09	0.813	2.09	0.808	1.84	0.788	2.09	0.800	2.09	0.817
2.34	0.827	2.34	0.829	1.97	0.799	2.34	0.819	2.34	0.833
2.59	0.850	2.59	0.846	2.09	0.809	2.59	0.835	2.59	0.850
2.84	0.867	2.84	0.862	2.34	0.827	2.84	0.848	2.84	0.863
3.09	0.886	3.09	0.874	2.59	0.841	3.09	0.866	3.09	0.874
3.34	0.901	3.34	0.892	2.84	0.860	3.34	0.881	3.34	0.885
3.59	0.915	3.59	0.906	3.09	0.868	3.59	0.890	3.59	0.895
3.84	0.931	3.84	0.920	3.34	0.879	3.84	0.903	3.84	0.906
4.09	0.944	4.09	0.931	3.59	0.893	4.09	0.910	4.09	0.915
4.35	0.953	4.35	0.945	3.84	0.905	4.35	0.922	4.35	0.926
4.59	0.964	4.59	0.956	4.09	0.921	4.59	0.931	4.59	0.936
4.84	0.974	4.84	0.965	4.35	0.933	4.84	0.944	4.84	0.946
5.09	0.983	5.09	0.974	4.59	0.945	5.09	0.951	5.09	0.954
5.35	0.989	5.35	0.981	4.84	0.955	5.35	0.961	5.35	0.964
5.60	0.994	5.60	0.988	5.09	0.961	5.60	0.970	5.60	0.968
5.84	0.997	5.84	0.992	5.35	0.968	5.84	0.977	5.84	0.979
6.09	1.000	6.09	0.995	5.60	0.977	6.09	0.985	6.09	0.979
6.34	1.000	6.34	1.000	5.84	0.986	6.34	0.988	6.34	0.989
6.60	1.000	*****	*****	6.09	0.988	6.60	0.992	6.60	0.997
*****	*****	*****	*****	6.34	0.993	6.85	0.996	6.85	1.000
*****	*****	*****	*****	6.60	0.997	7.09	1.000	7.09	1.000
*****	*****	*****	*****	6.85	1.000	7.34	1.000	7.34	1.000

TABLE 3.2- 2 RUN 4, UC/UG= 0.76, RC= 2620., PG0, AIR INJECTION

X/YC	20.0		75.0		150.0
UG M/S	21.3		21.3		21.3
Y/YC	U/UG	Y/YC	U/UG	Y/YC	U/UG
.00	0.000	0.00	0.000	0.00	0.000
.09	0.450	0.09	0.403	0.09	0.367
.11	0.564	0.11	0.481	0.12	0.443
.14	0.628	0.14	0.525	0.15	0.491
.19	0.657	0.19	0.549	0.21	0.552
.24	0.718	0.24	0.597	0.25	0.582
.34	0.761	0.34	0.629	0.36	0.613
.44	0.822	0.54	0.674	0.50	0.642
.54	0.843	0.74	0.718	0.71	0.670
.69	0.853	0.94	0.748	0.95	0.703
.84	0.840	1.14	0.749	1.36	0.748
.99	0.823	1.39	0.808	1.85	0.798
1.19	0.804	1.64	0.831	2.35	0.841
1.44	0.791	2.14	0.861	2.86	0.875
1.69	0.799	2.64	0.884	3.35	0.909
1.94	0.811	3.39	0.919	3.85	0.929
2.44	0.861	4.14	0.956	4.35	0.956
2.94	0.911	4.89	0.985	4.86	0.976
3.44	0.954	5.89	0.999	5.61	0.991
3.94	0.981	6.89	1.000	6.35	0.997
4.44	0.988	*****	*****	7.11	1.000
4.94	0.999	*****	*****	7.85	1.000
5.44	1.000	*****	*****	*****	*****
5.94	1.000	*****	*****	*****	*****

TABLE 3.2- 3 RUN 1. UC/UG= 1.23. RC= 4170.. PGO. AIR INJECTION

X/YC	20.0		75.0		150.0
UG M/S	21.0		21.0		21.0
Y/YC	U/UG	Y/YC	U/UG	Y/YC	U/UG
.00	0.000	0.00	0.000	0.00	0.000
.09	0.816	0.09	0.519	0.09	0.451
.11	0.944	0.11	0.599	0.12	0.544
.13	1.023	0.13	0.672	0.15	0.608
.17	1.075	0.18	0.716	0.21	0.638
.24	1.126	0.28	0.797	0.27	0.685
.34	1.167	0.43	0.846	0.43	0.721
.44	1.202	0.58	0.890	0.63	0.766
.54	1.210	0.78	0.944	0.88	0.812
.64	1.204	1.03	0.981	1.13	0.847
.79	1.166	1.28	0.997	1.63	0.912
.94	1.129	1.53	0.996	2.13	0.949
1.04	1.088	1.78	0.987	2.63	0.963
1.14	1.057	2.03	0.977	3.37	0.965
1.29	1.008	2.53	0.957	4.13	0.969
1.39	0.978	3.03	0.951	5.13	0.981
1.49	0.951	3.53	0.954	6.12	0.994
1.64	0.911	4.28	0.977	7.13	0.999
1.84	0.881	5.08	0.997	8.13	1.000
2.09	0.870	5.83	1.000	9.13	1.000
2.34	0.881	6.53	1.000	*****	*****
2.74	0.919	*****	*****	*****	*****
3.24	0.957	*****	*****	*****	*****
3.74	0.987	*****	*****	*****	*****
4.24	0.997	*****	*****	*****	*****
4.74	1.000	*****	*****	*****	*****
5.24	1.000	*****	*****	*****	*****

TABLE 3.2- 4 RUN 10. UC/UG= 1.85. RC= 6330.. PG0. AIR INJECTION

X/YC	10.0		20.0		40.0		60.0		80.0
UG M/S	20.2		20.3		20.2		20.1		20.3
Y/YC	U/UG	Y/YC	U/UG	Y/YC	U/UG	Y/YC	U/UG	Y/YC	U/UG
.00	0.000	0.00	0.000	0.00	0.000	0.00	0.000	0.00	0.000
.10	1.375	0.10	1.536	0.10	1.167	0.10	1.015	0.10	0.908
.13	1.717	0.13	1.673	0.16	1.363	0.14	1.124	0.16	1.053
.16	1.906	0.16	1.729	0.22	1.430	0.16	1.171	0.22	1.122
.22	2.119	0.22	1.813	0.28	1.468	0.22	1.233	0.28	1.147
.28	2.152	0.28	1.852	0.34	1.507	0.28	1.269	0.34	1.187
.34	2.165	0.34	1.889	0.41	1.536	0.34	1.311	0.41	1.212
.41	2.152	0.41	1.899	0.47	1.553	0.41	1.338	0.47	1.241
.47	2.127	0.47	1.894	0.53	1.565	0.47	1.368	0.53	1.254
.53	2.114	0.53	1.889	0.59	1.572	0.53	1.383	0.59	1.279
.59	2.069	0.59	1.862	0.66	1.571	0.59	1.401	0.66	1.291
.66	2.028	0.66	1.834	0.72	1.568	0.66	1.416	0.72	1.305
.72	1.970	0.72	1.803	0.78	1.566	0.72	1.422	0.78	1.312
.78	1.926	0.78	1.776	0.84	1.556	0.78	1.429	0.84	1.325
.84	1.839	0.91	1.691	0.91	1.545	0.84	1.432	0.91	1.332
.97	1.700	1.03	1.621	1.03	1.523	0.91	1.430	0.97	1.338
1.09	1.548	1.16	1.538	1.16	1.489	0.97	1.430	1.03	1.342
1.22	1.403	1.28	1.466	1.28	1.462	1.03	1.430	1.09	1.343
1.34	1.256	1.41	1.381	1.41	1.423	1.09	1.426	1.16	1.344
1.47	1.132	1.53	1.302	1.53	1.392	1.16	1.419	1.22	1.343
1.59	1.015	1.66	1.220	1.66	1.351	1.22	1.414	1.28	1.343
1.72	0.815	1.78	1.201	1.78	1.317	1.34	1.400	1.34	1.341
1.84	0.884	1.91	1.157	1.91	1.278	1.47	1.381	1.41	1.336
1.97	0.870	2.03	1.031	2.03	1.243	1.59	1.362	1.47	1.332
2.09	0.865	2.16	0.988	2.16	1.203	1.72	1.342	1.59	1.325
2.22	0.878	2.28	0.958	2.28	1.174	1.84	1.321	1.72	1.311
2.34	0.890	2.41	0.940	2.41	1.136	1.97	1.301	1.84	1.301
2.47	0.900	2.53	0.940	2.53	1.108	2.09	1.276	2.09	1.272
2.72	0.925	2.66	0.940	2.66	1.071	2.22	1.257	2.34	1.244
2.97	0.945	2.91	0.949	2.78	1.052	2.47	1.213	2.59	1.215
3.22	0.965	3.16	0.967	3.03	1.015	2.72	1.169	2.84	1.183
3.47	0.975	3.41	0.978	3.28	0.995	2.97	1.128	3.09	1.155
3.72	0.989	3.66	0.989	3.53	0.990	3.22	1.088	3.34	1.128
3.97	0.997	3.91	0.994	3.78	0.991	3.47	1.056	3.59	1.096
4.22	0.999	4.16	0.999	4.03	0.995	3.72	1.031	3.84	1.072
4.47	0.997	4.41	1.000	4.28	0.998	3.97	1.015	4.09	1.048
4.72	1.000	4.66	1.000	4.53	1.000	4.22	1.007	4.35	1.028
4.97	1.000	*****	*****	5.03	1.000	4.47	1.000	4.59	1.015
*****	*****	*****	*****	*****	*****	4.72	1.000	4.84	1.009
*****	*****	*****	*****	*****	*****	*****	*****	5.09	1.004
*****	*****	*****	*****	*****	*****	*****	*****	5.35	1.000

TABLE 3.2- 4 RUN 10. UC/UG= 1.85. RC= 6330.. PG0. AIR INJECTION

X/YC	100.0
UG M/S	20.3
Y/YC	U/UG
.00	0.000
.10	0.824
.16	0.891
.22	0.991
.28	1.053
.34	1.076
.41	1.114
.47	1.135
.59	1.174
.72	1.213
.84	1.240
.97	1.261
1.09	1.277
1.22	1.292
1.34	1.294
1.47	1.300
1.59	1.298
1.72	1.297
1.84	1.288
1.97	1.283
2.09	1.275
2.22	1.266
2.34	1.257
2.59	1.236
2.84	1.214
3.09	1.194
3.34	1.168
3.59	1.148
3.84	1.122
4.09	1.103
4.35	1.080
4.59	1.062
4.84	1.045
5.09	1.032
5.35	1.021
5.60	1.013
5.84	1.009
6.09	1.004
6.34	1.004

A 32 6

TABLE 3.2- 5 RUN 2. UC/UG= 0.575 RC= 5150.. PG0. ARCTON -12

X/YC	10.0		40.0		100.0
UG M/S	10.1		10.1		10.1
Y/YC	U/UG	Y/YC	U/UG	Y/YC	U/UG
.00	0.000	0.00	0.000	0.00	0.000
.10	0.460	0.10	0.440	0.10	0.300
.16	0.597	0.16	0.507	0.22	0.444
.22	0.653	0.22	0.540	0.35	0.483
.35	0.672	0.35	0.565	0.60	0.530
.47	0.683	0.47	0.610	0.85	0.561
.60	0.685	0.60	0.635	1.10	0.590
.72	0.646	0.85	0.696	1.35	0.630
.85	0.690	1.10	0.717	1.60	0.668
1.10	0.707	1.35	0.720	1.85	0.690
1.35	0.731	1.60	0.770	2.10	0.735
1.60	0.716	1.85	0.798	2.35	0.755
1.85	0.788	2.10	0.815	2.60	0.780
2.10	0.870	2.35	0.800	2.85	0.808
2.35	0.900	2.60	0.840	3.35	0.885
2.60	0.935	2.85	0.910	3.85	0.895
2.85	0.960	3.11	0.930	4.35	0.935
3.10	0.986	3.36	0.990	4.85	0.966
3.35	1.000	3.61	1.000	5.35	1.000

TABLE 3.2- 6 RUN 6. UC/UG= 1.645 RC=14250.. PG0. ARCTON -12

X/YC	10.0		40.0		100.0
UG M/S	9.8		9.8		9.8
Y/YC	U/UG	Y/YC	U/UG	Y/YC	U/UG
.00	0.000	0.00	0.000	0.00	0.000
.10	1.370	0.10	1.130	0.10	0.935
.16	1.540	0.17	1.275	0.22	1.092
.22	1.635	0.22	1.362	0.35	1.160
.35	1.770	0.35	1.485	0.60	1.234
.47	1.850	0.47	1.570	0.85	1.365
.60	1.860	0.60	1.650	1.10	1.400
.72	1.875	0.85	1.630	1.35	1.485
.85	1.890	1.10	1.740	1.60	1.448
.98	1.740	1.35	1.462	1.85	1.455
1.10	1.560	1.60	1.480	2.10	1.412
1.35	1.432	1.85	1.400	2.35	1.393
1.60	1.165	2.10	1.325	2.60	1.392
1.85	1.370	2.35	1.248	2.85	1.341
2.10	0.950	2.60	1.186	3.35	1.340
2.35	0.950	2.85	1.065	3.85	1.230
2.60	0.975	3.10	1.042	4.35	1.180
2.85	0.990	3.35	1.002	4.85	1.120
3.10	1.000	3.60	1.000	5.35	1.000

TABLE 3.2- 7 RUN 1, UC/UG= 0.583 RC= 965., PG2, AIR INJECTION

X/YC	0.5		14.4		44.0		67.0		92.5
UG M/S	10.0		10.2		11.3		12.2		13.5
Y/YC	U/UG	Y/YC	U/UG	Y/YC	U/UG	Y/YC	U/UG	Y/YC	U/UG
.00	0.000	0.00	0.000	0.00	0.000	0.00	0.000	0.00	0.000
.10	0.390	0.10	0.308	0.10	0.351	0.10	0.392	0.10	0.441
.13	0.433	0.13	0.339	0.13	0.477	0.13	0.438	0.13	0.565
.16	0.473	0.16	0.346	0.16	0.525	0.16	0.486	0.16	0.654
.19	0.613	0.22	0.502	0.19	0.548	0.19	0.593	0.19	0.687
.22	0.683	0.28	0.555	0.22	0.605	0.22	0.648	0.22	0.704
.28	0.728	0.34	0.650	0.28	0.671	0.25	0.680	0.25	0.733
.34	0.751	0.41	0.674	0.34	0.702	0.28	0.698	0.28	0.762
.59	0.756	0.47	0.708	0.41	0.737	0.34	0.747	0.31	0.772
.84	0.718	0.53	0.722	0.47	0.754	0.41	0.764	0.34	0.783
.91	0.678	0.59	0.733	0.53	0.775	0.47	0.792	0.41	0.809
.97	0.501	0.66	0.738	0.59	0.790	0.53	0.806	0.47	0.817
1.00	0.439	0.72	0.743	0.66	0.802	0.59	0.819	0.53	0.834
1.03	0.360	0.78	0.743	0.72	0.815	0.66	0.827	0.59	0.841
1.06	0.290	0.84	0.747	0.78	0.825	0.72	0.840	0.66	0.857
1.09	0.315	0.97	0.758	0.84	0.836	0.78	0.846	0.72	0.859
1.13	0.349	1.09	0.771	0.91	0.844	0.84	0.856	0.84	0.876
1.16	0.367	1.22	0.788	1.03	0.857	0.91	0.863	0.97	0.888
1.22	0.501	1.34	0.810	1.16	0.870	0.97	0.875	1.09	0.902
1.28	0.570	1.47	0.830	1.28	0.881	1.03	0.878	1.22	0.912
1.34	0.683	1.59	0.854	1.41	0.895	1.09	0.881	1.34	0.923
1.41	0.694	1.72	0.874	1.53	0.904	1.16	0.886	1.47	0.931
1.53	0.764	1.84	0.895	1.66	0.916	1.28	0.900	1.59	0.942
1.66	0.803	1.97	0.912	1.91	0.933	1.41	0.911	1.72	0.949
1.91	0.859	2.22	0.944	2.16	0.952	1.53	0.920	1.84	0.959
2.16	0.904	2.47	0.968	2.41	0.967	1.66	0.930	1.97	0.963
2.41	0.929	2.72	0.983	2.66	0.983	1.78	0.939	2.09	0.970
2.66	0.964	2.97	0.991	2.91	0.992	1.91	0.947	2.22	0.975
2.91	0.972	3.22	0.998	3.16	0.997	2.16	0.959	2.34	0.980
3.41	0.990	3.47	0.999	3.41	0.999	2.41	0.973	2.47	0.983
3.91	0.998	3.72	1.000	3.66	0.999	2.66	0.983	2.59	0.989
4.41	0.999	3.97	1.000	3.91	0.999	2.91	0.990	2.72	0.992
4.91	1.000	*****	*****	4.16	0.999	3.16	0.994	2.97	0.997
5.41	1.000	*****	*****	4.41	1.000	3.41	0.997	3.22	0.999
*****	*****	*****	*****	4.66	1.000	3.66	0.999	3.47	1.000
*****	*****	*****	*****	*****	*****	3.91	1.000	3.72	1.000
*****	*****	*****	*****	*****	*****	4.16	1.000	3.97	1.000
*****	*****	*****	*****	*****	*****	4.66	1.000	4.47	1.000
*****	*****	*****	*****	*****	*****	5.16	1.000	*****	*****
*****	*****	*****	*****	*****	*****	5.66	1.000	*****	*****

TABLE 3.2- 7 RUN 1. UC/UG= 0.583 RC= 965.. PG2. AIR INJECTION

X/YC	144.0
UG M/S	16.9
Y/YC	U/UG
.00	0.000
.10	0.485
.13	0.582
.16	0.703
.19	0.739
.22	0.745
.25	0.773
.28	0.794
.34	0.816
.41	0.839
.47	0.848
.53	0.863
.59	0.873
.66	0.886
.72	0.891
.84	0.906
.97	0.884
1.09	0.933
1.22	0.943
1.34	0.951
1.47	0.958
1.59	0.966
1.72	0.973
1.84	0.978
1.97	0.983
2.22	0.989
2.47	0.996
2.72	0.999
2.97	1.000
3.22	1.001
3.47	1.001
3.72	1.000
3.97	1.000
4.22	1.000
4.47	1.000
4.72	1.000
4.97	1.000

TABLE 3.2- 8 RUN 5, UC/UG= 2.21 RC= 3470., PG2, AIR INJECTION

X/YC	0.0		14.4		44.0		67.0		92.5
UG M/S	9.3		9.6		10.6		11.5		12.8
Y/YC	U/UG	Y/YC	U/UG	Y/YC	U/UG	Y/YC	U/UG	Y/YC	U/UG
.00	0.000	0.00	0.000	0.00	0.000	0.00	0.000	0.00	0.000
.10	1.753	0.10	1.381	0.10	0.997	0.10	0.718	0.10	0.670
.13	2.508	0.13	1.628	0.13	1.199	0.13	0.927	0.13	0.785
.16	2.588	0.16	1.902	0.16	1.268	0.16	1.029	0.16	0.919
.19	2.595	0.19	1.989	0.19	1.316	0.19	1.058	0.19	0.964
.22	2.607	0.22	2.060	0.22	1.359	0.22	1.091	0.22	0.980
.34	2.607	0.25	2.120	0.25	1.396	0.25	1.140	0.25	1.002
.59	2.609	0.28	2.183	0.28	1.413	0.28	1.165	0.28	1.037
.72	2.615	0.34	2.226	0.34	1.459	0.34	1.203	0.34	1.068
.84	2.607	0.41	2.256	0.41	1.486	0.41	1.238	0.41	1.096
1.09	2.524	0.47	2.272	0.47	1.500	0.47	1.252	0.47	1.106
1.13	2.357	0.53	2.264	0.53	1.518	0.53	1.270	0.53	1.129
1.16	1.982	0.59	2.245	0.59	1.530	0.59	1.289	0.59	1.146
1.19	1.253	0.66	2.215	0.66	1.536	0.66	1.308	0.66	1.159
1.22	0.770	0.72	2.174	0.72	1.543	0.72	1.317	0.72	1.168
1.28	0.324	0.78	2.123	0.84	1.549	0.78	1.325	0.78	1.175
1.34	0.407	0.84	2.084	0.97	1.537	0.84	1.337	0.84	1.189
1.41	0.477	0.97	1.958	1.09	1.530	0.97	1.342	0.91	1.193
1.47	0.555	1.09	1.829	1.22	1.513	1.09	1.346	0.97	1.199
1.53	0.640	1.22	1.673	1.34	1.485	1.22	1.345	1.03	1.202
1.66	0.770	1.34	1.558	1.47	1.460	1.34	1.338	1.16	1.210
1.78	0.834	1.47	1.412	1.59	1.437	1.47	1.333	1.28	1.213
1.91	0.881	1.59	1.295	1.84	1.381	1.59	1.324	1.41	1.213
2.03	0.915	1.72	1.207	2.09	1.321	1.72	1.314	1.53	1.212
2.28	0.958	1.84	1.137	2.34	1.258	1.97	1.286	1.66	1.210
2.53	0.990	1.97	1.083	2.59	1.199	2.22	1.258	1.91	1.200
2.78	0.990	2.09	1.045	2.84	1.155	2.47	1.230	2.16	1.186
3.03	1.010	2.22	1.017	3.09	1.126	2.72	1.202	2.41	1.175
3.28	1.000	2.34	1.006	3.34	1.084	2.97	1.172	2.66	1.156
3.53	1.008	2.59	1.000	3.59	1.055	3.22	1.145	2.91	1.139
4.03	1.000	2.84	0.996	3.84	1.037	3.47	1.110	3.16	1.122
4.53	1.000	3.09	1.000	4.09	1.022	3.72	1.084	3.41	1.103
*****	*****	3.34	0.996	4.35	1.012	3.97	1.080	3.66	1.089
*****	*****	3.84	0.996	4.59	1.005	4.47	1.033	3.91	1.076
*****	*****	4.35	1.000	4.84	1.004	4.97	1.014	4.16	1.059
*****	*****	4.84	1.000	5.35	1.001	5.47	1.008	4.66	1.035
*****	*****	5.35	1.000	5.84	1.000	5.97	1.002	5.16	1.021
*****	*****	5.84	1.000	6.34	1.000	6.47	1.000	5.66	1.011
*****	*****	*****	*****	*****	*****	6.97	0.997	6.16	1.006
*****	*****	*****	*****	*****	*****	7.47	1.001	6.66	1.002

A 3211

TABLE 3.2- 8 RUN 5. UC/UG= 2.21 RC= 3470.. PG2. AIR INJECTION

X/YC 144.0
UG M/S 16.4

Y/YC	U/UG
.00	0.000
.10	0.585
.13	0.692
.16	0.815
.19	0.850
.22	0.859
.25	0.883
.28	0.905
.34	0.927
.41	0.955
.47	0.966
.53	0.983
.59	0.994
.66	1.009
.72	1.017
.78	1.026
.84	1.035
.91	1.045
.97	1.050
1.03	1.056
1.16	1.067
1.28	1.074
1.41	1.077
1.53	1.081
1.66	1.084
1.78	1.085
1.91	1.085
2.03	1.079
2.16	1.081
2.41	1.077
2.66	1.072
2.91	1.066
3.16	1.058
3.41	1.053
3.91	1.043
4.41	1.030
4.91	1.019
5.41	1.010
5.91	1.005

TABLE 3.2- 9 RUN 1. UC/UG= 0.583 RC= 965.. PG3. AIR INJECTION

X/YC	9.7		44.0		68.3		92.5		150.0
UG M/S	10.2		12.4		14.9		18.5		54.2
Y/YC	U/UG	Y/YC	U/UG	Y/YC	U/UG	Y/YC	U/UG	Y/YC	U/UG
.00	0.000	0.00	0.000	0.00	0.000	0.00	0.000	0.00	0.000
.10	0.221	0.10	0.408	0.10	0.428	0.10	0.494	0.10	0.756
.13	0.335	0.13	0.457	0.13	0.527	0.13	0.716	0.13	0.884
.16	0.452	0.16	0.477	0.16	0.568	0.16	0.777	0.16	0.912
.22	0.539	0.19	0.544	0.19	0.650	0.19	0.795	0.19	0.954
.28	0.657	0.22	0.590	0.22	0.721	0.22	0.828	0.22	0.970
.34	0.686	0.28	0.678	0.25	0.757	0.25	0.859	0.25	0.979
.41	0.730	0.34	0.723	0.28	0.771	0.28	0.872	0.28	0.981
.47	0.739	0.41	0.794	0.34	0.818	0.31	0.877	0.34	0.990
.53	0.759	0.47	0.821	0.41	0.838	0.34	0.894	0.41	0.992
.59	0.765	0.53	0.850	0.47	0.856	0.41	0.911	0.47	0.995
.66	0.773	0.59	0.860	0.53	0.866	0.47	0.917	0.59	0.998
.72	0.776	0.66	0.874	0.59	0.880	0.53	0.927	0.72	0.999
.78	0.782	0.72	0.879	0.66	0.887	0.59	0.936	0.84	0.999
.84	0.784	0.78	0.891	0.72	0.897	0.66	0.942	0.97	1.000
.97	0.789	0.84	0.907	0.78	0.903	0.72	0.946	1.09	1.000
1.09	0.801	0.91	0.913	0.84	0.910	0.78	0.952	1.34	1.000
1.22	0.816	1.03	0.926	0.91	0.917	0.84	0.957	*****	*****
1.34	0.833	1.16	0.935	0.97	0.921	0.91	0.963	*****	*****
1.47	0.848	1.28	0.946	1.03	0.928	0.97	0.964	*****	*****
1.59	0.853	1.41	0.963	1.09	0.935	1.03	0.967	*****	*****
1.72	0.872	1.53	0.972	1.16	0.938	1.09	0.972	*****	*****
1.84	0.887	1.66	0.983	1.28	0.946	1.22	0.978	*****	*****
1.97	0.903	1.91	0.993	1.41	0.957	1.34	0.982	*****	*****
2.22	0.937	2.16	0.997	1.53	0.964	1.47	0.986	*****	*****
2.47	0.958	2.41	0.998	1.66	0.971	1.59	0.989	*****	*****
2.72	0.978	2.66	1.000	1.78	0.975	1.72	0.993	*****	*****
2.97	0.991	2.91	1.000	1.91	0.981	1.84	0.995	*****	*****
3.22	0.998	3.16	1.000	2.16	0.989	1.97	0.997	*****	*****
3.47	1.000	3.41	1.000	2.41	0.995	2.09	0.998	*****	*****
*****	*****	3.66	1.000	2.66	0.998	2.22	1.000	*****	*****
*****	*****	3.91	1.001	2.91	0.999	*****	*****	*****	*****
*****	*****	4.16	1.001	3.16	0.999	*****	*****	*****	*****
*****	*****	4.41	1.000	3.41	1.000	*****	*****	*****	*****
*****	*****	4.66	1.000	3.66	1.000	*****	*****	*****	*****
*****	*****	4.91	1.000	*****	*****	*****	*****	*****	*****

TABLE 3.2-10 RUN 5. UC/UG= 2.213 RC= 3470.. PG3. AIR INJECTION

X/YC	9.7		44.0		68.3		92.5		150.0
UG M/S	9.7		11.9		14.1		19.1		53.7
Y/YC	U/UG	Y/YC	U/UG	Y/YC	U/UG	Y/YC	U/UG	Y/YC	U/UG
.00	0.000	0.00	0.000	0.00	0.000	0.00	0.000	0.00	0.000
.10	1.421	0.10	1.140	0.10	0.897	0.10	0.585	0.10	0.782
.13	1.836	0.13	1.258	0.13	1.038	0.13	0.815	0.13	0.882
.16	1.978	0.16	1.314	0.16	1.099	0.16	0.874	0.16	0.920
.19	2.033	0.19	1.411	0.19	1.210	0.19	0.888	0.19	0.966
.22	2.082	0.22	1.489	0.22	1.249	0.22	0.913	0.22	0.978
.25	2.161	0.25	1.534	0.25	1.276	0.25	0.940	0.25	0.984
.28	2.213	0.28	1.556	0.28	1.291	0.28	0.956	0.28	0.978
.34	2.238	0.34	1.665	0.34	1.337	0.31	0.962	0.34	1.000
.41	2.266	0.41	1.702	0.41	1.358	0.34	0.977	0.41	1.003
.47	2.276	0.47	1.743	0.47	1.387	0.41	1.000	0.47	1.008
.53	2.253	0.53	1.758	0.53	1.398	0.47	1.008	0.53	1.011
.59	2.242	0.59	1.782	0.59	1.416	0.53	1.023	0.59	1.014
.66	2.200	0.66	1.788	0.66	1.422	0.59	1.033	0.66	1.015
.72	2.177	0.72	1.790	0.72	1.435	0.66	1.045	0.72	1.016
.78	2.113	0.78	1.795	0.78	1.440	0.72	1.048	0.78	1.017
.84	2.082	0.84	1.793	0.84	1.445	0.78	1.054	0.84	1.017
.97	1.980	0.97	1.777	0.97	1.446	0.91	1.064	0.91	1.017
1.09	1.861	1.09	1.753	1.09	1.445	1.03	1.066	0.97	1.017
1.22	1.746	1.22	1.734	1.22	1.440	1.16	1.067	1.03	1.017
1.34	1.617	1.34	1.707	1.34	1.431	1.28	1.065	1.09	1.017
1.47	1.514	1.47	1.679	1.47	1.418	1.41	1.064	1.16	1.017
1.59	1.400	1.59	1.643	1.59	1.407	1.53	1.061	1.22	1.016
1.72	1.304	1.72	1.606	1.72	1.392	1.66	1.056	1.28	1.016
1.84	1.216	1.84	1.571	1.97	1.365	1.78	1.051	1.34	1.015
1.97	1.149	1.97	1.542	2.22	1.328	1.91	1.044	1.47	1.014
2.09	1.089	2.09	1.505	2.47	1.299	2.03	1.039	1.59	1.013
2.22	1.046	2.22	1.463	2.72	1.260	2.16	1.032	1.72	1.012
2.34	1.013	2.34	1.421	2.97	1.229	2.28	1.029	1.84	1.013
2.59	0.991	2.59	1.358	3.22	1.195	2.41	1.019	1.97	1.010
2.84	0.991	2.84	1.283	3.47	1.157	2.53	1.012	2.09	1.009
3.09	0.991	3.09	1.212	3.72	1.124	2.66	1.006	2.34	1.007
3.34	0.999	3.34	1.145	3.97	1.095	2.78	1.000	2.59	1.006
3.84	0.999	3.84	1.059	4.47	1.052	*****	*****	2.84	1.003
4.35	1.000	4.35	1.020	4.97	1.018	*****	*****	3.09	1.002
4.84	0.999	4.84	1.000	5.47	1.006	*****	*****	3.59	1.000
5.35	1.000	5.35	1.000	5.97	1.002	*****	*****	*****	*****
*****	*****	5.84	1.000	6.47	1.000	*****	*****	*****	*****

TABLE 3.2-11 RUN 2. UC/UG= 0.553 RC= 1970.. PG4. AIR INJECTION

X/YC	24.0		43.3		68.5		93.5		123.0
UG M/S	19.5		18.5		17.2		16.4		15.5
Y/YC	U/UG	Y/YC	U/UG	Y/YC	U/UG	Y/YC	U/UG	Y/YC	U/UG
.00	0.000	0.00	0.000	0.00	0.000	0.00	0.000	0.00	0.000
.10	0.230	0.10	0.349	0.10	0.316	0.10	0.338	0.10	0.312
.13	0.282	0.13	0.374	0.13	0.369	0.13	0.407	0.16	0.410
.16	0.346	0.16	0.430	0.16	0.402	0.16	0.454	0.22	0.437
.19	0.363	0.19	0.465	0.19	0.408	0.19	0.466	0.28	0.469
.22	0.415	0.22	0.479	0.22	0.433	0.22	0.477	0.34	0.482
.28	0.490	0.28	0.511	0.28	0.477	0.28	0.508	0.41	0.496
.34	0.537	0.34	0.535	0.34	0.494	0.34	0.523	0.47	0.502
.41	0.575	0.41	0.546	0.41	0.517	0.41	0.538	0.53	0.515
.47	0.598	0.47	0.568	0.47	0.531	0.47	0.546	0.59	0.524
.53	0.631	0.53	0.582	0.53	0.543	0.53	0.559	0.66	0.533
.59	0.649	0.59	0.597	0.59	0.557	0.59	0.566	0.72	0.539
.66	0.671	0.66	0.612	0.66	0.571	0.66	0.574	0.78	0.551
.72	0.677	0.72	0.632	0.72	0.573	0.72	0.584	0.84	0.551
.78	0.692	0.78	0.644	0.78	0.595	0.78	0.591	0.91	0.568
.84	0.709	0.84	0.663	0.84	0.606	0.84	0.599	0.97	0.568
.97	0.734	0.91	0.672	0.91	0.619	0.91	0.613	1.03	0.588
1.09	0.766	0.97	0.688	0.97	0.623	0.97	0.615	1.16	0.591
1.22	0.787	1.09	0.727	1.09	0.649	1.09	0.636	1.28	0.604
1.34	0.811	1.22	0.748	1.22	0.671	1.22	0.649	1.41	0.620
1.47	0.846	1.34	0.778	1.34	0.700	1.34	0.669	1.53	0.638
1.59	0.862	1.47	0.798	1.47	0.716	1.47	0.686	1.66	0.648
1.72	0.888	1.59	0.825	1.59	0.747	1.59	0.703	1.78	0.670
1.84	0.910	1.72	0.854	1.72	0.769	1.84	0.731	2.03	0.693
1.97	0.933	1.97	0.891	1.97	0.804	2.09	0.769	2.28	0.719
2.09	0.947	2.22	0.929	2.22	0.844	2.34	0.797	2.53	0.749
2.34	0.976	2.47	0.955	2.47	0.878	2.59	0.834	2.78	0.775
2.59	0.992	2.72	0.976	2.72	0.911	2.84	0.847	3.03	0.797
2.84	0.997	2.97	0.989	2.97	0.942	3.09	0.889	3.53	0.844
3.09	0.999	3.22	0.995	3.22	0.961	3.59	0.935	4.03	0.894
3.34	1.000	3.47	1.000	3.72	0.990	4.09	0.969	4.53	0.930
3.59	1.000	3.72	1.000	4.22	1.000	4.59	0.988	5.03	0.962
3.84	1.000	3.97	1.000	4.72	1.000	5.09	0.997	5.53	0.980
4.09	1.000	4.47	1.000	5.22	1.000	5.60	1.000	6.03	0.992
4.35	1.000	4.97	1.000	5.72	1.000	6.09	1.000	6.53	0.997
4.59	1.000	5.47	1.000	6.22	1.000	*****	*****	7.03	1.000
4.84	1.000	5.97	1.000	*****	*****	*****	*****	7.53	1.000

TABLE 3.2-12 RUN 1, UC/UG= 1.853 RC= 6330., PG4, AIR INJECTION

X/YC	24.0		43.3		68.5		93.5		123.0
UG M/S	19.1		18.0		16.6		15.7		14.8
Y/YC	U/UG	Y/YC	U/UG	Y/YC	U/UG	Y/YC	U/UG	Y/YC	U/UG
.00	0.000	0.00	0.000	0.00	0.000	0.00	0.000	0.00	0.000
.10	1.435	0.10	1.171	0.10	1.163	0.10	0.920	0.10	0.922
.13	1.701	0.13	1.425	0.13	1.263	0.13	1.121	0.16	1.152
.16	1.789	0.16	1.494	0.16	1.329	0.16	1.163	0.22	1.185
.19	1.828	0.19	1.520	0.22	1.377	0.19	1.213	0.28	1.241
.22	1.856	0.22	1.553	0.28	1.424	0.22	1.258	0.34	1.262
.28	1.910	0.28	1.628	0.34	1.478	0.28	1.305	0.41	1.301
.34	1.931	0.34	1.658	0.41	1.515	0.34	1.350	0.47	1.320
.41	1.962	0.41	1.704	0.47	1.533	0.41	1.385	0.53	1.350
.47	1.973	0.47	1.722	0.53	1.556	0.47	1.409	0.59	1.363
.53	1.972	0.53	1.741	0.59	1.581	0.53	1.436	0.66	1.391
.59	1.955	0.59	1.748	0.66	1.594	0.59	1.451	0.72	1.404
.66	1.926	0.66	1.757	0.72	1.606	0.66	1.478	0.78	1.421
.78	1.880	0.72	1.762	0.78	1.614	0.72	1.498	0.84	1.432
.91	1.811	0.78	1.764	0.84	1.622	0.78	1.511	0.91	1.447
1.03	1.751	0.84	1.751	0.91	1.630	0.84	1.526	1.03	1.468
1.16	1.665	0.97	1.735	0.97	1.634	0.91	1.532	1.16	1.488
1.28	1.593	1.09	1.704	1.03	1.636	0.97	1.549	1.28	1.504
1.41	1.504	1.22	1.675	1.16	1.626	1.09	1.559	1.41	1.507
1.53	1.424	1.34	1.633	1.28	1.614	1.22	1.568	1.53	1.512
1.66	1.358	1.47	1.596	1.41	1.602	1.34	1.568	1.66	1.511
1.78	1.293	1.59	1.553	1.53	1.585	1.47	1.565	1.78	1.507
2.03	1.156	1.72	1.509	1.66	1.556	1.59	1.559	1.91	1.504
2.28	1.059	1.97	1.417	1.91	1.518	1.84	1.544	2.03	1.500
2.53	1.010	2.22	1.329	2.16	1.461	2.09	1.512	2.16	1.494
2.78	1.000	2.47	1.240	2.41	1.413	2.34	1.478	2.41	1.478
3.03	1.000	2.72	1.157	2.66	1.358	2.59	1.439	2.66	1.450
3.28	1.000	2.97	1.089	2.91	1.304	2.84	1.402	2.91	1.428
3.53	1.000	3.22	1.044	3.16	1.245	3.09	1.366	3.16	1.404
3.78	1.000	3.47	1.017	3.66	1.152	3.59	1.292	3.41	1.382
4.03	1.000	3.72	1.006	4.16	1.070	4.09	1.220	3.91	1.327
*****	*****	3.97	1.000	4.66	1.026	4.59	1.146	4.41	1.275
*****	*****	4.22	1.000	5.16	1.010	5.09	1.090	4.91	1.221
*****	*****	4.47	1.000	5.66	1.000	5.60	1.042	5.41	1.173
*****	*****	4.72	1.000	*****	*****	6.09	1.021	5.91	1.125
*****	*****	4.97	1.000	*****	*****	6.60	1.006	6.41	1.081
*****	*****	5.22	1.000	*****	*****	7.09	1.000	6.91	1.049
*****	*****	*****	*****	*****	*****	*****	*****	7.41	1.026
*****	*****	*****	*****	*****	*****	*****	*****	7.91	1.010
*****	*****	*****	*****	*****	*****	*****	*****	8.41	1.000

END

A.3.3 CONCENTRATION PROFILES

TABLE NO	RUN	UC/UG	RC	PRESSURE GRADIENT	INJECTED GAS	PAGE
1	9	0.550	1970.	PGO	AIR	A33 1
2	4	0.760	2620.	PGO	AIR	A33 3
3	1	1.230	4170.	PGO	AIR	A33 4
4	10	1.850	6330.	PGO	AIR	A33 5
5	2	0.575	5150.	PGO	ARCTON-12	A33 7
6	6	1.645	14250.	PGO	ARCTON-12	A33 8
7	1	0.583	965.	PG2	AIR	A33 9
8	5	2.210	3470.	PG2	AIR	A3310
9	2	0.553	1970.	PG4	AIR	A3311
10	1	1.853	6330.	PG4	AIR	A3312

A 3300

END

TABLE 3.3- 1 RUN 9, UC/UG= 0.55, RC= 1970., PGO, AIR INJECTION

X/YC	10.0		20.0		50.0		75.0		100.0
ETA	0.88		0.82		0.49		0.38		0.31
Y/YC	C/CS	Y/YC	C/CS	Y/YC	C/CS	Y/YC	C/CS	Y/YC	C/CS
.00	1.000	0.00	1.000	0.00	1.000	0.00	1.000	0.00	1.000
.10	0.995	0.16	0.985	0.10	0.971	0.16	0.990	0.10	0.965
.22	0.995	0.29	0.950	0.16	0.995	0.34	0.956	0.22	0.996
.47	0.915	0.47	0.833	0.34	0.956	0.59	0.926	0.47	0.977
.72	0.655	0.98	0.516	0.59	0.870	0.72	0.866	0.72	0.985
.98	0.505	1.22	0.340	0.84	0.724	0.84	0.863	0.97	0.901
1.22	0.446	1.48	0.425	1.09	0.614	0.97	0.829	1.22	0.887
1.48	0.247	1.72	0.287	1.59	0.360	1.22	0.718	1.34	0.810
1.72	0.134	1.97	0.156	1.84	0.306	1.47	0.593	1.47	0.734
1.80	0.037	2.10	0.115	2.22	0.216	1.84	0.464	1.59	0.730
2.47	0.000	2.60	0.041	2.72	0.105	2.34	0.275	1.84	0.622
*****	*****	3.10	0.000	3.22	0.041	2.84	0.199	2.09	0.567
*****	*****	*****	*****	3.72	0.011	3.09	0.108	2.34	0.466
*****	*****	*****	*****	4.22	0.000	3.59	0.042	2.84	0.319
*****	*****	*****	*****	*****	*****	4.09	0.000	3.09	0.235
*****	*****	*****	*****	*****	*****	*****	*****	3.59	0.169
*****	*****	*****	*****	*****	*****	*****	*****	4.09	0.061
*****	*****	*****	*****	*****	*****	*****	*****	4.59	0.029
*****	*****	*****	*****	*****	*****	*****	*****	5.35	0.000

END

TABLE 3.3- I RUN 9, UC/UG= 0.55, RC= 1970., PG0, AIR INJECTION

X/YC	125.0		150.0		175.0		200.0
ETA	0.27		0.24		0.21		0.20
Y/YC	C/CS	Y/YC	C/CS	Y/YC	C/CS	Y/YC	C/CS
.00	1.000	0.00	1.000	0.00	1.000	0.00	1.000
.22	0.982	0.22	0.985	0.22	0.986	0.22	0.997
.47	0.961	0.47	0.951	0.47	0.933	0.47	0.984
.72	0.885	0.72	0.912	0.72	0.930	0.72	0.896
.97	0.861	0.97	0.917	0.97	0.906	0.97	0.922
1.22	0.811	1.22	0.859	1.22	0.857	1.22	0.864
1.34	0.797	1.47	0.798	1.47	0.845	1.47	0.837
1.47	0.761	1.59	0.756	1.59	0.752	1.84	0.760
1.59	0.720	1.72	0.752	1.84	0.768	2.34	0.634
1.84	0.660	1.84	0.721	2.34	0.613	2.59	0.574
2.09	0.597	1.97	0.695	2.59	0.597	2.84	0.531
2.34	0.488	2.09	0.600	2.84	0.512	3.09	0.472
2.84	0.384	2.59	0.485	3.34	0.436	3.59	0.415
3.09	0.330	3.09	0.411	3.59	0.349	4.35	0.263
3.59	0.202	4.09	0.200	4.59	0.122	5.09	0.064
4.09	0.108	4.59	0.095	5.09	0.079	5.60	0.048
4.59	0.041	4.59	0.041	5.60	0.040	6.09	0.018
5.35	0.000	5.35	0.000	5.35	0.000	6.60	0.000
5.35	0.000	5.35	0.000	5.35	0.000	*****	*****

A 33 2

END

TABLE 3.3- 2 RUN 4, UC/UG= 0.76, RC= 2620., PG0, AIR INJECTION

X/YC	20.0		75.0		150.0
ETA	0.91		0.57		0.35
Y/YC	C/CS	Y/YC	C/CS	Y/YC	C/CS
.00	1.000	0.00	1.000	0.00	1.000
.06	1.000	0.06	1.000	0.06	1.000
.53	0.830	0.53	1.000	0.93	0.960
1.06	0.470	1.11	0.840	1.43	0.860
1.53	0.250	1.66	0.600	1.92	0.740
1.66	0.190	2.24	0.370	2.55	0.570
2.11	0.070	2.53	0.250	3.40	0.330
2.24	0.040	2.67	0.240	3.90	0.210
2.66	0.000	3.11	0.100	4.40	0.140
*****	*****	3.66	0.070	5.05	0.070
*****	*****	4.24	0.020	5.65	0.030
*****	*****	4.67	0.000	6.30	0.000

END

TABLE 3.3- 3 RUN 1, UC/UG= 1.23, RC= 4170., PG0, AIR INJECTION

X/YC	20.0		75.0		150.0
ETA	0.92		0.63		0.50
Y/YC	C/CS	Y/YC	C/CS	Y/YC	C/CS
.00	1.000	0.00	1.000	0.00	1.000
.06	1.000	0.06	1.000	0.06	1.000
.53	0.860	0.53	0.960	0.53	0.970
1.11	0.590	1.11	0.800	1.11	0.890
1.66	0.350	1.66	0.620	1.66	0.780
2.24	0.090	2.24	0.450	2.06	0.610
2.67	0.010	2.66	0.280	2.24	0.580
3.11	0.000	2.67	0.340	2.53	0.500
*****	*****	3.24	0.160	2.67	0.500
*****	*****	3.67	0.090	3.11	0.350
*****	*****	*****	*****	3.66	0.240
*****	*****	*****	*****	4.24	0.160
*****	*****	*****	*****	4.67	0.120
*****	*****	*****	*****	6.00	0.000

A 33 4
END

TABLE 3.3- 4 RUN 10, UC/UG= 1.85, RC= 6330., PG0, AIR INJECTION

X/YC	10.0		20.0		40.0		60.0		80.0
ETA	0.96		0.94		0.78		0.68		0.60
Y/YC	C/CS	Y/YC	C/CS	Y/YC	C/CS	Y/YC	C/CS	Y/YC	C/CS
.00	1.000	0.00	1.000	0.00	1.000	0.00	1.000	0.00	1.000
.10	1.003	0.10	1.000	0.10	1.000	0.10	0.945	0.10	1.000
.41	0.921	0.16	1.005	0.22	0.979	0.16	0.994	0.22	0.994
.53	0.880	0.28	0.936	0.34	0.907	0.22	1.000	0.34	0.965
.66	0.825	0.41	0.935	0.47	0.904	0.34	0.977	0.47	0.921
1.09	0.572	0.53	0.861	0.59	0.856	0.47	0.944	0.66	0.901
1.22	0.492	0.78	0.752	0.72	0.823	0.53	0.902	0.84	0.845
1.34	0.397	0.91	0.682	0.84	0.746	0.59	0.896	1.03	0.814
1.47	0.298	1.03	0.655	1.03	0.678	0.72	0.855	1.28	0.734
1.97	0.137	1.28	0.558	1.28	0.643	0.84	0.811	1.47	0.686
2.22	0.037	1.53	0.437	1.53	0.547	0.97	0.790	1.72	0.628
2.47	0.000	1.78	0.320	1.78	0.464	1.09	0.741	2.09	0.555
*****	*****	2.03	0.221	2.03	0.329	1.16	0.778	2.59	0.470
*****	*****	2.28	0.103	2.53	0.279	1.34	0.693	3.09	0.369
*****	*****	2.53	0.061	2.78	0.144	1.59	0.641	3.59	0.234
*****	*****	2.91	0.000	3.28	0.059	2.09	0.543	4.09	0.164
*****	*****	*****	*****	3.80	*****	2.47	0.414	4.59	0.082
*****	*****	*****	*****	*****	*****	3.22	0.247	5.00	0.000
*****	*****	*****	*****	*****	*****	4.20	0.000	*****	*****

END

TABLE 3.3- 4 RUN 10, UC/UG= 1.85, RC= 6330., PG0, AIR INJECTION

X/YC	100.0
ETA	0.55
Y/YC	C/CS
.00	1.000
.22	0.991
.34	1.000
.72	0.910
.97	0.838
1.22	0.753
1.72	0.645
1.97	0.604
2.22	0.578
2.59	0.471
3.09	0.436
3.59	0.352
4.09	0.229
4.59	0.173
5.60	0.045
6.50	0.000

A 33 6
END

TABLE 3.3- 5 RUN 2. UC/UG= 0.575 RC= 5150.. PGO. ARCTON -12

X/YC	10.0		40.0		100.0
ETA	1.00		0.93		0.74
Y/YC	C/CS	Y/YC	C/CS	Y/YC	C/CS
.00	1.000	0.00	1.000	0.00	1.000
.10	0.995	0.10	1.000	0.10	1.000
.16	1.000	0.16	1.000	0.22	0.977
.22	1.000	0.22	0.995	0.35	0.985
.35	1.000	0.35	0.984	0.60	0.935
.47	1.000	0.47	0.950	0.85	0.935
.60	0.975	0.60	0.915	1.10	0.905
.72	0.970	0.85	0.807	1.35	0.840
.85	0.875	1.10	0.715	1.60	0.778
1.10	0.660	1.35	0.652	1.85	0.735
1.35	0.430	1.60	0.490	2.10	0.620
1.60	0.380	1.85	0.394	2.35	0.588
1.85	0.210	2.10	0.332	2.60	0.510
2.10	0.000	2.35	0.300	2.85	0.448
2.35	0.000	2.60	0.278	3.35	0.248
2.60	0.000	2.85	0.131	3.85	0.220
2.85	0.000	3.11	0.126	4.35	0.179
3.10	0.000	3.36	0.000	4.85	0.103
3.35	0.000	3.61	0.000	5.35	0.000

END

TABLE 3.3- 6 RUN 6, UC/UG= 1.645 RC=14250., PG0, ARCTON -12

X/YC	10.0		40.0		100.0
ETA	1.00		0.98		0.91
Y/YC	C/CS	Y/YC	C/CS	Y/YC	C/CS
.00	1.000	0.00	1.000	0.00	1.000
.10	0.998	0.10	1.000	0.10	1.000
.16	0.986	0.17	0.990	0.22	0.988
.22	0.998	0.22	0.996	0.35	1.000
.35	0.995	0.35	0.980	0.60	0.995
.47	0.985	0.47	0.965	0.85	0.968
.60	0.967	0.60	0.932	1.10	0.912
.72	0.932	0.85	0.820	1.35	0.846
.85	0.860	1.10	0.746	1.60	0.810
.98	0.845	1.35	0.775	1.85	0.755
1.10	0.795	1.60	0.708	2.10	0.716
1.35	0.664	1.85	0.633	2.35	0.666
1.60	0.538	2.10	0.523	2.60	0.580
1.85	0.140	2.35	0.441	2.85	0.545
2.10	0.000	2.60	0.312	3.35	0.400
2.35	0.000	2.85	0.174	3.85	0.306
2.60	0.000	3.10	0.103	4.35	0.222
2.85	0.000	3.35	0.051	4.85	0.100
3.10	0.000	3.60	0.000	5.35	0.000

A 33 8
END

TABLE 3.3- 7 RUN 1. UC/UG= 0.583 RC= 965.. PG2. AIR INJECTION

X/YC	14.4		44.0		92.5		144.0
FTA	0.85		0.40		0.21		0.16
Y/YC	C/CS	Y/YC	C/CS	Y/YC	C/CS	Y/YC	C/CS
.00	1.000	0.00	1.000	0.00	1.000	0.00	1.000
.10	1.008	0.10	0.926	0.10	0.944	0.10	1.001
.22	0.980	0.16	1.002	0.16	1.000	0.16	0.922
.34	0.892	0.28	0.967	0.28	0.964	0.28	0.902
.47	0.820	0.41	0.876	0.41	0.935	0.41	0.877
.59	0.700	0.53	0.849	0.53	0.929	0.53	0.872
.72	0.601	0.66	0.742	0.66	0.853	0.66	0.824
.84	0.501	0.78	0.655	0.84	0.778	0.84	0.793
1.09	0.336	0.91	0.601	1.09	0.649	1.09	0.705
1.34	0.213	1.03	0.501	1.34	0.530	1.34	0.611
1.59	0.122	1.16	0.432	1.59	0.456	1.59	0.513
1.84	0.065	1.41	0.373	1.84	0.420	1.84	0.433
2.22	0.024	1.66	0.286	2.09	0.295	2.22	0.247
.00	0.000	1.91	0.227	2.34	0.222	2.72	0.148
*****	*****	2.41	0.100	2.59	0.169	3.22	0.061
*****	*****	2.91	0.032	2.97	0.096	3.72	0.000
*****	*****	3.16	0.000	3.22	0.055	*****	*****
*****	*****	*****	*****	3.47	0.037	*****	*****
*****	*****	*****	*****	3.72	0.009	*****	*****

A 33 9

END

TABLE 3.3- 8 RUN 5. UC/UG= 2.21 RC= 3470.. PG2. AIR INJECTION

X/YC	14.4		44.0		92.5		144.0
ETA	0.94		0.61		0.44		0.35
Y/YC	C/CS	Y/YC	C/CS	Y/YC	C/CS	Y/YC	C/CS
.00	1.000	0.00	1.000	0.00	1.000	0.00	1.000
.10	1.018	0.10	1.015	0.10	0.825	0.10	1.000
.16	1.000	0.16	0.999	0.16	0.859	0.16	0.956
.28	0.950	0.28	0.990	0.28	0.835	0.28	0.923
.41	0.877	0.41	0.971	0.41	0.846	0.41	0.915
.53	0.826	0.53	0.888	0.66	0.769	0.53	0.886
.66	0.734	0.66	0.844	0.91	0.717	0.66	0.856
.78	0.702	0.84	0.829	1.16	0.697	0.78	0.878
.97	0.638	1.09	0.761	1.41	0.660	0.91	0.842
1.09	0.595	1.34	0.705	1.66	0.623	1.03	0.817
1.22	0.559	1.59	0.635	1.91	0.556	1.28	0.775
1.47	0.450	2.09	0.518	2.16	0.529	1.53	0.717
1.72	0.325	2.59	0.367	2.66	0.421	1.78	0.675
1.97	0.222	3.09	0.264	3.16	0.384	2.03	0.633
2.22	0.108	3.59	0.139	3.66	0.317	2.41	0.579
2.59	0.023	4.09	0.062	4.16	0.245	2.91	0.508
2.84	0.000	4.59	0.023	5.16	0.115	3.41	0.450
*****	*****	5.35	0.000	6.16	0.038	4.41	0.300
*****	*****	*****	*****	7.16	0.006	5.41	0.242
*****	*****	*****	*****	*****	*****	0.00	0.067

A 3310
END

TABLE 3.3- 9 RUN 2. UC/UG= 0.553 RC= 1970.. PG4. AIR INJECTION

X/YC	24.0		43.3		68.5		93.5
ETA	0.69		0.46		0.35		0.30
Y/YC	C/CS	Y/YC	C/CS	Y/YC	C/CS	Y/YC	C/CS
.00	1.000	0.00	1.000	0.00	1.000	0.00	1.000
.10	1.001	0.10	0.999	0.10	1.000	0.10	0.944
.16	0.953	0.16	0.941	0.16	0.957	0.16	0.993
.22	0.970	0.28	0.927	0.28	0.956	0.28	1.008
.34	0.903	0.41	0.892	0.41	0.930	0.41	0.959
.47	0.812	0.53	0.870	0.53	0.888	0.53	0.890
.59	0.712	0.66	0.793	0.66	0.851	0.66	0.885
.72	0.674	0.78	0.768	0.78	0.858	0.78	0.893
.84	0.588	0.91	0.718	0.97	0.820	0.91	0.901
1.09	0.459	1.09	0.630	1.22	0.770	1.09	0.840
1.34	0.332	1.34	0.514	1.47	0.724	1.34	0.872
1.59	0.247	1.59	0.434	1.72	0.641	1.59	0.788
1.84	0.155	1.97	0.270	1.97	0.549	1.84	0.704
2.09	0.087	2.22	0.176	2.22	0.471	2.09	0.664
2.34	0.041	2.72	0.084	2.72	0.313	2.59	0.525
2.59	0.018	3.22	0.025	3.22	0.170	3.09	0.403
2.84	0.008	3.72	0.003	3.72	0.066	4.09	0.167
*****	*****	*****	*****	4.72	0.005	5.09	0.042
*****	*****	*****	*****	*****	*****	6.09	0.000

END

TABLE 3.3-10 RUN 1. UC/UG= 1.853 RC= 6330.. PG4. AIR INJECTION

X/YC	24.0		43.3		68.5		93.5
ETA	0.92		0.77		0.64		0.58
Y/YC	C/CS	Y/YC	C/CS	Y/YC	C/CS	Y/YC	C/CS
.00	1.000	0.00	1.000	0.00	1.000	0.00	1.000
.10	1.018	0.10	0.993	0.10	1.005	0.10	0.995
.16	0.968	0.16	1.004	0.16	0.997	0.16	1.000
.22	0.959	0.22	0.960	0.28	0.990	0.28	0.999
.28	0.942	0.34	0.960	0.41	0.964	0.41	0.969
.34	0.899	0.47	0.938	0.53	0.935	0.53	0.971
.41	0.839	0.59	0.830	0.66	0.856	0.66	0.913
.53	0.829	0.72	0.820	0.78	0.867	0.78	0.898
.66	0.767	0.84	0.625	0.91	0.828	0.91	0.894
.78	0.705	0.97	0.625	1.03	0.781	1.09	0.845
.91	0.693	1.09	0.625	1.16	0.740	1.34	0.784
1.03	0.629	1.34	0.628	1.41	0.701	1.59	0.722
1.16	0.576	1.59	0.557	1.66	0.590	1.84	0.692
1.28	0.544	1.97	0.479	1.91	0.574	2.09	0.625
1.53	0.454	2.47	0.307	2.41	0.483	2.59	0.536
1.78	0.340	2.97	0.173	2.91	0.383	3.09	0.463
2.03	0.225	3.47	0.058	3.66	0.139	3.59	0.378
2.53	0.076	3.97	0.017	4.66	0.064	4.59	0.261
3.03	0.010	*****	*****	5.65	*****	5.60	0.115

A 3312

END

TABLE 3.4 WALL SHEAR STRESS

	PGO		PGO		PGO		PGO	
RUN	9		10		15		19	
UC/UG	0.55		1.85		0.583		2.21	
RC	1970.		6330.		965.		3470.	
	UTAU	CF/2	UTAU	CF/2	UTAU	CF/2	UTAU	CF/2
X/YC								
12.5	0.675	1.05	1.73	7.32	0.425	1.80	1.09	13.30
32.5	0.700	1.11	1.90	8.88	0.410	1.68	1.16	15.30
52.5	0.888	1.79	1.77	7.68	0.475	2.23	1.00	11.20
72.5	0.815	1.47	1.38	4.63	0.525	2.66	0.91	9.26
92.5	0.888	1.74	1.37	4.54	0.510	2.45	0.82	7.27
112.5	0.855	1.59	1.31	4.07	0.520	2.60	0.80	6.97
132.5	0.886	1.71	1.26	3.78	0.505	2.41	0.74	5.86
152.5	0.865	1.62	1.18	3.26	0.512	2.44	0.71	5.38
192.5					0.520	2.45	0.68	4.93

NOTE UTAU (M/S)
CF/2=CF/2*10**3

A 34 1
END

TABLE 3.4 (CONTD) WALL SHEAR STRESS

	PG1		PG1		PG2		PG2	
RUN	1		5		1		5	
UC/UG	0.583		2.21		0.583		2.21	
RC	965.		3470.		965.		3470.	
	UTAU	CF/2	UTAU	CF/2	UTAU	CF/2	UTAU	CF/2
X/YC								
12.5	0.402	1.50	0.91	10.70	0.402	1.53	1.06	11.70
32.5	0.455	1.81	1.18	14.30	0.426	1.52	1.24	14.10
52.5	0.582	2.73	1.05	10.50	0.570	2.36	1.07	9.30
72.5	0.668	3.34	0.99	8.54	0.670	2.82	1.015	7.14
92.5	0.635	2.77	0.885	6.24	0.700	2.65	0.94	5.21
112.5	0.685	3.00	0.885	5.72	0.792	2.88	0.965	4.62
132.5	0.695	2.84	0.852	4.86	0.840	2.70	0.98	3.94
152.5	0.729	2.88	0.825	4.18	0.940	2.74	1.03	3.49
192.5	0.790	2.81	0.880	3.89	1.220	2.90	1.27	3.30

NOTE UTAU (M/S)
CF/2=CF/2*10**3

END

TABLE 3.4 (CONTD) WALL SHEAR STRESS

	PG3		PG3		PG4		PG4	
RUN	1		5		1		5	
UC/UG	0.583		2.21		0.55		1.85	
RC	965.		3470.		1970.		6330.	
	UTAU	CF/2	UTAU	CF/2	UTAU	CF/2	UTAU	CF/2
X/YC								
12.5	0.368	1.19	1.08	11.40	0.482	0.58	1.60	6.74
32.5	0.568	2.22	1.21	11.40	0.595	1.00	1.90	10.90
52.5	0.700	2.59	1.10	7.17	0.615	1.19	1.72	10.20
72.5	0.830	2.58	1.12	5.31	0.536	1.01	1.29	6.43
92.5	1.03	2.73	1.20	4.00	0.580	1.30	1.25	6.61
112.5	1.28	2.58	1.41	3.37	0.495	1.00	1.14	6.06
132.5	1.73	2.47	1.82	2.98	0.462	0.96	1.06	5.70
152.5	2.37	1.74	2.48	2.05	0.450	0.95	0.97	5.13

NOTE UTAU (M/S)
CF/2=CF/2*10**3

A 343
END

TABLE 4.1 ADIABATIC-WALL EFFECTIVENESS AND HEAT TRANSFER COEFFICIENT

APPARATUS B, YC = 4.75 (MM), T/YC = 0.35

RUN	1		2		3		4	
UC/UG	0.379		0.616		0.824		1.04	
M	0.348		0.571		0.766		0.969	
RC	1862.		3077.		4172.		5306.	
	ETA	NUC	ETA	NUC	ETA	NUC	ETA	NUC
X/YC								
1.0	1.033	8.8	1.036	13.6	1.021	15.10	1.020	19.40
3.1	1.002	10.10	1.066	10.40	1.036	12.60	1.014	16.80
4.1	1.002	10.40	1.051	11.40	1.040	12.20	1.018	16.10
6.2	0.964	8.77	1.010	11.30				
8.3	0.905	9.67	0.985	11.50	0.960	12.80	0.979	14.70
12.4	0.620	13.00	0.940	9.98	0.887	11.80	0.936	12.80
16.5	0.508	13.10	0.883	9.53	0.841	10.70	0.891	12.20
24.8	0.407	9.80	0.786	8.52	0.802	8.50	0.841	9.50
33.1	0.341	9.07	0.689	9.06	0.757	8.41	0.807	9.58
41.3	0.297	8.62	0.617	8.91	0.716	8.26	0.771	8.97
49.5	0.253	8.07	0.562	8.52	0.676	8.11	0.745	8.78
57.8	0.230	7.89	0.522	8.06	0.636	7.97	0.707	8.42

A 41 1

END

TABLE 4.1 (CONTD) ADIABATIC-WALL EFFECTIVENESS AND HEAT TRANSFER COEFFICIEN

APPARATUS B. YC= 4.75 (MM). T/YC = 0.35

RUN	5		6		7	
UC/UG	1.278		2.285		3.546	
M	1.179		2.098		3.362	
RC	6361.		10535.		16206.	
	ETA	NUC	ETA	NUC	ETA	NUC
X/YC						
1.0	0.998	20.2	1.034	33.1	0.996	40.6
3.1	0.988	21.0	1.034	26.1	1.011	28.6
4.1	0.995	19.2	1.032	27.1	1.006	31.1
6.2			1.025	27.6		
8.3	0.981	16.9	1.036	30.1	0.979	34.4
12.4	0.953	15.3	0.989	26.0	0.957	30.4
16.5	0.919	14.9	0.959	24.4	0.927	31.7
24.8	0.879	11.4	0.901	19.8	0.837	21.2
33.1	0.834	10.7	0.847	18.9	0.766	22.0
41.3	0.791	10.3	0.790	15.9	0.702	20.3
49.5	0.759	9.9	0.741	14.3	0.666	18.3
57.8	0.726	9.6	0.691	12.7	0.641	17.0

A 41 2

END

TABLE 4.2 ADIABATIC-WALL EFFECTIVENESS AND HEAT TRANSFER COEFFICIENT

APPARATUS B. YC= 4.75 (MM). T/YC= 1.0

RUN	8		9	
UC/UG	0.629		2.07	
M	0.586		1.905	
RC	3114.		10140.	
	ETA	NUC	ETA	NUC
X/YC				
1.0	1.022	13.9	0.989	28.6
3.1	1.03	13.4	1.010	19.5
4.1	1.030	13.4	1.003	21.4
6.2	0.970	12.9	0.979	23.6
8.3	0.928	12.2	0.955	23.1
12.4	0.825	10.0	0.890	20.6
16.5	0.716	9.7	0.819	20.2
24.8	0.581	8.7	0.739	15.3
33.1	0.504	9.3	0.710	14.0
41.3	0.455	8.4	0.673	12.7
49.5	0.416	7.9	0.647	11.6
57.8	0.403	7.6	0.629	10.8

A 42 1

END

APPENDIX A. 5.

Computer programme for the prediction of the adiabatic-wall effectiveness and the heat-transfer coefficient downstream of a two dimensional film cooling slot.

A listing of the computer programme referred to in chapter 6 is provided in this section, along with a listing of the source programme and specimen inputs and outputs. The present programme is a version of the computer programme of reference (49), modified on the lines described in chapter 6, to predict the flow development, adiabatic- or impervious- wall effectiveness and the heat-transfer coefficient downstream of a film cooling slot.

A list of the subroutines in the present programme and brief particulars of the modifications in each subroutine are given below.

List of Subroutines.

1.	MAIN	13.	POLYFT
2.	BEGIN1	14.	PRE
3.	BEGIN2	15.	RAD
4.	CHOP	16.	READY
5.	COEFF	17.	SLIP
6.	CONST	18.	SOLVE
7.	DENSTY	19.	SOURCE
8.	ENTRN	20.	VEFF
9.	FBC	21.	VISCO
10.	LENGTH	22.	WALL
11.	MASS	23.	WF1
12.	OUTPUT	24.	WF2

Brief particulars of subroutines.

1. MAIN.

a. Step Length is selected as explained in chapter 6 (p.98).

b. The wall value of the conserved property φ is computed from a new expression for the slip coefficients, which is based on the integrated form of the partial differential equation and satisfies the integral conservation equations.(69).

c. The free stream velocity is computed from a modified formulation which ensures compatibility of the pressure gradient term at the outer edge of the layer and the adjacent grid points.

d. The termination condition. Integration is normally stopped after 151 integrations and the next set of data is then processed. Integration can be stopped at any intermediate stage, by setting the index KSTOP to 1 (for instance if the velocity should become negative).

e. Subroutines START and ENPLOT are of relevance only when the output is to be plotted on a CALCOMP plotter. If such a facility is not available, dummy subroutines of the above names should be introduced.

2. BEGIN1.

a. Input options. Three options are provided, depending on the value of the index KSP (= 0,1,2). The implications of these options are as follows:

KSP= 0 This signifies that (i) the mass fraction of the slot fluid is taken as the conserved property φ , and that the flow is isothermal; (ii) the velocity profile at the slot exit is composed of three power-law profiles, as sketched in Fig.6.1.1; the (dimensional) values of the velocities are computed from the value of the velocity ratio, the slot Reynolds number and the slot-height.

KSP=1. signifies that the velocity profile at slot exit is selected from a set of experimental profiles which is stored within the subroutine, in an array named VSCK; the values of the variable KVR determines the profile which is used for the calculation.

KSP=2. signifies that (i) the temperature is taken as the conserved property (ie. the specific heat C_p is assumed to be constant and equal to 0.24 kcal/kg deg K; (ii) the heat flux at the wall is to be specified: if zero, an adiabatic wall is assumed; and (iii) if the heat flux at the wall is not equal to zero, the values of the Nusselt number (NUC) are printed out; a data set specifying a non-zero heat flux must be preceded by a data set with identical initial conditions and an adiabatic wall, so that adiabatic wall temperatures on which the Nusselt number is based , may be calulated and stored.

The conserved-property profile at slot exit is assumed to be of a top-hat shape (ie. unity in the slot and zero outside it.)

Typical inputs corresponding to the three values of KSP are listed at the end of the computer programme.

b. Lip thickness ratio, t/y_C (TYC) is read in and a values of the coefficient ξ (eq. 6.2.1) is calculated on the basis of equation 6.2.2.

c. MU. This index controls the nature of the eddy viscosity and diffusivity. When MU is set to 0, the eddy viscosity and diffusivity are computed from the Prandtl mixing-length hypothesis (eq.5.0.1). If MU is given a value of 1, the eddy diffusivity is bridged across the zero-diffusivity region(s) by a straight line(s) (see Fig.5.2.2) and if MU is set to 2, both the eddy viscosity and diffusivity are bridged.

d. Experimental data such as profiles of velocity and mass fraction and effectiveness, for comparison can be read into the programme. These may later be plotted (as described in OUTPUT subroutine), along with the predictions.

3. BEGIN2. This is a portion of the subroutine BEGIN of reference (49), in which the ω-values at grid points and slip-values for the initial profiles are computed.

4. CHOP. This subroutine is used only in connection with the plotting of profiles on a CALCOMP plotter. Its function is to select data points which lie within the limits TMAX and TMIN, which are arguments of this subroutine.

5. COEFF. This subroutine has been modified for the bridging of the eddy viscosity and diffusivity profiles and for augmenting the eddy diffusivity as a function of the lip thickness ratio (see Fig.6.2.1).

6. CONST. The requisite constants are set in this subroutine. The laminar viscosity and density of air are computed at 25°C and 30 in. of mercury.

7. DENSTY. For a binary gas mixture, the density is calculated assuming ideal gas relations. When temperature is the conserved property, the density is taken to be inversely

proportional to the temperature (KSP= 2).

8. ENTRN. This subroutine is unaltered from the version in reference (49).

9. FBC. The appropriate heat flux at the wall is set in this subroutine: for an impervious or adiabatic wall, AJFS is set to 0. For a non-zero (constant) heat-flux, AJFS is set to correspond to the value of Q.

10. LENGTH. This subroutine has been re-written to perform the following operations: (i) to classify the velocity profile being calculated; and (ii) to select the characteristic lengths and velocity, as indicated in the sketch below.

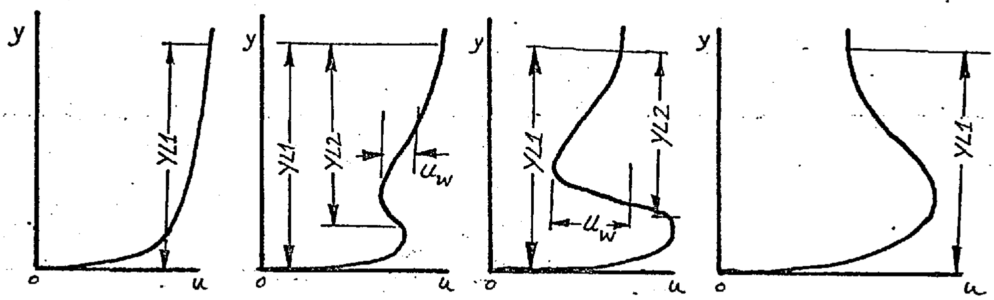

KASE= 1 2 3 4

11. MASS. The mass flux through the wall is set to zero.

12. OUTPUT . This subroutine prepares the quantities which are printed out, such as profiles of velocity, mass fraction, integral quantities, effeftiveness, Nusselt number etc. It also prepares profile data for plotting on a CALCOMP plotter.

a. Profiles of velocity and conserved property are printed out, if the the index KPROF is set to 1, at the values of x/y_C correreponding to the experimental profiles, or those stored in the array named ZX.

b. Other information is stored after every ten integrations and printed out after completion of the desired number of integrations (151 in this case).

c. Plotting predicted and experimental profiles. This involves the use of a CALCOMP plotter and related subroutines are used only when the index KDRAW is set to 1. If the compiler does not have provision for such a plotter, the following dummy subroutines should be inroduced, which merely return control to the calling subroutines:

PLØT, SCALE, AXIS, LINE, NUMBER, SYMBØL, START and ENPLØT.

d. The subroutine OUTPUT has an argument ISEP, which causes a print out if ISEP assumes a value of 1. ISEP can be set to 1 for example, if separation occurs (TAUI = 0.).

13. POLYFT. This subroutine is for fitting least-squares polynomials through a set of points. In the lisitng, a dummy subroutine is shown, since the example illustrated does not require the use of this subroutine.

14. PRE. The pressure gradient DPDX is computed, corresponding to the value of K_p, which is read in as input.

15. RAD. The present examples are for a plane two-dimensional case (KRAD=0) and R1 is set to unity.

16. READY. The expression used for calculating normal distances is slightly different (and more accurate) from that in the book. The resulting difference in the values of y is small.

17. SLIP. The slip value at a wall, for the conserved property and velocity is now obtained by a new formulation, which involves the partial defferential equations. The original version used a one-dimensional solution near the wall.

18. SOLVE. This subroutine remains unaltered.

19. SOURCE. The source term for the conserved property (mass fraction) is set to zero, since the substances are chemically inert.

20. VEFF. This subroutine is unaltered.

21. VISCO, The laminar viscosity is determined through the 'square root' formula for binary mixtures and a power law in the case of the non-isothermal case.

22. WALL.

a. Provision is made to stop integration if the velocity near the wall goes negative, for instance in adverse pressure gradients.

b. Two additional quantities are computed in this subroutine: BVI and PCI. The former is a non-dimensional eddy viscosoty and the latter is a non-dimensional stream function, at $\omega_{2.5}$. These quantities are needed in the computation of slip values of velocity and conserved property.

c. The computation of BETA has been deleted.

23. WF1. For large positive pressure gradients, TERM can go negative and since a negative number cannot be raised to a power, TERM is set to a small positive value, when this occurs.

22. WF2. This subroutine is unaltered.

A list and explanations of the FORTRAN symbols used in the input and output sections of the programme are given below.

EXPLANATION OF NAMES USED IN THE INPUT AND OUTPUT.

INPUT.

NAME	MEANING	UNITS
KDRAW	Plotting subroutines are called if KDRAW =1, but not if KDRAW = 0.	
NSETS	Number of sets of data to be processed.	
TITLE	Title in alpha-numeric form: one card.	
KSP	Values of KSP specify the input options. (See example at the end of the programme-lisitng).	
UCG	Slot to mainstream velocity ratio.	
RC	Slot Reynolds number.	
YC	Slot height.	mm.
TYC	Lip-thickness to slot height ratio.	
WT	Molecular weight of secondary gas.	
FPG	Pressure gradient parameter, $K_p \times 10^6$.	

NAME	MEANING	UNITS
KPROF	KPROF of 1 produces a print out of computed profiles; while no profiles are printed for KPROF of 0.	
KVR	The value of this index selects the velocity profile stored in subroutine BEGIN1 (for KSP=1).	
TCG	Slot to mainstream temperature ratio.	
TC	Temperature of coolant at slot exit.	^{o}C.
Q	Heat flux at the wall.	W/m^2.
F	Mass fraction (or temperature), normalised with the wall-value.	
NVEL	Number of experimental velocity profiles to be read in.	
NPHI	Number of experimental conserved-property profiles to be read in.	
NETA	Non-zero value implies effectiveness data (experimental) to be read in.	
XV	Value of x/y_C for an experimental velocity profile.	
XFI	Value of x/y_C for an experimental φ profile.	
IN	Number of data-points in an experimental profile.	
NRUN	Run designation.	
NEF	Number of data points for effectiveness.	
PAT(1,I)	Value of x/y_C	
PAT(2,I)	Value of experimental effectiveness corresponding to PAT(1,I).	

OUTPUT.

KCOUNT	Data-set number.	
XYC	x/y_C, the non dimensional distance from the slot.	
INTG	number of integrations performed.	
U/UG	non-dimensional velocity.	
Y/YC	y-values, normalised with the slot height.	
FI/FIW	conserved-property profiles, normalised with the wall values.	
ETA	effectiveness, or non-dimensional wall temperature.	
R2	momentum-thickness Reynolds number.	
RPHI2	R_{φ}	
SS*E3	Wall-shear stress coefficient, multiplied by 500.	
H12	Shape factor of the velocity profile (H).	
UMAX	maximum velocity	m/s
YMAX	value of y at which velocity is a maximum, normalised with the slot height.	
UHALF	(UMAX + UG) / 2	m/s
YHALF	Value of y at which u = UHALF.	
UG	Free stream velocity	m/s

NAME	MEANING	UNITS
NUC	Nusselt number Nu_C for KSP=2 and $Q \neq 0$.	--
AMG	Entrainment rate, $\dot{m}''_E/\rho_G\, u_G$ (for KSP = 0,1, and 2 (Q=0)).	
UTAU	Friction velocity $\sqrt{\tau_S/\rho_G}$	m/s.

```
$IBFTC MANE
C******                         APPENDIX  5
C       PREDICTION OF EFFECTIVENESS AND HEAT TRANSFER COEFFICIENT
C       DOWNSTREAM OF A TWO DIMENSIONAL FILM COOLING SLOT.
C******
      COMMON /GEN/PEI,AMI,AME,DPDX,PREF(2),PR(2),P(2),DEN,ANU,XU,XD,XP,
     1XL,DX,INTG,CSALFA
     1/I/N,NP1,NP2,NP3,NEQ,NPF,KEX,KIN,KASE,KRAD
     1/B/BETA,GAMA(2),TAUI,TAUE,AJI(2),AJE(2),INDI(2),INDE(2)
     1/V/U(43),F(2,43),R(43),RHO(43),EM(43),Y(43)
     1/C/SC(43),AU(43),BU(43),CU(43),A(2,43),B(2,43),C(2,43)
      COMMON /L/AK,ALMG
      COMMON /STOP/ KSTOP
      COMMON/S/ SBAR,EVIS(90),EM(90)
      COMMON/COUNT/KCOUNT
      COMMON /JAY/ JCOMP,KDRAW,NSETS,KSP
      COMMON/SHAPE/ LOOK,YL1,YL2,YDIV,UW,XI
      COMMON/CON/ UG,UCO,YC,XYC,FPC,FAT(20)
      COMMON/ABC/SF,S,EV1,PCI,A2,B2,C2
      JCOMP =0
      READ (5,200) KDRAW,NSETS
  200 FORMAT(I1,I2)
      IF(KDRAW.EQ.1) CALL START
      LOOK=0
      DIMENSION YS(90),US(90)
      KCOUNT=0
   16 CONTINUE
      KCOUNT=KCOUNT+1
      INTG=0
      KSTOP=0
      SBAR=0.
      ISEP=0
      XL=20.
      CALL CONST
      CALL BEGIN1
      AMI=0.
      AME=0.
      GO TO 25
   15 CALL READY
   25 CONTINUE
      INTG=INTG+1
      L=1
      DO 50 I=1,NP3
      IF(I.EQ.2.OR.I.EQ.NP2) GO TO 50
      YS(L)=Y(I)
      US(L)=U(I)
      L=L+1
   50 CONTINUE
      KOLD=LOOK
      CALL LENGTH(YS,US,NP1,.01,LOOK,YL1,YL2,YDIV,UW)
      IF(LOOK.EQ.0) WRITE(6,53) XU,INTG,(U(I),Y(I),I=1,NP3)
   53 FORMAT(32H UNRECOGNISABLE VELOCITY PROFILE/3H XU,E10.3,5H INTG,I3,
     12X/(2X,E10.3,5X,E10.3))
      IF(LOOK.EQ.0) KSTOP=1
      IF(KOLD.EQ.LOOK) GO TO 51
   51 CONTINUE
$EOF
```

```
      CALL ENTRN
C   CHOICE OF FORWARD STEP
      FRA=0.025
      DX=FRA*PL1/(R(1)*AMI-R(NP3)*AME)
      IF(DX.GT.0.3*Y(NP3)) DX=0.3*(Y(NP3))
      IF(DX.GT.0.15*Y(NP3).AND.XU/YC.LT.20.) DX=.15*Y(NP3)
      IF(DX.GT..05*Y(NP3).AND.XU/YC.LT.10.) DX=.05*Y(NP3)
      XD=XU+DX
   77 CONTINUE
      CALL PRE(XU,XD,DPDX)
      IF(KASE.EQ.2) GO TO 26
      IF(KIN.EQ.1)CALL MASS(XU,XD,AMI)
      IF(KEX.EQ.1)CALL MASS(XU,XD,AME)
      CALL WALL
   26 CALL OUTPUT(ISEP)
 4444 FORMAT(6H ITEST,I4/)
      CALL COEFF
C SETTING UP VELOCITIES AT A FREE BOUNDARY
C*****  AS FROM FIDEQ  20   30.10.68
      DUG=(-1.)*(XD-XU)*DPDX/(RHO(NP3)*U(NP3)*U(NP3))
      DUG=DUG/(1.+DUG)
      IF(KEX.EQ.2) U(NP3)=U(NP3)+ DUG*U(NP3)
      IF(KIN.EQ.2)U(1)=SQRT(U(1)*U(1)-2.*(XD-XU)*DPDX/RHO(1))
      CALL SOLVE(AU,BU,CU,U,NP3)
      DO 250 I=3,NP2
      IF(U(I).LT.0.) KSTOP=1
  250 IF(Y(I).LT.Y(I-1)) KSTOP =1
      IF(KSTOP.EQ.1) WRITE(6,251) INTG,XU,(I,U(I),Y(I),AU(I),BU(I),
     1CU(I),I=2,NP2)
      IF(KSTOP.EQ.1) CALL OUTPUT(1)
  251 FORMAT(26H NEGATIVE VELOCITIES OR DY/2X,I3,5X,F8.5/
     1(2X,I3,3X,5(E10.3,2X)))
C  SETTING UP VELOCITIES AT A SYMMETRY LINE
      IF(KIN.NE.3) GO TO 71
      U(1)=U(2)
      IF(KRAD.EQ.0)U(1)=.75*U(2)+.25*U(3)
   71 IF(KEX.EQ.3)U(NP3)=.75*U(NP2)+.25*U(NP1)
   72 CONTINUE
      IF(NEQ.EQ.1) GO TO 30
      DO 45 J=1,NPH
      DO 46 I=2,NP2
      AU(I)=A(J,I)
      BU(I)=B(J,I)
   46 CU(I)=C(J,I)
      DO 47 I=1,NP3
   47 SC(I)=F(J,I)
      CALL SOLVE(AU,BU,CU,SC,NP3)
      DO 48 I=1,NP3
   48 F(J,I)=SC(I)
      IF(KASE.EQ.2) GO TO 81
C  SETTING UP WALL VALUES OF F
C***** THIS EXPRESSION FOR F(1,1) INSERTED FROM FISLOT2,55    31.12.68
      IF(KIN.EQ.1.AND.INDI(J).EQ.2)F(J,1)=(F(J,2)-A2*F(J,3)-C2)/B2
      IF(KEX.EQ.1.AND.INDE(J).EQ.2)F(J,NP3)=((1.+BETA+GAMA(J))*F(J,NP2)-
     1(1.+BETA-GAMA(J))*F(J,NP1))*.5/GAMA(J)
C  SETTING UP SYMMETRY-LINE VALUES OF F
$EOF
```

```
   81 IF(KIN.NE.3) GO TO 82
      F(J,1)=F(J,2)
      IF(KRAD.EQ.0)F(J,1)=.75*F(J,2)+.25*F(J,3)
   82 IF(KEX.EQ.3)F(J,NP3)=.75*F(J,NP2)+.25*F(J,NP1)
   45 CONTINUE
   30 XP=XU
      XU=XD
      PEI=PEI+DX*(R(1)*AMI-R(NP3)*AME)
C  THE TERMINATION CONDITION
      IF(KSTOP.EQ.1) GO TO 16
      IF(INTG.LT.151) GO TO 15
      IF(KCOUNT.LT.NSETS) GO TO 16
      IF(KDRAW.EQ.1) CALL ENPLOT(12.)
      STOP
      END
$IBFTC BEG1      DECK
      SUBROUTINE BEGIN1
      COMMON /GEN/PEI,AMI,AME,DPDX,PREF(2),PR(2),F(2),DEN,AMU,XU,XD,XP,
     1XL,DX,INTG,CSALFA
     1/I/N,NP1,NP2,NP3,NEQ,NPH,KEX,KIN,KASE,KRAD
     1/B/BETA,GAMA(2),TAUI,TAUE,AJI(2),AJE(2),INDI(2),INDE(2)
     1/V/U(43),F(2,43),R(43),RHO(43),OM(43),Y(43)
      COMMON/AMP/WT,PC,TC
      COMMON/CON/UC,UCC,YC,XYC,FPG,FAT(20)
      COMMON /JAY/ JCOMP,KDRAW,NSETS,KSP
      COMMON /X/TITLE(12),XV(10),YX(10,70),UX(10,70),FIX(10,70),NVEL,NPH
     1I,NETA,NUM(10),PAT(2,100),XC,NRUN,NFI(10),NFE,YXE(10,70),XEI(10)
      COMMON/COUNT/KCOUNT
      COMMON/GROWTH/LOCAT,YI(50),YE(50)
      COMMON /MUCODE/ MU
      COMMON/BVIS/BMU
      COMMON/COOL/TG,TCC,FC,FCG
      COMMON/KCAL/KETA,KHGW,KHG2W,KHBAL,KFRCE,C,RC,IYC
      COMMON/SHAPE/ LOOK,YL1,YL2,YDIV,UW,XI
      DIMENSION VSCK(5,40)
C*****
C********   SLOT VELOCITY PROFILES FROM REF (30)
C*****
      DATA (VSCK(1,I),I=1,37)/0.,0.,.52,.58,.62,.67,.72,.76,.79,.82,.84,
     1 .84,.845,.85,3*.85,.84,.84,.80,.76,.67,.40,0.0,0.0,0.0,.67,.74,
     2 .78,.82,.86,.90,.92,.96,.98,.98,1.0/
      DATA (VSCK(2,I),I=1,37) /0.0,0.0,.60,.65,.70,.77,.82,.87,.91,
     1.94,.98,.98,.985,.99,1.0,1.0,.99,.98,.98,.96,.92,.82,.40,
     23*0.,.67,.74,.78,.82,.86,.90,.92,.96,.98,.99,1.0/
      KETA=0
      KHGW=0
      MU=1
      KRAD=0
C*****   INPUT
      READ(5,60) TITLE
C  INITIAL VELOCITY PROFILE
      NPHI=0
      NVEL=0
      NFE=0
      NETA=0
      C =0
$EOF
```

```
      TCG=1.0
      TC=25.
      WT=28.96
      EMU=AMU
      FPG=0.
C***** FPG STANDS FOR K*10**6
      READ(5,106)  KSP
      IF(KSP.EQ.0) READ(5,6) UCG,RC,YC,TYC,WT,FPG,KPRCF
      IF(KSP.EQ.1) READ(5,7) UCG,RC,YC,TYC,WT,FPG,KPRCF,KVR
      IF(KSP.EQ.2) READ(5,8) UCG,RC,YC,TYC,WT,FPG,KPRCF,TCG,TC,Q
C*****   INPUT OF EXPERIMENTAL DATA FOR COMPARISON
      READ(5,50) NVEL,NPHI,NETA
      IF(NVEL.EQ.0) GO TO 53
      DO 52 J=1,NVEL
      READ(5,51) XV(J),IN,(YX(J,I),UX(J,I),I=1,IN)
      NUM(J)=IN
   52 CONTINUE
      IF(NPHI.EQ.0) GO TO 53
      DO 54 J=1,NPHI
      READ(5,55) XFI(J),IN,(YXF(J,I),FIX(J,I),I=1,IN)
      NFI(J)=IN
   54 CONTINUE
   53 CONTINUE
      IF(NETA.EQ.0) GO TO 56
      READ(5,57) NRUN,NEE,(PAT(1,I),PAT(2,I),I=1,NEE)
 56   CONTINUE
      TC=TC+ 460.
      TG= TC/TCG
C***    MOLECULAR VISCOSITY FOR ARGON, ARCTON -12 AND HYDROGEN
      KETA=1
      KHGW=0
      IF(Q.NE.0.)  KETA=0
      IF(Q.NE.0.)  KHGW=1
      IF(WT.EQ.0.) WT=28.96
      IF(WT.EQ.39.94)  BMU=AMU*(2125./1716.)
      IF(WT.EQ.120.93) BMU= AMU*(127 ./1716.)
      IF(WT.EQ.2.) BMU=AMU*(841.1/1716.)
      IF(KSP.EQ.2) BMU= AMU*(TC/485.)**0.70
      X0=0.
      N=34
      T=TYC*YC
      YC=YC/12./25.4
      T=T/12./25.4
      UC=BMU*RC/(DEN*WT/28.96*YC)
      IF(KSP.EQ.2)  UC= RC* BMU/(DEN*TG/TC*YC)
      UC=UC/UCG
C***      ASSUMPTION    UC/UCMAX = 0.9
      IF(KSP.EQ.0.OR.KSP.EQ.2)  UC=UC/0.9
C***      XI  FROM  EQ.  6.2.2
       XI=0.28*TYC**2.0
C***
      XU=0.
      NEQ=2
      NPH=NEQ-1
      NP1=N+1
      NP2=N+2
$EOF
```

```
      NP3=N+3
C     INITIAL PROFILE STARTING FROM THE WALL
      KASE=1
      KEX=2
      KIN=1
      Y(1)=0.
      U(1)=0.
      F(1,1)=1.0
C****** ASSUMPTION    Y,G,C,/ YC =  2.5
      GW2=2.5*YC
      Y(NP3)=YC+GW2+T
      U(NP3)=UG
      F(1,NP3)=0.
      EX1=1./7.
      EX2=0.5
      EX3=0.5
      I1=6
      I2=12
      I3=19
      I4=24
      DO 999 I=3,12
  999 Y(I)=Y(1)+YC*0.5*FLOAT(I-2)/10.
      Y(3)=Y(3)*1.5
      DO 997 I=13,24
  997 Y(I)=Y(12)+YC*0.5*FLOAT(I-12)/12.
      IF(KSP.EQ.1) GO TO 1001
      DO 998 I=3,12
      IF(I.LE.I1) U(I)=0.99*UC*(Y(I)/Y(I1)) ** EX1
      IF(I.GT.I1)  U(I)=U(I1)+(UC-U(I1)) / (Y(I2)-Y(I1)) *(Y(I)-Y(I1))
  998 F(1,I)=1.0
      DO 996 I=13,24
      IF(I.LE.I3) U(I)=U(I2)+(UC-0.99*UC)/(Y(I2)-Y(I3))*(Y(I)-Y(I2))
      IF(I.GT.I3) U(I)=U(I3)*((Y(I)-Y(I4))/(Y(I3)-Y(I4))) **EX2
  996 F(1,I) =1.0
 1001   CONTINUE
      Y(25)=Y(24)+T/2.
      Y(26)=Y(25)+T/2.
      F(1,25)=0.
      F(1,26)=0.
      DO 995 I=27,35
  995 Y(I)=Y(26)+FLOAT(I-26)/10.*GW2
      IF(KSP.EQ.1) GO TO 1002
      DO 994 I=27,35
      EX3=1./7.
      U(I)= UG*((Y(I)-Y(26)) / (Y(NP3)-Y(26))) ** EX3
  994 F(1,I)=0.0
 1000 CONTINUE
      GO TO 1003
 1002   CONTINUE
      DO 1004 I=1,NP3
      U(I)=VSCK(KVR,I)*UG
      IF(I.LE.24) F(1,I)=1.0
 1004  IF(I.GT.24) F(1,I)=0.0
 1003 U(24)=0.5*U(23)
      U(25)=0.5*U(24)
      U(26)=0.5*U(27)
$EOF
```

```
C     BEGIN SUBROUTINE SPLIT HERE ON 9.10.67(BRP) INTO BEGIN1 AND BEGIN2
      CALL BEGIN2
6     FORMAT(6F6.3,I1,5X)
7     FORMAT(6F6.3,I1,5X,I1,5X)
8     FORMAT( 6F6.3,I1,5X,3F6.3)
   50 FORMAT(3I2)
   51 FORMAT(F6.3,I2/(12F6.3))
   55 FORMAT(F6.3,I2/(12F6.3))
57    FORMAT(2I2,1X/(12F6.2))
   60 FORMAT(12A6)
   61  FORMAT(6X,F6.4)
100   FORMAT(6X,I2)
      RETURN
      END
$IBFTC BEG2
      SUBROUTINE BEGIN2
      COMMON /GEN/PEI,AMI,AME,DPDX,PREF(2),PR(2),P(2),DEN,AMU,XU,XD,XP,
     1XL,DX,INTG,CSALFA
     1/I/N,NP1,NP2,NP3,NEQ,NFH,KEX,KIN,KASE,KRAD
     1/B/BETA,GAMA(2),TAUI,TAUE,AJI(2),AJE(2),INDI(2),INDE(2)
     1/V/U(43),F(2,43),R(43),RHO(43),CM(43),Y(43)
      COMMON/AME/WT,PC,TC
      COMMON/CON/UG,UCG,YC,XYC,EPG,FAT(20)
      COMMON /JAY/ JCOMP,KDRAW,NSETS,KSP
      COMMON /X/TITLE(12),XV(10),YX(10,70),UX(10,70),FIX(10,70),NVEL,NPH
     1I,NETA,NUM(10),PAT(2,100),XC,NRUN,NFI(10),NEF,YXF(10,70),XFI(10)
      COMMON/COUNT/KCOUNT
      COMMON/MUCOEF/MU
      COMMON/BVIS/ BMU
      COMMON/COOL/ TC,TCC,HC,HCC
C***** CONTINUATION OF BEGIN1
C  CALCULATION OF SLIP VELOCITIES AND DISTANCES
      BETA=.143
      GO TO (71,72,73),KIN
   71 U(2)=U(3)/(1.+2.*BETA)
      Y(2)=Y(3)*BETA/(2.+BETA)
      GO TO 74
   72 U11=U(1)*U(1)
      U13=U(1)*U(3)
      U33=U(3)*U(3)
      SQ=84.*U11-12.*U13+9.*U33
      U(2)=(16.*U11-4.*U13+U33)/(2.*(U(1)+U(3))+SQRT(SQ))
      Y(2)=Y(3)*(U(2)+U(3)-2.*U(1))*.5/(U(2)+U(3)+U(1))
      GO TO 74
   73 IF(KRAD.NE.0) GO TO 89
      U(2)=(4.*U(1)-U(3))/3.
      Y(2)=0.
      GO TO 74
   89 U(2)=U(1)
      Y(2)=Y(3)/3.
   74 GO TO (75,76,77),KEX
   75 U(NP2)=U(NP1)/(1.+2.*BETA)
      Y(NP2)=Y(NP3)-(Y(NP3)-Y(NP1))*BETA/(2.+BETA)
      GO TO 78
   76 U11=U(NP1)*U(NP1)
      U13=U(NP1)*U(NP3)
$EOF
```

```
      U33=U(NP3)*U(NP3)
      SQ=84.*U33-12.*U13+9.*U11
      U(NP2)=(16.*U33-4.*U13+U11)/(2.*(U(NP1)+U(NP3))+SQRT(SQ))
      Y(NP2)=Y(NP3)-(Y(NP3)-Y(NP1))*(U(NP2)+U(NP1)-2.*U(NP3))*.5/
     1(U(NP2)+U(NP1)+U(NP3))
      GO TO 78
   77 U(NP2)=(4.*U(NP3)-U(NP1))/3.
      Y(NP2)=Y(NP3)
   78 CONTINUE
      IF(NEG.EQ.1) GO TO 45
      J=1
C     CALCULATION OF CORRESPONDING SLIP VALUES
      GAMA(J)=.143
      GO TO (81,82,83),KIN
   81 F(J,2)=F(J,1)+(F(J,3)-F(J,1))*(1.+BETA-GAMA(J))/(1.+BETA+GAMA(J))
      GO TO 84
   82 F(J,2)=F(J,1)+(F(J,3)-F(J,1))*(U(2)+U(3)-8.*U(1))/(5.*(U(2)+U(3))
     1+8.*U(1))
      GO TO 84
   83 F(J,2)=F(J,1)
      IF(KRAD.EQ.0)F(J,2)=(4.*F(J,1)-F(J,3))/3.
   84 GO TO (85,86,87),KEX
   85 F(J,NP2)=F(J,NP3)+(F(J,NP1)-F(J,NP3))*(1.+BETA-GAMA(J))/(1.+BETA-
     1GAMA(J))
      GO TO 88
   86 F(J,NP2)=F(J,NP3)+(F(J,NP1)-F(J,NP3))*(U(NP2)+U(NP1)-8.*U(NP3))/
     1(5.*(U(NP2)+U(NP1))+8.*U(NP3))
      GO TO 88
   87            F(J,NP2)=(4.*F(J,NP3)-F(J,NP1))/3.
   88 CONTINUE
   45 CONTINUE
      CALL DENSTY
C     CALCULATION OF RADII
      CALL RAD(XU,R(1),CSALFA)
      IF(CSALFA.EQ.0..OR.KRAD.EQ.0) GO TO 27
      DO 28 I=2,NP3
28    R(I)=R(1)+Y(I)*CSALFA
      GO TO 29
   27 DO 30 I=2,NP3
   30 R(I)=R(1)
   29 CONTINUE
C      CALCULATION OF OMEGA VALUES
      OM(1)=0.
      OM(2)=0.
      DO 49 I=3,NP2
   49 OM(I)=OM(I-1)+.5*(RHO(I)*U(I)*R(I)+RHO(I-1)*U(I-1)*R(I-1))*
     1(Y(I)-Y(I-1))
      PEI=OM(NP2)
       DO 59 I=3,NP1
   59 OM(I)=OM(I)/PEI
      OM(NP2)=1.
      OM(NP3)=1.
      IF(NEG.EQ.1)RETURN
      DO 65 J=1,NP1
      IF(KEX.EQ.1)INDE(J)=1
      IF(KIN.EQ.1) INDI(J)=1
$EOF
```

```
   69 CONTINUE
      RETURN
      END
$IBFTC CHP
      SUBROUTINE CHOP(TAU,ETA,NUM,TMAX,TMIN,NEWN)
      DIMENSION TAU(1),ETA(1),TS(90),ES(90)
      NEWN=0
      J=1
      DO 11 I=1,NUM
      IF(TAU(I).LE.TMAX.AND.TAU(I).GE.TMIN) GO TO 10
      GO TO 11
   10 TS(J)=TAU(I)
      ES(J)=ETA(I)
      NEWN=J
      J=J+1
   11 CONTINUE
      DO12 I=1,NEWN
      TAU(I)=TS(I)
   12 ETA(I)=ES(I)
      RETURN
      END
$IBFTC COFF     DECK
      SUBROUTINE COEFF
      COMMON /GEN/PEI,AMI,AME,DPDX,PREF(2),FR(2),F(2),DEN,AMU,XU,XD,XP,
     1XL,DX,INTG,CSALFA
     1/I/N,NP1,NP2,NP3,NEQ,NFF,KEX,KIN,KASE,KRAD
     1/B/BETA,GAMA(2),TAUI,TAUE,AJI(2),AJE(2),INDI(2),INDE(2)
     1/V/U(43),F(2,43),R(43),RHO(43),EM(43),Y(43)
     1/C/SC(43),AU(43),BU(43),CU(43),A(2,43),B(2,43),C(2,43)
      COMMON /L/AK,ALMG
      COMMON /MUCODE/MU
      DIMENSION G1(43),G2(43),G3(43),D(2,43),S1(43),S2(43),S3(43)
      COMMON/S/ SE/R,FVIS(90),EM(90)
      COMMON/ABC/SF,S,DVI,PCI,A2,B2,C2
      COMMON/SHAPE/ LOCK,YL1,YL2,YDIV,UW,XI
      DIMENSION PK(90),IK(90),AJ(90),BJ(90)
      KOUNT=0
      IF(KOUNT.EQ.0) GO TO 100
  101 DO 2 I=2,NP1
2     CALL VEFF(I,I+1,EM(I-1))
      IF(MU.EQ.0) GO TO 100
      J=1
C****     BRIDGING PROCEDURE
C*****
      PKI= EM(2)
      DO 10 I=3,N
C****       GAMA ADD FROM EQ 6.2.1
      EMUAD=RHO(I)*XI*UW*YL2
       IF(EM(I).GE.EM(I-1))GO TO 10
      IF(EM(I-1).LE.EM(I-2)) GO TO 10
      IF(J.EQ.1) GO TO 8
      IC=I-1
      PKO= EM(I-1)+EMUAD
      YO= Y(I-1)
      DO 9 K=II,IC
9     EM(K)= PKI + (PKO-PKI)*(Y(K)-YI) /(YO-YI)
$EOF
```

```
      II=I0
      PKI=PK0
      YI=Y0
      J=J+1
      GO TO 10
8      II=I-1
       PKI= EM(I-1)
       YI= Y(I-1)
       J=J+1
10    CONTINUE
C   CALCULATION OF SMALL C 'S
  100 SBAR=0.
      DO 98 I=2,NP1
      RA=.5*(R(I+1)+R(I))
      RH=.5*(RHO(I+1)+RHO(I))
      UM=.5*(U(I+1)+U(I))
      EMU=EM(I-1)
      IF(KOUNT.EQ.0) CALL VEFF (I,I+1,EMU)
      DSBAR=EMU*(U(I+1)-U(I))*(U(I+1)-U(I))/(Y(I+1)-Y(I))/U(NP3)/U(NP3)
     1/U(NP3)/DEN
      IF(KOUNT.EQ.0) EVIS(I-1)=EMU
      SBAR=SBAR+DSBAR
   98 SC(I)=RA*RA*RH*UM*EMU/(PEI*PEI)
CADJUSTMENT OF EMU AT 2.5 AND N+1.5  MAY 1968 ,(DES)
      IF(KIN.NE.1) GO TO 299
C**** ADJUSTMENT  AS PER VAN DRIEST HYPOTHESES
      EMU2=BVI*PCI*0.125*(RHO(2)+RHO(3))*(U(2)+U(3))*(Y(2)+Y(3))
      CALL VEFF (2,3, EMU)
      SC(2) = SC(2)*EMU2/EMU
  299 IF(KEX.NE.1) GO TO 300
      T= TAUE+ DPDX*(Y(NP3)-0.5*(Y(NP1) + Y(NP2)))-
     1 AME*.5*(U(NP1)+U(NP2))
      EMUNP1=T*(Y(NP3)-.5*(Y(NP1)+Y(NP2)))/(BETA*
     1  (U(NP1) + U(NP2)))
      CALL VEFF(NP1,NP2,EMU)
      SC(NP1)=SC(NP1)*EMUNP1/EMU
  300 CONTINUE
C   THE CONVECTION TERM
      SA=R(1)*AMI/PEI
      SB=(R(NP3)*AME-R(1)*AMI)/PEI
      DX=XD-XU
      IF(KOUNT.NE.1) GO TO 102
      DO 103 I=3,NP1
      CMD=CM(I+1)-CM(I-1)
      P2=.25/DX
      P3=P2/CMD
      P1=(CM(I+1)-CM(I))*P3
      P3=(CM(I)-CM(I-1))*P3
      P2=3.*P2
      AJ(I)=2./CMD
      BJ(I)=SC(I-1)*AJ(I)/(CM(I)-CM(I-1))
      AJ(I)=SC(I)*AJ(I)/(CM(I+1)-CM(I))
      DO 34 J=1,NPH
      C(J,I)=-P1*F(J,I+1)-P2*F(J,I)-P3*F(J,I-1)
      CALL SOURCE (J,I,CS,D(J,I))
      C(J,I)=-C(J,I)+CS-F(J,I)*D(J,I)
$EOF
```

```
      A(J,I)=AJ(I)/PREF(J)
      B(J,I)=BJ(I)/PREF(J)
   34 CONTINUE
  103 CONTINUE
      IF(KOUNT.EQ.1) GO TO 104
  102 CONTINUE
      DO 71 I=3,NP1
      CMD=CM(I+1)-CM(I-1)
      P2=.25/DX
      P3=P2/CMD
      P1=(CM(I+1)-CM(I))*P3
      P3=(CM(I)-CM(I-1))*P3
      P2=3.*P2
      Q=SA/CMD
      R2=-SB*.25
      R3=R2/CMD
      R1=-(CM(I+1)+3.*CM(I))*R3
      R3=(CM(I-1)+3.*CM(I))*R3
      G1(I)=P1+Q+R1
      G2(I)=P2+R2
      G3(I)=P3-Q+R3
      CU(I)=-P1*U(I+1)-P2*U(I)-P3*U(I-1)
C  THE DIFFUSION TERM
      AU(I)=2./CMD
      BU(I)=SC(I-1)*AU(I)/(CM(I)-CM(I-1))
      AU(I)=SC(I)*AU(I)/(CM(I+1)-CM(I))
      IF(NEQ.EQ.1) GO TO 33
C  SOURCE TERM FOR VELOCITY EQUATION
   33 S1(I)=DPDX*DX
      S2(I)=P2*S1(I)/(RHO(I)*U(I))
      S3(I)=P3*S1(I)/(RHO(I-1)*U(I-1))
      S1(I)=P1*S1(I)/(RHO(I+1)*U(I+1))
      CU(I)=-CU(I)-2.*(S1(I)+S2(I)+S3(I))
      S1(I)=S1(I)/U(I+1)
      S2(I)=S2(I)/U(I)
      S3(I)=S3(I)/U(I-1)
   71 CONTINUE
      KOUNT=1
      IF(NEQ.GT.1)    GO TO 101
  104 CONTINUE
C  COEFFICIENTS IN THE FINAL FORM
      DO 91 I=3,NP1
      RL=1./(G2(I)+AU(I)+BU(I)-S2(I))
      AU(I)=(AU(I)+S1(I)-G1(I))*RL
      BU(I)=(BU(I)+S3(I)-G3(I))*RL
   91 CU(I)=CU(I)*RL
      IF(NEQ.EQ.1) GO TO 76
      DO 92 J=1,NPH
      DO 92 I=3,NP1
      RL=1./(G2(I)+A(J,I)+B(J,I)-D(J,I))
      A(J,I)=(A(J,I)-G1(I))*RL
      B(J,I)=(B(J,I)-G3(I))*RL
   92 C(J,I)=C(J,I)*RL
   76 CALL SLIP
      RETURN
      END
$EOF
```

```
$IBFTC CON1
      SUBROUTINE CONST
      COMMON /GEN/PEI,ANI,ANE,DPDX,PREF(2),PR(2),P(2),DEN,AMU,XU,XD,XP,
     1XL,DX,INTG,CSALFA
      COMMON /L/AK,ALMG
     1/L1/YL,UMAX,UMIN,FR,YIP,YEM
      COMMON/AMB/WT,PO,TO
      COMMON/COUNT/KCOUNT
      AK= 0.4187
      ALMG=.09
    3 CONTINUE
      FR=.01
      PREF(1)=1.0
      PREF(2)=1.7
      P(1)=-2.
      PR(1)=.71
C     REFERENCE AMBIENT CONDITION
      PO=30.
      TO=25.
      TO=TO*1.8+492.
      DEN=1.34*PO/TO
      AMU=1.285/10.**5.*(TO/500.)**.768
      RETURN
      END
$IBFTC DEN1
      SUBROUTINE DENSTY
      COMMON /GEN/PEI,ANI,ANE,DPDX,PREF(2),PR(2),P(2),DEN,AMU,XU,XD,XP,
     1XL,DX,INTG,CSALFA
     1/V/U(43),F(2,43),R(43),RHO(43),CM(43),Y(43)
     1/I/N,NP1,NP2,NP3,NEQ,NPH,KEX,KIN,KASE,KRAD
      COMMON /AMB/ WT,PO,TO
      COMMON/JAY/JCOMP,KDRAW,ASETS,KSP
      COMMON /COOL/ TC,TCG,HG,HCG
      IF(KSP.EQ.2) GO TO 50
      RHF1=1.34*PO/TO*WT/28.96
      DO 45 I=1,NP3
   45 RHO(I)=1./ (F(1,I)/RHF1+(1.-F(1,I))/DEN)
      RETURN
C***** CASE OF SLOT ENTHALPY EQUALS UNITY
50    DO 51 I=1,NP3
51    RHO(I)=DEN/(1.+F(1,I)*(TCG-1.))
      RETURN
      END
$IBFTC ENT
      SUBROUTINE ENTRN
      COMMON/SHAPE/ LOOK,YL1,YL2,YDIV,UW,XI
      COMMON /GEN/PEI,ANI,ANE,DPDX,PREF(2),PR(2),P(2),DEN,AMU,XU,XD,XP,
     1XL,DX,INTG,CSALFA
      COMMON /L/AK,ALMG
     1/V/U(43),F(2,43),R(43),RHO(43),CM(43),Y(43)
     1/I/N,NP1,NP2,NP3,NEQ,NPH,KEX,KIN,KASE,KRAD
     1/L1/YL,UMAX,UMIN,FR,YIP,YEM
C  THIS SUBROUTINE USES THE MIXING-LENGTH HYPOTHESIS
      YL=YL1
      GO TO (71,72,73),KIN
   71 GO TO 74
$EOF
```

```
   72 AMI=8.*RHO(1)*((ALNG*YL)/(Y(2)+Y(3)))**2*ABS(U(2)+U(3)-2.*U(1))
      GO TO 74
   73 AMI=0.
   74 GO TO (81,82,83),KEX
   81 RETURN
   82 AME=-8.*RHO(NP3)*((ALNG*YL)/(Y(NP1)+Y(NP2)-2.*Y(NP3)))**2*ABS(
     1U(NP1)+U(NP2)-2.*U(NP3))
      RETURN
   83 AME=0.
      RETURN
      END
$IBFTC FEC1
      SUBROUTINE FEC(X,IPF,IND,AJES)
      COMMON/KCAL/KETA,KHGW,KHG2W,KHBAL,KPROF,G,RC,TYC
      COMMON /JAY/ JCOMP,KDRAW,NSETS,KSP
      COMMON /CON/PSI,AMI,AME,DPEX,PREF(2),PR(2),F(2),DEN,AMU,XU,XD,XP,
     1XL,DX,INTG,CSALFA
      COMMON /COOL/ TC,TCG,HG,HCG
      COMMON/COUNT/KCOUNT
      IND=2
      AJES=0.
C*****   Q IN W/M2
      IF(KSP.EQ.2.AND.KHGW.EQ.1) AJES= Q/(3600.*0.24*3.16*TG*(TCG-1.))
      RETURN
      END
$IBFTC INTP
      SUBROUTINE INTPOL (U,Y,N,UD,YD,ND)
      DIMENSION U(N),Y(N),UD(ND),YD(ND)
C*****    LINEAR INTERPOLATION
      I=1
      DO 5 ID=1,ND
      IF(YD(ID).GE.Y(N)) GO TO 9
    8 IF(YD(ID).GE.Y(I).AND.YD(ID).LT.Y(I+1))  GO TO 7
      GO TO 6
    7 UD(ID)=U(I)+(U(I+1)-U(I)) /(Y(I+1)-Y(I))*(YD(ID)-Y(I))
      IF(YD(ID+1).GE.Y(I+1)) I=I+1
      GO TO 5
    6 CONTINUE
      I=I+1
      IF(I.LT.N) GO TO 8
    5 CONTINUE
      RETURN
    9 J=ID
      DO 11 ID=J,ND
   11 UD(ID)=U(N-1)+(U(N)-U(N-1))/(Y(N)-Y(N-1))*(YD(ID)-Y(N-1))
      RETURN
      END
$IBFTC LEN1
      SUBROUTINE LENGTH (Y,U,N,ER,KASE,YL1,YL2,YDI,UW)
      DIMENSION Y(20),U(20),EK(5),IK(5)
      J=1
      YL1=0.
      YL2=0.
      YDIV=0.
      KASE=0
      UW=0.
$EOF
```

```
      DO 10 I=1,N
      IF(U(I).GE. U(I-1)) GO TO 5
      UMIN=U(I)
      IF(U(I-1).GE.U(I-2)) J=J+1
      GO TO 10
    5 PK(J)=U(I)
      IK(J)=I
      IF(J.GE.2) KASE=2
   10 CONTINUE
      J1=IK(1)
      IK(1)=0
      J2=IK(2)
      IK(2)=0
      J3=IK(3)
      IK(3)=0
      J4=IK(4)
      IK(4)=0
      IF(PK(1).GT.U(N).AND.Y(J1).LT.Y(N).AND.J.GE.2) KASE=4
      IF(KASE.NE.4) GO TO 11
      DO 25 I=J1,N
      IF(U(I).LT.(1.-FR)*U(N)) KASE=3
   25 CONTINUE
   11 CONTINUE
      YDIV=Y(J1)
      UDIV=PK(1)
      IF(UDIV.EQ.U(N)) KASE=1
C***** U WAKE TAKEN AS DIFFERENCE BETWEEN UMIN AND MEAN OF UMAX AND UO
      IF(KASE.EQ.3.OR.KASE.EQ.2) UW=0.5*(PK(1)+U(N))- UMIN
C      SEARCH NEAR E BOUNDARY
      DIF=FR*U(N)
      J=N
   13 J=J-1
      UJ1=U(J)-U(N)
      IF(ABS(UJ1).GE.DIF)  GO TO 14
      GO TO 13
   14 A1=1.
      IF(UJ1.LT.0.) A1=-1.
      YEM=Y(J+1)+(Y(J)-Y(J+1)) * (U(N)+A1*DIF-U(J+1))/
     1(U(J)-U(J+1))
      YL1=YEM
      IF(KASE.EQ.1.OR.KASE.EQ.4) GO TO 20
C     SEARCH FOR YEN
      DIF =FR*PK(1)
      J=J1
   15 J=J+1
      UJ1=U(J)-U(J1)
      IF(ABS(UJ1).GE.DIF) GO TO 16
      GO TO 15
   16 YEN=Y(J)+(Y(J)-Y(J-1)) / (U(J)-U(J-1)) * (U(J1)-DIF-U(J))
      YL2=YEM-YEN
C     SEARCH FOR YEO
      DIF =FR*PK(1)
      J=J1
   17 J=J-1
      UJ1=U(J)-U(J1)
      IF(ABS(UJ1).GE.DIF) GO TO 18
$EOF
```

```
      GO TO 17
   18 A1=1.
      IF(UJ1.LT.0.) A1=-1.
      YEE= Y(J+1)+(Y(J)-Y(J+1))*(U(J1)+A1*DIF-U(J+1))/(U(J)-U(J+1))
   20 CONTINUE
      RETURN
      END
$IEFTC MAS1
      SUBROUTINE MASS(XU,XD,AM)
      AM=0.
      RETURN
      END
$IBFTC OTPT
      SUBROUTINE OUTPUT(ISEP)
C     MODIFIED ON 20TH JUNE,1967
      COMMON /GEN/RE1,AM1,AME,DPDX,PREF(2),PR(2),P(2),DEN,AMU,XU,XD,XP,
     1XL,DX,INTG,CSALFA
     1/C/SC(43),AU(43),BU(43),CU(43),A(2,43),B(2,43),C(2,43)
     1/V/U(43),F(2,43),R(43),RHO(43),EM(43),Y(43)
      COMMON/L/AK,ALMG
     1/L1/YL,UMAX,UMIN,FR,YIP,YEM
     1/I/N,NP1,NP2,NP3,NEQ,NPH,KEX,KIN,KASE,KRAD
     1/B/BETA,GAMA(2),TAUI,TAUE,AJI(2),AJE(2),INDI(2),INDE(2)
      COMMON /GEN/ UG,UCG,YG,XYG,FPG,FAT(20)
      COMMON /JAY/ JCOMP,KDRAW,NSETS,KSP
      DIMENSION UMS(60),ELT(60),ARG(70),DEL2(50),RD2(50),DFF12(50),RPFI2
     1(50),H12(50),ERPF(50),YPR(70),YS(70),SS(50),T(70),CR(2,20),ZX(20),
     1UM(50),YM(50),UH(50),YH(50),ANG(50),UTAU(50),ETAD(50)
     1,ETAX(50),XETA(50),CEX(5),SMOOTH(50)
      COMMON /AMB/ WT,PO,TO
      COMMON /STOP/ KSTOP
      COMMON/S/SEAR,EVIS(90),EM(90)
      COMMON/COUNT/KCOUNT
      COMMON /X/TITLE(12),XV(10),YX(10,70),UX(10,70),FIX(10,70),NVEL,NPH
     1I,NETA,NUM(10),PAT(2,100),XC,NRUN,NFI(10),NEF,YXF(10,70),XFI(10)
      COMMON/COOL/TC,TCC,FC,FCG
      COMMON/GROWTH/LOCAT,YI(50),YE(50)
      COMMON/SHAPE/ LOCK,YL1,YL2,YDIV,UW,XI
      COMMON/KCAL/KETA,KEGW,KEG2W,KEBAL,KPRCF,C,RC,TYC
      COMMON /AEC/ SF,S,BVI,PCI,A2,B2,C2
      COMMON/FLUX/QI
      DATA ((CR(I,J),J=1,9),I=1,2)/1.0,3.0,3.0,-6.0,3.0,3.0,-6.0,
     13.0,3.0,1.0,0.0,0.0,9.67,0.0,0.0,9.67,0.0,0.0/
      TC=TCC*TC
      NO=1
      IF(KPRCF.EQ.1)  NO=0
      IF(INTG.NE.1) GO TO 15
C     L.S. CUBIC FIT TO EXPERIMENTAL EFFECTIVENESS DATA    8.4.69
      IF(NETA.LE.0) GO TO 700
      DEVSQ=0.
      DEVL=F(1,1)
      IF(KSP.EQ.7) DEVL=(F(1,1)-F(1,NP3))/(F(1,NP3)*(TCC-1.))
      DO 701 I=1,NEF
      ARG(I)=PAT(2,I)
  701 ELT(I)=PAT(1,I)
      DO 702 I=1,50
$EOF
```

```
702   ANG(I)=0.
      CALL POLYFT(ELT,ANG,NEF,3,CEX,CEXC,SMOOTH,STDV)
      DEVL=CEXO+XC*(CEX(1) + XO*(CEX(2)+CEX(3)*XC))-DEVL
700   CONTINUE
      DO 350 I=1,NP3
      EM(I)=0.
  350 EVIS(I)=0.
      WRITE(6,29)
      WRITE(6,942) KCOUNT
      WRITE(6,260) TITLE
      YCDUM= YC*12.*25.4
      WRITE(6,60) KSP,UCG,FC,YCDUM,TYC,WT,FPG,TCG,TC,G
      WRITE(6,504) AK,ALNG,FFFF(1),XI
      WRITE(6,49)(EM(I),I=1,NP3)
      IF(NVEL.EQ.0) GO TO 302
      WRITE(6,555)
      IF(NC.EQ.0) WRITE(6,556)
C******** VALUES OF X/YC AT WHICH PROFILES ARE PRINTED OUT
      DO 200 I=1,NVEL
  200 ZX(I)=XV(I)
  302 CONTINUE
      ZX(NVEL+1)=0.
      ZX(NVEL+2)=1.0
      NV3=NVEL+3
      NV12=NVEL+12
      DO 750 I=NV3,NV12
750   ZX(I)=ZX(I-1)*2.
15    CONTINUE
      DXYC=DX/YC
      XYC=XU/YC+XC
      KY=0
      IF(ISEP.EQ.1) GO TO 55
      IF(INTG.NE.1) GO TO 75
      IT=1
      JT=1
      JPROF=1
      L=9
      IF(NVEL.GT.6) L=NVEL
   75 DO 28 I=1,L
      D=ZX(I)-XYC
      IF(INTG.EQ.151.AND.XYC.LT.ZX(6)) D=0.0
      IF(ABS(D).LT.DXYC.AND.D.GE.0.) GO TO 27
   28 CONTINUE
      GO TO 26
   27 KY=1
      IF(INTG.EQ.1) KY =0
      JPLOT=I
      IFP=0
      IF(NPHI.EQ.0) GO TO 26
      DO 230 I=1,NPHI
  230 IF(ABS(ZX(JPLOT)-XPI(I)).LE.0.5*YC)IFP=I
   26 CONTINUE
      IF(KY.EQ.1.AND.INTG.NE.IT) GO TO 25
      IF(INTG.NE.IT) RETURN
      IT= IT+10
   25 CONTINUE
$EOF
```

```
      JAM=JT+NEE
C******** STORING INFORMATION AFTER EVERY TEN INTEGRATIONS
      PAT(1,JAM)=XYC
      PAT(2,JAM)=F(1,1)
C     STORING ADIABATIC WALL TEMPERATURES
      ETAD(JAM)= PAT(2,JAM)
      IF(KETA.NE.1) GO TO 740
      ETAX(JT)=ETAD(JAM)
      XETA(JT)=XYC
      NETAX=JT
740   CONTINUE
C***    UMS IN M/S
      UMS(JAM)= U(NP3)*0.3048
      DLT(JAM)=12.*Y(NP3)
C     SEARCH FOR MAXIMUM AND HALF VELOCITY POINTS
      UM(JAM)=0.
      YM(JAM)=0.
      DO 800 I=3,NP3
      IF(U(I).LT.UM(JAM))   GO TO 800
      UM(JAM)= U(I)*0.3048
      YM(JAM)=Y(I)/YC
  800 CONTINUE
      UH(JAM)=(UM(JAM)+U(NP3))/2.
      DO 801 I=1,NP3
      IF(Y(I).LT.YM(JAM)*YC)  GO TO 801
      IF(UH(JAM).LE.U(I).AND.UH(JAM).GE.U(I+1)) GO TO 802
  801 CONTINUE
      GO TO 803
  802 YH(JAM)=(Y(I)+(Y(I+1)-Y(I))/(U(I)-U(I+1))*(U(I)-UH(JAM)))*12.
      YH(JAM)=YH(JAM)/YC/12.
  803 CONTINUE
      UH(JAM)=UH(JAM)*0.3048
      IF(KSP.EQ.9) SS(JAM)=TAUI/(DEN*UM(JAM)*UM(JAM))*1000.
      AMG(JAM)=AMS/DEN/UM(JAM)
C*****  COMPUTATION OF NAELA (STORED UNDER AMG)  8.4.69
      IF(NETA.LE.0) GO TO 703
      IF(JT.EQ.1)   GO TO 703
      DEV= DEX0+XYC*(DEX(1)+XYC*(DEX(2)+XYC*DEX(3)))-PAT(2,JAM)
      DEVSQ=DEVSQ+0.5*(DEV*DEV + DEVL*DEVL)*(PAT(1,JAM)-PAT(1,JAM-1))
      AMG(JAM) = SQRT(DEVSQ* YC / XU)
      DEVL=DEV
  703 CONTINUE
      IF(U(NP3).EQ.0.) GO TO 5001
      SS(JAM)=TAUI/(DEN*U(NP3)*U(NP3))*1000.
      UTAU(JAM)= SQRT(TAUI/DEN)*0.3048
C********* CALCULATION OF INTEGRAL QUANTITIES AND SHAPE FACTORS
      DO 76 I=2,NP2
   76 YS(I-1)=Y(I)
      UOMI=RHO(1)*(U(3)+U(2))*(U(3)+U(2))*(Y(3)+Y(2))/(U(NP3)*8.0*
     1(2./PCI-1.)*PEI)
      UOMI=UOMI+(OM(3)-OM(2))*(3.*U(3)+U(2))/(8.0*U(NP3))
      DO 112 I=3,NP1
  112 UOMI=UOMI+(OM(I+1)-OM(I))*(U(I+1)+U(I))/(2.*U(NP3))
      D2=PEI/(DEN*U(NP3))*(1.-UOMI)
      IF(KRAD.EQ.1) D2=D2/R(1)
      DEL2(JAM)=D2*12.
$EOF
```

```
      RD2(JAM)=U(NP3)*D2*DEN/AMU
      D2=0.
      DO 61 I=3,NP2
      IM1=I-1
   61 D2=D2+0.5*(F(1,I)+F(1,IM1)-2.*F(1,NP3))*(DM(I)-DM(IM1))
      D2=PEI/(DEN*U(NP3)*(F(1,1)-F(1,NP3)))*D2
      IF(KRAD.EQ.1) D2=D2/R(1)
      RPHI2(JAM)=U(NP3)*D2*DEN/AMU
      ERPH(JAM)=RPHI2(JAM)*F(1,1)
      D2=Y(NP3)-PEI/(DEN*U(NP3))
      IF(KRAD.EQ.1) D2=(Y(NP3)+0.5*Y(NP3)*Y(NP3)*CSALFA/R(1)) - PEI/
     1(DEN*U(NP3)*R(1))
      H12(JAM)=12.*D2/DEL2(JAM)
 5001 CONTINUE
  149 CONTINUE
      IF(KY.EQ.1) GO TO 24
      IF(INTG.NE.JPROF)GO TO 5
   24 CONTINUE
      IF(NC.NE.1) WRITE(6,20)XYC,INTG
   20 FORMAT(//5H XYC=,F6.1,5X,5H INTG,I3)
      DO 56 I=1,NP3
      IF(U(NP3).EQ.0.) GO TO 5000
      ARG(I)=U(I)/U(NP3)
      T(I)=(F(1,I)-F(1,NP3)) / (F(1,1)-F(1,NP3))
 5000 IF(KSP.EQ.9) ARG(I)=U(I)/UM(JAM)
      YPR(I)=Y(I)/YC
      IF(KSP.EQ.9) YPR(I)=Y(I)/(YH(JAM)*YC)
   56 CONTINUE
      T(NP2)=T(NP3)
C******** PRINTING OUT PROFILE INFORMATION
      IF(NC.EQ.1) GO TO 508
      WRITE(6,57) (ARG(I),I=1,NP3)
      WRITE(6,58) (YPR(I),I=1,NP3)
      WRITE(6,59) (T(I),I=1,NP3)
 508  CONTINUE
C******** PLOTTING PREDICTED PROFILES
      IF(KDRAW.NE.1) GO TO 300
      JCOMP=JCOMP+1
      IF(JCOMP.EQ.10)  CALL PLOT(7.75,-20.33,-3)
      IF(JCOMP.EQ.10) JCOMP=1
      CALL PLOT(OR(1,JCOMP),OR(2,JCOMP),-3)
      YMAX=5.0
      IF(YPR(NP3).GT.YMAX) YMAX=YPR(NP3)
      UMAX=FLOAT(IFIX(UCC)+1)
      YPR(N+4)=YMAX
      ARG(N+4)=UMAX
      T(N+4)=0.
      CALL SCALE(YPR,5.0,N+4,1)
      CALL SCALE(ARG,3.0,N+4,1)
      CALL AXIS(0.0,0.0,4HY/YC,4,5.0,90.0,YPR(N+5),YPR(N+6))
      CALL AXIS(0.0,0.0,1H ,1,3.0,0.0,ARG(N+5),ARG(N+6))
      YPR(N+4)=YPR(N+3)
      ARG(N+4)=ARG(N+3)
      CALL LINE(ARG,YPR,N+4,1,0,1)
      IF(NEQ.EQ.1) GO TO 206
      CALL SCALE(T,3.0,N+4,1)
$EOF
```

```
      CALL AXIS(0.0,5.0,6HFI/FIW,6,3.0,0.0,T(N+5),T(N+6))
      T(N+4)=T(N+3)
      CALL LINE(T,YPR,N+4,1,0,1)
      CALL SYMBOL (1.0,4.0,0.125,6H X/YC=,0.0,6)
      CALL NUMBER(2.0,4.0,0.125,ZX(JPLOT),0.0,1)
      IF(JCOMP.NE.1.AND.JCOMP.NE.4.AND.JCOMP.NE.7) GO TO 840
      CALL SYMBOL (2.,-0.7,.125,TITLE,0.0,72)
C      DRAWING A4 SIZE BORDER
      CALL PLOT(-1.37,-1.0,3)
      CALL PLOT(-1.37,7.5,2)
      CALL PLOT(4.505,7.5,2)
      CALL PLOT(4.505,7.0,2)
      CALL PLOT(4.505,7.5,2)
      CALL PLOT(10.38,7.5,2)
      CALL PLOT(10.38,-1.,2)
      CALL PLOT(10.38,-1.0,2)
      CALL PLOT(-1.37,-1.,2)
      CALL PLOT(0.,0.,3)
  840 CONTINUE
  200 CONTINUE
C********  PLOTTING EXPERIMENTAL PROFILES
  300 IF(NVEL.EQ.0) GO TO 207
      IF(JPLOT.GT.NVEL)  GO TO 207
      NU=NUM(JPLOT)
      NUM1=NU+1
      DO 205 I=1,NUM1
      YPR(I)=YX(JPLOT,I)/YC/12.
      YX(JPLOT,I)=YPR(I)
      ARG(I)=UX(JPLOT,I)
  205 IF(KSP.EQ.10) ARG(I)=UX(JPLOT,I)/U(NP3)
      IF(KDRAW.NE.1) GO TO 736
      CALL CHOP(YPR,ARG,NU,YMAX,0.0,KN)
      NU=KN
      NUM1=NU+1
      YPR(NUM1)=YMAX
      ARG(NUM1)=UMAX
      CALL SCALE(YPR,5.0,NUM1,1)
      CALL SCALE(ARG,3.0,NUM1,1)
      CALL AXIS(0.0,0.0,1H ,1,0.0,90.0,YPR(NU+2),YPR(NU+3))
      CALL AXIS(0.0,0.0,1H ,1,0.0,0.0,ARG(NU+2),ARG(NU+3))
      CALL LINE(ARG,YPR,NUM1,1,-1,4)
  736 IF(IFP.EQ.0) GO TO 207
      NF=NFI(IFP)
      NF1=NF+1
      DO 233 I=1,NF1
      YPR(I)=YXF(IFP,I)/YC/12.
      YXF(IFP,I)=YPR(I)
  233 T(I)=FIX(IFP,I)
      IF(KDRAW.NE.1) GO TO 207
      CALL CHOP(YPR,T,NF,YMAX,0.0,KN)
      NF=KN
      NF1=NF+1
      YPR(NF1)=YMAX
      T(NF1)=0.0
      CALL SCALE(YPR,5.0,NF1,1)
      CALL SCALE(T,3.0,NF1,1)
$EOF
```

```
      CALL AXIS(0.0,0.0,1H ,1,0.0,90.0,YPR(NF+2),YPR(NF+3))
      CALL AXIS(0.0,0.0,1H ,1,0.0,0.0,T(NF+2),T(NF+3))
      CALL LINE(T,YPR,NF1,1,-1,9)
  207 CONTINUE
      IF(KY.EQ.1) GO TO 5
   80 CONTINUE
      JPROF=JPROF+21
    5 JT=JT+1
      IF(INTG.NE.151) RETURN
C******** PRINTING OUT EFFECTIVENESS,INTEGRAL AND OTHER QUANTITIES
      WRITE(6,501)
   55 NEF=NEF+1
C     COMPUTING H FROM TAD AND TW AND Q
      IF(KHGW.NE.1) GO TO 741
      J=1
      NH=JAM-NEF+1
      DO 742 I=NEF,JAM
      ARG(J)=PAT(1,I)
      T(J)=ETAD(I)
742   J=J+1
      CALL INTPOL(ETAX,XETA,NETAX,YPR,ARG,NH)
      DO 743 I=1,NH
      AMG(I)=3600.*QI/(TG*(TCG-1.)*(T(I)-YPR(I)))
C****** THIS EXPRESSION VALID WHEN SLOT ENTHALPY IS TAKEN AS UNITY (KSP
      IF(KSP.EQ.2) AMG(I)= 3600.*0.24/(T(I)-YPR(I))*CI
C     NUSSELT NUMBER BASED ON SLOT CONDITIONS
      COND= AMU*0.24/PR(1)*3600.
      AMG(I)=AMG(I)*YC/COND
743   CONTINUE
 741   CONTINUE
      WRITE(6,70) (PAT(1,I),PAT(2,I),RD2(I),RPHI2(I),SS(I),H12(I),
     1UM(I),YM(I),UH(I),YH(I),UMS(I),AMG(I),UTAU(I),          I=NEF,JAM)
   70 FORMAT(//101H   X/YC    ETA         R2       RPHI2   SS*E3          H12  U
     1MAX       YMAX    UHALF    YHALF     UG    NUC OR AMG,4X,5H UTAU,2X,
     1//(
     11X,F6.2,2X,F6.4,1X,F9.2,2X,F7.1,2X,F6.3,2X,F6.3,2X,F6.2,2X,F6.3,2X
     1,F6.2,2X,F6.3,2X,F6.2,2X,E10.3,2X,F6.3,2X          ))
      NEF=NEF-1
      IF(NETA.LE.0) GO TO 301
      WRITE(6,71) NRUN,CEXO,(CEX(I),I=1,3),STDV,(PAT(1,I),PAT(2,I),
     1SMOOTH(I),I=1,NEF)
  301 CONTINUE
      JCOMP=9
71    FORMAT(/32H EXPERIMENTAL EFFECTIVENESS DATA//,5H RUN ,I2/
     127H COEFFICIENTS OF L.S. CUBIC/3H C0,4X,E12.5/3H C1,4X,E12.5/
     23H C2,4X,E12.5/3H C3,4X,E12.5//5H STDV,2X,E12.5/
     16H X/YC ,2X,3HETA,2X,6HSMOOTH//(F6.1,2X,F6.4,2X,F6.4))
  206 FORMAT(30X,12A6)
942   FORMAT(/8H KCOUNT ,I2/)
   29 FORMAT(1H1)
60    FORMAT(9H*********,3X,6H INPUT//4H KSP,5X,1H=,I3,12X,
     110H UC/UG    =,F7.3,10X, 10H RC        =,F9.1/ 10H YC (MM) =,
     1F6.2,9X, 10H T/YC     =,F5.2,12X, 10H M.WT.C  =,F8.2/
     110H KP*10**6=,F6.2,9X, 10H TC/TG    =,F6.3,11X,10H TC DEG K=,F7.1/
     110H QW W/M2 =F8.1//9H*********)
57     FORMAT(//(2X,4HU/UC,4X,15(F6.3,1X)))
$EOF
```

```
58     FORMAT(/(2X,5HY/YC ,3X,15(F6.3,1X)))
59      FCRMAT(/(2X,5HF1/F1W,2X,15(F6.4,1X)))
  502 FORMAT(2X,4HEVIS,4X,8(1PE10.3,3X))
  503 FORMAT(15X,7(4X,1PE10.3))
505     FCRMAT(/(2X,6HENU/NU,2X,15(F6.1,1X)))
506    FCRMAT(/(2X,8HEDIF/NU , 15(F6.0,1X)))
4444   FCRMAT(6H ITEST,I4/)
504     FCRMAT(9H*********,3X,24H MIXING LENGTH CCNSTANTS//
      12H K,7X,1H=,F7.3,8X,10H LAMBDA  =,F5.2,12X,10H SIGMA T =,F6.2/
      13H X1,6X,1H=,F8.4//9H*********)
49     FCRMAT(9H*********,3X,13H CMEGA VALUES//(15F8.4))
555     FCRMAT(9H*********,3X,7H CUTPUT/)
556    FCRMAT(9H*********,3X,20H PRCFILE INFCRMATICN/)
501    FCRMAT(/9H*********,3X,35H WALL,INTEGRAL AND CTHER PRCPERTIES/)
       RETURN
       END
$IBFTC PRE1
       SUBRCUTINE PRE(XU,XD,DPDX)
       COMMCN /GEN/PEI,AMI,AME,DPDX,PREF(2),PR(2),P(2),DEN,AMU,XU,XD,XP,
      1XL,DX,INTG,CSALFA
      1/V/U(43),F(2,43),R(43),RHC(43),CM(43),Y(43)
      1/I/N,NP1,NP2,NP3,NEC,NFI,KEX,KIN,KASE,KRAD
       COMMCN /CCN/ UG,UCG,YC,XYC,FPG,FAT(20)
C***** FPG REPRESENTS K * 10**6
       DPDX=(-1.)*DEN*DEN*U(NP3)*U(NP3)*U(NP3)*FPG/(AMU*10.**6)
       RETURN
       END
$IBFTC RAD1
C***** THIS SUBRCUTINE TRANSFERRED FRCM FISLOT2 55 31.12.1968
       SUBRCUTINE RAD(X,R1,CSALFA)
       COMMCN /GEN/PEI,AMI,AME,DPDX,PREF(2),PR(2),P(2),DEN,AMU,XU,XD,XP,
      1XL,DX,INTG,CSAL
      1/V/U(43),F(2,43),R(43),RHC(43),CM(43),Y(43)
      1/I/N,NP1,NP2,NP3,NEC,NFI,KEX,KIN,KASE,KRAD
       COMMCN /JAY/ JCCMP,KDRAW,NSETS,KSP
C       LIST NAMES CHANGED IN THIS SUBRCUTINE
       CSALFA=1.
       IF(KIN.EQ.3) GC TC 17
       IF(KRAD.EQ.0) GC TO 16
       IF(KSP.EQ.13) GC TC 15
       IF(X.EQ.0.) GO TC 15
       R1=R(1)*(R(1)-2.*AMI*(X-XP)/(RHC(1)*U(1)))
       IF(R1.LT.0.)R1=0.
       R1=SQRT(R1)
       RETURN
C*****   R1 CCRRESPONDS TC APPARATUS  B
15     R1=1.427/12.
       CSALFA=-1.
       RETURN
   16 R1=1.
       RETURN
   17 R1=0.
       RETURN
       END
$IBFTC RDY
       SUBRCUTINE READY
$ECF
```

```
      COMMON /GEN/PEI,ANI,ANE,DPDX,PREF(2),FR(2),P(2),DEN,AMU,XU,XD,XP,
     1XL,DX,INTG,CSALFA
     1/V/U(43),F(2,43),R(43),RHO(43),CM(43),Y(43)
     1/I/N,NP1,NP2,NP3,NEQ,NPH,KEX,KIN,KASE,KRAD
     1/B/BETA,GAMA(2),TAUI,TAUE,AJI(2),AJE(2),INDI(2),INDE(2)
      COMMON/ABC/SF,S,EVI,PCI,A2,B2,C2
      CALL DENSTY
      CALL RAD(XU,R(1),CSALFA)
C  Y NEAR THE I BOUNDARY
      GO TO (71,72,73),KIN
C****** EXPRESSIONS FOR Y(2) AND Y(3) CHANGED ON 6.3.69
   71 RU25=0.25*(RHO(2)+RHO(3))*(U(2)+U(3))
      Y(2)=CM(3)*(0.5/RU25/PCI-1./(RU25+RHO(3)*U(3)))
      GO TO 74
   72 Y(2)=12.*CM(3)/((3.*RHO(2)+RHO(3))*(U(2)+U(3)+4.*U(1)))
      GO TO 74
   73 Y(2)=.5*CM(3)/(RHO(1)*U(1))
   74 Y(3)=CM(3)*0.5/PCI/RU25+ CM(3)/(RU25+RHO(3)*U(3))
      IF(Y(2).LT.0..OR.Y(3).LT.0.) WRITE(6,7) Y(2),Y(3),BETA,CM(3),
     1RHO(2),RHO(3),U(2),U(3),INTG,XU
    7 FORMAT(//6H READY/8(3X,E10.3),2X,I3,3X,F6.3)
C  Y 'S FOR INTERMEDIATE GRID POINTS
      DO 50 I=4,NP1
   50 Y(I)= Y(I-1)+2.*(CM(I)-CM(I-1))/ (RHO(I-1)*U(I-1) + RHO(I)*U(I))
C  Y NEAR THE E BOUNDARY
      Y(NP2) = Y(NP1) + (CM(NP2)-CM(NP1)) / (1.5*RHO(NP1)*U(NP1)
     1 +0.5*RHO(NP2)*U(NP2))
      GO TO (81,82,83),KEX
   81 Y(NP3)=Y(NP2)+(1.+BETA)*(CM(NP2)-CM(NP1))*4./((RHO(NP1)+3.*RHO(NP2
     1))*(U(NP1)+U(NP2)))
      GO TO 84
   82 Y(NP3)=Y(NP2)+12.*(CM(NP2)-CM(NP1))/((RHO(NP1)+3.*RHO(NP2))*(U(NP2
     1)+U(NP1)+4.*U(NP3)))
      GO TO 84
   83 Y(NP3)=Y(NP2)+.5*(CM(NP2)-CM(NP1))/(RHO(NP3)*U(NP3))
   84 IF(CSALFA.EQ.0..OR.KRAD.EQ.0) GO TO 51
      DO 52 I=2,NP3
   52 Y(I)=2.*Y(I)*PEI/(R(1)+SQRT(ABS(R(1)*R(1)+2.*Y(I)*PEI*CSALFA)))
      GO TO 56
   51 DO 54 I=2,NP3
   54 Y(I)=PEI*Y(I)/R(1)
   56 CONTINUE
      Y(NP2)=2.*Y(NP2)-Y(NP1)
C  CALCULATION OF RADII
      DO 57 I=2,NP3
      IF(KRAD.EQ.0)R(I)=R(1)
      IF(KRAD.NE.0) R(I)= R(1)+Y(I)*CSALFA
   57 CONTINUE
      RETURN
      END
$IBFTC SLP
      SUBROUTINE SLIP
C***** THIS SUBROUTINE TRANSFERRED FROM EISLOT2 55 31.12.1968
      COMMON /GEN/PEI,ANI,ANE,DPDX,PREF(2),PR(2),P(2),DEN,AMU,XU,XD,XP,
     1XL,DX,INTG,CSALFA
     1/I/N,NP1,NP2,NP3,NEQ,NPH,KEX,KIN,KASE,KRAD
$EOF
```

```
     1/V/U(43),F(2,43),R(43),RHC(43),CM(43),Y(43)
     1/B/BETA,GAMA(2),TAUI,TAUE,AJI(2),AJE(2),INDI(2),INDE(2)
      COMMON /L/AK,ALMG
     1/C/SC(43),AU(43),BU(43),CU(43),A(2,43),B(2,43),C(2,43)
      COMMON/ABC/SE,S,BVI,PCI,A2,B2,C2
      COMMON/FLUX/GI
C   SLIP COEFFICIENTS NEAR THE I BOUNDARY FOR VELOCITY EQUATION
      CU(NP2)=0.
      GO TO (71,72,73),KIN
C****** SLIP COEFFICIENTS TO INCLUDE CONVECTION IN INNER-HALF INTERVAL
      REAL MI,ME
71    YCON=PCI*(.5*(Y(2)+Y(3))/DX
      G25=.25*(RHC(3)+RHC(2))*(U(2)+U(3))
      MI=AMI/G25
      ME=AME/G25
      CM25=(CM(3)+CM(2))*0.125
      D=1.5*YCON+S+MI*(1.+CM25)-ME*(R(NP3)/R(1))*CM25+BVI
      AU(2)=(-1.)*(.5*YCON+S+MI*(1.-CM25) + ME*(R(NP3)/R(1))*CM25-BVI)/D
      BU(2)=2.*(S+MI)/D
      CU(2)=(YCON*(1.5*U(2)+.5*U(3))-(Y(3)+Y(2))*DPDX/G25)/D
      GO TO 74
   72 SQ=84.*U(1)*U(1)-12.*U(1)*U(3)+9.*U(3)*U(3)
      BU(2)=8.*(2.*U(1)+U(3))/(2.*U(1)+7.*U(3)+SQRT(SQ))
      AU(2)=1.-BU(2)
      GO TO 74
   73 BU(2)=0.
      CALL VEFF(2,3,EMU)
      AK1=1./DX-DPDX/(RHC(1)*U(1)*U(1))
      AK2=-U(1)*AK1+DPDX/(RHC(1)*U(1))
      AJ=RHC(1)*U(1)*.25*(Y(2)+Y(3))**2/EMU
      IF(KRAD.EQ.0) GO TO 75
      AU(2)=2./(2.+AJ*AK1)
      CU(2)=-.5*AJ*AK2*AU(2)
      GO TO 74
   75 CU(2)=1./(2.+3.*AJ*AK1)
      AU(2)=CU(2)*(2.-AJ*AK1)
      CU(2)=-CU(2)*4.*AJ*AK2
C   SLIP COEFFICIENTS NEAR THE E BOUNDARY FOR VELOCITY EQUATION
   74 GO TO (81,82,83),KEX
   81 AU(NP2)=0.
      BU(NP2)=1./(1.+2.*BETA)
      GO TO 84
   82 SQ=84.*U(NP3)*U(NP3)-12.*U(NP3)*U(NP1)+9.*U(NP1)*U(NP1)
      AU(NP2)=8.*(2.*U(NP3)+U(NP1))/(2.*U(NP3)+7.*U(NP1)+SQRT(SQ))
      BU(NP2)=1.-AU(NP2)
      GO TO 84
   83 AU(NP2)=0.
      CALL VEFF(NP1,NP2,EMU)
      BK1=1./DX-DPDX/(RHC(NP3)*U(NP3)*U(NP3))
      BK2=-U(NP3)*BK1+DPDX/(RHC(NP3)*U(NP3))
      BJ=RHC(NP3)*U(NP3)*.25*(2.*Y(NP3)-Y(NP1)-Y(NP2))**2/EMU
      CU(NP2)=1./(2.+3.*BJ*BK1)
      BU(NP2)=CU(NP2)*(2.-BJ*BK1)
      CU(NP2)=-CU(NP2)*4.*BJ*BK2
   84 IF(NEQ.EQ.1)RETURN
C   SLIP COEFFICIENTS NEAR THE I BOUNDARY FOR OTHER EQUATIONS
$EOF
```

```
      DO 54 J=1,NPH
      C(J,2)=0.
      C(J,NP2)=0.
      GO TO (41,42,43),KIN
   41 CALL FBC(XD,J,INDI(J),GI)
      IF(INDI(J).EQ.1) GO TO 61
      VPH= BVI/ PREF(J)
      T= D- (S+BVI) + VPH
      A(J,2) =(-1.)/T*(0.5*YCON+MI*(1.0-.25*OM(3))+.25*ME*OM(3)*R(NP3)/
     1R(1)-VPH)
      B(J,2)=0.
      C(J,2)=(YCON*(1.5*F(J,2)+.5*F(J,3))+2.*GI/(.25*(RHO(2)+RHO(3))*(U(
     12)+U(3)) )) /T
C     CALCULATION OF A2,B2,C2 FOR OBTAINING WALL VALUES OF F
      TD=T+SF
      A2=(A(J,2)*T-SF)/TD
      B2=2.0*(SF+MI)/TD
      C2=YCON*(1.5*F(J,2)+.5*F(J,3))/TD
      GO TO 44
   61 F(J,1)=GI
      A(J,2)=(1.+BETA-GAMA(J))/(1.+BETA+GAMA(J))
      B(J,2)=1.-A(J,2)
      GO TO 44
   42 A(J,2)=(U(2)+U(3)-8.*U(1))/(5.*(U(2)+U(3))+8.*U(1))
      B(J,2)=1.-A(J,2)
      GO TO 44
   43 B(J,2)=0.
      CALL SOURCE(J,1,CS,DS)
      AK1=1./DX-DS
      AK2=-AK1*F(J,1)-CS
      AJF=AJ*PREF(J)
      IF(KRAD.EQ.0) GO TO 45
      A(J,2)=2./(2.+AJF*AK1)
      C(J,2)=-.5*AJF*AK2*A(J,2)
      GO TO 44
   45 C(J,2)=1./(2.+3.*AJF*AK1)
      A(J,2)=C(J,2)*(2.-AJF*AK1)
      C(J,2)=-C(J,2)*4.*AJF*AK2
C   SLIP COEFFICIENTS NEAR THE E BOUNDARY FOR OTHER EQUATIONS
   44 GO TO (51,52,53),KEX
   51 CALL FBC(XD,J,INDE(J),GE)
      IF(INDE(J).EQ.1) GO TO 31
      AJE(J)=GE
      B(J,NP2)=1.
      A(J,NP2)=0.
      C(J,NP2)=-8.*(1.+2.*BETA)*PREF(J)*AJE(J)/(AK*AK*BETA*(1.+BETA)*
     1(1.+BETA)*(RHO(NP1)+3.*RHO(NP2))*U(NP1))
      GO TO 54
   31 F(J,NP3)=GE
      B(J,NP2)=(1.+BETA-GAMA(J))/(1.+BETA+GAMA(J))
      A(J,NP2)=1.-B(J,NP2)
      GO TO 54
   52 B(J,NP2)=(U(NP2)+U(NP1)-8.*U(NP3))/(5.*(U(NP2)+U(NP1))+8.*U(NP3))
      A(J,NP2)=1.-B(J,NP2)
      GO TO 54
   53 A(J,NP2)=0.
$EOF
```

```
      CALL SOURCE(J,NP3,CS,DS)
      BK1=1./DX-DS
      BK2=-BK1*F(J,NP3)-CS
      EJF=EJ*PREF(J)
      C(J,NP2)=1./(2.+3.*PJF*BK1)
      B(J,NP2)=C(J,NP2)*(2.-EJF*BK1)
      C(J,NP2)=-C(J,NP2)*4.*EJF*BK2
   54 CONTINUE
      RETURN
      END
$IBFTC SLV
      SUBROUTINE SOLVE(A,B,C,F,NP3)
C     THIS SOLVES EQUATIONS OF THE FORM
C     F(I) = A(I)*F(I+1) + B(I)*F(I-1) + C(I)
C     FOR I=2,NP2
      DIMENSION A(NP3),B(NP3),C(NP3),F(NP3)
      NP2=NP3-1
      B(2) = B(2)*F(1) + C(2)
      DO 48 I=3,NP2
      T = 1./(1.-B(I)*A(I-1))
      A(I) = A(I)*T
   48 B(I) = (B(I)*B(I-1) + C(I))*T
      DO 50 I=2,NP2
      J=NP2-I+2
   50 F(J)=A(J)*F(J+1)+B(J)
      RETURN
      END
$IBFTC SORC
      SUBROUTINE SOURCE(J,I,CS,DS)
      CS=0.
      DS=0.
      RETURN
      END
$IBFTC VEF1
      SUBROUTINE VEFF(I,IP1,EMU)
      COMMON /GEN/PEI,AMI,AME,DPDX,PREF(2),PR(2),P(2),DEN,AMU,XU,XD,XP,
     1XL,DX,INTG,CSALFA
     1/V/U(43),F(2,43),R(43),RHO(43),EM(43),Y(43)
     1/I/N,NP1,NP2,NP3,NEQ,NFF,KEX,KIN,KASE,KRAD
      COMMON /L/AK,ALMG
     1/L1/YL,UMAX,UMIN,FR,YIE,YEM
      COMMON/SHAPE/ LOCK,YL1,YL2,YDIV,UW,XI
C  THIS SUBROUTINE USES THE MIXING-LENGTH HYPOTHESIS
      AL=ALMG*YL1
      IF(KIN.EQ.1) YM=(Y(I)+Y(IP1))*0.5
      IF(KEX.EQ.1) YM=Y(NP3)-0.5*(Y(I)+Y(IP1))
      IF(YM.LT.AL/AK) AL=AK*YM
   66 EMU=.5*(RHO(I)+RHO(IP1))*AL*AL*ABS((U(I)-U(IP1))/(Y(I)-Y(IP1)))
      RETURN
      END
$IBFTC VIS1
      FUNCTION VISCO(I)
      COMMON /GEN/PEI,AMI,AME,DPDX,PREF(2),PR(2),P(2),DEN,AMU,XU,XD,XP,
     1XL,DX,INTG,CSALFA
      COMMON/BVIS/ BMU
      COMMON/V/U(43),F(2,43),R(43),RHO(43),EM(43),Y(43)
$EOF
```

```
      COMMON/AME/WT,PC,TO
      COMMON/JAY/JCOMP,KDRAW,NSETS,KSP
     1/I/N,NP1,NP2,NP3,NEQ,NPH,KEX,KIN,KASE,KRAD
      COMMON/COOL/TC,TCG,FC,FCG
      IF(KSP.EQ.2) GO TO 50
C******** VISCOSITY OF A BINARY MIXTURE 'SQUARE-ROOT'FORMULA
      ENB=F(1,I)/(F(1,I)+WT/28.96*(1.-F(1,I)))
      ENA=1.-ENB
      VISCO=(ENA*AMU*SQRT(28.96)+ENB*BMU*SQRT(WT))/
     1 (ENA*SQRT(28.96)+ENB*SQRT(WT))
      RETURN
C***** ENTHALPY AS CONSERVED PROPERTY
C****** TEMP NON DIM WITH SLOT VALUES
50    VISCO= AMU*(1.+F(1,I)*(TCG-1.))**0.76
      RETURN
      END
$IBFTC WALL
      SUBROUTINE WALL
C  THIS DECK TRANSFERRED FROM FISLOT 2 ON 4TH JUNE 1968
      COMMON/ABC/SF,S,EVI,POI,A2,B2,C2
      COMMON /GEN/PEI,AMI,AME,DPDX,PREF(2),PR(2),P(2),CEN,AMU,XU,XD,XP,
     1XL,DX,INTG,CSALF/
     1/V/U(43),F(2,43),R(43),RHO(43),OM(43),Y(43)
     1/I/N,NP1,NP2,NP3,NEQ,NPH,KEX,KIN,KASE,KRAD
     1/B/BETA,GAMA(2),TAUI,TAUE,AJI(2),AJE(2),INDI(2),INDE(2)
      COMMON /L/AK,ALNG
      COMMON /STOP/ KSTOP
C  CALCULATION OF BETA FOR THE E BOUNDARY
      IF(U(3).LT.0.) KSTOP=1
      IF(U(2).LT.0.) KSTOP=1
      IF(KSTOP.EQ.1) WRITE (6,5)
    5 FORMAT( 23H NEGATIVE VELOCITIES)
      IF(KSTOP.EQ.1) RETURN
      IF(KEX.NE.1) GO TO 15
      YI=Y(NP3)-.5*(Y(NP1)+Y(NP2))
      UI=.5*(U(NP2)+U(NP1))
      RH=.25*(3.*RHO(NP2)+RHO(NP1))
      RE=RH*UI*YI/VISCO(NP3)
      FP=DPDX*YI/(RH*UI*UI)
      AM=AME/(RH*UI)
      CALL WF1(RE,FP,AM,S)
      BETA=SQRT(ABS(S+FP+AM))/AK
      TAUE=S*RH*UI*UI
      IF(NEQ.EQ.1) GO TO 36
C  CALCULATION OF GAMA 'S FOR THE E BOUNDARY
      DO 35 J=1,NPH
      CALL WF2(RE,FP,AM,PR(J),PREF(J),P(J),SF)
      GAMA(J)=(SF+AM)*PREF(J)/(AK*AK*BETA)
      IF(INDE(J).EQ.1)AJE(J)=SF*RH*UI*(F(J,NP2)+F(J,NP1)-2.*F(J,NP3))*.5
   35 CONTINUE
   36 IF(KIN.NE.1)RETURN
C  CALCULATION OF BETA FOR THE I BOUNDARY
   15 YI=.5*(Y(2)+Y(3))
      UI=.5*(U(2)+U(3))
      RH=.25*(3.*RHO(2)+RHO(3))
      RE=RH*UI*YI/VISCO( 1 )
$EOF
```

```
      FP=DPDX*YI/(RH*UI*UI)
      AM=AMI/(RH*UI)
      XYZ=VISCO(1)
      IF(RE.LE.0.)WRITE(6,32)INTG,XU,RE,U(2),U(3),Y(2),Y(3),RHO(2),RHO(3
     1),XYZ
   32 FORMAT(6H WALL /3X,I3,3X,F7.4,8(2X,E10.3))
      CALL WF1(RE,FP,AM,S)
      TAUI=S*RH*UI*UI
C****
C****  CALCULATION OF  VEFF2.5 AND PCI   2.5                    6.3.69
C******
       T1=ABS(S+FP*AM)
C*****   VAN DRIEST,S CONSTANT  A* TAKEN EQUAL TO 11
      PWR=(-1.)*RE*SQRT(T1)*AK/11.
      DAMP=1.-EXP(PWR)
      VPLUS= 0.5 + SQRT(0.25 + AK*AK*RE*RE*T1*DAMP*DAMP)
      EVI=  VPLUS/RE + T1
      PCI = VPLUS/(VPLUS+ T1*RE)
      IF(NEQ.EQ.1) RETURN
C  CALCULATION OF GAMA 'S FOR THE I BOUNDARY
      DO 38 J=1,NPH
      CALL WF2(RE,FP,AM,PR(J),PREF(J),P(J),SF)
      GAMA(J)=(SF+AM)*PREF(J)/(AK*AK*BETA)
      IF(INDI(J).EQ.1)AJI(J)=SF*RH*UI*(2.*F(J,1)-F(J,2)-F(J,3))*.5
   38 CONTINUE
      RETURN
      END
$IBFTC WF1S
      SUBROUTINE WF1(R,F,AM,S)
      COMMON /L/AK,ALMG
      AKS=AK*AK/.16
      RT=R*AKS
      IF(RT.LE.0.) WRITE(6,16) R,AK
      IF(RT.LE.0.)RETURN
      ST=1./RT-.04741*RT**(-.7)+.01111*RT**(-.174)
   16 FORMAT(4H WF1,2X,2E10.3)
      IF(F.EQ.0.) GO TO 15
      FT=F/AKS
      TERM=1.-25.*FT*RT/(57344.+RT**2.5)**.4
      IF(TERM.LT.0.) TERM=.0001
      ST=ST*TERM**1.6
   15 S=ST*AKS
      RETURN
      END
$IBFTC WF2S
      SUBROUTINE WF2(R,F,AM,  PR ,PRT,P,S)
C***** THIS SUBROUTINE TRANSFERRED FROM FIS10T2 55 31.12.1968
      COMMON /L/AK,ALMG
      AKS=AK*AK/.16
      RT=R*AKS
      IF(RT.LE.0.) RETURN
      PT=P*AK*2.5
      A=1./PR
      A=A+10.**(-A)
      S1=1./(PR*PT)
      S2=.0111*RT**(-.174)
$EOF
```

```
$DATA
004
      SAMPLE DATA   KSP= 0
 KSP   0
0.75  2000. 2.54  0.50  39.94 0.00  0
0000000
      SAMPLE DATA   KSP = 1
 KSP  01
0.[illegible] 5850. 6.30  0.128 28.96 0.00  0       1
0[illegible]00
      SAMPLE DATA KSP = 2
 K[illegible]P  02
0.[illegible]5 2000. 2.54  0.50  28.96 0.00  0       1.20  60.0  0.00
0[illegible]000
      SAMPLE DATA   KSP= 2 AND C NOT EQUAL TO ZERO
 KSP  02
0.75  2000. 2.54  0.50  28.96 0.00  0       1.20  60.0  600.0
0000000
$EOF
```

```
      S2=S2/(PRT*(1.+FT*SQRT(S2)))
      IF(S1.LE.0..OR. S2.LE.0.) RETURN
      S=(S1**A+S2**A)**(1./A)
      IF(F.EQ.0.) GO TO 15
      FT=F/AKS
      SSEP=1.32/PRT*RT**(-.3333)*(FT+17.)**(-1.165)
      FD=.01*RT
      FD= 25.*FT*FD/(1.+FD)
      IF(FD.GT.0.)FD=FD**.8
      S=S*(1.-FD)+FD*SSEP
   15 S=S*AKS
      RETURN
      END
$IBFTC PLY
      SUBROUTINE POLYFT(X,Y,N,NPOL,C,CC,SMOOTH,STDV)
      DIMENSION X(N),Y(N),C(NPOL),SMOOTH(N)
C***** THIS IS A DUMMY
      RETURN
      END

C********************           SAMPLE  INPUT
```

SAMPLE DATA KSP= 0

******** INPUT

KSP	= 0	UC/UG	= 0.750	RC	= 2000.0
YC (MM)	= 2.54	T/YC	= 0.50	M.WT.C	= 39.94
KP*10**6	= 0.00	TC/TG	= 1.000	TC DEG K	= 485.0
QW W/M2	= 0.0				

****
******** MIXING LENGTH CONSTANTS

K	= 0.419	LAMBDA	= 0.09	SIGMA T	= 1.00
XI	= 0.0700				

****
******** OMEGA VALUES

0.0000	0.0000	0.0187	0.0263	0.0424	0.0593	0.0766	0.0939	0.1113	0.1286	0.1460	0.1634	0.1780	0.1925
0.2214	0.2358	0.2503	0.2646	0.2783	0.2903	0.3004	0.3082	0.3130	0.3261	0.3433	0.3842	0.4417	0.5037
0.6366	0.7062	0.7775	0.8503	0.9244	1.0000	1.0000							

******** WALL,INTEGRAL AND OTHER PROPERTIES

X/YC	ETA	R2	RPHI2	SS*E3	H12	UMAX	YMAX	UHALF	YHALF	UG	NUC OR AMG	UTAU
0.00	1.0000	1361.86	2521.7	10.035	1.239	14.56	4.000	9.50	2.610	14.56	-0.498E 00	1.458
0.95	0.9980	1362.98	2526.9	6.129	0.705	14.56	3.795	9.50	2.476	14.56	-0.227E 00	1.140
1.91	0.9841	1375.04	2562.9	5.416	0.694	14.56	3.850	9.50	2.512	14.56	-0.171E 00	1.071
3.86	0.9391	1397.42	2686.0	4.618	0.700	14.56	3.948	9.50	2.575	14.56	-0.126E 00	0.989
5.85	0.8917	1417.89	2828.9	4.114	0.712	14.56	4.031	9.50	2.630	14.56	-0.105E 00	0.934
7.88	0.8500	1436.82	2967.8	3.747	0.726	14.56	4.107	9.50	2.679	14.56	-0.929E-01	0.891
9.95	0.8144	1454.54	3097.9	3.463	0.741	14.56	4.177	9.50	2.725	14.56	-0.858E-01	0.857
15.92	0.7351	1499.70	3432.6	2.926	0.780	14.56	4.366	9.50	2.849	14.56	-0.816E-01	0.787
24.66	0.6634	1556.31	3803.9	2.517	0.825	14.56	4.634	9.50	3.023	14.56	-0.831E-01	0.730
31.74	0.6248	1597.66	4039.7	2.347	0.851	14.56	4.843	9.50	3.159	14.56	-0.804E-01	0.705
39.13	0.5921	1638.52	4263.6	2.244	0.871	14.56	5.048	9.50	3.294	14.56	-0.760E-01	0.689
54.81	0.5368	1720.97	4703.5	2.124	0.903	14.56	5.446	9.50	3.553	14.56	-0.678E-01	0.671
63.10	0.5127	1763.04	4925.1	2.084	0.916	14.56	5.639	9.50	3.679	14.56	-0.647E-01	0.664
71.67	0.4905	1805.82	5148.9	2.050	0.928	14.56	5.831	9.50	3.804	14.56	-0.623E-01	0.659
89.68	0.4507	1893.70	5603.7	1.995	0.950	14.56	6.215	9.50	4.055	14.56	-0.591E-01	0.650
108.86	0.4163	1984.93	6067.8	1.950	0.969	14.56	6.607	9.50	4.311	14.56	-0.571E-01	0.643
127.13	0.3891	2070.09	6493.7	1.914	0.985	14.56	6.970	9.50	4.547	14.56	-0.559E-01	0.637
129.22	0.3862	2079.73	6541.6	1.910	0.987	14.56	7.011	9.50	4.574	14.56	-0.558E-01	0.636
150.82	0.3597	2178.31	7025.8	1.875	1.003	14.56	7.431	9.50	4.848	14.56	-0.547E-01	0.630
173.69	0.3360	2280.84	7521.4	1.842	1.018	14.56	7.866	9.50	5.132	14.56	-0.538E-01	0.625

```
KCOUNT  2
                                   SAMPLE DATA   KSP = 1
********   INPUT

KSP        =  1               UC/UG     =  0.750             RC          =   5850.0
YC (MM)    =  6.30            T/YC      =  0.13              M.WT.C      =   28.96
KP*10**6=     0.00            TC/TG     =  1.000             TC DEG K=   485.0
QW W/M2    =     0.0

********
********   MIXING LENGTH CONSTANTS

K          =  0.419           LAMBDA    =  0.09              SIGMA T  =   1.00
XI         =  0.0046

********
********   OMEGA VALUES

 0.0000  0.0000  0.0115  0.0163  0.0270  0.0384  0.0507  0.0639  0.0776  0.0919  0.1066  0.1215  0.1339  0.1465
 0.1716  0.1841  0.1966  0.2090  0.2211  0.2327  0.2432  0.2511  0.2556  0.2590  0.2639  0.3085  0.3710  0.4383
 0.5837  0.6617  0.7424  0.8257  0.9117  1.0000  1.0000

********   WALL,INTEGRAL AND OTHER PROPERTIES
```

X/YC	ETA	R2	RPHI2	SS*E3	H12	UMAX	YMAX	UHALF	YHALF	UG	NUC OR ANG	UTAU
0.00	1.0000	3913.04	5659.1	2.237	1.611	19.12	3.628	12.47	2.367	19.12	-0.557E 00	0.904
0.90	1.0023	3912.47	5646.8	1.946	1.395	19.12	3.626	12.47	2.366	19.12	-0.261E 00	0.843
1.81	1.0017	3925.65	5650.5	1.956	1.377	19.12	3.684	12.47	2.403	19.12	-0.198E 00	0.846
2.00	1.0012	3928.42	5653.2	1.959	1.375	19.12	3.694	12.47	2.410	19.12	-0.190E 00	0.846
3.68	0.9918	3954.37	5707.2	1.966	1.366	19.12	3.781	12.47	2.467	19.12	-0.150E 00	0.848
3.87	0.9903	3957.31	5716.1	1.964	1.365	19.12	3.790	12.47	2.473	19.12	-0.147E 00	0.847
5.59	0.9742	3983.86	5811.3	1.935	1.363	19.12	3.866	12.47	2.522	19.12	-0.128E 00	0.841
7.54	0.9539	4013.18	5935.3	1.883	1.363	19.12	3.943	12.47	2.573	19.12	-0.115E 00	0.830
7.93	0.9497	4019.00	5961.2	1.871	1.363	19.12	3.958	12.47	2.582	19.12	-0.113E 00	0.827
9.53	0.9333	4042.10	6066.4	1.826	1.364	19.12	4.016	12.47	2.620	19.12	-0.106E 00	0.817
14.43	0.8875	4109.74	6380.3	1.698	1.370	19.12	4.182	12.47	2.728	19.12	-0.946E-01	0.788
15.69	0.8770	4126.33	6456.8	1.670	1.372	19.12	4.222	12.47	2.754	19.12	-0.926E-01	0.781
21.49	0.8322	4199.73	6805.6	1.566	1.379	19.12	4.396	12.47	2.868	19.12	-0.853E-01	0.757
30.96	0.7577	4312.20	7475.8	1.474	1.385	19.12	4.654	12.47	3.036	19.12	-0.762E-01	0.734
35.18	0.7237	4360.67	7827.7	1.453	1.385	19.12	4.759	12.47	3.105	19.12	-0.729E-01	0.729
49.92	0.6166	4526.55	9189.0	1.421	1.381	19.12	5.094	12.47	3.323	19.12	-0.639E-01	0.721
62.41	0.5458	4665.44	10382.2	1.412	1.376	19.12	5.350	12.47	3.490	19.12	-0.588E-01	0.718
65.63	0.5303	4701.10	10686.2	1.411	1.375	19.12	5.413	12.47	3.531	19.12	-0.577E-01	0.718
82.29	0.4640	4885.18	12215.7	1.406	1.368	19.12	5.724	12.47	3.734	19.12	-0.536E-01	0.717
99.88	0.4125	5078.86	13741.4	1.402	1.362	19.12	6.034	12.47	3.936	19.12	-0.508E-01	0.716
118.60	0.3717	5282.[illegible]	15253.9	1.397	1.357	19.12	6.347	12.47	4.141	19.12	[illegible]	0.715

KCCUNT 5

SAMPLE DATA KSP = 2

******** INPUT

```
KSP        =  2          UC/UG    =  0.750        RC        =    2000.0
YC (MM)    =  2.54       T/YC     =  0.50         M.WT.C    =    28.96
KP*1C**6=   0.00         TC/TG    =  1.200        TC DEG K=    520.0
QW W/M2  =    0.0
```

****
******** MIXING LENGTH CCNSTANTS

```
K          =  0.419      LAMBDA   =  0.09         SIGMA T =  1.00
XI         =  0.0700
```

****
******** CMEGA VALUES

```
 C.000C  0.0000  0.0129  0.0182  0.0294  0.0411  0.0531  0.0651  0.0771  0.0891  0.1011  0.1132  0.1233  0.1333
 0.1534  0.1634  0.1733  0.1833  0.1928  0.2011  0.2081  0.2135  0.2168  0.2275  0.2472  0.2941  0.3599  0.4311
 C.5834  0.6632  0.7449  0.8284  0.9133  1.0000  1.0000
```

******** WALL,INTEGRAL AND OTHER PROPERTIES

X/YC	ETA	R2	RPHI2	SS*E3	H12	UMAX	YMAX	UHALF	YHALF	UG	NUC OR AMG	UTAU
0.00	1.0000	1564.37	2154.8	6.485	2.427	20.51	4.000	13.38	2.610	20.51	-0.498E 00	1.652
0.96	0.9966	1565.69	2162.5	3.842	1.806	20.51	3.812	13.38	2.487	20.51	-0.228E 00	1.271
1.92	0.9742	1576.45	2212.3	3.413	1.782	20.51	3.865	13.38	2.521	20.51	-0.172E 00	1.198
3.87	0.9046	1596.78	2382.8	2.969	1.766	20.51	3.956	13.38	2.581	20.51	-0.126E 00	1.118
5.87	0.8348	1615.72	2582.1	2.691	1.762	20.51	4.034	13.38	2.632	20.51	-0.105E 00	1.064
7.90	0.7726	1633.44	2790.3	2.485	1.762	20.51	4.104	13.38	2.678	20.51	-0.926E-01	1.023
9.97	0.7232	1650.21	2981.2	2.325	1.763	20.51	4.170	13.38	2.720	20.51	-0.851E-01	0.989
15.91	0.6225	1693.65	3463.5	2.026	1.770	20.51	4.342	13.38	2.832	20.51	-0.769E-01	0.923
24.58	0.5456	1749.54	3952.4	1.811	1.777	20.51	4.574	13.38	2.984	20.51	-0.738E-01	0.873
31.55	0.5056	1791.50	4265.8	1.742	1.772	20.51	4.747	13.38	3.097	20.51	-0.707E-01	0.856
38.77	0.4724	1833.85	4566.0	1.708	1.763	20.51	4.917	13.38	3.208	20.51	-0.672E-01	0.848
53.97	0.4187	1921.35	5152.2	1.681	1.740	20.51	5.247	13.38	3.423	20.51	-0.606E-01	0.841
63.56	0.3922	1976.02	5501.4	1.672	1.725	20.51	5.440	13.38	3.549	20.51	-0.576E-01	0.839
70.14	0.3763	2013.40	5734.1	1.668	1.716	20.51	5.567	13.38	3.632	20.51	-0.559E-01	0.838
87.27	0.3416	2110.20	6316.6	1.657	1.693	20.51	5.886	13.38	3.840	20.51	-0.527E-01	0.835
105.37	0.3127	2211.72	6901.8	1.646	1.672	20.51	6.209	13.38	4.051	20.51	-0.507E-01	0.832
124.44	0.2881	2317.95	7491.5	1.634	1.653	20.51	6.539	13.38	4.266	20.51	-0.493E-01	0.829
126.40	0.2858	2328.84	7550.7	1.633	1.651	20.51	6.572	13.38	4.288	20.51	-0.491E-01	0.829
144.51	0.2669	2428.92	8087.3	1.622	1.635	20.51	6.878	13.38	4.488	20.51	-0.482E-01	0.826
165.61	0.2484	2544.66	8691.2	1.609	1.618	20.51	7.230	13.38	4.717	20.51	-0.474E-01	0.823

KCOUNT 4

SAMPLE DATA KSP= 2 AND Q NOT EQUAL TO ZERO

******** INPUT

KSP =	2	UC/UG =	0.750	RC =	2000.0
YC (MM) =	2.54	T/YC =	0.50	M.WT.C =	28.96
KP*10**6=	0.00	TC/TG =	1.200	TC DEG K=	520.0
QW W/M2 =	600.0				

****
******** MIXING LENGTH CONSTANTS

K =	0.419	LAMBDA =	0.09	SIGMA T =	1.00
XI =	0.0700				

****
******** OMEGA VALUES

0.0000	0.0000	0.0129	0.0182	0.0294	0.0411	0.0531	0.0651	0.0771	0.0891	0.1011	0.1132	0.1233	0.1333
0.1534	0.1634	0.1733	0.1833	0.1928	0.2011	0.2081	0.2135	0.2168	0.2275	0.2472	0.2941	0.3599	0.4311
0.5834	0.6632	0.7449	0.8284	0.9133	1.0000	1.0000							

******** WALL,INTEGRAL AND OTHER PROPERTIES

X/YC	ETA	R2	RPHI2	SS*E3	H12	UMAX	YMAX	UHALF	YHALF	UG	NUC OR ANG	UTAU
0.00	1.0000	1564.37	2154.8	6.485	2.427	20.51	4.000	13.38	2.610	20.51	0.000E-38	1.652
0.96	1.0664	1565.99	2022.5	3.850	1.807	20.51	3.812	13.38	2.487	20.51	0.173E 02	1.273
1.92	1.0570	1576.79	2042.2	3.417	1.783	20.51	3.865	13.38	2.522	20.51	0.146E 02	1.199
3.87	1.0048	1597.18	2151.8	2.968	1.768	20.51	3.957	13.38	2.581	20.51	0.120E 02	1.118
5.87	0.9476	1616.15	2285.6	2.688	1.765	20.51	4.035	13.38	2.633	20.51	0.107E 02	1.063
7.90	0.8953	1633.91	2422.9	2.480	1.765	20.51	4.106	13.38	2.679	20.51	0.982E 01	1.022
9.97	0.8545	1650.70	2543.1	2.319	1.768	20.51	4.172	13.38	2.722	20.51	0.918E 01	0.988
15.92	0.7720	1694.19	2828.5	2.018	1.777	20.51	4.346	13.38	2.835	20.51	0.807E 01	0.922
24.60	0.7125	1750.14	3085.6	1.803	1.786	20.51	4.580	13.38	2.988	20.51	0.722E 01	0.871
31.57	0.6822	1792.15	3240.4	1.733	1.783	20.51	4.755	13.38	3.102	20.51	0.682E 01	0.854
38.81	0.6564	1834.54	3387.3	1.699	1.776	20.51	4.927	13.38	3.214	20.51	0.655E 01	0.846
54.04	0.6134	1922.12	3667.7	1.670	1.756	20.51	5.260	13.38	3.432	20.51	0.619E 01	0.838
63.66	0.5920	1976.82	3828.2	1.661	1.743	20.51	5.455	13.38	3.559	20.51	0.603E 01	0.836
70.26	0.5792	2014.24	3932.1	1.656	1.735	20.51	5.585	13.38	3.643	20.51	0.593E 01	0.835
87.45	0.5518	2111.08	4181.7	1.645	1.715	20.51	5.908	13.38	3.854	20.51	0.573E 01	0.832
105.62	0.5294	2212.65	4417.5	1.633	1.697	20.51	6.235	13.38	4.068	20.51	0.556E 01	0.829
124.77	0.5109	2318.93	4641.5	1.620	1.681	20.51	6.570	13.38	4.286	20.51	0.540E 01	0.826
126.74	0.5092	2329.82	4663.3	1.619	1.679	20.51	6.604	13.38	4.308	20.51	0.539E 01	0.825
144.95	0.4955	2429.94	4855.5	1.607	1.665	20.51	6.915	13.38	4.511	20.51	0.527E 01	0.822
166.17	0.4826	2545.74	5061.3	1.593	1.651	20.51	7.272	13.38	4.744	20.51	0.514E 01	0.819

2879